NEW MEXICO DEPARTMENT OF TRANSPORTATION

RESEARCH BUREAU

Innovation in Transportation

Load Rating Bridges with No As-Built Plans or Non-Engineered Bridges

Prepared by:
New Mexico State University
Department of Civil Engineering
Box 30001, MSC 3CE
Las Cruces, NM 88003-8001

Prepared for:
New Mexico Department of Transportation
Research Bureau
7500B Pan American Freeway NE
Albuquerque, NM 87109

In Cooperation with:
The US Department of Transportation
Federal Highway Administration

Final Report

JUNE 2015

USDOT FHWA SUMMARY PAGE

1. Report No. NM13STR-01	**2. Government Accession No.**	**3. Recipient's Catalog No.**
4. Title and Subtitle Load Rating Bridges with No As-Built Plans or Non-Engineered Bridges		**5. Report Date** June 2015 **6. Performing Organization Code**
7. Author(s) David V. Jáuregui, Craig M. Newtson, Brad D. Weldon, Carlos V. Aguilar, Tamara M. Cortez, Dagmawie D. Shikurye, and Yongguan Ouyang		**8. Performing Organization Report No.**
9. Performing Organization Name and Address New Mexico State University Department of Civil Engineering 3035 S. Espina Street Las Cruces, NM 88003		**10. Work Unit No. (TRAIS)** **11. Contract or Grant No.**
12. Sponsoring Agency Name and Address NMDOT Research Bureau 7500B Pan American Freeway PO Box 94690 Albuquerque, NM 87199-4690		**13. Type of Report and Period Covered** Final Report (5/17/13 – 7/31/15) **14. Sponsoring Agency Code**
15. Supplementary Notes		

16. Abstract

Off-system concrete bridges with no design plans are currently a concern in New Mexico as many exist throughout the State. Load rating of these bridges is problematic since the design documentation is limited or missing, thus creating uncertainties regarding the safe load limits for legal vehicles. Only a few states in the United States have formal procedures for load rating concrete bridges without plans. This project was conducted for the New Mexico Department of Transportation to develop a load rating procedure for planless concrete bridges, in particular prestressed structures. In accordance with the *AASHTO Manual for Bridge Evaluation*, a reinforced concrete slab bridge and five prestressed concrete bridges (including two double T-beam, two box girder, and one I-girder) were evaluated using advanced analyses and experimental methods (including load testing and/or non-destructive material evaluation techniques). A multi-step procedure was implemented that included estimating the material properties from past specifications and amount of prestressing steel via Magnel diagrams; verifying the steel estimate with a rebar scanner; testing the bridge at both diagnostic and proof loads based on strain and acoustic emission measurements; and rating the bridges using the proof test results. Rating factors were determined for AASHTO and New Mexico legal loads based on the serviceability limit state (i.e., concrete cracking). Using the AASHTOWare Bridge Rating (BrR) program, rating factors were also computed for the strength limit state (i.e., shear or flexural capacity) based on the measured bridge dimensions and estimated material properties. For the reinforced concrete slab bridge, only the BrR evaluation was needed. The serviceability ratings from proof testing and strength ratings from the BrR program were ultimately compared to determine the final load ratings and need for posting the bridges.

17. Key Words Load rating; Concrete bridges; Bridge testing; Inspection; Non-destructive evaluation	**18. Distribution Statement** Available from NMDOT Research Bureau		
19. Security Classification (of this report)	**20. Security Classification (of this page)**	**21. No. of pages**	**22. Price**
Form DOT F 1700.7 (8-72)			

PROJECT NO. NM13STR-01

LOAD RATING BRIDGES WITH NO AS-BUILT PLANS OR NON-ENGINEERED BRIDGES

Final Report
May 17, 2013 – July 31, 2015

A Report on Research Sponsored by:

Research Bureau
New Mexico Department of Transportation
7500B Pan American Freeway NE
PO Box 94690
Albuquerque, NM 87199-4690
(505) 841-9145
research.bureau@state.nm.us
http://nmdotresearch.com

Prepared by:

David V. Jáuregui, Craig M. Newtson, Brad D. Weldon, Carlos V. Aguilar, Tamara M. Cortez, Dagmawie D. Shikurye, and Yongguan Ouyang

Department of Civil Engineering
New Mexico State University
3035 S. Espina Street
PO Box 30001, MSC 3CE
Las Cruces, NM 88003

PREFACE

The objective of the project is to develop methods to determine bridge load ratings and posting loads for concrete bridges in New Mexico with no as-built plans and to use these methods to perform load ratings on a selected group of bridges. The project includes four major tasks including: (1) coordinate with NMDOT for data collection and regulatory / administrative requirements for the selected bridges; (2) review procedures from other state departments of transportation (DOTs) for load rating of bridges with no as-built plans or non-engineered bridges; (3) perform a literature search to determine the available relevant research and best practices; and (4) develop load testing and rating procedures for the selected bridges. The bridge assessment procedures are developed in accordance with the AASHTO *Manual for Bridge Evaluation* using diagnostic and proof load testing methods, non-destructive material evaluation techniques, and advanced analysis methods. Final load ratings for the selected bridges are provided in the NMDOT standard rating form. The primary goal for future implementation is to determine load ratings or posting loads for all locally owned bridges in New Mexico with no as-built plans.

NOTICE

DISCLAIMER

ABSTRACT

Off-system concrete bridges with no design plans are currently a concern in New Mexico as many exist throughout the State. Load rating of these bridges is problematic since the design documentation is limited or missing, thus creating uncertainties regarding the safe load limits for legal vehicles. Only a few states in the United States have formal procedures for load rating concrete bridges without plans. This project was conducted for the New Mexico Department of Transportation to develop a load rating procedure for planless concrete bridges, in particular prestressed structures. In accordance with the *AASHTO Manual for Bridge Evaluation*, a reinforced concrete slab bridge and five prestressed concrete bridges (including two double T-beam, two box girder, and one I-girder) were evaluated using advanced analyses and experimental methods (including load testing and/or non-destructive material evaluation techniques). A multi-step procedure was implemented that included estimating the material properties from past specifications and amount of prestressing steel via Magnel diagrams; verifying the steel estimate with a rebar scanner; testing the bridge at both diagnostic and proof loads based on strain and acoustic emission measurements; and rating the bridges using the proof test results. Rating factors were determined for AASHTO and New Mexico legal loads based on the serviceability limit state (i.e., concrete cracking). Using the AASHTOWare Bridge Rating (BrR) program, rating factors were also computed for the strength limit state (i.e., shear or flexural capacity) based on the as-built bridge dimensions and estimated material properties. For the reinforced concrete slab bridge, only the BrR evaluation was performed. The serviceability ratings from proof testing and strength ratings from the BrR program were ultimately compared to determine the final load ratings and need for posting the bridges.

ACKNOWLEDGEMENTS

This research would not have been possible without the assistance provided by many individuals from the New Mexico Department of Transportation (NMDOT), Federal Highway Administration (FHWA), Dona Ana County (DAC), City of Albuquerque, and New Mexico Department of Public Safety (NMDPS). From the NMDOT and FHWA, the authors wish to thank Mr. Ray Trujillo (State Bridge Engineer), Mr. Jeff Vigil (Bridge Management Engineer), Mr. Gary Kinchen (Bridge Rating Engineer), and Dr. Thiet Nguyen (New Mexico Division Bridge Engineer) for supporting the research project. Mr. Scott McClure (Research Bureau Chief) and Dr. David Hadwiger (Research Staff Manager) are gratefully acknowledged for their oversight of the study and the guidance provided by other members of the technical panel including Mr. Ben Najera, Mr. Will Dodge, Mr. Earl Franks, and Mr. Patrick Romero is appreciated. For the assistance they provided in securing the vehicles, weight scales, overload permits, and traffic control measures needed for the bridge testing, the NMSU research team would like to especially recognize the following individuals: NMDOT – Mr. Ernest Sedillo (Anthony Patrol Yard Supervisor), Mr. Danny Silva (Hatch Patrol Yard Supervisor), Mr. Nick Lucero (North Urban Patrol Yard Supervisor), Ms. Margaret Haynes (District 3 Maintenance Engineer), Mr. Joseph Valdez (Bridge Management Analyst), Ms. Leslie Sanchez (Bridge Management Analyst), Mr. Frank Martinez (District 2 Bridge Inspector), and Mr. Joe Garcia (Artesia Patrol Yard Supervisor); DAC – Mr. Robert Armijo (County Engineer) and Ms. Dara Gomez (Inspector); City of Albuquerque – Mr. David Silva (Bridge Engineer) and Mr. Tommy Rivera (Street Operation / Maintenance Supervisor); and NMDPS – Lieutenant David Abeita, Ms. Lucretia Maez, Sergeant Sammy Clouthier, and Lieutenant Mike Weatherly. In addition, numerous truck drivers and traffic control personnel from NMDOT Districts 1, 2, and 3 did excellent jobs in following the NMSU load testing procedures and their cooperation is gratefully acknowledged.

METRIC CONVERSION FACTORS PAGE

APPROXIMATE CONVERSIONS TO SI UNITS				
SYMBOL	**WHEN YOU KNOW**	**MULTIPLY BY**	**TO FIND**	**SYMBOL**
LENGTH				
in	inches	25.4	millimeters	mm
ft	feet	0.305	meters	m
yd	yards	0.914	meters	m
mi	miles	1.61	kilometers	km
AREA				
in^2	square inches	645.2	square millimeters	mm^2
ft^2	square feet	0.093	square meters	m^2
yd^2	square yard	0.836	square meters	m^2
ac	acres	0.405	hectares	ha
mi^2	square miles	2.59	square kilometers	km^2
VOLUME				
fl oz	fluid ounces	29.57	milliliters	mL
gal	gallons	3.785	liters	L
ft^3	cubic feet	0.028	cubic meters	m^3
yd^3	cubic yards	0.765	cubic meters	m^3
NOTE: volumes greater than 1000 L shall be shown in m^3				
MASS				
oz	ounces	28.35	grams	g
lb	pounds	0.454	kilograms	kg
T	short tons (2000 lb)	0.907	megagrams (or "metric ton")	Mg (or "t")
TEMPERATURE (exact degrees)				
^oF	Fahrenheit	5 (F-32)/9 or (F-32)/1.8	Celsius	^oC
ILLUMINATION				
fc	foot-candles	10.76	lux	lx
fl	foot-Lamberts	3.426	candela/m^2	cd/m^2
FORCE and PRESSURE or STRESS				
lbf	poundforce	4.45	newtons	N
lbf/in^2	poundforce per square inch	6.89	kilopascals	kPa

TABLE OF CONTENTS

LIST OF TABLES

LIST OF FIGURES

1. INTRODUCTION

1.1 BACKGROUND

Bridge load rating is the process of determining the safe load-carrying capacity of a bridge using analytical methods, experimental methods, or a combination of the two. In the U.S., the load rating methods and corresponding procedures are specified by the American Association of State Highway and Transportation Officials (AASHTO) in the AASHTO *Manual for Bridge Evaluation* (2011). This manual is hereafter referred to as the AASHTO *Manual* in this report. Load ratings are used by the New Mexico Department of Transportation (NMDOT) to manage the State's bridge infrastructure to assure public safety, assist in the efficient allocation of bridge repair and replacement resources, and facilitate the movement of goods and services on the State's public roadways.

The majority of the State's bridges have documentation and conventional structural systems (e.g., girder and deck, flat slab, rigid frame) such that these bridges can readily be load rated by normal analytical methods. Yet many bridges exist that are difficult to evaluate solely by analytical means such as those without available documentation (i.e., as-built plans), and certain non-engineered structures that either lack plans and/or were constructed using alternative structural systems without well-defined load paths. As in several other states, the majority of bridges in New Mexico that do not have plans are older off-system (i.e., locally owned by a city or county) concrete bridges. Typical timber and steel bridges can be field measured to obtain the information needed to perform an analytical load rating. For concrete bridges, however, it is a major challenge to obtain the location and size of steel reinforcement inside the main concrete members, which is essential for the load rating analysis. In the absence of plans, conservative assumptions are usually made to define the reinforcement parameters and concrete properties for use in the analysis. In some cases, the load ratings are established based on engineering judgment and an assessment of the current bridge condition without an actual structural analysis. Ratings determined under these principles may result in much uncertainty and have a low confidence level.

1.2 RESEARCH OBJECTIVE

The objective of this project is to develop methods to determine bridge load ratings and posting loads for concrete bridges in New Mexico with no as-built plans and to use these methods to perform load ratings on a selected group of bridges. The project consists of four major tasks which are listed below:

> **Task 1** – Coordinate with NMDOT personnel to gather and compile relevant data, as well as regulatory and administrative requirements, to perform the load rating analysis.

Task 2 – Review procedures from no fewer than six (6) other state DOT's, or as available, which have addressed the issue of load rating of bridges with no as-built plans.

Task 3 – Perform a literature search to determine the available relevant research and best practices, and how this information may be used to address the problem.

Task 4 – Develop and test procedures on a select group of concrete bridges.

The bridge assessment procedures are developed in accordance with the AASHTO *Manual* using diagnostic and proof load testing methods, non-destructive material evaluation techniques, and advanced analysis methods. The load rating approach and final ratings for the selected bridges are provided in the NMDOT standard rating form. The primary goal for future implementation is to determine load ratings or posting loads for all locally owned bridges in New Mexico with no as-built plans.

1.3 ORGANIZATION OF REPORT

The study presented herein focuses on the development of a load rating procedure for reinforced and prestressed concrete bridges with no design plans. The procedure involves some or all of the following activities: detection of steel reinforcement using Magnel diagrams in accordance with the applicable AASHTO design specifications; detection and confirmation of steel reinforcement estimate with a Hilti PS 250 Ferroscan; validation of the concrete strength with a Windsor Probe; diagnostic and/or proof load testing and strain measurements; load rating for serviceability using the proof test results according to the AASHTO *Manual*; and load rating for strength using the AASHTOWare Bridge Rating (BrR) program based on the Load Factor Rating (LFR) and Load and Resistance Factor Rating (LRFR) methods.

Chapter 2 provides a literature review of previous research related to the load testing of bridges without plans. In addition, the chapter summarizes the results from the department of transportation (DOT) surveys submitted by 14 states regarding the general policies and load testing procedures (if any) for rating bridges without plans. Finally, a summary of the general load rating approach developed for this project is given. Chapter 3 describes the six bridges selected for evaluation in this project that included five prestressed concrete bridges (two double T-beam, two box beam, and one I-girder) and one reinforced concrete slab bridge. In addition, the bridge measurements and properties obtained from field measurements are provided as well as the bridge conditions from the in-depth inspection reports.

In Chapter 4, the procedure for estimating the number and layout of steel strands in the prestressed concrete bridges using Magnel diagrams is covered. The equations used to develop the Magnel diagrams for both composite and non-composite behavior are described and strand estimates are provided for each prestressed concrete bridge. Chapter 5 provides the non-destructive testing results from the Hilti Ferroscan. For the prestressed concrete bridges, the Ferroscan results are compared with the Magnel strand estimates from Chapter 4. The size, location, and concrete cover of the mild shear reinforcement measured with the Ferroscan is also presented. In addition, for the reinforced concrete slab bridge, the Ferroscan measurements of the longitudinal steel bars are given. Chapter 6 provides the non-destructive testing results of the concrete strengths for the different bridges from the Windsor Probe.

Chapter 7 covers the diagnostic testing of three prestressed concrete bridges (NMDOT bridge numbers 7701, 7722, and 8761) including the preparatory calculations, instrumentation plans, truck configurations, and strain measurements for each bridge. In addition, the test phases for each bridge as well as the truck paths applied during the diagnostic tests are discussed to determine the critical paths for the proof tests. Chapter 8 discusses the proof testing of the five prestressed concrete bridges (NMDOT bridge numbers 7701, 7722, 8588, 8761, and 8825) similar to the diagnostic tests. Chapter 9 presents the final load ratings for each bridge. For the prestressed concrete bridges, legal load ratings based on serviceability (i.e., concrete cracking) using the results of the proof tests are computed in accordance with the AASHTO *Manual*. In addition, legal load ratings based on strength using the AASHTOWare BrR models are calculated for all bridges. For Bridge 8676, the reinforced concrete slab bridge, no load tests were conducted and only the BrR ratings were calculated. A comparison of the legal load ratings and final recommendations regarding the capacity of each bridge are finally given. Chapter 10 provides a summary of the project and the main conclusions drawn from the load ratings of the selected concrete bridges without plans that were evaluated.

Appendix A provides guidance on the use of the Hilti Ferroscan and Windsor Probe for prestressed concrete bridges with double T-beam, box beam, and I-girder superstructures as well as reinforced concrete slab bridges. Appendix B contains a paper highlighting the results from acoustic emission monitoring of Bridge 7701, a prestressed concrete double T-beam bridge. The monitoring was performed during the proof test of the bridge and was a joint effort between New Mexico State University (NMSU) and the University of South Carolina. Appendix C contains the final NMDOT load rating forms for the six concrete bridges.

2. LITERATURE REVIEW, STATE SURVEYS, AND GENERAL PROCEDURE

2.1 LITERATURE REVIEW

A literature review was performed using several search engines, a few of which included the ASCE Civil Engineering Database (CEDB), Web of Science, Google Scholar, TRB Transport Research International Documentation (TRID), and Engineering Village. The search focused on work performed over the last 10 years and related primarily to proof load testing and load rating of concrete bridges without plans. Summaries of the historical studies related to load testing and the most recent investigations found in the literature are provided in the following paragraphs.

In the 80's and 90's, several state DOTs used load testing to determine the capacity ratings for a bridge including Alabama (Conner et al. 1997), Florida (Shahawy and Garcia 1990, Shahawy 1995), Michigan (Saraf et al. 1996), and New York (Kissane et al. 1980). A study to develop nondestructive load testing procedures for bridge assessment was conducted under Project 12-28(13) of the National Cooperative for Highway Research Program (NCHRP) by Pinjarkar et al. (1990) and Lichtenstein (1993). The procedures developed in NCHRP Project 12-28(13) actually serve as the basis of "Section 8: Nondestructive Load Testing" provided in the AASHTO *Manual*. It is important to note that a significant amount of the diagnostic and proof load testing were conducted by the aforementioned states prior to the year 2000 and slowed down after many bridges in the state inventory were tested. Furthermore, the majority of the proof tests were performed on reinforced concrete and steel bridges, with only a few on prestressed concrete bridges.

Recently, a major project was conducted by the Georgia Institute of Technology for the Georgia Department of Transportation. The project involved several tasks including an appraisal of the start-of-the-art of bridge condition assessment (Wang et al. 2009); bridge evaluation through load testing and advanced analysis (O'Malley et al. 2009, Wang et al. 2011a); and the development of guidelines for bridge condition assessment, evaluation and load rating in Georgia (Ellingwood et al. 2009, Wang et al. 2011b). The Iowa DOT (Wipf et al. 2003), Delaware DOT (Chajes and Shenton 2006), and Vermont Agency of Transportation (Jeffrey et al. 2009) have also sponsored research within the last ten years to develop bridge testing capabilities for load rating purposes. However, the testing method of choice in the four states mentioned above has been diagnostic testing rather than proof testing.

Apart from the U.S., both Canada and Switzerland have a long history in testing bridges. Much of the Canadian research was performed by the Ontario Ministry of Transportation (Bakht and Jeager 1990). In Switzerland, most of the load tests performed were acceptance proof tests on new bridges before they were opened to traffic (Ladner 1985, Markey 1991). Suggestions for extending the testing procedures and evaluation criteria of the Swiss approach to existing bridges were provided by Moses et al. (1994). A major project was recently conducted in Europe entitled Assessment and Rehabilitation of Central European Highway Structures (ARCHES) that focused on the use of soft, diagnostic, and proof load testing for bridge evaluation (Casas et al. 2009).

Outside of the ARCHES project, just a few other studies were discovered related to diagnostic and proof load testing of concrete bridges without plans (Bernhardt and DeKolb 2003, Bernhardt et al. 2004, Hag-Elsafi and Kunin 2006, Shenton et al. 2007, Commander et al. 2009). Again, the bridge type consisted mainly of reinforced concrete members (i.e., non-prestressed) and with the exception of Bernhardt and DeKolb (2003) and Bernhardt et al. (2004) the evaluation was based on the diagnostic testing approach. With regards to proof load testing, several studies were found that focused on the computation of target proof load factors based on probability-based methods (Gómez and Casas 2008, Gómez and Casas 2010, Wisniewski et al. 2012, Casas and Gómez 2013). However, a significant amount of information is needed regarding the traffic characteristics which is not available for the select group of concrete bridges in New Mexico.

2.2 STATE SURVEYS

A total of 14 state DOTs (including Alabama, California, Colorado, Delaware, Florida, Iowa, Michigan, Ohio, Oregon, Pennsylvania, Texas, Vermont, Virginia, and Washington) completed the questionnaire that was sent out regarding their load rating procedures for bridges without plans. The list of the survey questions is provided below:

- Are bridges without plans a problem in your state?
- How many on-system and off-system bridges within your state are without plans?
- Of the bridges without plans, how many are concrete, steel, and timber?
- What commercial software(s) are used for load rating?
- How are bridges without plans load rated in your state?
- Does your state conduct non-destructive load testing to aid in load rating? If so, what type of tests are conducted and how many bridges are tested per year?
- Are there any formal policies and procedures in place for how bridge tests are conducted for load rating purposes?
- Does your state DOT conduct the testing in-house, contract with consultants for testing, or a combination of both?
- What sort of preparatory work is done before bridges are tested?
- Specifically for concrete bridges without plans, how are initial estimates of concrete strength and amount of reinforcement found?
- What instrumentation do you employ while conducting tests?
- For proof tests, what are the loading schemes used?
- How is damage (spalls, delaminations, etc.) taken into consideration prior and during the proof test? How often does an unexpected failure occur during a proof test?
- How long does a typical proof test take?

The responses from the 14 state DOTs are summarized in the following paragraphs. For certain states having more experience in load testing, a follow-up phone interview was also conducted.

2.2.1 Alabama, California, Colorado, Florida and Iowa

The five states of Alabama, California, Colorado, Florida and Iowa were contacted and each state filled out the questionnaire related to the evaluation of bridges without plans. Mr. Will Potter (Senior Structures Design Engineer, Florida DOT) was also contacted for a phone interview since he has significant experience with load testing bridges. Three out of the five states (Alabama, California, and Colorado) indicated that their state experiences problems with bridges without plans. California appears to have the highest number of all five, indicating that over 500 bridges (over 250 for both on and off-system) have no plans in their state. Iowa had the lowest amount; less than 50 bridges are without plans. All states except Iowa stated that a respectable amount of these bridges are concrete. Three of the five states use VIRTIS to perform load ratings in their state; in addition, other programs such as LUSAS and Brufem are used for load rating purposes.

Overall, the majority of these five states indicated that load testing is not used to evaluate concrete bridges without plans. Alabama, California, Colorado and Iowa all use a combination of inspection and engineering judgement to determine a load rating for concrete bridges without plans. Colorado indicated that 1-5 bridges are tested per year; however, Mr. Mac Hasan (Bridge Rating Coordinator, Colorado DOT) mentioned, "When plans are not available and the structure shows no signs of distress, inventory and operating ratings are determined by a Colorado licensed professional engineer". In addition, Mr. Eric Christie (Assistant State Maintenance Engineer – Bridges, Alabama DOT) stated that bridges without plans are never load tested, and further explained that

> "All load tests are done on structures that we have plans or can obtain measurements. No concrete superstructures without plans have been load tested. The purpose of the test is to see if the actual capacity is greater than the theoretical, which from past experience has been the case."

Mr. Potter stated that in the 1980's and 1990's, load testing was extensively used throughout Florida to load rate bridges without plans; an estimated 10 to 20 bridges were tested every year. Since testing has been ongoing for years, many of the suspect bridges have already been tested and rated, thus resulting in only 3-4 bridges now being tested per year.

California and Colorado will both immediately post a limit on a bridge if a small rating factor is calculated. Alabama and Iowa, however, will conduct a deeper investigation to determine if the bridge absolutely needs to be posted. For example, Mr. Christie stated that Alabama will create a finite element model to "come up with a more refined moment analysis". If the model indicates the bridge must still be posted, a load test will be conducted. All states, except for California,

indicated that load testing is used for load rating bridges; however, only Florida and Iowa will load test bridges without plans, with Iowa only using diagnostic testing.

Based on the four states that employ load testing, in-depth inspections are performed and structural analyses are conducted before the tests. In addition, the AASHTO *Manual* is referenced for unknown variables (for example, strength of concrete for a bridge without plans). Both strain and deflection gauges are most commonly used when it comes to conducting proof tests. Alabama and Colorado use dump trucks for proof testing, while Florida has specialized load testing trucks. Both Alabama and Florida mentioned that only two trucks are used for proof testing. All three states indicated that the planning and execution of proof tests can take up to 2 or 3 months. This includes the logistics, instrumentation, and actual implementation of the proof test. The actual loading of the bridge takes, on average, 6-10 hours to complete.

2.2.2 Michigan, Ohio, Oregon, Texas and Washington

This section summarizes the questionnaire responses of five additional representative state DOTs (Michigan, Ohio, Oregon, Texas and Washington) and feedback from phone interviews conducted with load rating engineers. All of the aforementioned states attested that bridges with no as built plans are of concern. It was revealed that 50-150 are on-system bridges in the states of Ohio, Oregon, and Washington (Oregon specifically mentioned 125 on-system bridges have no plans). In addition, there are more than 250 off-system bridges in Ohio, 110 in Oregon, and an unknown number of off-system bridges with no plans in Washington State. Of bridges without plans, 1-20 are timber bridges, more than 100 are steel bridges, and the remaining are concrete bridges in the state of Ohio. In Oregon, 195 are concrete, 36 are steel, and 4 are timber bridges while Washington stated that almost all bridges without plans are concrete bridges. All these state DOTs use different types of software for load rating. For example, Ohio uses the VIRTIS load rating software while BRASS-Girder LRFD (from Wyoming DOT) and Midas Civil is used for load rating in Oregon along with Excel spreadsheets and MathCAD. Washington uses a software developed in-house for load rating bridges.

For bridges without plans, Oregon has specific load rating procedures that depend on the type of bridge. If the bridge is made of steel or timber, field measurements are taken so that the loading on the bridge and the member capacities can be calculated, thus allowing the bridge to be load rated analytically. If the bridge is comprised of prestressed concrete members, Oregon will review the standard drawings (corresponding to the size and span length of the prestressed members) that were in place at the time that the bridge was constructed to estimate the material properties and the amount of prestressing strands in the member so that it can be rated (ODOT 2013a, ODOT 2013b). For conventionally reinforced concrete bridges without plans, Oregon follows a series of steps to assign inventory and operating rating factors for the bridge (ODOT 2013a, ODOT 2013b).

The states of Michigan and Washington follow "engineering judgment" in the rating of bridges without plans as described in a memo issued by the Federal Highway Administration (FHWA) on February 2, 2011 (FHWA 2011). Michigan subsequently issued a bridge advisory to provide further guidance in following the FHWA memo (MDOT 2012). This advisory references Section 6.1.4 of the AASHTO *Manual* that states the following:

> "For bridges where necessary details, such as reinforcement in a concrete bridge, are not available from plans or field measurements, a physical inspection of the bridge by a qualified inspector and evaluation by a qualified engineer may be sufficient to establish an approximate load rating based on rational criteria."

and

> "A concrete bridge with unknown details need not be posted for restricted loading if it has been carrying normal traffic for an appreciable period of time and shows no distress. The bridge shall be inspected regularly to verify satisfactory performance."

and

> "Knowledge of the live load used in the original design, the current condition of the structure, and live load history may be used to provide a basis for assigning a safe load capacity. Bridge owners may consider nondestructive proof load tests to establish a safe load capacity for such bridge."

Furthermore, the ratings shall be determined by the engineer upon careful consideration of all available information including, but not limited to, the following: year of construction and material properties of members; assumed design (inventory) loading and controlling operating vehicle; measurable structural dimensions; condition of load carrying components; redundancy of load path; changes since original construction; and comparable structures of known design (MDOT 2012).

The Texas Department of Transportation (TxDOT) follows the flow chart given in Figure 2.1 for load rating of concrete bridges with no plans. If a concrete bridge with unknown reinforcement has a long history of carrying unrestricted traffic and there are no signs of structural distress, the bridge can be rated for the State Legal Load (i.e., HS-20 design load) at the Operating Level (TxDOT 2013); hence, the operating rating is taken as unity for this case. The inspection frequency and need for posting are subsequently determined based on the age of the structure and the condition ratings of the deck, superstructure, and substructure. If structural distress is found, a quantitative analysis is required to determine the load rating. Examples are provided in the TxDOT

(2013) Bridge Inspection Manual to illustrate the load rating of different concrete bridge types including a flat slab concrete bridge designed between 1930 and 1960, a multi-beam concrete bridge built between 1940 and 1965, and a prestressed concrete beam bridge built after 1955.

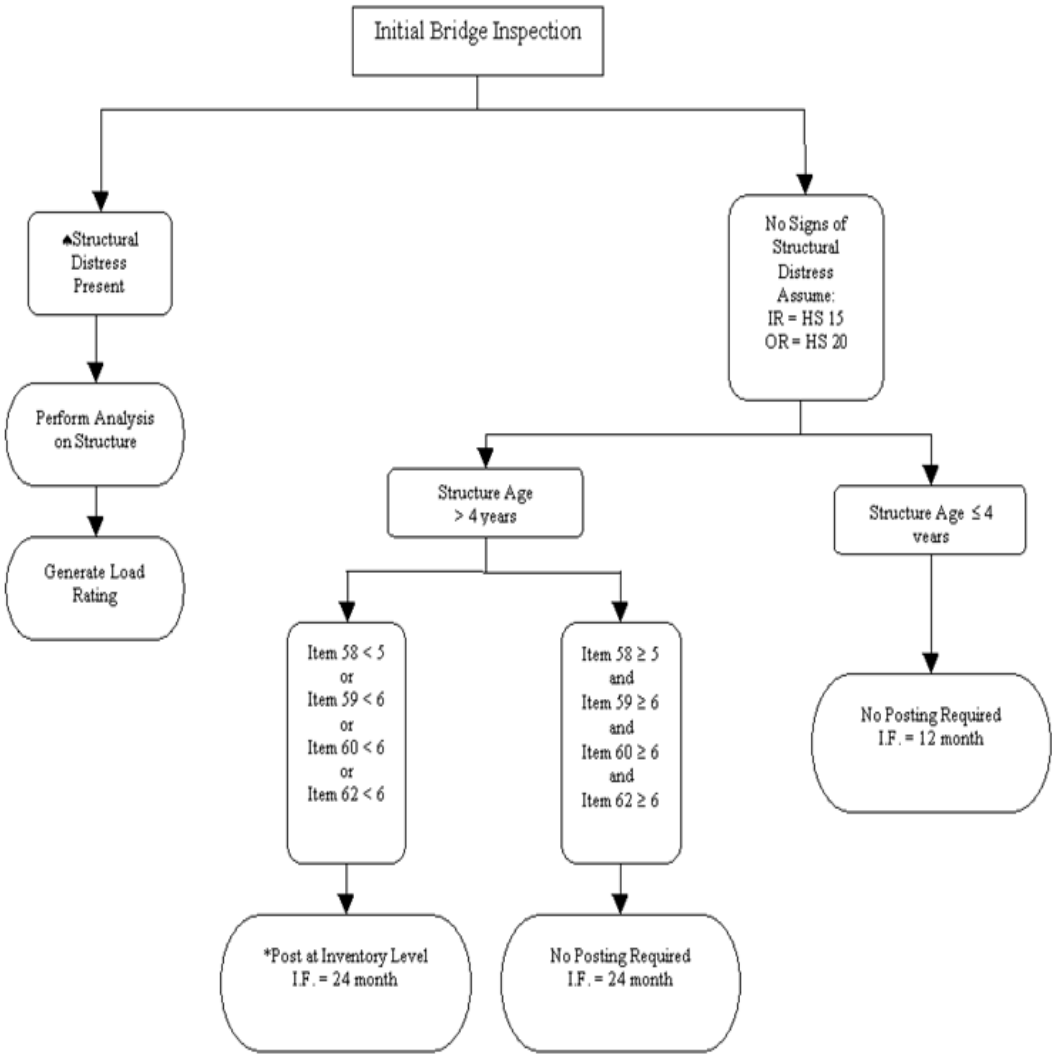

Figure 2.1. Rating procedure for concrete bridges without plans in Texas (TxDOT 2013).

Aside from the information provided in the manual, Mr. Bernie Carrasco (Engineering Assistant – Bridge Division, TxDOT) was also interviewed by phone. A few of the interview highlights are provided below:

- Both proof and diagnostic testing has been used, however, it is not done often
- No other experimental methods have been used
- No formal policies or procedures are in place for bridge testing
- Majority of work is done in house, or with a university (not certain if consultants have been used)

- Software used include in-house spreadsheets, Bridge Analysis and Rating (BAR7) program developed by the Pennsylvania Department of Transportation (PennDOT), VIRTIS, RM Bridge developed by Bentley, PGSuper developed by Bridgesight Inc., RISA-3D, ANSYS, LUSAS
- Washington and Oregon are good states to contact
- Rebar scanner, ground penetrating radar rarely used
- For proof tests, dump trucks and water trucks have been used (for water trucks, tandem axle is about 34 kips); loading is dependent on bridge configuration
- Distress is controlling trigger to stop loading bridges (e.g., large deflections, increase in cracks/crack sizes)
- Hard to estimate number of bridges without plans (not a major concern in Texas)
- For bridges without plans: ON-SYSTEM – 5 or better needs no load posting, <4 is posted; OFF-STSTEM: 6 or better needs no load posting, <5 is posted (@ HS-15)

The states of Oregon and Ohio use non-destructive testing on occasion to investigate the load carrying capacity of bridges with no plans and typically hire consultants to conduct the tests. Strain and deflection gauges are the primary instruments used during testing while dump trucks loaded with predefined loads are used as a means of loading. Oregon reported that 2-3 days are typically required for setting up and installing the sensors, testing the equipment, tracing errors and shorts in the wiring, and monitoring ambient traffic to verify the equipment is working properly. An entire day is then allotted to perform the proof test according to the AASHTO *Manual* which stipulates that the loads be incremented up to the target proof load. The load effects of partially loaded dump trucks in both single and multiple lane configurations is first evaluated, and then the trucks are loaded further with additional gravel up to the next load level. The axle weights for the new loading are re-measured and the truck returns to the bridge for the next phase of the test. This is repeated until either the target load level is reached, or the bridge instrumentation begins to show that the bridge response is approaching the stress or deflection limits determined from the pre-test analysis performed to develop the load test plan for the bridge.

2.2.3 Delaware, Pennsylvania, Vermont and Virginia

Vermont and Delaware stated that bridges without plans are an issue in their states while Virginia is concerned only with bridges on highway routes with high traffic volume; Pennsylvania replied that bridges without plans are not a problem. As for the number of bridges without plans, Virginia has over 250 bridges (including on-system and off-system); Pennsylvania has over 250 on-system bridges; and Vermont and Delaware each have less than 150 on-system bridges. Virginia does not separate on-system and off-system bridges, while Vermont and Pennsylvania each have over 250 off-system bridges without plans in their state; the number of off-system bridges without plans in Delaware is unknown. In all four states, concrete bridges are the most common types of bridges without plans. Mr. Jonathan Mallard, the load rating program manager for the Virginia DOT,

mentioned that since most steel bridges can be measured in the field, and properties can be determined from historic manuals, the plans can be easily recreated. For this reason, the lack of plans for steel bridges is not as large a concern as concrete bridges.

Virginia and Delaware both mentioned that load testing has been considered to aid in the load rating of bridges without plans. Virginia, however, indicated that load testing is not common, and engineering judgment is predominately used, as in the states of Vermont and Pennsylvania. Specific policies for load rating bridges without plans using engineering judgment are currently being developed in Vermont while the Pennsylvania Department of Transportation (PennDOT) has policies already in place that can be found in Chapter 3 of the state's Bridge Safety Inspection Manual (PennDOT 2010a). The chapter states that factors such as the bridge condition, material properties, load path redundancy, traffic characteristics, performance of bridge under loading, and bridge restrictions should be considered in arriving at a bridge rating based on engineering judgment (PennDOT 2010a). The following statement is also contained in the chapter as a guide for the load rating of bridges without plans (PennDOT 2010a):

> "In PA, the vast majority of bridges either have sufficient design drawings or the properties of the members can be verified through field measurements to support an engineering analysis. However, for many older concrete or masonry structures (including slabs, beams, and arches), the structural components either cannot be measured (arches) or critical details (e.g., reinforcement details) are not known with sufficient confidence to evaluate through computations. For these structures, a rating based on engineering judgment by a qualified engineer familiar with the bridge and the factors listed above may be appropriate. A suggested method for applying engineering judgment alone to determine the ratings of such bridges without plans is contained in Appendix IP 03-B".

The appendix referred to in the above statement contains the document titled *Guidelines for Live Load Rating of Selected Concrete Bridges Without Plans Using Engineering Judgment* (PennDOT 2010b). Using these guidelines, the operating and inventory ratings along with the inspection frequency for selected bridges without plans may be determined based on the condition rating and distress level of the controlling bridge member.

Towards the end of Chapter 3 (PennDOT 2010a), it is stated that testing should only be used as a last resort if "the structure cannot be accurately modeled by analysis, the structural response to live load is in question, or as a last means to avoid a weight restriction on a significant structure". Similar to Pennsylvania, Vermont indicated that no load testing is done in their state to establish load ratings for bridges without plans. Out of the four states, only Virginia and Delaware mentioned that load testing is used to assist with load rating; Pennsylvania mentioned that testing is employed, but for non-load rating purposes, and Vermont does not use load testing in their state.

Both Virginia and Delaware regularly conduct diagnostic and proof tests, averaging between 1-5 tests per year. Mr. Jonathan Mallard described the testing in Virginia, stating that,

> "In the past, Virginia has done a modified combination of the two (proof and diagnostic tests), where modeling has been done prior to testing, but then trucks of varying loads have been positioned at varying locations on the bridge. The maximum load used during testing is typically a legal load that can be transported to the bridge site, and rarely does that load reach the target proof load dictated by the Manual for Bridge Evaluation. During testing, bridges are instrumented to observe member behavior in real-time, but the bridge is not visually inspected after each run during the test."

Although both states use testing to aid in load rating, neither have any formal policies on how these tests should be performed.

Finally, both Virginia and Delaware indicated that modeling and inspection are performed before any load test is performed. While Virginia conducts the test in-house, Delaware will contract with consultants for testing. To estimate the concrete strength, Virginia uses a combination of physical inspection and reference data from the AASHTO *Manual*. Delaware also uses the AASHTO *Manual* along with concrete core testing. For instrumentation, both states use primarily strain and deflection gauges, along with dump trucks to load the bridges. Virginia has not tested any bridges with severe damage (i.e., such that it was considered crucial). Delaware, on the other hand, models the bridge with the defects in place, and carefully monitors the damage throughout the test. Overall, both states have not experienced any unexpected failure during proof testing; Virginia uses a modified proof test with lower loads and therefore, failure is less likely. On average, proof testing in both states takes over 9 hours to complete, including instrumentation, testing, and clean-up.

2.3 GENERAL PROCEDURE

From the AASHTO *Manual* and the review of the literature and other state DOT procedures, it was recognized that the proof testing procedures were developed primarily for reinforced concrete and steel bridges at the strength limit state and operating load level. Specific guidance for proof testing of prestressed concrete bridges is lacking. Due to the high likelihood of exceeding the cracking moment based on the target proof load specified in the AASHTO *Manual*, it was decided that the load testing conducted in this study would be planned and conducted based on the Service III limit state (i.e., concrete cracking) rather than the Strength I limit state for prestressed concrete bridges. This greatly facilitates the load testing since a much smaller target proof load is required. In addition, this approach limits the amount of damage (if any) imposed on the bridge during testing. It is important to note that the AASHTO *Manual* allows the optional check at the Service III limit state to be considered for the legal load rating.

Based on the literature review and state surveys, a basic procedure for field testing of prestressed concrete bridges without plans was developed. First, the total number and eccentricity of the prestressing strands in the bridge beams are estimated using Magnel diagrams (Krishnamurthy 1983). This approach was previously used by Hag-Elsafi and Kunin (2006) to evaluate a post-tensioned bulb-T beam bridge in New York and Taylor et al. (2011) to evaluate several prestressed double-tee beam bridges in Colorado. Material properties are obtained from the AASHTO *Manual*, AASHTO Standard Specifications, and/or the State's provisions. Second, a Hilti PS 250 Ferroscan is used to detect the steel in the prestressed concrete beams and check the strand estimate and also determine the layout of the shear reinforcement. In addition, the concrete strength is estimated using a Windsor probe instrument. Third, a diagnostic load test is performed to measure the beam strains under a truck load approximately 60% of the target proof load determined based on the prestressing strand estimate and allowable tensile stress at service. The objectives of this test are to determine the critical transverse truck paths (i.e., ones producing the largest measured strains) and compare the measurements with analytical predictions. Diagnostic load testing is required mainly when the quality of bridge construction is poor and thus, such a test is not necessary for all bridges. Fourth, a proof load test is conducted following critical truck paths and under increasing truck loading until the allowable tensile stress or the target proof load is reached (whichever comes first).

3. DESCRIPTIONS OF SELECTED CONCRETE BRIDGES

The six bridges shown in Table 3.1 were chosen for load testing primarily based on proximity to Las Cruces, NM. Four of the bridges are located in District 1, one in District 2, and one in District 3. All the bridges have two-way traffic but an effort was made to choose bridges with different skew angles and ADTs. One bridge was chosen from each of four concrete bridge categories (including a reinforced concrete slab bridge and prestressed concrete double T-beam, box beam, and I-girder bridges). Diagnostic and/or proof tests were conducted on the prestressed concrete bridges but not the reinforced concrete slab bridge for reasons to be discussed later in the report.

Table 3.1. New Mexico concrete bridges without plans selected for load rating.

Bridge No.	Bridge Type	Year Built	District	Span Length	Roadway Width	Skew Angle	ADT
7701	T-Beam	1974	1	30	23	0	509
8676 *	Slab	1986	1	31	22.4	0	156
7722	Box	1966	1	44.4	21.1	16	823
8761	T-Beam	1989	1	33.3	35.9	28	823
8588	I-Girder	1973	2	74.1	32.2	15	2405
8825	Box	1990	3	42	44	0	592

Notes: * - Bridge 8676 was load rated but not load tested.

In-depth inspections of the six chosen bridges were first performed to document the site conditions, as-built configurations, and current physical conditions of the superstructures. These inspections were important for establishing regulatory and administrative requirements for the nondestructive load testing and load ratings of these structures including the personnel and equipment needed for test preparation, traffic control, underbridge access, and bridge loading. The NMDOT Districts 1, 2, and 3 provided the needed assistance before, during, and after the load testing.

Inspection reports for the select group of bridges listed in Table 3.1 were provided by the NMDOT Bridge Bureau. During the first quarter of FY2014 of this project, field visits were made to the first four bridges given in the table (i.e., nos. 7701, 8676, 7722, and 8761) and preliminary drawings were generated based on the measured geometry and member sizes. All of these bridges are located in District 1, three of which are owned by Doña Ana County and one is owned by Grant County. Mr. Robert Armijo (County Engineer, Doña Ana County) and Mr. Justin Reese (Director of Public Works, Grant County) were informed of the research project and also asked to review their in-house files for any available information on these bridges. Descriptions of the District 1 bridges along with highlights of the field visits and inspection reports are given below. Descriptions of the box girder bridge located in District 3 (Bridge 8825) and the I-girder bridge located in District 2 (Bridge 8588) are also provided which were visited during the second and third quarters of FY2014 of the project, respectively, to obtain the bridge details and verify the bridge conditions. For these bridges, assistance was provided by Mr. David Silva (Bridge Engineer, City of Albuquerque) in District 3 and Mr. Frank Martinez (Bridge Inspector, NMDOT) in District 2 for the load testing.

3.1 BRIDGE NO. 7701, P/C DOUBLE T-BEAM

This bridge, constructed in 1974, is a single-span, prestressed concrete bridge with a 31 ft. span. The bridge consists of nine double T-beams, each of which is 33 in. wide, 19.5 in. deep, and 32 ft. long. The bridge beams are placed directly next to one another, allowing for the beam flanges to act as the deck, and the beam ends rest on 12 in. long bearing seats. Each beam has seven shear keys on the top flange at 4 ft. 3 in. center-to-center spacing and each shear key is 1 foot long and four inches wide. There is no wearing surface and the overall bridge width is 24 ft. 9 in., while the roadway width is 23 ft. 5 in. from curb to curb. The exterior beams have concrete curbs that are 8 inches wide and 13 inches deep. In addition, the exterior beams have side mounted guardrails, with W6 I-beam posts spaced at 51 in. and extending 26 in. above the concrete curb. The guardrail is 12.5 in. deep, and runs along the entire length of the bridge. Overall, the entire structure is 33 ft. 4 in. long (including the prestressed beams and backwalls) by 26 ft. 2 in. wide (based on the backwall length). The bridge carries County Road B-31 over an irrigation canal near NM-478. See pictures given in Figure 3.1.

Figure 3.1. Bridge No. 7701 (prestressed concrete double T-beam) in NMDOT District 1.

Overall, the bridge is in fair condition. The most recent inspection report from November 7th, 2013, indicates a rating of 6 for the deck and superstructure, and a 6 for the substructure. The topside of the beam flanges have transverse, horizontal and map cracking up to 1/32 in. with heavy abrasion and small spalls. The exterior beams have less abrasion and damage, most likely due to less exposure to traffic. The underside of the flanges have map and longitudinal cracks up to 1/32 in. with minor spalls. Some of the longitudinal cracks are developing between the beam stems and the flanges. The stems of the beams have horizontal cracks up to 1/8 in. at the supports. Beam 6 has some vertical cracking up to 1/32 in. originated from the flange-stem transition; however, these cracks are not full depth. Beam 9 has a few spalls up to six inches by six inches with four inches of exposed shear reinforcement on the south side of the stem, near abutment one. The beams are numbered from north to south and the abutments are numbered from west to east. Overall, the beams are in satisfactory condition, as no full-depth flexural cracks were found.

The shear keys located on the top flanges of the beams all vary in condition. Each shear key consists of two steel angles, welded together with a short piece of rebar. The exterior keys are all covered with concrete and appear to be functioning properly. Between beams 4 and 5, six of the seven shear keys are broken and not functioning. In addition, the keys between beams 6 and 7 are damaged and not working well. The condition of each shear key was noted for purposes of planning the load testing. The bridge carries an Average Daily Traffic (ADT) of 511 according to the most recent inspection report; this number seems high, however, as much less traffic was observed during the recent field visits. The truck ADT was not specified in the inspection report.

3.2 BRIDGE NO. 8761, P/C DOUBLE T-BEAM

This is a simple-span bridge with five double-tee prestressed concrete beams and a 28 degree skew. The bridge was originally built in 1989 but based on the field visit and inspection report (dated 12/13/2012), two exterior beams were added later to widen the bridge. The bridge serves 2-way traffic with a total width (out-to-out) of 40 ft., and total length of 36 ft. The individual beam size is 96 in. wide by 27 in. deep by 36 ft. long including a 0.5 ft. bearing length at each end. There is no deck slab on the bridge meaning the beam flanges serve as the deck. The flange thickness is 6 in. while the stem thickness varies from 5.75 in. at the top to 3.75 in. at the bottom. The bridge carries West Afton Road over the West Side Canal near NM-28. See pictures given in Figure 3.2.

The latest condition ratings are 5 for the concrete deck, 5 for the T-beam superstructure, and 6 for the substructure. The inspection report also stated that the edges of the double-tee girders have diagonal cracks at the ends. The girders are numbered 1 through 5 from south to north and the abutments are numbered 1 and 2 from east to west. Girders 1 and 5 have horizontal cracks near abutment 2 and honeycombing along the beam edges. Spalls were found on the undersides of girder 2 (3 in. by 8 in.), girder 4 (3 in. by 6 in.), and girder 5 (3 in. by 5 in.). Overall, the concrete girders are in fair condition. The concrete breastwalls have vertical cracks up to 1/16 in. with heavy scaling and minor leaching. Abutment 1 has delamination up to 20 in. by 21 in. The concrete breastwalls and abutments are in satisfactory condition overall. The bridge rails (NMDOT metal type “A”) are in good condition overall with minor surface rust and paint peeling. The ADT is reported as 827 and the future ADT is 1048 (with 3% truck traffic) for year 2032.

Figure 3.2. Bridge No. 8761 (prestressed concrete double T-beam) in NMDOT District 1.

3.3 BRIDGE NO. 7722, P/C BOX GIRDER

This bridge was constructed in 1966. It is a simple-span bridge with a 44.4 ft. beam length and a 6.1 ft. vertical clearance over an irrigation channel. The bridge has a 16 degree skew and seven box girders (PCI-AASHTO section type BI-36) that are 36 in. wide and 27 in. deep. The wearing surface is a 4 in. asphalt overlay and the roadway width is 21 ft. The bridge has steel rails on each side with varying spacing and number of rail posts; the north exterior beam supports seven rail posts evenly spaced at 8 ft. center-to-center and each extending 26 in. above the asphalt overlay while the south exterior beam supports five posts evenly spaced at 11.1 ft. center-to-center. The exterior beams also support two gas utility pipelines suspended from each rail post. The bridge carries County Road B-108 near NM-185. See pictures given in Figure 3.3.

From the latest inspection report (dated 1/16/2014), the deck, superstructure, and substructure were all rated a 6. The topsides of the girders are unobservable due to the asphalt overlay and the undersides have map cracks up to 1/32 in. with minor to moderate leaching and honeycombing. The girders are numbered from north to south and girder 6 has a spall located close to midspan that is 24 in. long by 2 in. wide with an exposed prestressing strand (3/8 in. diameter) over a distance of 13 in. The vertical faces of the exterior girders have minor vertical and map cracks up to 1/32 in. with honeycombing. The asphalt material is falling through the joints between all the girders. The gap is 2 1/8 in. between girders 1 and 2 and 1 1/4 in. between girders 6 and 7 (note

that the gap measurements were taken from the underside of the bridge). Overall, the bridge is in satisfactory condition. The metal bridge rails are also in fair condition overall (with minor to heavy surface rust, minor traffic damage, and paint peeling) but the north rail is not attached at the northwest corner of the structure. The approach roadway has transverse and map cracks up to 1/4 in., wheel rutting, minor to moderate raveling, and an overall rough riding surface.

Figure 3.3. Bridge No. 7722 (prestressed concrete box girder) in NMDOT District 1.

The latest inspection report gave an ADT of 827. The future ADT was estimated to be 1,048 in the year 2032 with a truck ADT of 3%. The inspection report also mentioned that the box beams were post-tensioned; however, no evidence of post-tensioning was observed during the field visit. Significant gaps were observed on the bridge soffit between the exterior girders and the adjacent interior girders as mentioned earlier suggesting that the bridge was widened sometime in the past. In addition, there are large openings in the asphalt overlay at the exterior-interior girder joints and concrete work was also done on the abutments which provided further evidence of the widening.

3.4 BRIDGE NO. 8825, P/C BOX GIRDER

Bridge 8825 was constructed in 1990 and is located in Bernalillo County, Albuquerque, NM. It is a simple-span bridge with a maximum span length of 42.0 ft. and vertical clearance of 3 ft. over Mariposa Arroyo. The superstructure consists of ten prestressed concrete box girders (section type 5B20) which are 60 in. wide and 20 in. deep. The roadway has a 3 in. thick asphalt overlay and a curb-to-curb width of 44.0 ft. The concrete curbs are 10 in. thick and 6 ft. wide, and extend past the exterior beams a distance of 3 ft. on each side. The curbs support 50 in. tall guardrail with W8x24 posts evenly spaced at 9 ft. 4 in. that are connected by three HSS 5X3 horizontal members spaced 12 in. apart. The bridge carries Mojave Street near the intersection with Homestead Drive. See pictures given in Figure 3.4.

Figure 3.4. Bridge No. 8825 (prestressed concrete box girder) in NMDOT District 3.

According to the latest inspection report (dated 11/6/2013), the bridge is regularly inspected on a 24 month interval and the sufficiency rating is 99.9%. The deck and superstructure were given condition ratings of 6 and the substructure was rated a 7. No signs of bridge widening were observed. The topsides of the box beams are unobservable due to the asphalt overlay. The overlay has transverse cracks at both ends of the bridge and longitudinal reflective cracks over the beam

joints which have been sealed. On the underside, the beams showed leaching with heavy water stains at the longitudinal joints and some rust stains. A minor spall was found on the west beam measuring 3 in. x 3 in. The steel bridge rail has been repainted and the northwest anchor is damaged. The current ADT is 587 and the projected ADT is 697 for the year 2031.

3.5 BRIDGE NO. 8588, P/C I-GIRDER

This bridge, constructed in 1973, is a single-span, prestressed concrete girder bridge with a 74.1 ft. maximum span length. The bridge has a 15° skew and six I-girders (PCI-AASHTO Type III), each 45 in. deep and 75 ft. long. The girders rest on 2 in. thick by 7 in. long elastomeric bearing pads and are spaced 6 ft. 6 in. on center. The overall structure width is 39 ft. 2 in. (39 ft. 10 in. along the skew). Concrete diaphragms, measuring 22 in. deep and 72.75 in. wide along the skew, are located at the ends and mid-span. The girders support a 7.5 in. thick cast-in-place concrete deck, which is topped with a ¼ in. chip seal overlay. The east side of the bridge has a 5 ft. 2 in. wide, 12 in. thick sidewalk that overhangs the bridge deck by 2 ft.; the west side has no sidewalk. The bridge rails on both sides of the bridge are supported by ten W8x21 steel posts on each side. The inner eight posts are spaced at 9 ft. 2 in., while the exterior two posts are spaced at 7 ft. The east side rails are composed of three HSS sections; the top rail is 3 in. x 3 in. and the bottom two are 5 in. x 3 in. The west side rails consist of two 5 in. x 3 in. HSS sections. The bridge measures 36 ft. 4 in. from rail to rail, and 32 ft. 7 in. from the west side rail to the east side sidewalk (not along the skew). Overall, the deck has a length of 75 ft. while the overall structure is 77.1 ft. long. The bridge carries County Road 53 over Eagle Draw near US-82 in Artesia, NM. See pictures given in Figure 3.5.

Overall, the bridge is in fair condition. The most recent inspection report (dated 8/13/2014) has ratings of 5 for the deck, and 6 for the superstructure and substructure. The topside of the deck has spalled areas with exposed rebar. The edges of the deck have hairline vertical, transverse cracks and regions of heavy scaling (mainly on the west side). The underside of the deck has hairline transverse cracks with light leaching, as well as areas of honeycombing; there is also evidence of patchwork on the underside. In addition, the inspectors noted that the majority of the deck is delaminated. The bridge girders have transverse and vertical cracks up to 1/32 in. near the supports. Girders one, four and six have spalls up to 4 in. by 6 in. with some exposed corroded rebar. The concrete diaphragms have small transverse and vertical cracks, with 1 in. x 1 in. popouts, exposed snap ties, and honeycombing up to 1 ft. x 1 ft. The average daily traffic (ADT) is listed as 1232, while the future ADT for the year 2033 is 1432; the truck ADT is estimated as 20%.

Figure 3.5. Bridge No. 8588 (prestressed concrete I-girder) in NMDOT District 2.

3.6 BRIDGE NO. 8676, R/C SLAB

This bridge, constructed in 1986, is a reinforced concrete slab bridge with a 31 ft. simple span. The slab is 16 in. thick with a 2-in. haunch. The topside acts as the riding surface and the ends rest on full height concrete abutments with 2 ft. 6 in. bearing lengths. The overall bridge width is 25 ft. and roadway width is 22 ft. 8 in. between rails. The approach roadway is 22 ft. 2 in. wide including shoulders and the guardrails are W-beams on wood posts with wood blockouts. In addition, the bridge has metal railings consisting of two 3 in. deep by 5 in. wide steel rails (spaced 13 in. on center) on W8x21 steel posts (spaced at 9 ft. 9 in. or 7 ft. 9.5 in. on center) that extend 2 ft. 5.5 in. above the slab. The entire structure is 36 ft. long (including the slab and backwalls). The bridge carries Cottonwood Drive over Sapillo Creek near NM-35. See pictures given in Figure 3.6.

In general, the bridge is in good condition. The most recent inspection report from March 7th, 2013, indicates a rating of 7 for the deck, superstructure, and substructure. The top side of the slab has map, longitudinal, and transverse cracking up to 1/16 in. with small “D” (i.e., hairline) cracks near the approaches. The slab edges have vertical cracks up to 1/32 in. toward the middle of the span and at 6-in. to 12-in. spacing. The underside of the slab has diagonal and longitudinal

cracking up to 1/32 in. as well. In addition, the slab bottom has minor leaching and honeycombing. Despite not having a wearing surface, the concrete slab has no major issues. The bridge carries an ADT of 156, with a future ADT of 199, which appears high based on the recent field visit. The truck ADT was given as 3% in the latest inspection report.

Figure 3.6. Bridge No. 8676 (reinforced concrete slab) in NMDOT District 1.

4. ESTIMATE OF PRESTRESSING STRANDS

The amount of prestressing steel in the double T-beams of Bridges 7701 and 8761, and box beams of Bridges 7722 and 8825, was estimated using Magnel diagrams for HS-20, H-20, and H-15 truck loadings. The diagrams were formulated based on the serviceability criteria (i.e., allowable stresses) for compression and tension at transfer and service. The stresses were evaluated at the beam midspan and included the compressive stress at bottom of beam at transfer, tensile stress at bottom of beam at service, tensile stress at top of beam at transfer, and compressive stress at top of beam at service resulting in four equations. The equations, written in the form of inequalities for the inverse of the initial prestressing force ($1/P_i$), are as follows (Hag-Elsafi and Kunin 2006):

$$P1(e) = \frac{1}{P_i} \geq \frac{1}{A*\left(f_{bi}+\frac{M_{DL}}{S_b}\right)} + \frac{e}{S_b*\left(f_{bi}+\frac{M_{DL}}{S_b}\right)} \quad \text{(Eq. 4.1)}$$

$$P2(e) = \frac{1}{P_i} \leq \frac{-1}{A*\left(f_{ti}+\frac{M_{DL}}{S_t}\right)} + \frac{e}{S_t*\left(f_{ti}+\frac{M_{DL}}{S_t}\right)} \quad \text{(Eq. 4.2)}$$

$$P3(e) = \frac{1}{P_i} \leq k * \left(\frac{1}{A*\left(-f_{bf}+\frac{M_{Tot}}{S_b}\right)} + \frac{e}{S_b*\left(-f_{bf}+\frac{M_{Tot}}{S_b}\right)}\right) \quad \text{(Eq. 4.3)}$$

$$P4(e) = \frac{1}{P_i} \geq k * \left(\frac{-1}{A*\left(-f_{tf}+\frac{M_{Tot}}{S_t}\right)} + \frac{e}{S_t*\left(-f_{tf}+\frac{M_{Tot}}{S_t}\right)}\right) \quad \text{(Eq. 4.4)}$$

where *P1*, *P2*, *P3* and *P4* are the range of solutions that satisfy the serviceability criteria at the beam midspan based on the bottom stress at transfer (f_{bi}), top stress at transfer (f_{ti}), bottom stress at service (f_{bf}), and top stress at service (f_{tf}), respectively. In addition, e is the eccentricity of the prestressing steel; S_b and S_t are the section moduli at the bottom and top of the beam; A is the cross-sectional area of the beam; k is the factor for prestress losses; and M_{DL} and M_{Tot} are the dead load moment and total moment (i.e., dead load plus live load moments), respectively, at midspan.

For Bridge 8588, the amount of prestressing steel in the I-girders was estimated using Magnel diagrams for both non-composite and composite behavior since it was uncertain that interface shear reinforcement was used between the concrete deck and girders. For non-composite action, Eqs. (4.1) through (4.4) given above were used similarly to the other prestressed concrete bridges with double T-beams or box girders. The moment due to the girder self-weight (M_{SW}) was used in Eqs. (4.1) and (4.2) for P1 and P2 as no other dead load is present at the time of transfer. The total moment (M_{Tot}) used in Eqs. (4.3) and (4.4) for P3 and P4 at service included the dead load moments (due to the girder self-weight and the weights of the deck, diaphragms, wearing surface, sidewalks, and rails) plus the live load moment caused by the design truck.

For composite action, the I-girder stresses were again evaluated at midspan and included the compressive stress at bottom of beam at transfer, tensile stress at bottom of beam at service, tensile stress at top of beam at transfer, and compressive stress at top of beam at service. It is important to note that the stresses at the top and bottom of the deck at service are not affected by the prestressing force since the deck resists only superimposed dead loads and truck live load as part of the composite section. The prestressing force acts only on the non-composite girder section. Hence, the Magnel equations used for Bridge 8588 based on composite action are as follows:

$$P5(e) = \frac{1}{P_i} \geq \frac{1}{A*\left(f_{bi}+\frac{M_{SW}}{S_{b,NC}}\right)} + \frac{e}{S_b*\left(f_{bi}+\frac{M_{SW}}{S_{b,NC}}\right)} \quad \text{(Eq. 4.5)}$$

$$P6(e) = \frac{1}{P_i} \leq \frac{-1}{A*\left(f_{ti}+\frac{M_{SW}}{S_{t,NC}}\right)} + \frac{e}{S_t*\left(f_{ti}+\frac{M_{SW}}{S_{t,NC}}\right)} \quad \text{(Eq. 4.6)}$$

$$P7(e) = \frac{1}{P_i} \leq k * \left(\frac{1}{A*\left(-f_{bf}+\frac{M_{DL,NC}}{S_{b,NC}}+\frac{M_{DL,COMP}+M_{LL}}{S_{b,COMP}}\right)} + \frac{e}{S_b*\left(-f_{bf}+\frac{M_{DL,NC}}{S_{b,NC}}+\frac{M_{DL,COMP}+M_{LL}}{S_{b,COMP}}\right)}\right) \quad \text{(Eq. 4.7)}$$

$$P8(e) = \frac{1}{P_i} \geq k * \left(\frac{-1}{A*\left(-f_{tf}+\frac{M_{DL,NC}}{S_{t,NC}}+\frac{M_{DL,COMP}+M_{LL}}{S_{t,COMP}}\right)} + \frac{e}{S_t*\left(-f_{tf}+\frac{M_{DL,NC}}{S_{t,NC}}+\frac{M_{DL,COMP}+M_{LL}}{S_{t,COMP}}\right)}\right) \quad \text{(Eq. 4.8)}$$

where P5, P6, P7 and P8 are the range of solutions that satisfy the serviceability criteria at midspan based on the I-girder stresses at transfer and service. In Eqs. (4.5) through (4.8), e is the eccentricity of the prestressing steel relative to the non-composite girder centroid; $S_{b,NC}$, $S_{t,NC}$, $S_{b,COMP}$, and $S_{t,COMP}$ are the section moduli at the bottom and top of the girder for both non-composite and composite sections, respectively; A is the cross-sectional area of the non-composite girder; k is the factor for prestress losses; M_{SW} is the moment due to the girder self-weight at transfer; and $M_{DL,NC}$, $M_{DL,COMP}$, and M_{LL} are the dead load moments resisted by the non-composite and composite sections and live load moment, respectively, at midspan of the girder. It can be seen that at transfer, the equations remain the same for both fully non-composite (i.e., P1 and P2) and composite (i.e., P5 and P6) bridges, since only the beam dead load (self-weight) is considered. Note that for composite bridges, the girder resists some loads by non-composite action and others by composite section. In a fully non-composite bridge such as the double T-beam and box girder bridges investigated in this study, the total dead and live load moment (i.e., M_{Tot} in P3 and P4) is resisted by solely the beam or girder with no participation from a separate deck. In a composite bridge, the weights of the girder, deck, and diaphragms are resisted by the non-composite section while the superimposed dead load (due to the weights of the rails, sidewalk, and wearing surface) are resisted by the composite section.

4.1 BRIDGE NO. 7701, P/C DOUBLE T-BEAM

Since the bridge was constructed in 1974, the 11th Edition of the AASHO Standard Specifications for Highway Bridges (1973) was followed which would have been the most current specification at the time of construction of Bridge 7701. The concrete strength at release (f_{ci}') was assumed to be 4500 psi, which is slightly larger than the minimum of 4000 psi given in Section 1.6.19 of the AASHO specifications for pretensioned members. The concrete strength at 28 days (f_c') was assumed to be 5000 psi in accordance with Section 1.6.6 of the AASHO specifications and Section 506 of the 1970 Edition of the Standard Specifications for Road and Bridge Construction published by the New Mexico State Highway Department (NMSHD). Note that the strengths of f_{ci}' = 4500 psi and f_c' = 5000 psi agreed with historical information found by the NMDOT for off-system bridges in Doña Ana County. The prestressing steel was assumed to be 0.5-inch diameter, Grade 270, seven-wire, stress-relieved strands. The value for k, the amount of prestress loss, was estimated using the AASHO specifications (Section 1.6.7B) to be 23.6% and finally taken as 25%. The allowable stresses were taken from Section 1.6.6 of the AASHO specifications and are equal to the following values:

$$f_{bi} = 0.6f'_{ci} = 2700 \text{ psi}$$

$$f_{ti} = 3\sqrt{f_{ci}'} = 201.2 \text{ psi}$$

$$f_{bf} = 6\sqrt{f_c'} = 424.3 \text{ psi}$$

$$f_{tf} = 0.4f_c' = 2000 \text{ psi}$$

The dead load moment was computed based on the self-weight of an interior beam since there is no wearing surface or deck. As mentioned before, the live load moments were determined for HS-20, H-20, and H-15 truck loading. The impact and wheel distribution factors for live load were computed as 1.3 and 0.458, respectively, according to AASHO Sections 1.2.12 and 1.3.1.

Magnel diagrams for Bridge 7701 were generated for the three design trucks (i.e., HS-20, H-20, and H-15); Figure 4.1 shows the diagram for the H-20. In the figure, the P1 through P4 lines represent Eqs. (4.1) through (4.4) given previously to satisfy the serviceability criteria. Recall that the P1 and P2 lines correspond to the beam stresses at transfer and are thus, not affected by the design truck (i.e., the P1 and P2 lines stay the same regardless of live load used). The area enclosed by the four lines indicates the possible combinations of the initial prestressing force (P_i) and eccentricity (e) satisfying the beams stresses at transfer and service.

Table 4.1 summarizes the high prestress / low eccentricity combination (i.e., intersection of lines P3 and P4) and low prestress / high eccentricity combination (i.e., intersection of lines P2 and P3) determined for the design trucks. In the table, the effective prestressing force (P_e) was computed as kP_i with k equal to 0.75. To determine the area of the prestressing strand (A_s), P_i was divided by the initial stress in the strand at transfer (f_{pi}) which was assumed equal to 70% of the ultimate strand stress (f_{pu}) as specified in Section 1.6.6 of the AASHO specifications. The number of strands was finally computed by dividing A_s by the area of a single 0.5-inch diameter strand (equal to 0.153 in^2).

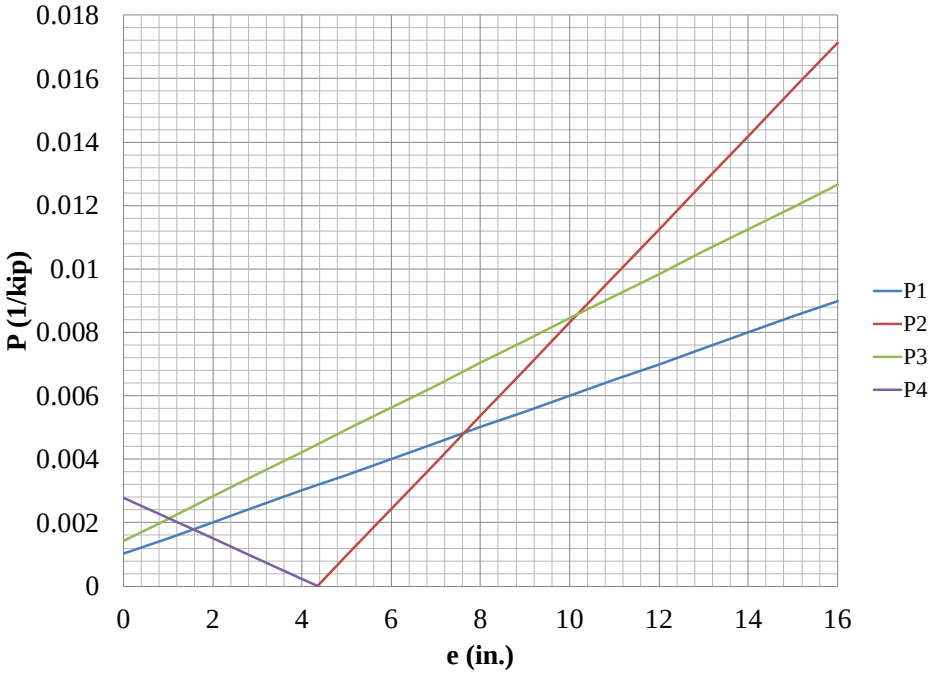

Figure 4.1. Magnel diagram for H-20 design truck (Bridge 7701).

Table 4.1. Estimate of prestressing strands for Bridge 7701.

Variable	HS-20		H-20		H-15	
	High P/T	Low P/T	High P/T	Low P/T	High P/T	Low P/T
$1/P_i$ x 10^{-3} (1/kip)	2.14	6.60	2.14	8.56	2.14	14.5
P_i (kip)	468.4	151.5	468.4	116.8	468.4	69.1
e (in.)	1.48	8.84	1.01	10.2	1.87	14.0
P_e (kip)	351.3	113.6	351.3	87.6	351.3	51.8
A_s (in^2)	2.48	0.801	2.48	0.618	2.48	0.366
No. of strands	16.2	5.24	16.2	4.04	16.2	2.39

Figure 4.2 shows the standard beam section for Bridge 7701. The centroid is located 13.28 in. from the bottom of the section. Assuming a distance of 3 in. to the center of the strand and a center-to-center strand spacing of 1 in. (based on historical information provided by the NMDOT), the eccentricities were 10.28 in. for two strands, 9.78 in. for four strands, and 9.28 in. for six strands. Note that the eccentricity of 14.0 in. for the H-15 truck loading is outside this eccentricity range meaning more steel than the equivalent of 2.39 strands will be needed. For example, at an eccentricity of 10 in., a total of four strands (i.e., greater than the 3.29 strand equivalent) would be required. Based on Table 4.1, it is evident that the geometry of the beam section is best suited for the H-20 design truck since the eccentricity of 10.2 in. agrees well with the possible strand patterns. For an eccentricity of 9.28 in., the steel equivalent increased to 4.32 strands which for practical purposes would require 6 strands. This number of strands agreed with the historical data provided by the NMDOT for off-system bridges in Doña Ana County and was also confirmed by the Ferroscan results (discussed later). The NMDOT historical data also indicated the bridge was designed for H-20 truck loading.

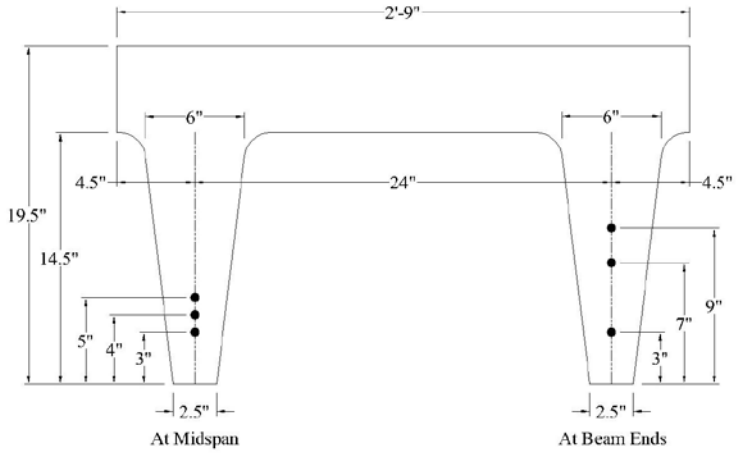

Figure 4.2. Standard beam section of Bridge 7701.

4.2 BRIDGE NO. 8761, P/C DOUBLE T-BEAM

As shown previously in Eqs. (4.1) through (4.4), the Magnel diagrams are based on the linear relationship between the inverse of the prestressing force and eccentricity. Similar to Bridge 7701, the stress limit equations for Bridge 8761 were evaluated at the top and bottom of the bridge beams at transfer and at service. Bridge 8761 was originally built in 1989 and subsequently widened in 2005. Consequently, the Magnel diagrams for the interior and exterior beams were developed based on the 13th (1983) and 17th (2002) editions, respectively, of the AASHTO Standard Specifications for Highway Bridges as discussed below.

1. Prestressing strands: the grade of prestressing strands may be determined based on the AASHTO *Manual*. Historical documentation was found for the bridge, however, that specified the grade as 270 ksi. Furthermore, the nominal strand diameter was given as 0.6 in. for the

exterior beam and 0.5 in. for the interior beam.

2. Concrete strengths at release and 28 days: according to the 13th AASHTO Standard Specification (1983), Section 9.15 states that the design of precast concrete members shall be based on a 28-day compressive strength between 5000 and 6000 psi. Subsequently, to estimate the design strength of the original bridge beams (i.e., interior beams), the concrete strength combinations shown in Table 4.2 were considered. Using the Magnel diagrams, the number of strands and cracking moments were obtained for the different combinations and the results varied very little. Thus, f_c' = 5500 psi and f_{ci}' = 4500 psi were selected which represented the average values given in Table 4.2. For the exterior beam, f_c' and f_{ci}' were taken as 6000 psi and 4500 psi, respectively, as given in the rehabilitation plans.

Table 4.2. Possible combinations of f_c' and f_{ci}' for original beam (Bridge 8761).

Variable	Magnitude (psi)		
f_c'	5000	5500	6000
f_{ci}'	4000	4000	4000
	4250	4500	4500
	4500	4750	5000
	4750	5000	5500

3. Prestress losses: for f_c' equal to 5000 psi, a prestress loss of 45,000 psi is specified in AASHTO Table 9.16.2.2 (1983) which amounts to 22% losses for 270 ksi grade prestressing strand. Similar to Bridge 7701, 20% prestress losses was conservatively assumed to estimate the number of strands in the interior and exterior beams.

4. Truck loading: the prestressing strand estimate was done for three types of AASHTO trucks. The maximum live load moments were 218.4 kip-ft, 291.2 kip-ft and 354.0 kip-ft (excluding the distribution and impact factors) for H15, H20, and HS20 loading, respectively.

5. Distribution factor: based on the field inspection, the shear keys for Bridge 8761 appear to be functioning. Thus, the wheel distribution factor for the interior beams was calculated according to Table 3.23.1 of the 13th AASHTO Standard Specification (1983) which specifies S/6 where S is the beam spacing. For S = 8 ft., the distribution factor equaled 1.333 for wheel loading or 0.667 for axle loading. For the exterior beam, the distribution factor was computed using the lever rule as specified in the 17th AASHTO Standard Specification (2002) which amounted to 0.645 for axle loading.

6. Dead load: the dead load moment was computed based on self-weight only for the interior beam of the original bridge and self-weight and the bridge railing for the exterior beam of the widened bridge.

From the Magnel diagrams, the number of strands and corresponding eccentricities for the three AASHTO trucks were estimated for Bridge 8761. Figures 4.3 and 4.4 show the Magnel diagrams for the interior and exterior beams for HS-20 truck loading and Tables 4.3 and 4.4 summarize the

results for the H-15, H-20, and HS-20 trucks. As shown in the tables, the eccentricities computed for the H-15 and H-20 trucks at the low-prestressing points exceeded the available eccentricity range of both beams, which suggests that neither the H-15 nor H-20 was the design truck. Furthermore, the historical documentation for the original bridge and the rehabilitation plans for the widened bridge both state HS-20 loading as the design truck. Based on the HS-20 truck, the strand estimate was 7.0 for the exterior beam, which would be rounded up to 8 (four strands in each stem). For the interior beam, the strand estimate was 10.1, which would be rounded up to 12 (six strands in each stem). Fewer strands were needed for the exterior beam due to the smaller distribution factor and also the larger strand diameter. Based on the estimated number of strands in each stem and assuming the strands are bundled with 2 in. cover (from the stem bottom to the center of the lowest strands), the maximum eccentricities were obtained. The maximum eccentricities for the exterior and interior beams are 18.46 in. and 18.48 in., respectively. From Tables 4.3 and 4.4, the estimated eccentricities of both beams for the HS-20 truck are less than the maximum eccentricities which was not the case for the H-15 and H-20 trucks as mentioned earlier. The Hilti Ferroscan instrument was used to further verify the strand estimates. The Ferroscan images provided reasonable proof that there are 3 unbundled strands in each stem of the exterior beam and 6 bundled strands in the interior beam stem. It is important to note that the detected number of strands in the exterior beam is less than the number estimated from the Magnel chart. Additional discussion of the Hilti Ferroscan results for Bridge 8761 is provided later in the report.

Figure 4.3. Magnel diagram for exterior beam under HS-20 design truck (Bridge 8761).

Figure 4.4. Magnel diagram for interior beam under HS-20 design truck (Bridge 8761).

Table 4.3. Estimate of prestressing strands for Bridge 8761 (exterior beam).

Variable	HS20		H20		H15	
	High P/T	Low P/T	High P/T	Low P/T	High P/T	Low P/T
$1/P_i$ x 10^{-3} (1/kip)	0.620	3.24	0.620	4.45	0.620	7.90
P_i (kip)	1613	308.6	1613	224.7	1613	126.6
e (in.)	1.43	16.8	0.935	20.4	0.366	30.6
P_e (kip)	1290	246.9	1290	179.8	1290	101.3
A_s (in^2)	7.97	1.52	7.97	1.11	7.97	0.625
No. of strands	36.7	7.00	36.7	5.10	36.7	2.90

Note: f_c' = 6000 psi, f_{ci}' = 4500 psi for exterior beam.

Table 4.4. Estimate of prestressing strands for Bridge 8761 (interior beam).

Variable	HS20		H20		H15	
	High P/T	Low P/T	High P/T	Low P/T	High P/T	Low P/T
$1/P_i$ x 10^{-3} (1/kip)	0.640	3.18	0.640	4.40	0.640	7.91
P_i (kip)	1563	314.5	1563	227.3	1563	126.4
e (in.)	1.58	16.4	1.05	20.0	0.440	30.1
P_e (kip)	1250	251.6	1250	181.8	1250	101.1
A_s (in^2)	7.72	1.55	7.72	1.12	7.72	0.624
No. of strands	50.4	10.1	50.4	7.30	50.4	4.10

Note: f_c' = 5500 psi, f_{ci}' = 4500 psi for interior beam.

4.3 BRIDGE NO. 7722, P/C BOX GIRDER

Bridge 7722 was built in 1966 and consequently, the provisions of the AASHO 8th Edition (1961) were used to estimate the number of prestressing strands and concrete compressive strength. Magnel diagrams (which are based on the linear relationships between the stresses at the extreme fibers *f*, the eccentricity *e*, prestressing force *P*, and the bending moment *M*) were used to capture the "safe zone" or the range of valid combinations of *e* and *P*. The basic equation for a non-composite section is shown below:

$$f = \frac{P}{A} \mp \frac{Pec}{I} \pm \frac{Mc}{I} \leq f_{allowable} \qquad \text{(Eq. 4.9)}$$

where *A*, *I* , and c are the area, moment of inertia, and centroid of the cross-section, respectively.

According to the 1961 AASHO Standard Specifications, the design of prestressed concrete members must conform to the requirements of Section 13 of Division 1 (PRESTRESSED CONCRETE). Accordingly, AASHO Section 1.13.18 states the following: "Unless otherwise specified, stress shall not be transferred from strand to concrete in pretensioned members until the compressive strength of the concrete as indicated by test cylinders cured by methods identical with the curing of the members is at least 4,000 psi". Hence, the concrete strength at release was taken as f_{ci}' = 4000 psi and the 28-day concrete strength was taken to be 500 psi higher than the release strength, f_c' = 4500 psi.

The AASHTO *Manual* was used to determine the strength of the prestressing strands. Section 6A.5.2.3 of the manual states that when the tensile strength of the prestressing strand is unknown, f_{pu} may be taken as 232 ksi for bridges constructed prior to 1963 and 250 ksi for those constructed in 1963 and later. Thus, based on the construction year (i.e., 1966), a tensile strength of f_{pu} = 250 ksi was assumed. Furthermore, the initial prestressing stress, f_{pi}, was assumed to be seventy percent of the ultimate tensile strength, f_{pi} = 175 ksi, and total losses were assumed to be twenty percent resulting in an effective prestress of f_{pe} = 140 ksi. Section 1.13.8 (B) of the 1961 AASHO Standard Specifications states that prestress losses due to all causes except friction may be taken as 35 ksi for pre-tensioned members and 25 ksi for post-tensioned members. Note that 35 ksi agrees with the assumption of 20% prestress loss discussed earlier. In the end, the prestressing steel was assumed to be Grade 250, seven-wire, low-relaxation strands with diameters of 0.375 in. and 0.4375 in. for the interior and exterior beams, respectively.

Allowable stresses were taken from AASHO Section 1.13.7 and are equal to the following values:

$$f_{bi} = 0.6f'_{ci} = 2400 \text{ psi}$$

$$f_{ti} = 3\sqrt{f_{ci}'} = 189.7 \text{ psi}$$

$$f_{bf} = 0 \text{ psi}$$

$$f_{tf} = 0.4f_c' = 1800 \text{ psi}$$

AASHO Section 1.2.12 requires that live load stresses produced by H or HS loadings be increased for superstructures, to account for dynamic, vibratory and impact effects. The dynamic impact allowance, *IM*, is given as:

$$IM = \frac{50}{L+125} \qquad \text{(Eq. 4.10)}$$

where L = length in feet of the portion of the span that is loaded to produce the maximum stress in the member. Bridge 7722 has a 44.5 ft span resulting in an impact factor of 0.295. According to AASHO Section 3-DISTRIBUTION OF LOADS, Subsection 1.3.1 (B) specifies the lateral distribution factor for interior concrete box girders as $S/8$ and $S/7$ in bridges designed for one traffic lane and two or more traffic lanes, respectively, where S is the average girder spacing in feet. For an exterior box girder, the distribution factor is $w_e/8$ where w_e is the girder width in feet.

Bridge 7722 consists of seven adjacent PCI-AASHTO BI-36 beams with a width (W) of 36 in. and height (H) of 27 in. as shown in Figure 4.5. The distribution factors are 0.375 and 0.429 for one traffic lane and two or more traffic lanes, respectively. Reconstruction marks on the abutments and wing walls, and longitudinal gaps between the exterior and interior beams provided evidence that the bridge roadway was widened by adding two exterior beams. Consequently, the distribution factors for the interior and exterior beams assumed that the bridge was only one lane wide for the original construction and two lanes after widening. Hence, the distribution factors were taken as 0.375 for the interior beam and 0.429 for the exterior beam to estimate the prestressing strand.

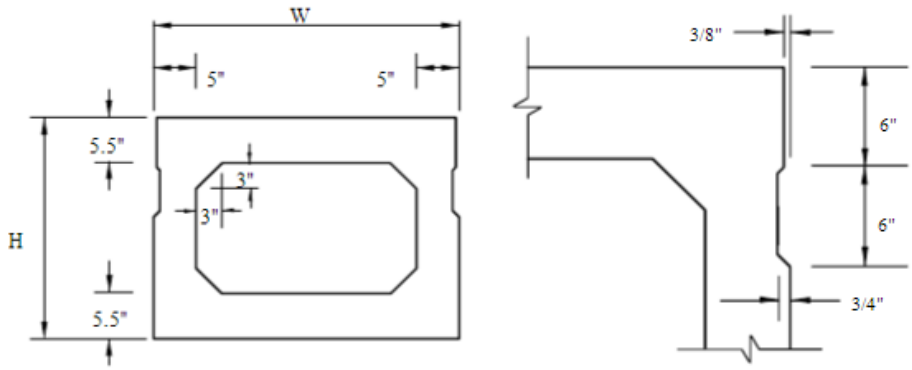

Figure 4.5. Standard AASHTO Type BI-36 box beam of Bridge 7722.

The amount of prestressing steel in the box beams of Bridge 7722 was estimated using Magnel diagrams. The diagrams were formulated based on the serviceability criteria (i.e., allowable stresses) for compression and tension at transfer and service at the beam midspan using Eqs. (4.1) through (4.4) given earlier. The dead load moment was computed based on the self-weight of a standard AASHTO BI-36 box beam and a 4.0-in. thick asphalt wearing surface. An additional dead load of 100 lb/ft was applied to the exterior beam to account for the weight of the utility pipeline and guardrail. The live load moments were determined for HS-20, H-20, and H-15 truck loadings. Table 4.5 summarizes the dead load and live load moments used to develop the Magnel diagrams for Bridge 7722. Higher moments were obtained for the exterior beam due to the larger amount of dead load and the larger distribution factor for live load.

Table 4.5. Dead load and live load beam moments for Bridge 7722.

Variable	Magnitude (kip-ft)	
	Interior beam	Exterior beam
Dead load moment	170.6	195.3
HS20 truck moment	129.6	147.2
H20 truck moment	94.9	108.6
H15 truck moment	71.2	81.5

Figures 4.6 and 4.7 show the Magnel diagrams for an exterior and interior beam, respectively, of Bridge 7722 under H-20 loading. As for the other bridges, the Magnel diagram analysis for Bridge 7722 was done to determine feasible solutions for the reciprocal of the initial prestressing force and eccentricity. Four inequalities were formulated based on the code requirements for the mid-span top and bottom stresses under initial and service load conditions, and then plotted to determine the region of valid solutions. This region of valid solutions is defined by the four intersection points of the inequality equations. Due to the geometry of the box beams, only two of these intersection points were found, contrary to the four points customary for other types of cross sections. Although the amount of prestressing force may be computed from these two points, the estimated force and the amount of steel corresponds to the highest level of prestressing and thus, will be unconservative. It was decided to vertically project the two points onto line P3 to obtain the smallest prestressing force which translates to a conservative estimate of the number of strands. Lines PP1 and PP2 shown in Figures 4.6 and 4.7 are the lines of projection. The high and low initial prestressing forces were then computed from the P3 expression at the points of intersection with lines PP1 and PP2, and further used to determine the effective prestress force P_e, area of steel A_s, and the number of strands.

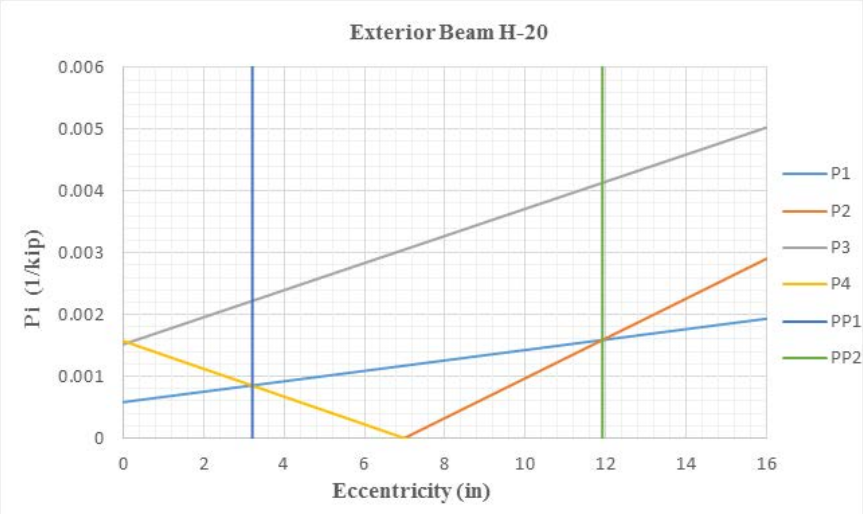

Figure 4.6. Magnel diagram for exterior beam under H-20 design truck (Bridge 7722).

Figure 4.7. Magnel diagram for interior beam under H-20 design truck (Bridge 7722).

Tables 4.6 and 4.7 summarize the Magnel diagram results for all three design trucks. The maximum eccentricity (assuming 2 in. of cover to the center of the strand) is 11.6 in. and the strand areas are 0.080 in^2 and 0.108 in^2 for 0.375 in. and 0.4375 in. diameters, respectively. From the tables, the prestressing steel was finally based on H-20 truck loading amounting to 14 strands for the exterior beam and 16 strands for the interior beam. Less strands were required for the exterior beam due to the larger strand diameter in spite of the larger moments under dead and live load.

Table 4.6. Estimate of prestressing strands for Bridge 7722 (exterior beam).

Variable	HS20		H20		H15	
	High P/T	Low P/T	High P/T	Low P/T	High P/T	Low P/T
$1/P_i$ x 10^{-4} (1/kip)	20.4	36.7	22.2	41.3	26.0	50.9
P_i (kip)	489.5	272.6	449.8	241.9	384.9	196.4
e (in.)	3.60	11.9	3.20	11.9	2.70	11.9
P_e (kip)	391.6	218.0	359.9	193.5	307.9	157.1
A_s (in^2)	2.80	1.56	2.60	1.38	2.20	1.12
No. of strands	25.9	14.4	23.8	12.8	20.4	10.4

Table 4.7. Estimate of prestressing strands for Bridge 7722 (interior beam).

Variable	HS20		H20		H15	
	High P/T	Low P/T	High P/T	Low P/T	High P/T	Low P/T
$1/P_i$ x 10^{-4} (1/kip)	22.3	41.0	24.4	46.1	26.2	50.7
P_i (kip)	448.4	244.2	410.5	216.7	381.8	197.4
e (in.)	3.10	11.5	2.80	11.5	2.60	11.5
P_e (kip)	358.7	195.4	328.4	173.4	305.5	157.9
A_s (in^2)	2.60	1.40	2.35	1.24	2.20	1.13
No. of strands	32.0	17.4	29.3	15.5	27.3	14.1

4.4 BRIDGE NO. 8825, P/C BOX GIRDER

Similar to the other bridges, the AASHTO *Manual* was used to determine the material properties of the concrete and the prestressing strands of Bridge 8825. Since the bridge was constructed in 1990, the 14th Edition of the AASHTO Standard Specifications (AASHTO 1989) was also used. For bridges constructed in 1963 and later, the ultimate tensile strength of the prestressing strand, f_{pu}, is specified as 250 ksi in the AASHTO *Manual*. The initial prestressing stress, f_{pi}, was assumed to be 70% of f_{pu} (f_{pi} = 175 ksi) and total losses were assumed to be 20% of f_{pi} (i.e., f_{pe} = 140 ksi). Note that Section 9.16.2.2 and Table 9.16.2.2 of AASHTO (1989) specify prestress losses equal to 45 ksi for pre-tensioned members which is slightly higher than the assumption of 20%. The prestress losses were initially taken as 20% to estimate the number of prestressing strands and then as 25% to calculate the cracking moment (discussed later). The prestressing steel was finally assumed to be Grade 250, seven-wire, low-relaxation strands with 0.5-in. diameter for both the interior and exterior beams.

The concrete strengths at release and 28 days were based off the 1989 AASHTO Standard Specifications. According to Sections 9.15 and 9.22 of these specifications, the minimum concrete strengths for prestressed concrete members are 5000 psi at 28 days and 4000 psi at release. Thus, the concrete strengths were assumed to be f_c' = 5000 psi and f_{ci}' = 4500 psi. From AASHTO Section 9.15.2, the allowable stresses equaled the following magnitudes: $f_{bi} = 0.6f_{ci}' = 2700$ psi; $f_{ti} = 3\sqrt{f_{ci}'} = 201.2$ psi; $f_{bf} = 6\sqrt{f_c'} = 424.3$ psi; and $f_{tf} = 0.4f_c' = 2000$ psi. From AASHTO (1989), the impact factor was computed as 0.30 for a span length of 42 ft. The lateral distribution factors for interior concrete box girders are specified as S/8 and S/7 for one traffic lane and two or more traffic lanes, respectively, where S is the average girder spacing in feet. Recall that Bridge 8825 consists of ten adjacent standard Type 5B20 beams with a width (W) of 60 in. and height (H) of 20 in. as shown in Figure 4.8.

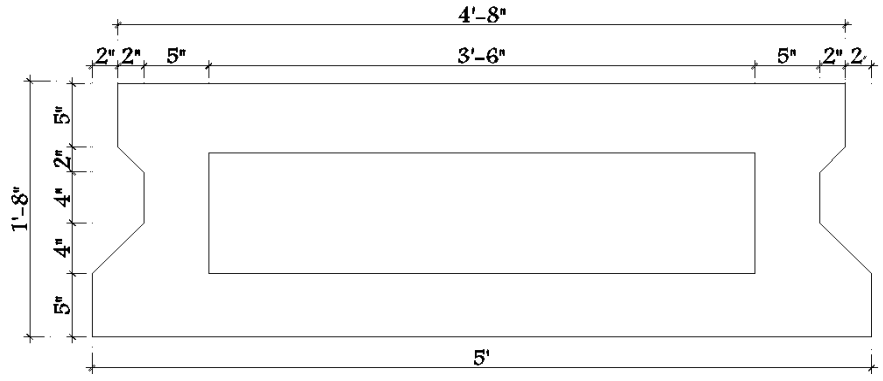

Figure 4.8. Standard Type 5B20 box beam of Bridge 8825.

Accordingly, the interior girder distribution factors were 0.625 and 0.714 for one traffic lane and two or more traffic lanes, respectively. For an exterior concrete box girder, the distribution factor is $w_e/8$ where w_e is the width of the exterior girder in feet which amounted to 0.625. Thus, the multiple lanes distribution factor for an interior girder controlled and was used to compute the live-load moments of 225.1 kip-ft, 169.4 kip-ft, and 127.3 kip-ft for HS-20, H-20, and H-15 truck loading, respectively. The dead load moment equaled 238.8 kip-ft and was computed based on the self-weight of a standard Type 5B20 box beam (0.748 kip/ft.), a 3.0-in. thick asphalt wearing surface, 6-ft. wide and 10-in. thick pedestrian sidewalks, and steel guard rails. The loads of the sidewalks and guard rails were evenly distributed among all beams.

Figure 4.9 shows the Magnel diagram for an exterior and interior beam of Bridge 8825 under HS-20 loading. Similar to Bridge 7722, only two of the intersection points were found, contrary to the four points customary for other types of cross sections. The high and low initial prestressing forces were computed from the P3 expression at the points of intersection with lines PP1 and PP2, and then used to determine the effective prestress force (P_e), area of steel (A_s), and the number of strands. Table 4.8 summarizes the Magnel diagram results for all three design trucks. Note that the maximum eccentricity (assuming 2 in. of cover to the center of the strand) is 8.8 in. and the strand area is 0.144 in^2. The amount of prestressing steel was finally selected based on HS-20 truck loading which amounted to 16 strands for both the exterior and interior beams.

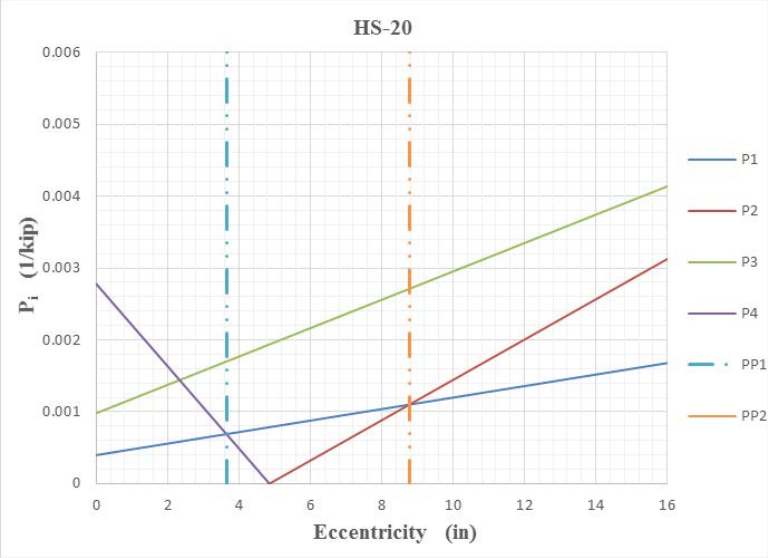

Figure 4.9. Magnel diagram for interior and exterior beams under HS-20 design truck (Bridge 8825).

Table 4.8. Estimate of prestressing strands for Bridge 8825 (interior and exterior beams).

Variable	HS20		H20		H15	
	High P/T	Low P/T	High P/T	Low P/T	High P/T	Low P/T
$1/P_i$ x 10^{-4} (1/kip)	16.5	25.8	18.6	31.0	21.0	36.7
P_i (kip)	607.2	387.9	537.3	322.4	475.5	272.9
e (in.)	3.60	8.80	3.20	8.80	2.80	8.80
P_e (kip)	485.7	310.3	429.9	257.9	380.4	218.3
A_s (in^2)	3.50	2.20	3.10	1.80	2.70	1.60
No. of strands	24.1	15.4	21.3	12.8	18.9	10.8

4.5 BRIDGE NO. 8588, P/C I-GIRDER

Since Bridge 8588 was constructed in 1973, the 10th Edition of the AASHO Standard Specifications for Highway Bridges (1969) was used, which would have been the most current specification at the time of construction. The concrete strength at release (*fci'*) was assumed to be 4500 psi, which is slightly larger than the minimum of 4000 psi given in Section 1.6.18 of the AASHO specifications for pretensioned members. The concrete strength at 28 days (*fc'*) was assumed to be 5000 psi in accordance with Section 1.6.7 of the AASHO specifications and Section 506 of the NMSHD Standard Specifications for Road and Bridge Construction (1970). The prestressing steel was assumed to be 0.5-inch diameter, Grade 270, seven-wire, stress-relieved strands. The value for *k*, the amount of prestress loss, was estimated using the AASHO specifications (Section 1.6.8B) to be 35000 psi, which amounts to 18.5%. The allowable stresses were taken from Section 1.6.7 of the AASHO specifications and are equal to the following values:

$$f_{bi} = 0.6f'_{ci} = 2700 \text{ psi}$$

$$f_{ti} = 3\sqrt{f_{ci}'} = 201.2 \text{ psi}$$

$$f_{bf} = 3\sqrt{f_c'} = 212.1 \text{ psi}$$

$$f_{tf} = 0.4f_c' = 2000 \text{ psi}$$

The live load moments were determined for HS-20, H-20, and H-15 truck loading. The impact and wheel distribution factors for live load were computed as 1.25 and 1.18, respectively, according to Sections 1.2.12 and 1.3.1 of the AASHO specifications.

A typical interior girder of Bridge 8588 was first evaluated by Magnel diagrams assuming full non-composite behavior. Figure 4.10 shows the diagram for the HS-20 design truck load. Based on the inequalities, the area greater than (i.e., above) the P1 line and less than (i.e., below) the P3 line do not overlap and thus, there is no design region that satisfies the top and bottom girder stresses at transfer and service. This suggests that Bridge 8588 was designed based on composite behavior; Figure 4.11 shows the Magnel diagram for this case. As shown in the figure, the consideration of composite action results in a design region of feasible prestress/eccentricity combinations that will satisfy the girder stresses at transfer and service.

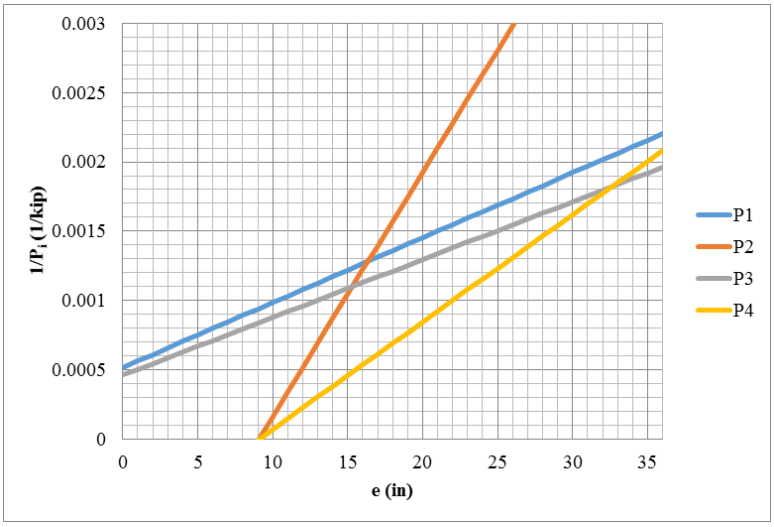

Figure 4.10. Magnel diagram for interior girder under HS-20 design truck assuming full non-composite behavior (Bridge 8588).

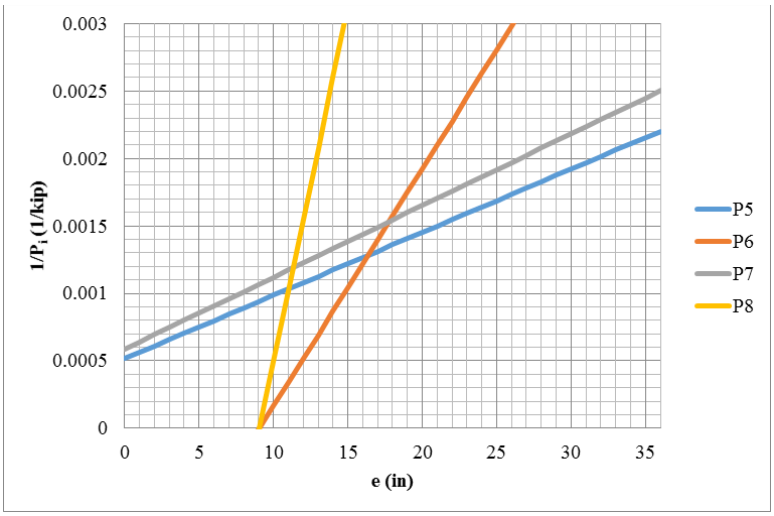

Figure 4.11. Magnel diagram for interior girder under HS-20 design truck assuming composite behavior (Bridge 8588).

Table 4.9 summarizes the high prestress / low eccentricity combination (i.e., intersection of lines P7 and P8) and low prestress / high eccentricity combination (i.e., intersection of lines P6 and P7) determined for the three design trucks. In the table, the effective prestressing force (P_e) was computed as kPi with k equal to 0.815. To determine the area of the prestressing strand (A_s), P_i was divided by the initial stress in the strand at transfer (f_{pi}) which was assumed equal to 70% of the ultimate strand stress (f_{pu}) as specified in Section 1.6.7A of the AASHO specifications. The number of strands was finally computed by dividing A_s by the area of a single 0.5-inch diameter strand (equal to 0.153 in^2).

Table 4.9. Estimate of prestressing strands for Bridge 8588 (interior girder).

Variable	HS20		H20		H15	
	High P/T	Low P/T	High P/T	Low P/T	High P/T	Low P/T
$1/P_i$ x 10^{-4} (1/kip)	10.3	15.7	9.95	18.3	9.78	19.7
P_i (kip)	969.0	635.3	1005	545.9	1023	507.6
e (in.)	11.0	18.0	10.2	18.3	9.84	18.3
P_e (kip)	789.5	517.7	818.9	444.8	833.1	413.6
A_s (in^2)	5.13	3.36	5.32	2.89	5.41	2.69
No. of strands	33.5	22.0	34.8	18.9	35.4	17.6

Figure 4.12 shows the standard beam section for Bridge 8588, an AASHTO Type III I-girder. The centroid of the non-composite section is located 20.3 in. from the bottom of the section. Therefore, assuming a 2-in. cover to the center of the strand, the maximum eccentricity possible is 18.3 inches. Note that for the H-20 and H-15 design trucks, the low prestress / high eccentricity point is controlled by this limit. Assuming a center-to-center strand spacing of 2 inches (based on the typical strand configurations for AASHTO I-girders), actual strand patterns were obtained to verify

the strand estimate. Based on Table 4.9, it appears that the geometry of the beam section is best suited for the HS-20 design truck since the smaller eccentricity of 18 inches agrees well with the possible strand patterns. In addition, it is likely that an HS-20 design truck was used for Bridge 8588 due to the span length (i.e., 73 ft. clear span). The actual eccentricity for 22 strands was calculated to be 17 inches. For this eccentricity, the steel equivalent increased to 22.8 strands which for practical purposes would require 24 strands. For 24 strands, the actual eccentricity amounted to 16.8 in., which slightly increased the steel equivalent to 23.0 strands which showed convergence and indicated that 24 strands was a probable design.

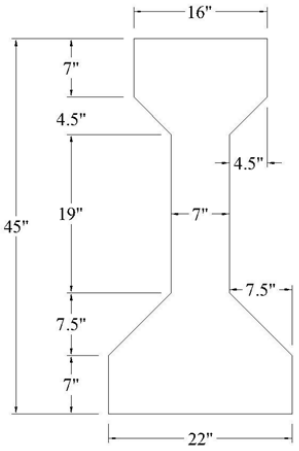

Figure 4.12. Standard AASHTO Type III I-girder of Bridge 8588.

5. DETECTION OF STEEL REINFORCEMENT

The Hilti PS 250 Ferroscan system was used to scan the location, size, and cover of the steel reinforcement (i.e., longitudinal strands and transverse bars) in the prestressed concrete beams of Bridges 7701, 8761, 7722, and 8825, and the longitudinal bars in the reinforced concrete slab of Bridge 8676. The Ferroscan has certain limitations that must be considered. First, the scanner is generally capable of providing accurate results only for the first layer of reinforcement and a minimum ratio of 2:1 is required for the center-to-center rebar spacing to concrete cover (from the concrete to steel surface). Second, the accuracy of the rebar size estimate is ±1 standard bar diameter and the reinforcement must be no deeper than 2.4 inches from the concrete surface. The steel depth must also be greater than 0.4 inches to obtain an accurate depth measurement. Third, the Ferroscan is most accurate for detecting steel reinforcing bars that meet the ASTM A615 / A615M-01b Standard Specification for Deformed and Plain Carbon-Steel Bars for Concrete Reinforcement. For prestressed concrete bridges, the imagescans of the prestressing strand are not as accurate due to the seven-wire strand arrangement. However, the Ferroscan gives good results of the shear reinforcement which are typically deformed or plain bars.

The Ferroscan system generates imagescans of a 2 ft. by 2 ft. area through use of a reference grid (see Figure 5.1) that is placed at the area of interest. The imagescans can be connected to produce blockscans of a larger area. For example, a blockscan of a 6 ft. by 6 ft. area can be obtained using a series of nine imagescans on a 3 by 3 grid. In this project, the blockscan application was used to connect the imagescans along the length of the double T-beam and box beam bridges. The blockscan feature was also used to connect imagescans of the reinforced concrete slab bridge. For ease of scanning, the 2 ft. by 2 ft. reference grid was adhered on a polypropylene, or plastic cardboard, backing. The backing is particularly useful for scanning beams with shallow depths since the backing provides a smooth surface for the scanner past the bottom of the beam. In addition, the reference grid can be more easily handled and consistently placed in the field.

Figure 5.1. 2 ft. x 2 ft. reference grid used for Hilti PS 250 Ferroscan.

5.1 BRIDGE NO. 7701, P/C DOUBLE T-BEAM

Bridge 7701 is a simple-span bridge with nine double T-beams. The Hilti PS 250 Ferroscan system was used to generate blockscans of the north exterior beam and the center beam (i.e., beams 1 and

5). Several other 2 ft. by 2 ft. areas on the remaining seven beams were also scanned to spot check the blockscans of beams 1 and 5. Furthermore, the blockscans were compared with the steel reinforcement layout found in historical documents provided by the NMDOT. Overall, the Ferroscan results agreed reasonably well with the historical data found for Bridge 7701. Beam 1 of the bridge was scanned starting at the east abutment and ending at the west abutment. Figure 5.2 shows the east half of the beam. As shown in the figure, the vertical shear reinforcement of beam 1 is unevenly spaced and looks to have been haphazardly placed. The rebar size estimate ranged from a #7 to a #3 diameter. After further review, it was found that the larger estimates of the vertical bar sizes occurred in areas where the vertical bars overlapped with a prestressing strand or the bar spacing was small. Overall, the imagescans gave an average cover of 1.18 in. for the vertical bars and a predominant bar size of #3 diameter. The most consistent results were obtained at locations where the 2:1 spacing-to-cover ratio requirement was met along the beam length.

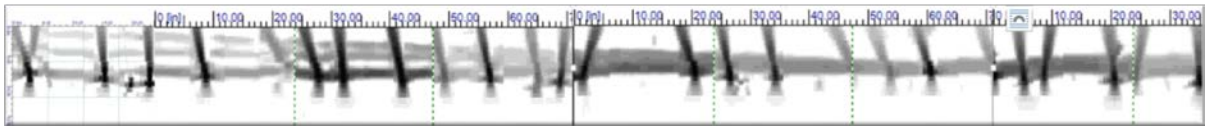

Figure 5.2. Blockscan of north exterior beam from east abutment to center line (Bridge 7701).

The blockscan of beam 1 also showed three longitudinal strands running along the beam length that are harped at approximately 0.4L. In the middle 20% of the beam length, the prestressing strands are tightly spaced which complicates the size estimate (aside from the fact that the strands are not standard rebars). Due to the seven-wire strand arrangement, the bar size estimate ranged from a #11 to a #3 diameter. As to the spacing, the historic drawing provided by the NMDOT and given in Figure 5.3 shows a 2 in. and 4 in. strand spacing near the abutments and a 1 in. spacing at the center of the beam which agreed with the blockscan shown above in Figure 5.2.

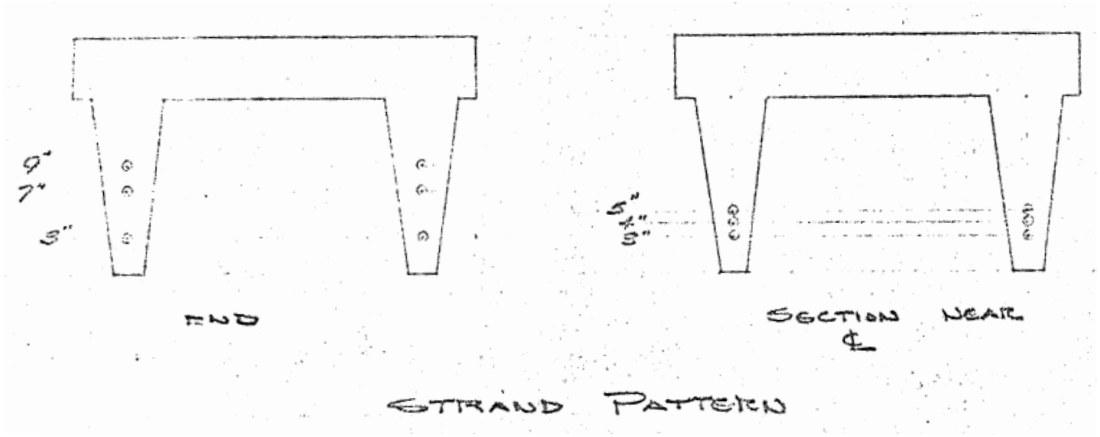

Figure 5.3. Historical beam drawing of Bridge 7701.

The interior beams of Bridge 7701 have the same geometry as the exterior beams and there was no indication that the bridge had been widened in the past. Based on the imagescans for the north exterior beam, however, there was a concern that the vertical shear reinforcement of the remaining beams was also placed inconsistently. The imagescans of the remaining beams showed that only

the north exterior beam had the misplaced vertical reinforcement. Figure 5.4 and Figure 5.5 given below show the Ferroscan images for different beams and locations to illustrate the similarities of the steel reinforcement layout. Note that the ends of the interior beams were not scanned due to the difficulties caused by the shallow beam depth and the abutment seats. Consequently, the vertical shear reinforcement is unknown in the end areas and was assumed to be similar to the configuration found away from the abutments.

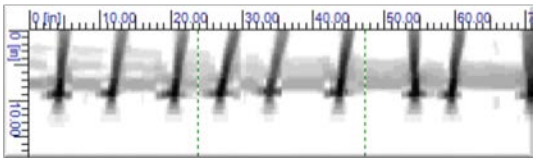

Figure 5.4. Blockscan of south exterior beam near harp point (Bridge 7701).

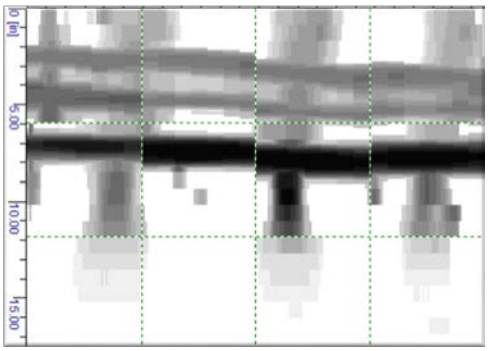

(a)

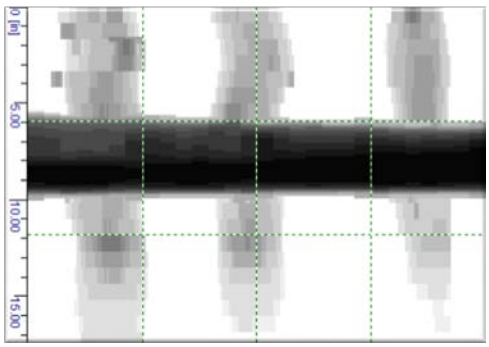

(b)

Figure 5.5. Imagescans in (a) harped and (b) non-harped areas of interior beam (Bridge 7701).

5.2 BRIDGE NO. 8761, P/C DOUBLE T-BEAM

Similar to Bridge 7701, the Hilti PS 250 Ferroscan system was used to detect the location, size, and cover of the steel reinforcement (including the prestressing strands and mild reinforcing bars) in the beams of Bridge 8761. Blockscans were generated for the south exterior beam (widening), south interior beam (original construction), center interior beam (original construction), and north

exterior beam (widening). Recall that the bridge was originally built in 1989 with three beams and later widened in 2005 with two additional beams. The rehabilitation plans for the 2005 bridge widening and the design calculations for the original 1989 bridge construction were provided by the NMDOT. The south exterior beam was scanned starting from the east abutment and ending at the west abutment. Figure 5.6 shows the elevation view of the beam given in the rehabilitation plans and Figure 5.7 shows the blockscan produced by the Ferroscan.

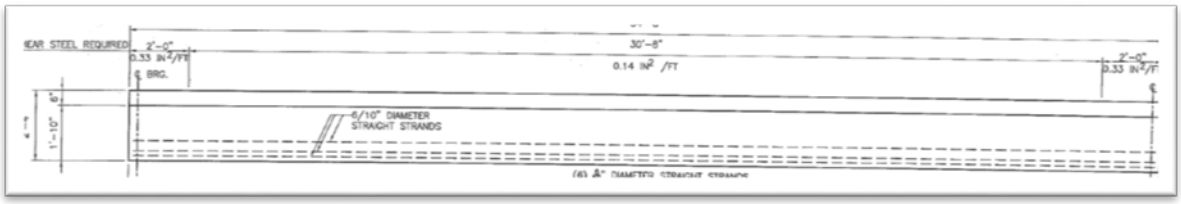

Figure 5.6. Elevation view of exterior beam of Bridge 8761 from rehabilitation plans.

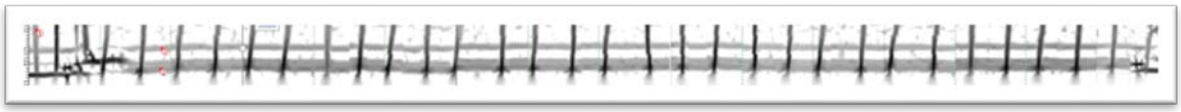

Figure 5.7. Blockscan of south exterior beam from east to west abutment (Bridge 8761).

The blockscan detected what appeared to be two longitudinal bars (one small diameter and one large diameter) and a series of vertical bars spaced approximately 12 in. on center as shown in Figure 5.7. The rehabilitation plans specify a 4 in. and 2 in. spacing between the three strands from top to bottom (see Figure 5.6). For a 0.6-in. diameter strand and a 2-in. strand spacing, the clear distance between strands is about 1.4 in. which is the minimum required for the Hilti Ferroscan. Between the top and center strands, the clear distance is approximately 3.4 in. which exceeds the Ferroscan minimum. For the top strand, the Ferroscan results gave a bar size ranging between #3 and #5. Note that the cross-sectional area of a 0.6-in. diameter strand is 0.217 in^2 which equates to a 0.530-in. diameter solid bar (i.e., a #4 bar) which is the average of the Ferroscan results. Due to the small spacing, the middle and bottom strands were more difficult to distinguish with the Ferroscan but the two strands could still be reasonably identified.

The Ferroscan results consistently gave a #3 bar size for the vertical steel. In addition, the average cover of the vertical steel was approximately 2.2 in. resulting in a 5:1 spacing-to-cover ratio, which exceeds the minimum 2:1 ratio required for accurate results. To determine the number of stirrup legs in each beam stem, blockscans were taken on the inside and outside faces of a single stem. Figures 5.8 and 5.9 show the blockscans of the north exterior beam near the east abutment taken on both faces of the stem and also viewed at different depth ranges (5 in. and 2 in.) through the concrete. In general, the Hilti Ferroscan is valid for the first layer of reinforcement and multiple layers can cause disturbances in the magnetic field. However, different reinforcement layers can be reasonably separated using the depth range feature of the Ferroscan software. This feature displays the Ferroscan results at different concrete depths and therefore identifies the reinforcement that is closest to the concrete surface. Figures 5.8 and 5.9 show that the vertical bars have the smallest cover on both sides of the stem which is a clear indication that the stirrup

has two legs and thus, the double T-beam is reinforced with a two-legged stirrup in each stem. The rehabilitation plans specified the required shear steel to be 0.33 in^2/ft for a distance of 2 ft. from the beam ends and 0.14 in^2/ft for the remaining 30.67 ft. of the beam length. As mentioned previously, the Ferroscan detected #3 vertical bars spaced at 12 in. which amounts to a shear steel area of 0.11 in^2/ft * 4 = 0.44 in^2/ft which exceeds the specified area of 0.33 in^2/ft.

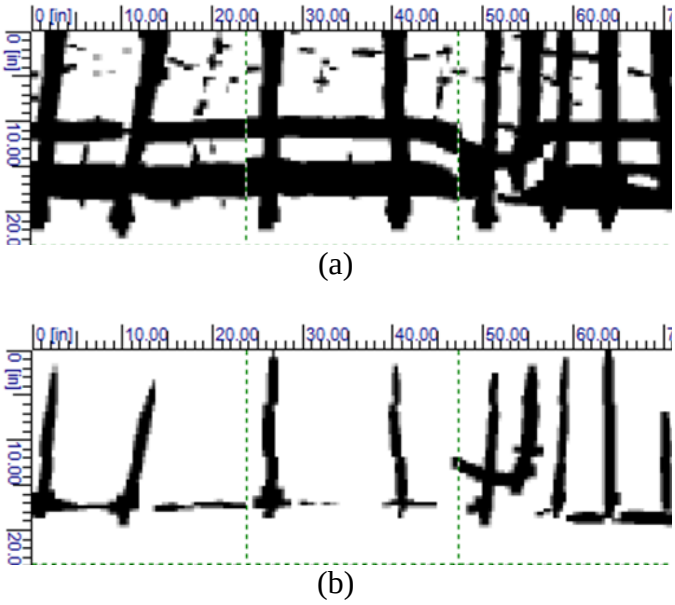

(a)

(b)

Figure 5.8. Blockscans on inside face of north exterior beam stem of Bridge 8761 at depth ranges of (a) 5 inches and (b) 2 inches.

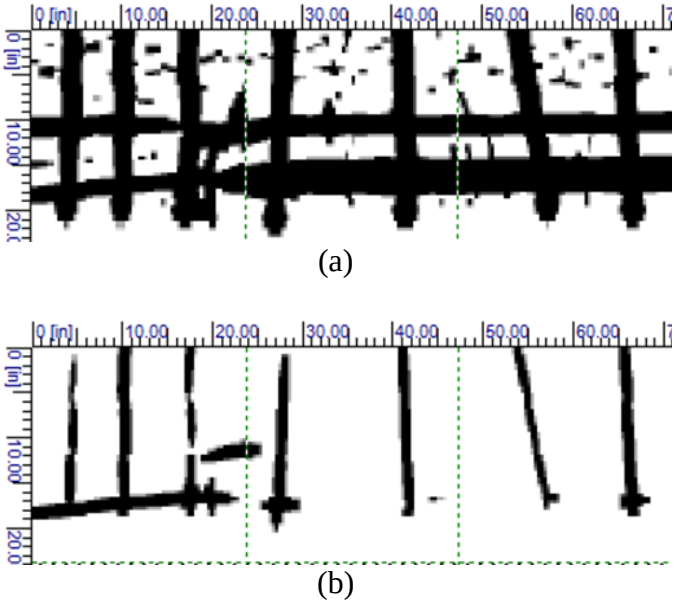

(a)

(b)

Figure 5.9. Blockscans on outside face of north exterior beam stem of Bridge 8761 at depth ranges of (a) 5 inches and (b) 2 inches.

As mentioned previously, the south interior beam and the center beam of the original bridge were scanned with the Hilti Ferroscan. The beams were scanned their full length from the east to west abutment and both beams showed similar results. Figure 5.10 shows the blockscan of half the south interior beam. As shown in the figure, the steel reinforcement appears as a clear grid pattern near the beam ends and a hazy grid further away. The original 1989 design calculations denoted two layers of 8x4x8/4 welded wire fabric as the shear reinforcement over a distance of 10 ft. from the beam ends and a single layer for the remainder of the beam which generally agrees with the steel layout obtained from the Ferroscan (but the bar size estimate was inconclusive). At the end of the wire mesh, the prestressing strands appear in the blockscan which according to the 1989 calculations are bundled with 0.5-in. spacing and harped at 40% of the beam length. Since the strands are bundled, there is no clear distance between the strands and thus, the Ferroscan could not provide an accurate estimate of the size and number of strands. Based on the blockscans obtained for the original beams of Bridge 8761, it is concluded that the Ferroscan provides less meaningful results in cases where the shear reinforcement consists of welded wire fabric or the prestressing strands are bundled.

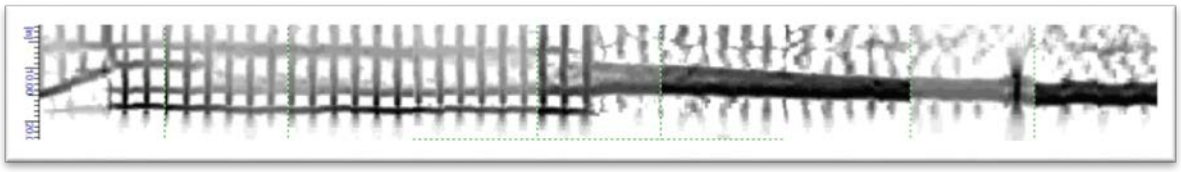

Figure 5.10. Blockscan of south interior beam from east abutment to center line (Bridge 8761).

5.3 BRIDGE NO. 7722, P/C BOX GIRDER

The Hilti PS 250 Ferroscan system was employed to determine the size, spacing, and locations of the steel reinforcement in the box beams of Bridge 7722. A standard AASHTO BI-36 box beam is shown in Figure 5.11 along with the available prestressing strand positions. The figure shows two available rows of prestressing strands in the bottom flange that may accommodate up to 34 strands placed at 2-in. center-to-center spacing. Additional strands may be placed vertically in the two webs and/or horizontally in the top flange particularly for controlling end stresses at release.

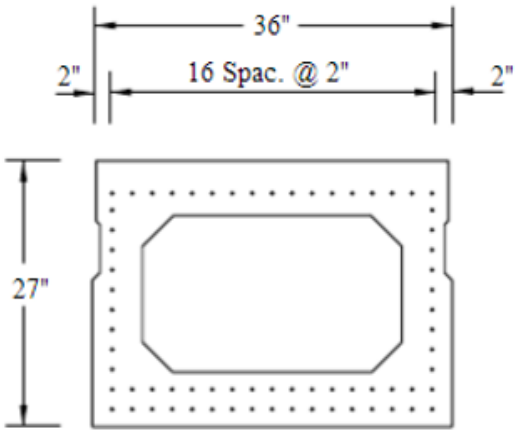

Figure 5.11. Prestressing strand layout for standard AASHTO Type BI-36 box beam.

The Hilti PS 250 gives the best results for the first layer of reinforcement and additional layers are difficult to interpret. Due to the close strand spacing and possibility of multiple strand layers, the scans obtained for Bridge 7722 were quite difficult to understand. Figure 5.12 shows an imagescan taken on the bottom side of an exterior beam. As shown in the figure, there are various shades of gray and strip widths in the imagescan due to different cover depths and spacings for the prestressing strands and mild reinforcement. The horizontal strips represent the prestressing strands while the vertical strips represent the shear reinforcement. In general, the darker gray regions in the magnetic field may be caused by multiple reinforcement layers, close strand spacing, and/or small cover depth. The Hilti PS 200 software provides some useful features for discerning the steel configuration. For instance, the depth range feature of the software may be used to analyze the larger bar scans and determine if the strands are in a single or multiple rows. However, the strand size and location may be inaccurate due to the interfering magnetic fields. An accurate depth measurement is also difficult to obtain and thus, the clarification of whether the bars lie parallel to each other or at different depths is uncertain. In summary, due to the magnetic interference caused by multiple strand layers and/or closely spaced strands, the Hilti PS 250 Ferroscan may have some difficulty in authenticating the steel configuration in the box beams of Bridge 7722. The locations may not be detected accurately since the center of a single gray bar in an imagescan does not necessarily signify the center of the reinforcement because the stands may be in multiple layers and/or closely spaced. The sizes and depths may also be inaccurate because the strand spacing is less than the required 1.4 inches.

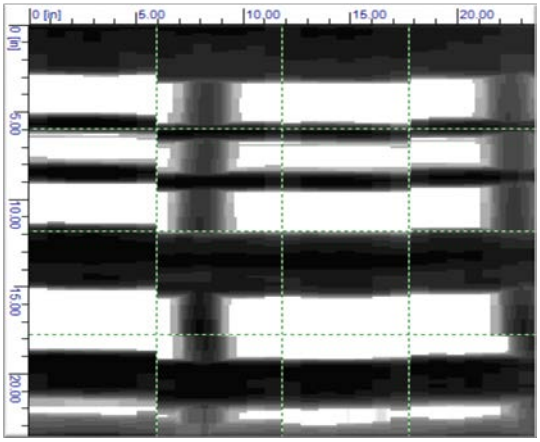

Figure 5.12. Imagescan on bottom side of exterior beam (Bridge 7722).

Several imagescans were taken at various locations on the bottom sides of the exterior and interior beams. Figure 5.13 shows a pair of imagescans (i.e., blockscan) between two interior beams displayed at different depth ranges. As shown in Figure 5.13(a), there are numerous wide, dark strips in the vertical direction representing the longitudinal prestressing strands. What is not clear is whether the strips represent closely spaced strands or multiple layers of strands, or both. Using the depth range feature in the Hilti PS 200 software, the imagescans were analyzed. This software option allows the user to pan in and out through the depth of the beam flange. Subsequently, the thin gray lines in the images begin to blur and disappear from view at shallower depths which is a clear indication that those strands are in the first layer and there are no multiple layers of strands

at those locations (see Figure 5.13(b)). On the other hand, the thick gray lines begin to separate into two or more bars, thus confirming the presence of multiple strands in more than one layer.

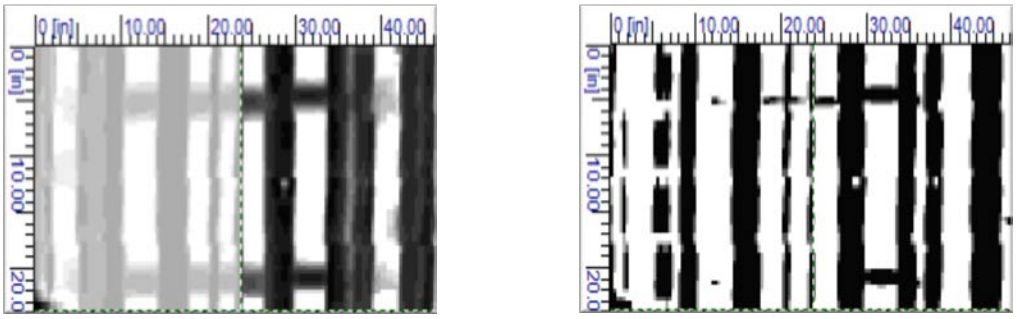

(a) (b)

Figure 5.13. Blockscans between two interior beams of Bridge 7722 at depth ranges of (a) 5 inches and (b) 2 inches.

Using this analysis technique, it was concluded that the interior beam has a maximum of 18 and a minimum of 14 strands in the bottom flange. Figure 5.14(a) shows the strand arrangement in the interior beam determined from the imagescans; strands marked with a red dot were identified with more certainty than those marked with a blue dot. Similarly, a maximum of 16 and a minimum of 12 strands were found in the exterior beam of Bridge 7722 (see Figure 5.14(b)). Note that a single layer of strands was detected in the exterior beam compared to multiple layers in the interior beam.

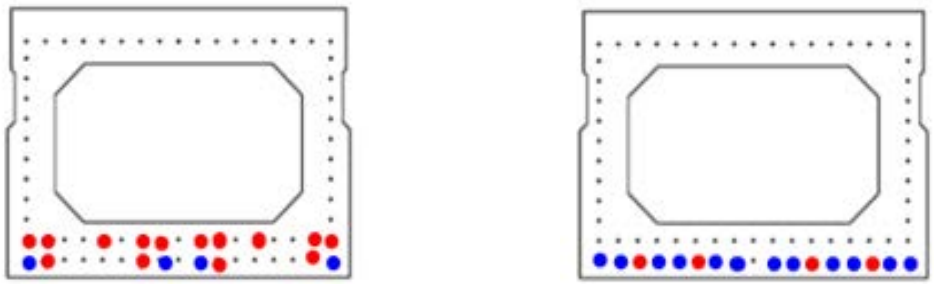

(a) (b)

Figure 5.14. Strand configuration in (a) interior and (b) exterior box beam of Bridge 7722 determined with Ferroscan.

Recall that the amount of steel estimated using the Magnel diagrams was 16 and 14 strands for the interior and exterior beams, respectively, which is the average number from the Ferroscan results. To estimate the size and location of the shear reinforcement, quick scans were performed on the exposed vertical faces of the exterior beams and on the bottom flanges of the interior beams. The scans clearly showed the transverse bars to be spaced at 16 inches center-to-center, however, the size estimate was not as conclusive due to the magnetic interference caused by the strands. Ultimately, the shear reinforcement was conservatively estimated as No. 3 bars (i.e., the smallest bar size) at a center-to-center spacing of 16 inches.

5.4 BRIDGE NO. 8825, P/C BOX GIRDER

To confirm the number of prestressing strands determined from the Magnel diagrams and also estimate the bar size and location of the shear reinforcement, scans were taken on the exposed vertical faces of the exterior beams and on the bottom faces of the interior beams. Recall that 16 prestressing strands were estimated earlier from the Magnel diagrams. Due to the large concrete cover of the prestressing strands, the scans of the beams of Bridge 8825 provided data of limited use. Figure 5.15 shows a blockscan taken on the bottom side of an interior beam. As shown in the figure, the prestressing strands appear as groups of speckled patterns. Several scans were made on the beam soffits to detect the prestressing strands but clear images were not obtained due to the large concrete cover as mentioned previously.

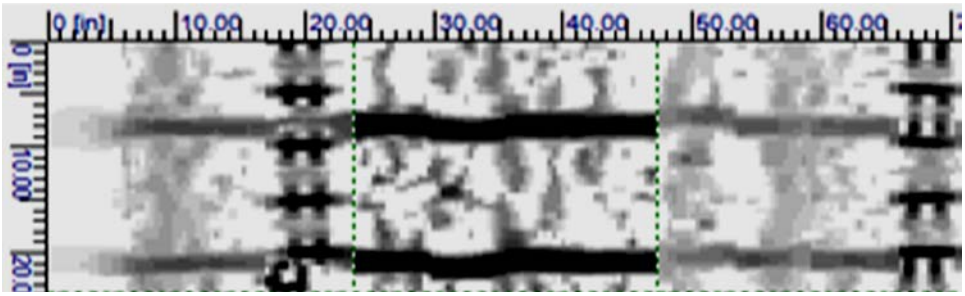

Figure 5.15. Blockscan of bottom face of interior beam (Bridge 8825).

Figure 5.16 is a blockscan taken on the side face of an exterior beam that clearly shows the shear reinforcement (i.e., transverse bars) at 12-in. spacing. The transverse bars are also visible in the blockscan given in Figure 5.15. However, the bar size estimate was not conclusive from either figure due to the magnetic interference caused by the strands. Ultimately, the shear reinforcement was conservatively assumed as No. 3 bars (i.e., the smallest bar size) at 12-in. spacing.

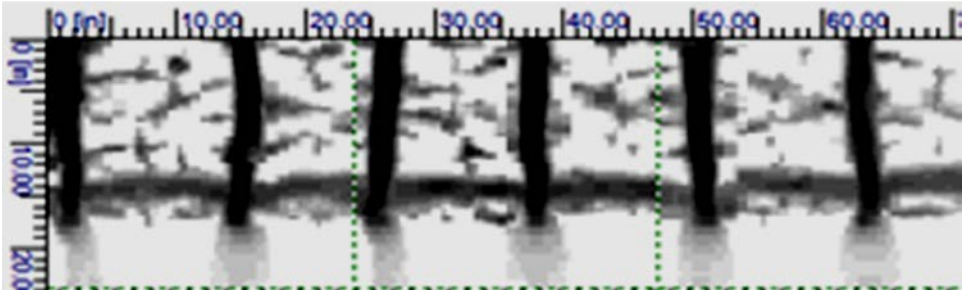

Figure 5.16. Blockscan of side face of exterior beam (Bridge 8825).

5.5 BRIDGE NO. 8588, P/C I-GIRDER

Similarly to the other bridges, the Hilti PS 250 Ferroscan was used to try and determine the size, spacing and location of the steel reinforcement (prestressed and non-prestressed) in the girders of Bridge 8588. The standard strand spacing for an AASHTO Type III I-girder allows a maximum

of 10 strands per layer in the bottom three strand layers of the girder as shown in Figure 5.17. Layers four, five and six can accommodate a maximum of 8, 6 and 4 strands, respectively. The remaining layers are situated in the girder web and top flange, and have only two strands per layer. The limitations of the Ferroscan system, in particular the minimum required bar spacing and incapability to detect the steel past the first layer of reinforcement complicated the measurement of strands in the girder bottom flange. Only the strands located near the faces of the girder could be accurately detected by the Ferroscan system. Figure 5.18 shows the imagescans taken on the bottom flange of the exterior girder near the beam end and at midspan.

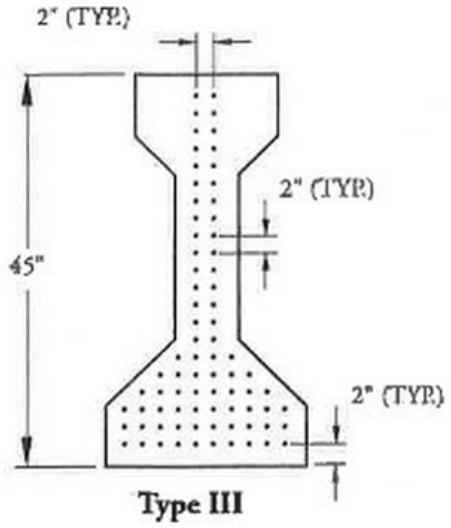

Figure 5.17. Prestressing strand layout for standard AASHTO Type III I-girder.

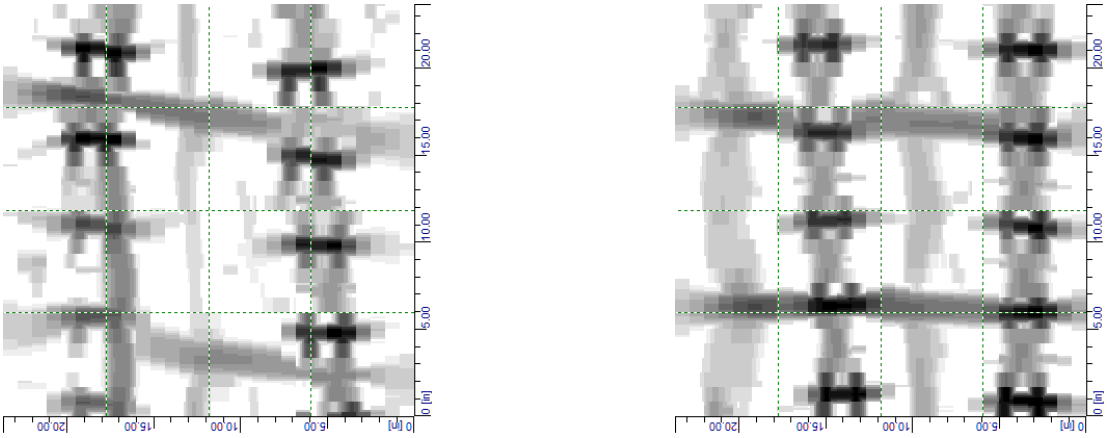

Figure 5.18. Imagescans at 5 in. depth range on soffit of bottom flange near (a) midspan and (b) abutment (Bridge 8588).

The vertical strips represent the prestressing strands while the horizontal strips are the mild shear reinforcement. As mentioned earlier, the darker shades of grey indicate multiple reinforcement layers, close strand spacing, and/or small cover depth. For multiple reinforcement layers, the interfering magnetic fields of each layer can generate scans with inaccurate depth, size and spacing

measurements. In addition, the prestressing strands may be bundled in certain areas which violates the required 1.4 in. spacing for the scan to provide accurate results. Ultimately, the results of the scan for an I-girder have limited use and provide minimal information on the location and amount of prestressing reinforcement.

The depth range feature of the Ferroscan was used to try and distinguish the different strand layers. Figure 5.18 is a full-depth scan of 5 in. and it appears that there are five strands at midspan, and 6 to 8 strands near the abutment. This is not a standard configuration since more strands would be expected at midspan if the strands were harped or equal strands if the strands were debonded. As shown in Figure 5.19, decreasing the scan depth to two inches causes the lighter shades of grey strips to disappear and only four strands remain in both the abutment and midspan scans. This is a possible indication that there are only 4 strands in the bottom layer.

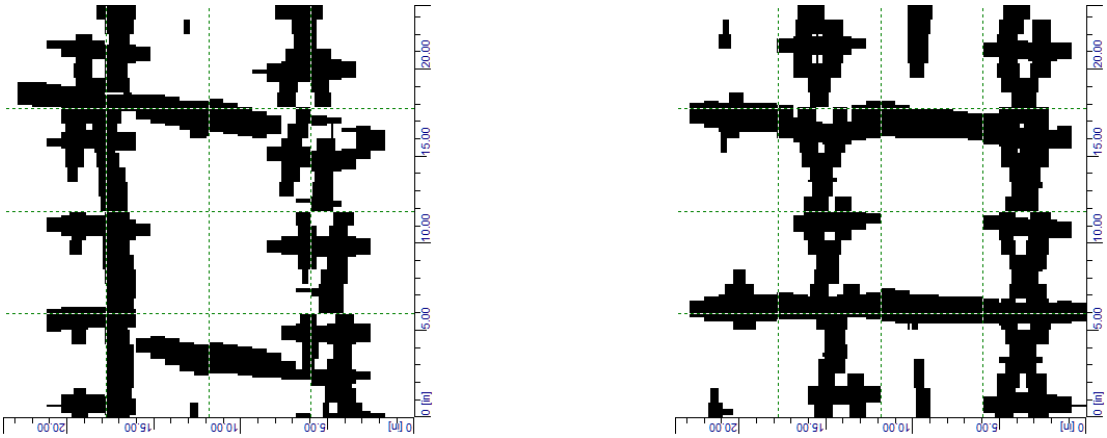

(a) (b)

Figure 5.19. Imagescans at 2 in. depth range on soffit of bottom flange near (a) midspan and (b) abutment (Bridge 8588).

The imagescans are 24 in. wide while the bottom flange width is only 22 in.; hence, there is a one inch overhang on each side of the imagescan that extends past the edge of the bottom flange. Note that the strand pattern that appears in the midspan scan is centered along the bottom flange width but is off center in the scan taken near the abutment. This shift may be due to poor placement of the strands and/or formwork during fabrication since the prestressing strand pattern should be symmetrical throughout the beam.

Recall that the prestress estimate from the Magnel diagrams amounted to 24 strands. However, only four strands are clear in the bottom layer of reinforcement from the imagescans which suggests that the majority of the strands were placed in the next two to four layers within the bottom flange. To try and determine the number of strands in these layers, a vertical imagescan was taken over the bottom flange height of seven inches as shown in Figure 5.20. The figure clearly shows the presence of strands over a vertical bandwidth of six inches, indicating that the bottom 3 layers have prestressing. Due to the scanner limitations, however, the amount of reinforcement could not be determined and thus, the prestress estimate from the Magnel diagrams needed to be relied upon without full confirmation from the Ferroscan.

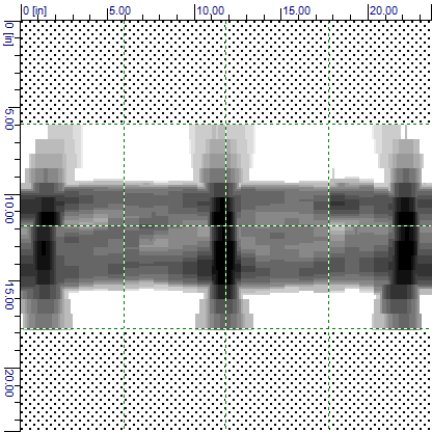

Figure 5.20. Imagescan at 5 in. depth range on side face of bottom flange near abutment (Bridge 8588).

Imagescans were also taken along the sides of the web near the abutment to check for harped strands and mild shear reinforcement as shown in Figure 5.21. The scans clearly show the shear stirrups but no evidence of harped strands indicating that debonding was likely employed. The shear reinforcement spacing was determined by taking quickscans along the web of both an interior and exterior beam. The scans gave a bar spacing of 21 inches near midspan and 9 inches near the abutment. The spacing transitions from 21 inches to 9 inches at a distance of 12 feet from the abutment. The imagescans of the web (see Figure 5.21) provided a size estimate of #3 bars.

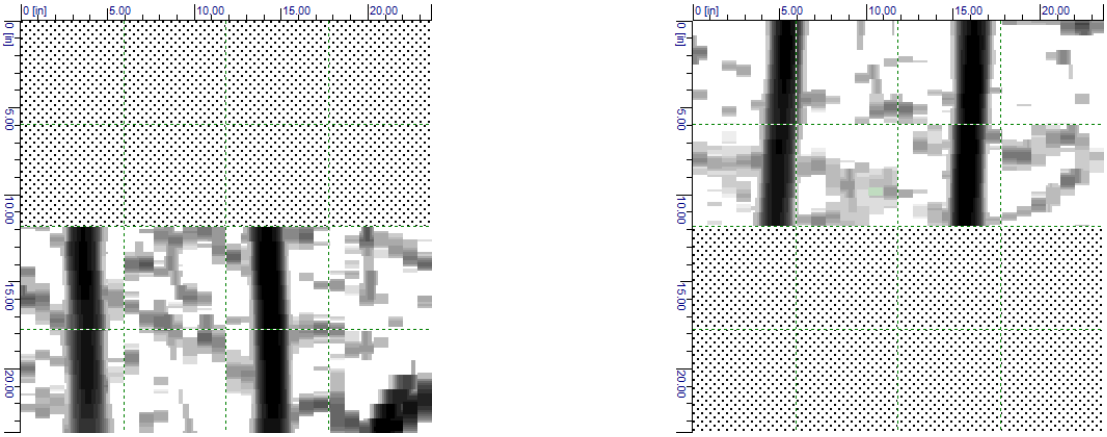

(a) (b)

Figure 5.21. Imagescans at 5 in. depth range on (a) bottom and (b) top regions of girder web near abutment (Bridge 8588).

5.6 BRIDGE NO. 8676, R/C SLAB

Bridge 8676 is a simple-supported slab bridge and thus, the bottom steel mat reinforcement configuration and concrete compressive strength are the principal factors affecting the load capacity. The Ferroscan system was used to scan a quarter of the bridge to determine the bottom steel reinforcement. As shown in Figure 5.22, the locations and lengths of the rebars are clear. In

addition, the bar size estimates were consistent and amounted to #8 bars (full length reinforcement) and #6 bars (partial length reinforcement). The spacing of the #6 and #8 bars is 12 inches. Figures 5.23 and 5.24 show the as-built drawings for the bridge. To determine the grade of the reinforcement, ten concrete slab bridges built during the 1970s to early 1990s whose plans are available were reviewed. Seven of the ten bridges built in 1982 or later used Grade 60 steel. Since Bridge 8676 was built in 1989, Grade 60 was assumed.

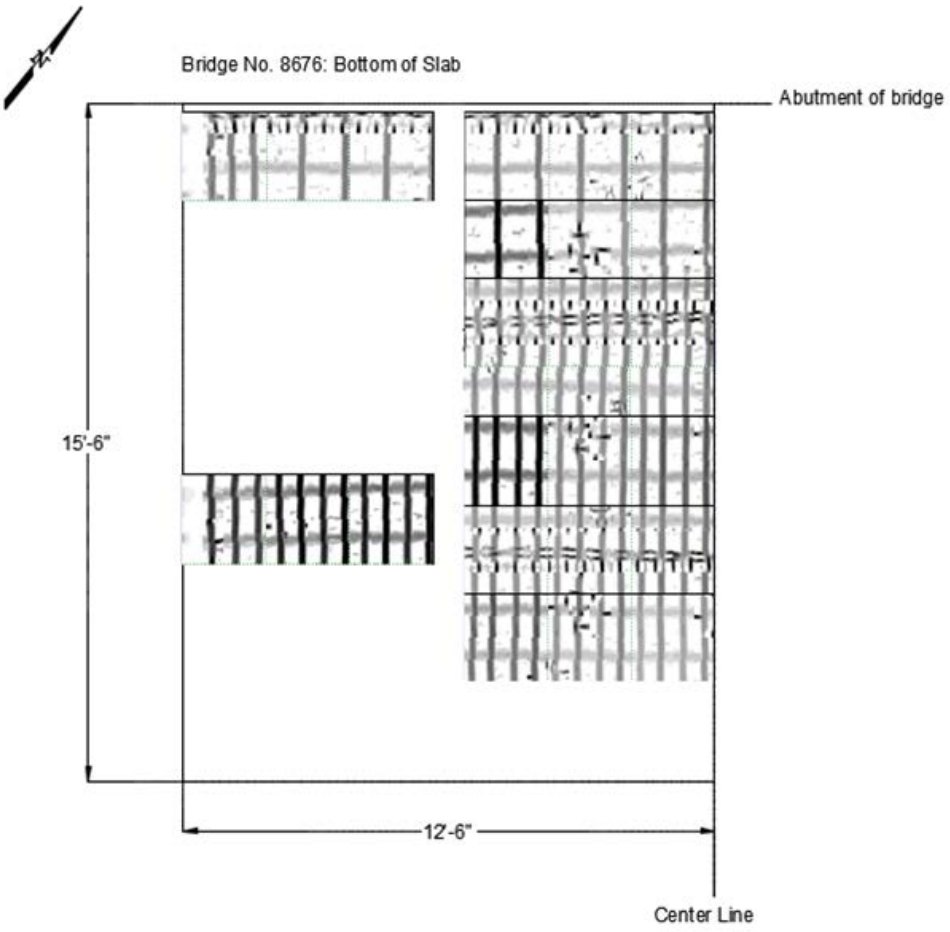

Figure 5.22. Ferroscan results for Bridge 8676.

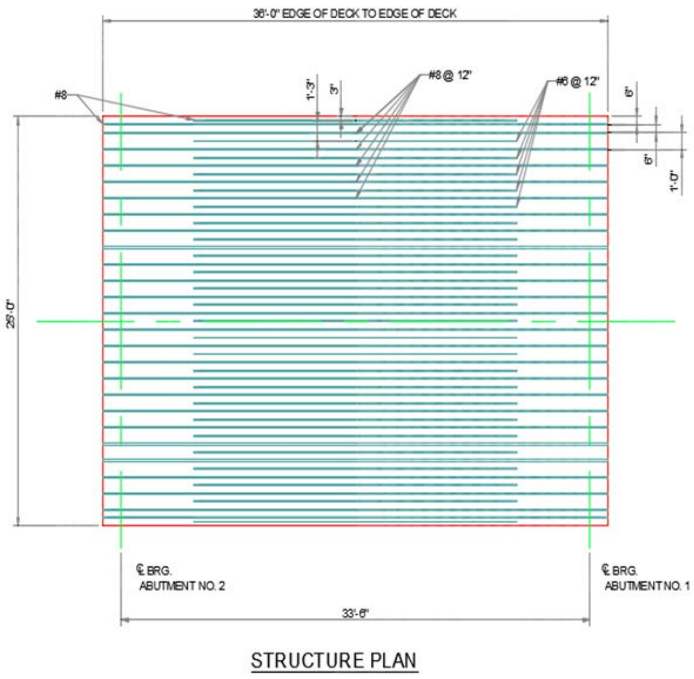

Figure 5.23. Structure plan of Bridge 8676 (as-built drawing).

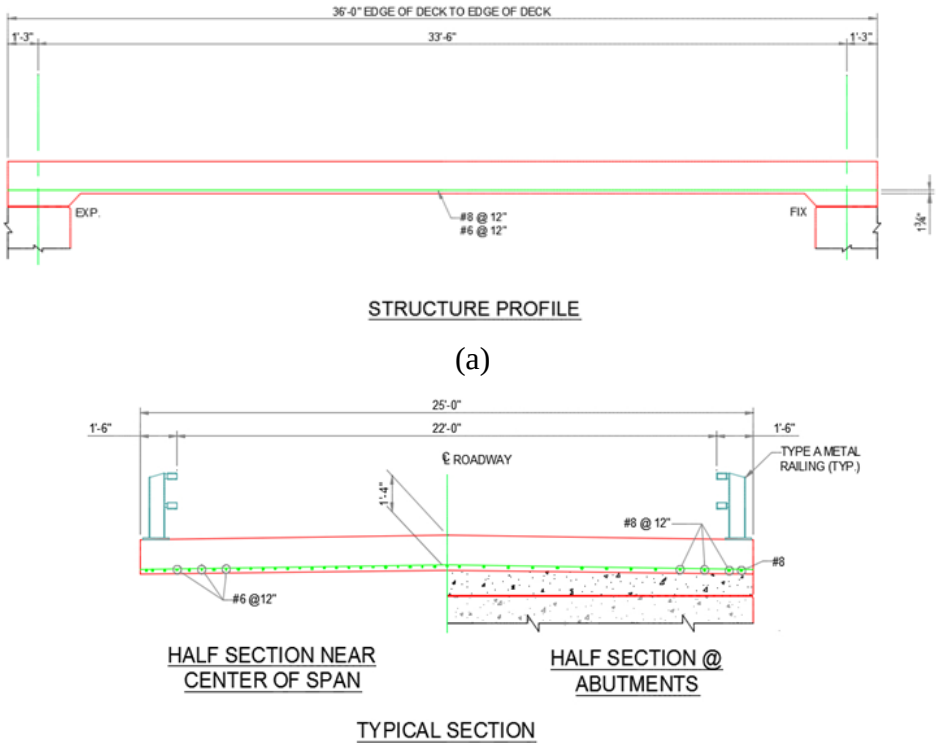

Figure 5.24. (a) Structure profile and (b) typical section of Bridge 8676 (as-built drawing).

6. VALIDATION OF CONCRETE STRENGTH

The Windsor probe penetration test is a non-destructive testing method for estimating the compression strength of in-situ concrete. The test was introduced to the United States in the 1960's and the depth of penetration of the probe is measured and used to estimate the concrete compressive strength. The correlation between the penetration and the compressive strength varies with the hardness of the coarse aggregate in the concrete mix. The Windsor Probe System WP-534 from James Instruments, Inc. was used in this project. Table 6.1 shows the correlation between the height of the exposed probe and the concrete compressive strength (based on Mohs' hardness of the coarse aggregate) for the WP-534 instrument.

The James Instruments WP-534 system can estimate the compressive strength of up to 17,000 psi concrete and calibration charts are provided for different aggregate hardness values. There are two power settings for the WP-534 instrument: low and standard. Table 6.1 provides the WP-534 chart for the standard power setting. Low power should be used only when the concrete is expected to have a compressive strength smaller than 3,000 psi. In this project, standard power was used because the compressive strengths of the selected concrete bridges for load testing were all expected to be larger than 3,000 psi. In addition, silver colored probes were used rather than gold since the former are designed to penetrate concrete with compressive strengths up to 17,000 psi. The test is conducted by holding the driving head of the WP-534 instrument perpendicular to the surface of the concrete, placing it on the firing template, and firing the probe into the concrete. A measuring cap and plate are then installed on the embedded probe and a calibrated micrometer is used to measure the exposed probe length to the nearest 0.025 inch. A Mineral Scratch test is finally done on the coarse aggregate to obtain the Mohs' hardness value and together with the exposed probe length are used to determine the concrete compressive strength from the table.

The ASTM C803 Standard Test Method for Penetration Resistance of Hardened Concrete specifies the procedures for the proper execution of Windsor probe testing in the field. The standard was followed to obtain the required samples and distribution of Windsor probes for the concrete bridges selected for this project. The probes cannot penetrate more than half the thickness of the concrete member and must be 4 inches from any edge of the concrete surface and 7 inches from any other probe. Furthermore, the probes must be fully embedded in the concrete and any loose probes must be discarded. A small hammer can be used to tap the probes to ensure proper embedment. A minimum of three embedded probe measurements are necessary to obtain statistically significant results. The ASTM C803 standard provides a "Precision for Resistance Testing with Probes" table that gives the range difference allowed between the three measurements. If the three exposed probes fall outside this range, a fourth measurement is required.

During the third quarter of FY2014, the Windsor probe testing was conducted on the two double T-beam concrete bridges located in Doña Ana County. For Bridge 7701, probes were shot into the top surfaces of the north and south exterior beams. Table 6.2 lists the lengths of the exposed probes and the estimated compressive strengths of the concrete. Based on the results given in the table, the average measured strength was approximately 7550 psi.

Table 6.1. Standard power table for James Instruments WP-534 Windsor probe system.

Standard Power Table (No.1)

Exposed Probe (inches)	PSI Mohs' N0. 3	Mpa Mohs' N0. 3	PSI Mohs' N0 .4	Mpa Mohs' N0.4	PSI Mohs' N0.5	Mpa Mohs' N0.5	PSI Mohs' N0.6	Mpa Mohs' N0.6	PSI Mohs' N0.7	Mpa Mohs' N0.7
2.025	**7175**	49.5003	**6675**	46.0508	**6150**	42.4288	**5600**	38.6344	**4975**	34.3225
2.05	**7325**	50.5351	**6850**	47.2581	**6350**	43.8086	**5800**	40.0142	**5175**	35.7023
2.075	**7500**	51.7425	**7025**	48.4654	**6525**	45.0159	**6000**	41.394	**5400**	37.2546
2.1	**7675**	52.9498	**7200**	49.6728	**6700**	46.2233	**6200**	42.7738	**5625**	38.8068
2.125	**7825**	53.9846	**7375**	50.8801	**6900**	47.6031	**6400**	44.1536	**5850**	40.3591
2.15	**8000**	55.192	**7550**	52.0874	**7075**	48.8104	**6600**	45.5334	**6050**	41.7389
2.175	**8175**	56.3993	**7725**	53.2947	**7250**	50.0177	**6800**	46.9132	**6275**	43.2912
2.2	**8325**	57.4341	**7900**	54.5021	**7450**	51.3975	**7000**	48.293	**6500**	44.8435
2.225	**8500**	58.6415	**8075**	55.7094	**7625**	52.6048	**7200**	49.6728	**6725**	46.3957
2.25	**8675**	59.8488	**8250**	56.9167	**7800**	53.8122	**7400**	51.0526	**6925**	47.7755
2.275	**8825**	60.8836	**8425**	58.1240	**7975**	55.0195	**7600**	52.4324	**7150**	49.3278
2.3	**9000**	62.091	**8600**	59.3314	**8175**	56.3993	**7800**	53.8122	**7375**	50.8801
2.325	**9175**	63.2983	**8775**	60.5387	**8350**	57.6066	**8000**	55.192	**7600**	52.4324
2.35	**9325**	64.3331	**8950**	61.7460	**8525**	58.8139	**8200**	56.5718	**7800**	53.8122
2.375	**9500**	65.5405	**9125**	62.9533	**8725**	60.1937	**8400**	57.9516	**8025**	55.3644
2.4	**9675**	66.7478	**9300**	64.1607	**8900**	61.4011	**8600**	59.3314	**8250**	56.9167
2.425	**9825**	67.7826	**9475**	65.3680	**9075**	62.6084	**8800**	60.7112	**8475**	58.4690
2.45	**10000**	68.99	**9650**	66.5753	**9275**	63.9882	**9000**	62.091	**8675**	59.8488
2.475	-	-	**9825**	67.7826	**9450**	65.1955	**9200**	63.4708	**8900**	61.4011
2.5	-	-	**10000**	68.99	**9625**	66.4028	**9400**	64.8506	**9125**	62.9533

Table 6.2. Windsor probe results for Bridge 7701.

Distance from West Abutment	South Exterior Beam		North Exterior Beam	
	Exposed Probe (in.)	Compressive Strength (psi)	Exposed Probe (in.)	Compressive Strength (psi)
2 ft. 0 in.	2.100	7200	2.200	7900
2 ft. 9 in.	2.200	7900	2.100	7200
4 ft. 3 in.	2.175	7725	2.150	7550

Note: Coarse aggregate hardness measured #4 on Mohs' scale.

For Bridge 8761, attempts were made to fire the Windsor probes into the interior beams (part of 1989 original construction) and the exterior beams (part of 2005 widening). Table 6.3 lists the Windsor probe results for the beams. As shown in the table, the Windsor probe testing was not

successful on the interior beams since all the probes continued to bend and break when shot into the concrete. Three probes were embedded into the exterior beams but only after several tries and the average compressive strength was approximately 7850 psi.

Table 6.3. Windsor probe results for Bridge 8761.

Distance from East Abutment	Interior Beam		Exterior Beam	
	Exposed Probe (in.)	Compressive Strength (psi)	Exposed Probe (in.)	Compressive Strength (psi)
3 ft. 6 in.	-----	-----	2.325	8350
5 ft. 4 in.	-----	-----	2.275	7975
18 ft. 8 in.	-----	-----	2.175	7250

Note: Coarse aggregate hardness measured #5 on Mohs' scale for exterior beam.

Attempts were made to fire the Windsor probes into the interior and exterior beams of Bridge 7722 and Bridge 8825. However, the testing was not successful on any of these bridge beams since the probes either were damaged or did not embed in the concrete (similar to Bridge 8761).

For Bridge 8676, the concrete compressive strength was assumed to be 4000 psi based on the year built. To verify the assumption, Windsor Probe testing was conducted and three probes were successfully embedded into the concrete. Table 6.4 shows the testing results for the top of slab at the southeast corner. Based on Mohs' hardness of 6, the average compressive strength was approximately 6400 psi.

Table 6.4. Windsor probe results for Bridge 8761.

Exposed Probe (in.)	Compressive Strength (psi)
2.175	6800
2.075	6000
2.125	6400

Note: Coarse aggregate hardness measured #6 on Mohs' scale.

Windsor Probe testing was conducted on both the girder and deck of Bridge 8588 to verify the assumed concrete strengths of 5000 psi and 3000 psi, respectively. A single attempt was made to measure the compressive strength of the bridge girder, however, the test was not successful as the probe did not embed in the concrete. No further attempts were not made due to previous negative experience with Windsor Probe testing of prestressed concrete members. On the contrary, successful tests were completed on the bridge deck. Table 6.5 shows the results from the Windsor Probe tests at the southwest corner of the deck. The data fell in compliance with the range variation

standard set by ASTM C803 and an average compressive strength of 7400 psi was obtained. Therefore, the assumed value of 3000 psi for the deck compressive strength was conservative.

Table 6.5. Windsor probe results for Bridge 8588.

Prestressed Girder		Concrete Deck	
Exposed Probe (in.)	Compressive Strength (psi)	Exposed Probe (in.)	Compressive Strength (psi)
-----	-----	2.175	6800
-----	-----	2.325	8000
-----	-----	2.250	7400

Note: Coarse aggregate hardness measured #6 on Mohs' scale for concrete deck.

7. DIAGNOSTIC LOAD TESTS

Using the information collected from the in-depth inspections, diagnostic load tests were planned and executed on double T-beam Bridges 7701 and 8761, and box beam Bridge 7722. Dump trucks with weights well below the target proof load were applied to the bridges along different transverse paths on the roadway. The bridges were instrumented heavily to capture the elastic response for use in planning the proof load test. The primary purpose of the diagnostic tests was to study the actual load path for each bridge and determine the critical truck paths (i.e., those that produce the largest measured strains). The critical paths were then used to develop the loading procedure for the proof tests.

Note that the final load ratings were not determined based on the diagnostic load tests. Rather the results from these tests were used to gain a basic understanding of the bridge response in the elastic region to properly plan the proof load test. Before the load tests were performed, the available bending moments for the beams were computed using the prestressing estimates from the Magnel diagrams to determine the largest load the bridge could resist without cracking. The available moments were converted to bending strains that represented the maximum strain levels the bridge beams could carry before initiation of cracking. Furthermore, the diagnostic tests provided live load distribution factors that were more representative of the bridge behavior than the design-based factors from the AASHTO specifications. In short, strain measurements from the diagnostic tests were used to determine the level of load in the proof tests that loading may need to be halted.

7.1 BRIDGE NO. 7701, P/C DOUBLE T-BEAM

On November 14, 2013, a diagnostic load test was performed on Bridge 7701 to get a feel for the equipment and to determine the critical truck paths for the proof load test (based on maximum measured strains and deflections of the nine beams). Due to the condition of the shear keys, the live load distribution between the beams was uncertain and thus, caution needed to be taken to avoid overloading the bridge. The diagnostic load test consisted of two phases. In the first phase, the front axle of a single 10 cubic-yard dump truck was positioned along seven transverse paths in an effort to maximize the load on each beam. For paths 1 and 7, the truck was positioned approximately 2 ft. from the curb and for paths 2 through 6, the truck was centered about beams 3 through 7, respectively. Figure 7.1 shows the wheel locations of the dump truck (spaced approximately 6.5 ft. apart) for paths 5 and 7.

For each path, the truck's font axle (weighing 14.72 kips) was moved along the bridge length in five steps as shown in Figure 7.2. In the first step, the front axle was stopped directly above the west support bearing of the bridge. In the next three steps, two through four, the front axle was stopped at distances of 4 ft., 8 ft., and 12 ft. from the bearing, respectively. In the fifth and final step, the front axle was placed one foot from the center line of the bridge (i.e., 14.5 ft. from the bearing). A similar scheme was used to load the bridge with side-by-side dump trucks in the second phase of testing using the front of the tandem axle as the reference (discussed later).

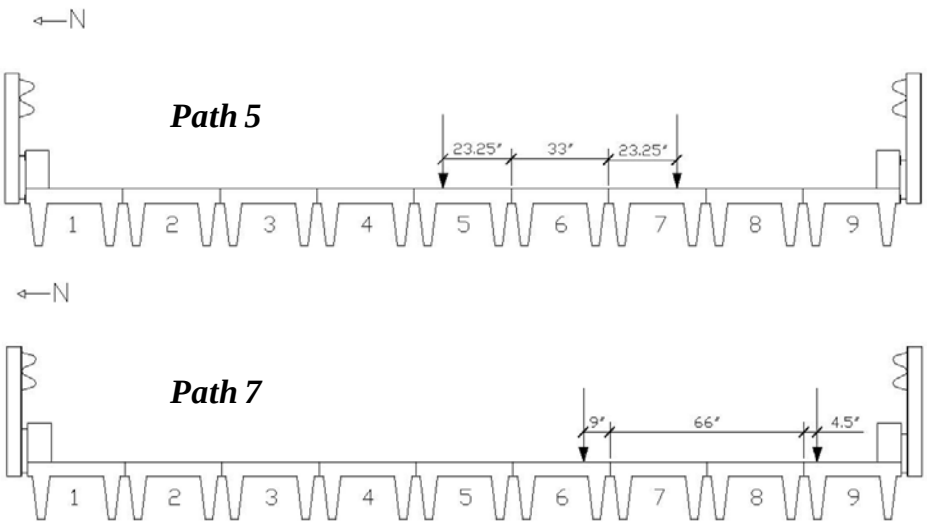

Figure 7.1. Transverse truck paths 5 and 7 for first phase of diagnostic testing (Bridge 7701).

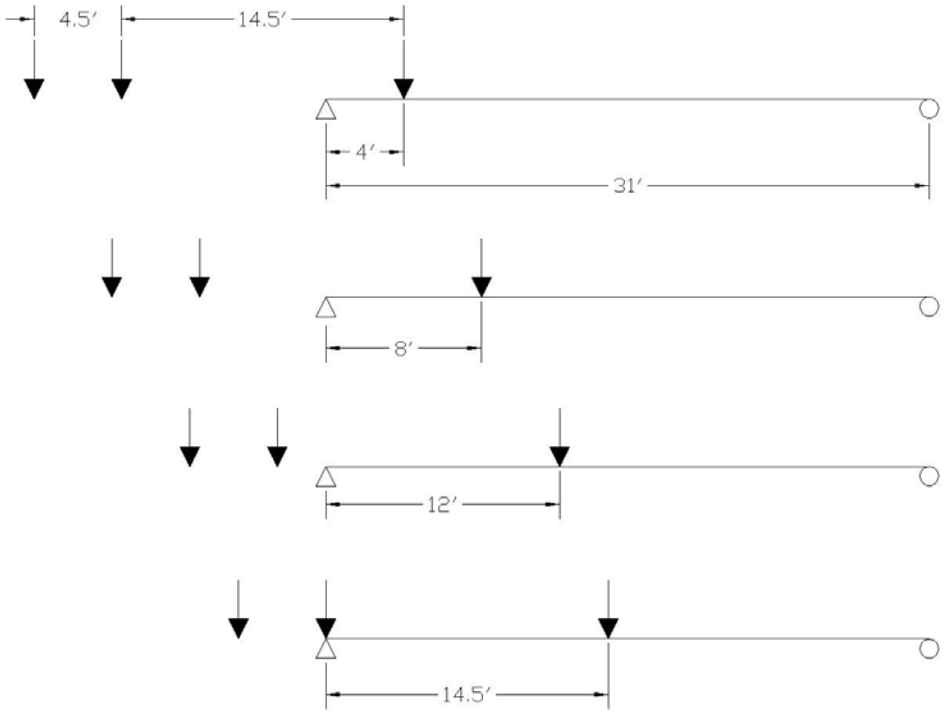

Figure 7.2. Longitudinal truck positions for first phase of diagnostic testing (Bridge 7701).

The BDI (Bridge Diagnostics, Inc.) structural testing system was used to measure strains and deflections of the beams under truck loading. The system has a total of 36 channels, six for deflection measurement and 30 for strain measurement. All 36 channels were used for the diagnostic load test; Figure 7.3 shows the instrumentation layout of Bridge 7701. As shown in the figure, strain transducers were placed on the beam stems at midspan and also at the third points.

The locations of the transducers over the beam height are shown in Figure 7.4. The deflection transducers were placed at the center of six of the beams (1 and 3 through 7) at midspan.

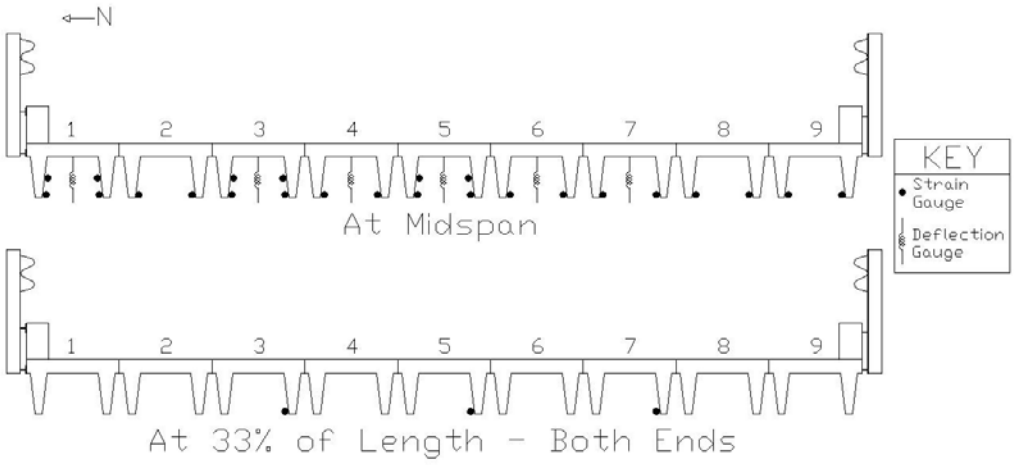

Figure 7.3. Instrumentation layout for diagnostic load testing (Bridge 7701).

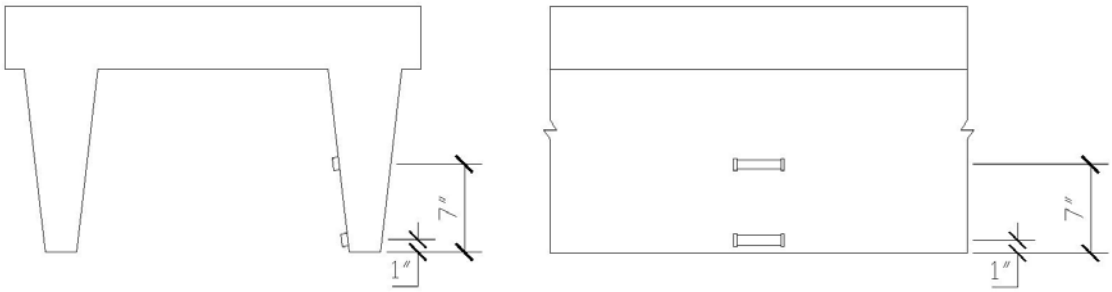

Figure 7.4. Strain transducer locations over beam height (Bridge 7701).

Using the estimate of the prestressing strands discussed earlier, calculations were done to determine the cracking moment, available moment, target moment, and test truck moment for an interior beam of Bridge 7701. In addition, the available strain and test truck strain were computed to aid in monitoring the bridge beams during the load test (discussed later). The cracking moment was found assuming a prestress loss of 30%; this percentage is higher than the 25% used in the initial estimate of the prestressing strand and thus, gives a more conservative estimate of the cracking moment. The cracking moment was determined using the following equation:

$$M_{cracking} = S_b * \left[P_e * \left(\frac{1}{A} + \frac{e}{S_b}\right) + f_{cr}\right] \quad \text{(Eq. 7.1)}$$

where f_{cr} is the modulus of rupture (equal to 7.5 times the square root of f_c' as given in Section 1.6.6B of the AASHO specifications). For f_c' equal to 5000 psi, f_{cr} equals 530 psi and the cracking moment equals 140.3 kip-ft. The available moment was found by subtracting the dead load moment from the cracking moment and thus represented the additional moment the beam could resist before cracking. For Bridge 7701, the dead load moment was simply the moment due to the

self-weight of an interior beam resulting in an available moment of 104.5 kip-ft. For the diagnostic load test, dump trucks with a tandem axle weight of 27.8 kips were used which is 82% of the Type 3 legal load. As mentioned previously, a smaller load was applied as a precautionary measure against cracking due to the suspect shear keys and uncertain live load distribution. The dump truck provided a test truck moment of 92.5 kip-ft. Note that if the live load distribution factor is equal to one, the test truck moment and the available moment are nearly equal. Using a factor of 0.458 as computed based on the AASHO specifications, the test truck moment reduced to 42.4 kip-ft. Due to the damage observed on many of the shear keys, the actual test truck moment was expected to fall somewhere between 42.4 kip-ft and 92.5 kip-ft. Hence, the test truck moment is less than or equal to the available moment suggesting that the bridge should remain uncracked.

Using the moments given above, the cracking strain and the expected test truck strain were calculated at the location one inch from the bottom of the beam stem (i.e., the transducer location). These values were then compared to the strain measurements during the load testing to monitor the bridge behavior for indications that cracking was imminent and also to check the actual live load distribution. The following equation was used to determine the strain values:

$$\varepsilon = \frac{M}{S_b * E_{design}} \qquad \text{(Eq. 7.2)}$$

where M is the available or test truck moment, S_b is the section modulus of the beam at the transducer location, and E_{design} is the modulus of elasticity of the beam. The available strain was calculated to be 493 με and the test truck strain (determined using the distribution factor of 0.458) amounted to 200 με. Apart from strain, the deflection under test truck loading was also computed as 0.441 in. using the live load distribution factor of 0.458. The deflection of 0.441 in. due to the test truck was then compared to the serviceability limit of L/800. For a 31.0 ft. span, the serviceability limit is 0.465 in. Attention was given to the deflection measurements during testing to ensure the serviceability limit was not exceeded. Table 7.1 summarizes the important findings presented in this section.

Table 7.1. Preparatory calculations for diagnostic load testing of Bridge 7701.

Moment	Value (kip-ft)	Strain	Value (με)	Deflection	Value (in.)
$M_{cracking}$ *	140.3	$\varepsilon_{available}$ **	493	Δ_{truck}	0.441
M_{DL}	35.8	ε_{truck} **	200	*L/800*	0.465
$M_{available}$	104.5				
M_{truck} ***	42.4				

Notes: * - Computed based on allowable tension of 7.5 times square root of f_c'.
** - Computed one inch from bottom of beam section.
*** - Computed based on load distribution factor of 0.458.

The diagnostic load test of Bridge 7701 required approximately six hours to complete. Installation of the strain transducers was done the day before the test, while the deflection transducers were installed the morning of the test. As mentioned previously, the test was executed in two phases.

For the first phase, the front axle of a single dump truck was used to load the bridge beams along seven transverse paths and four longitudinal locations per path (see Figures 7.1 and 7.2). The measured strains of the beams with the front axle located 14.5 ft. from the bearing are reported in Table 7.2 for all the transverse paths. The results correspond to the maximum values recorded at the 18 strain transducers located at the bottom of the beams at midspan. The beams and stems are numbered from north to south and are labeled B#S# (e.g., B1S1 corresponds to beam 1, stem 1).

From Table 7.2, the largest measured strains were 202 με and 152 με for transverse paths 5 and 7, respectively. Consequently, in the second phase of testing, two dump trucks were placed side-by-side with the first truck positioned in either path 5 or path 7 and the second truck placed approximately 2 ft. from the first truck in an effort to maximize the measured strains. As shown in Figure 7.5, the dump trucks were positioned in paths 1 and 5 for the first run, and then in paths 3 and 7 for the second run. In these two runs, the trucks were backed up onto the bridge and the load was applied by the tandem axle rather than the front axle. This was done in order to increase the applied load and also so the trucks could get off the bridge as quickly as possible in case that the cracking load was approaching. The locations where the trucks were stopped remained relatively the same using the front of the tandem axle as the reference as shown in Figure 7.6. The trucks were backed up one at a time, leaving them staggered for only a few moments.

Table 7.2. Maximum measured strains for first phase of diagnostic testing (Bridge 7701).

Transducer Location	Strain (με)						
	Path 1	Path 2	Path 3	Path 4	Path 5	Path 6	Path 7
B1S1	76	54	24	2	2	-3	-5
B1S2	116	108	26	13	-1	-2	-4
B2S1	112	**117**	32	1	3	1	-2
B2S2	49	61	86	27	8	3	-1
B3S1	48	68	83	14	6	4	0
B3S2	105	75	67	89	12	8	6
B4S1	**117**	72	69	83	15	10	4
B4S2	36	97	55	79	28	35	20
B5S1	61	84	69	65	**202**	14	11
B5S2	14	19	**106**	58	87	98	37
B6S1	16	16	103	48	84	95	33
B6S2	10	8	23	87	74	64	130
B7S1	11	7	34	**113**	75	81	**152**
B7S2	5	2	8	18	83	60	54
B8S1	5	4	5	22	86	62	59
B8S2	0	2	1	2	29	**102**	101
B9S1	-1	0	0	10	25	99	91
B9S2	-4	-1	-5	-18	12	40	100

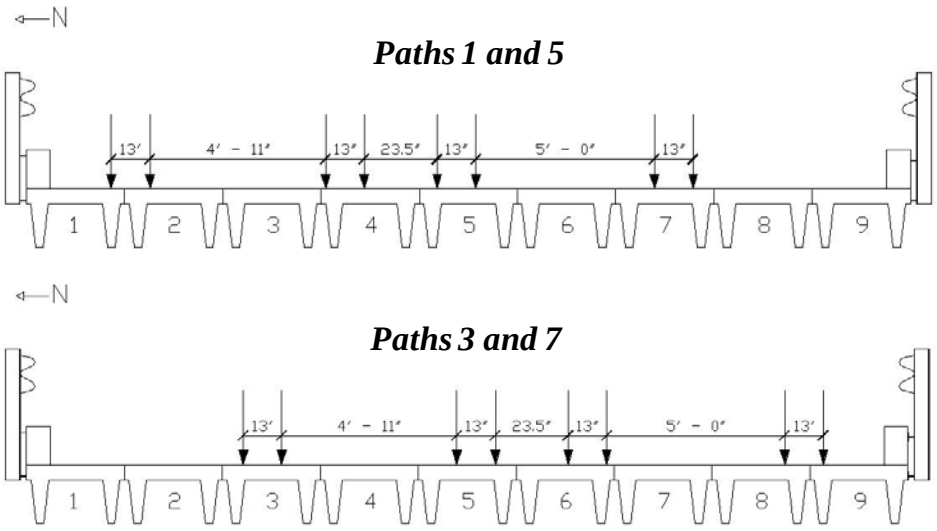

Figure 7.5. Transverse truck paths 1-5 and 3-7 for second phase of diagnostic testing (Bridge 7701).

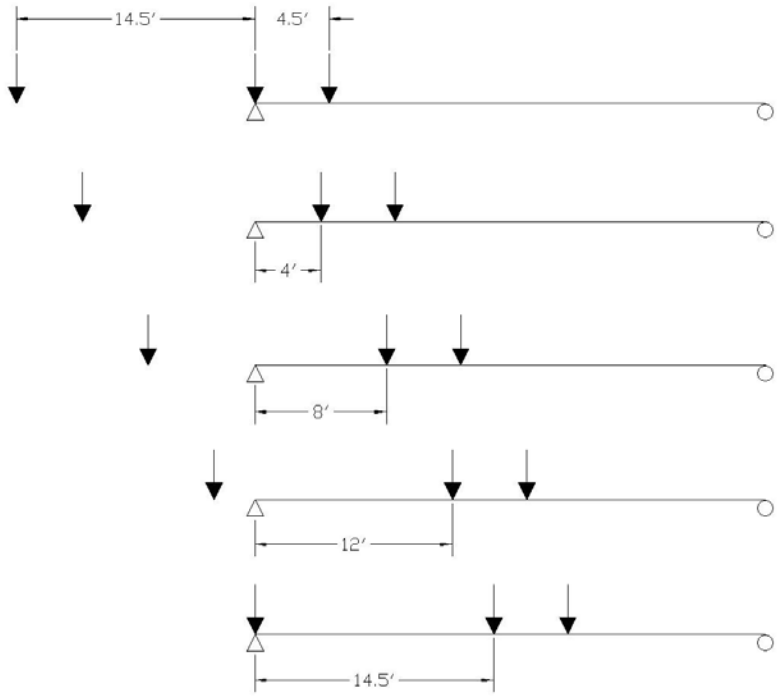

Figure 7.6. Longitudinal truck positions for second phase of diagnostic testing (Bridge 7701).

Table 7.3 shows the maximum measured strains during the second phase of testing. Based on these results, it is clear that the side-by-side trucks in paths 3 and 7 was the most critical. This loading arrangement resulted in measured strains as high as 312 με which is approximately 1.6

times the expected test truck strain of 200 με. This is a clear indication that the shear keys are not functioning as intended, which was a concern going into the test due to the visible damage. The measured strains given in Tables 7.2 and 7.3 were subsequently used to plan the proof load test, which was completed on March 26, 2014. Results from the proof load test will be provided later in the quarterly report.

Table 7.3. Maximum measured strains for second phase of diagnostic testing (Bridge 7701).

Transducer Location	Strain (με)	
	Paths 1 and 5	Paths 3 and 7
B1S1	132	41
B1S2	199	58
B2S1	199	60
B2S2	140	158
B3S1	148	147
B3S2	239	120
B4S1	230	125
B4S2	247	103
B5S1	**265**	**312**
B5S2	194	295
B6S1	188	288
B6S2	183	191
B7S1	199	289
B7S2	148	156
B8S1	162	165
B8S2	66	210
B9S1	64	221
B9S2	38	118

7.2 BRIDGE NO. 8761, P/C DOUBLE T-BEAM

Similar to Bridge 7701, a diagnostic load test was conducted on Bridge 8761 on February 27, 2014 to aid in planning a proof load test. Diagnostic testing served to compare the analytical and measured strains at a lower load level and to ultimately provide the critical truck locations and axle weights for proof testing. To monitor the bridge response, 28 strain gauges and 6 deflection gauges were installed as shown in Figure 7.7. The strain gauges were installed at midspan, and 20% and 80% of the bridge length on the beam stems; 22 gages were placed 1 inch from the bottom and 6 gages were placed 12 inches from the bottom.

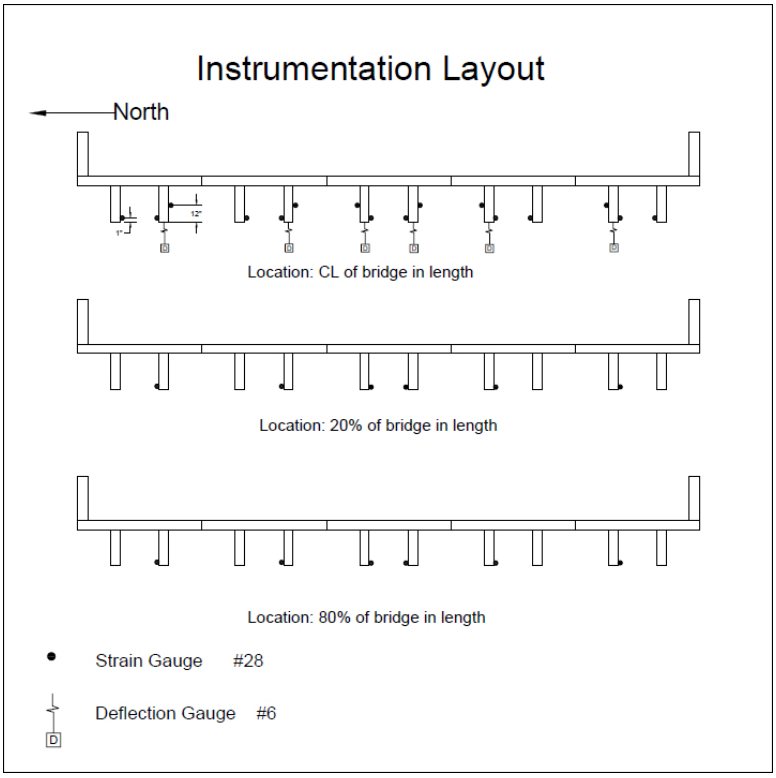

Figure 7.7. Instrumentation layout for diagnostic load testing (Bridge 8761).

Single-truck tests and double-truck tests (side-by-side and back-to-back) were conducted on Bridge 8761. For the single-truck tests (i.e., first phase), the truck was placed at the following paths (see Figure 7.8): center of each interior girder (paths 3, 5, and 7); center of each shear key between girders (paths 2, 4, 6, and 8); and 3 ft. from the edge of deck (paths 1 and 9). Along each path, the front axle of the dump truck was stopped 12 ft. and 16 ft. from the east abutment. Only two longitudinal positions were necessary for Bridge 8761 (compared to four for Bridge 7701) due to the small measured strains. Figure 7.9 shows the axle configurations and weights for the two dump trucks used for the diagnostic load tests. Truck #16766 was used for the single-truck tests since the front axle weight was larger. Based on the results of the single-truck tests, the truck paths for the double-truck tests were determined.

To safeguard against cracking the bridge beams during the load tests, the available moment for live load was determined, which equaled the cracking moment minus the moment due to dead load. The cracking moment was computed using Eq. (7.1) given earlier and assuming the prestress losses were 30% and the allowable tension was 6 times the square root of f_c'. As shown in Eq. (7.1), the cracking moment is based on the effective prestressing force and strand eccentricity. Recall that the number of strands and eccentricities for the interior and exterior girders were estimated using Magnel diagrams under HS-20 truck loading and confirmed by the historical information provided by the NMDOT and/or the Hilti Ferroscan results. For the exterior beam, the estimate was six 0.6-in. diameter strands with an eccentricity of 16.69 inches and for the interior girder, the estimate was twelve 0.6-in. diameter strands with an eccentricity of 18.23 inches.

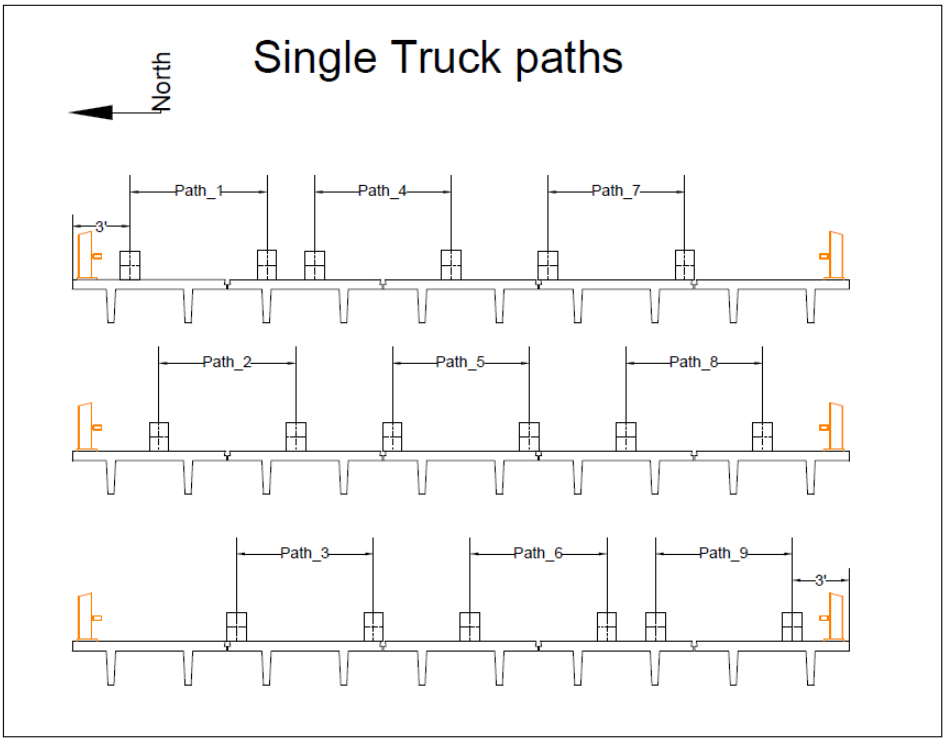

Figure 7.8. Transverse truck paths 1 through 9 for first phase of diagnostic testing (Bridge 8761).

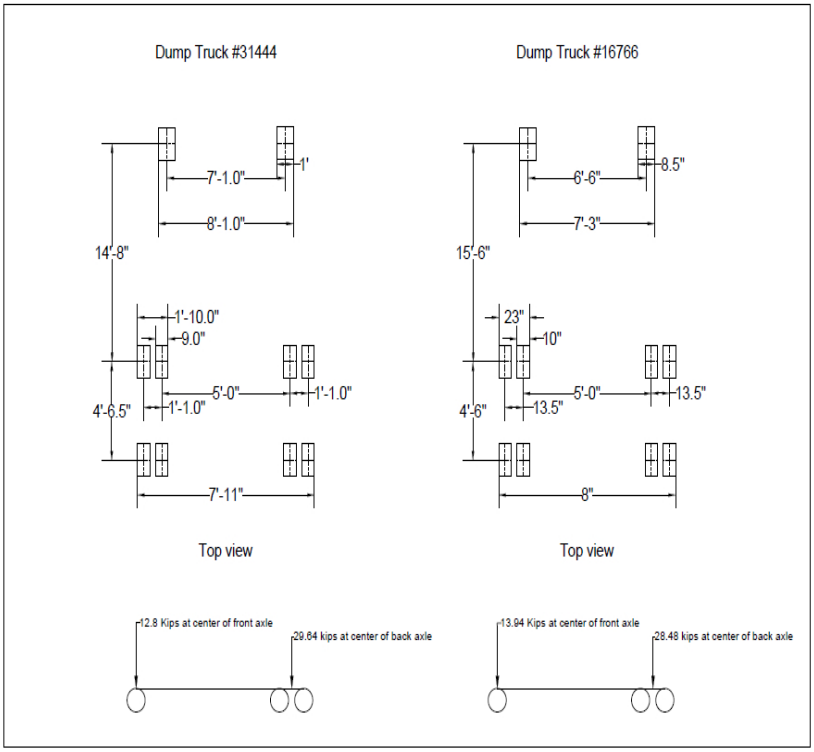

Figure 7.9. Axle configurations and weights of diagnostic test trucks (Bridge 8761).

Table 7.4 shows the beam calculations made in preparation for the diagnostic testing of Bridge 8761. As shown in the table, the available moment for the interior girder is larger than the moment caused by the test trucks and the state legal load, which indicates that the interior girder is satisfactory for diagnostic testing. For the exterior girder, the available moment is larger than the moment caused by the test truck but less than the moment caused by the State legal load. These moments suggest that the exterior girder is satisfactory for diagnostic testing but precaution should be taken during the proof test loading which simulates the State legal load. There are a couple of factors that will affect the behavior of the exterior beam. The first factor is the prestress loss of 30% which is conservative compared to the 22% prestress loss that was determined by AASHTO provisions. The second factor is the distribution factor. Due to the railing, a truck cannot be placed directly on the exterior girder meaning the distribution factor may be smaller than AASHTO.

Table 7.4. Preparatory calculations for diagnostic load testing of Bridge 8761.

Variable	Exterior	Interior
f_c' (psi)	6000	5500
E (ksi)	4415	4227
S_b (in^3)	1660	1717
Number of Strands	6	12
Area per Strand (in^2)	0.217	0.153
P_e (kip)	184.6	260.3
e (in.)	16.69	18.23
M_{cr} (kip-ft) *	355.1	506.4
M_{dl} (kip-ft)	158.4	146.9
$M_{available}$ (kip-ft)	196.7	359.5
M_{truck} (kip-ft) ***	151.9	159.3
M_{Type3} (kip-ft) ***	236.8	248.3
$\varepsilon_{available}$ (με) **	302.8	561.8
ε_{truck} (με) **	232.4	248.9
ε_{Type3} (με) **	362.3	388.0

Notes: * - Computed based on allowable tension of 6 times square root of f_c'.
** - Computed one inch from bottom of beam section.
*** - Computed based on load distribution factor of 0.667 for interior beam and 0.645 for exterior beam, and impact factor of 1.33 (for Type 3 legal load only).

The diagnostic load test of Bridge 8761 was conducted in three phases: first phase – a single dump truck was moved along the nine paths shown previously in Figure 7.8 and the front axle was stopped 12 ft. and 16 ft. from the east abutment; second phase – two dump trucks were placed side-by-side along paths 1 and 3, 4 and 6, and 7 and 9 (see Figure 7.10), and the back axles were stopped at midspan of the bridge; and the third phase – two dump trucks were placed back-to-back

along paths 1, 5, and 9 (see Figure 7.11). Tables 7.5 through 7.7 list the maximum measured strains for the three phases of testing. The beams and stems are labeled from north to south (e.g., B1S1 corresponds to the north stem of the north beam).

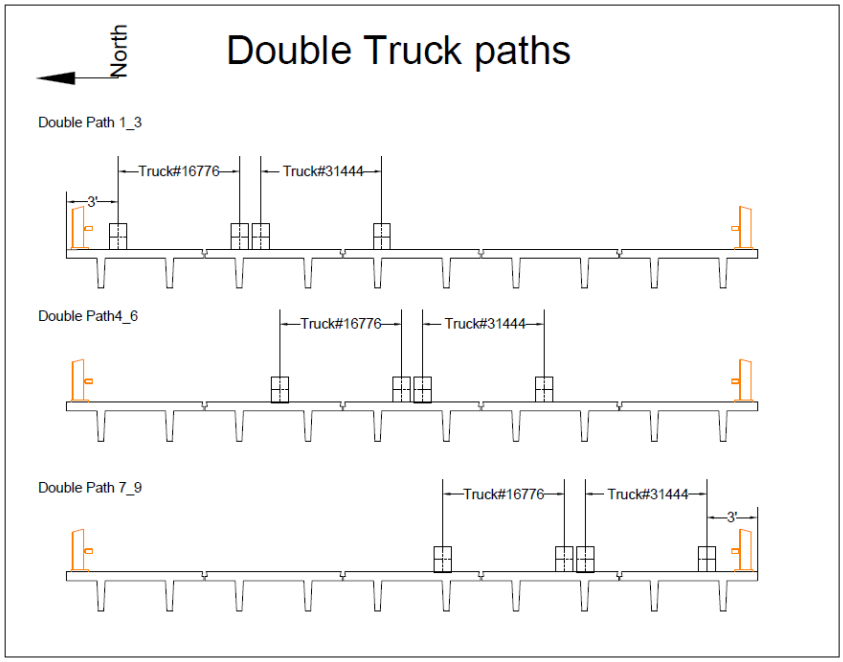

Figure 7.10. Transverse truck paths 1-3, 4-6, and 7-9 for second phase of diagnostic testing (Bridge 8761).

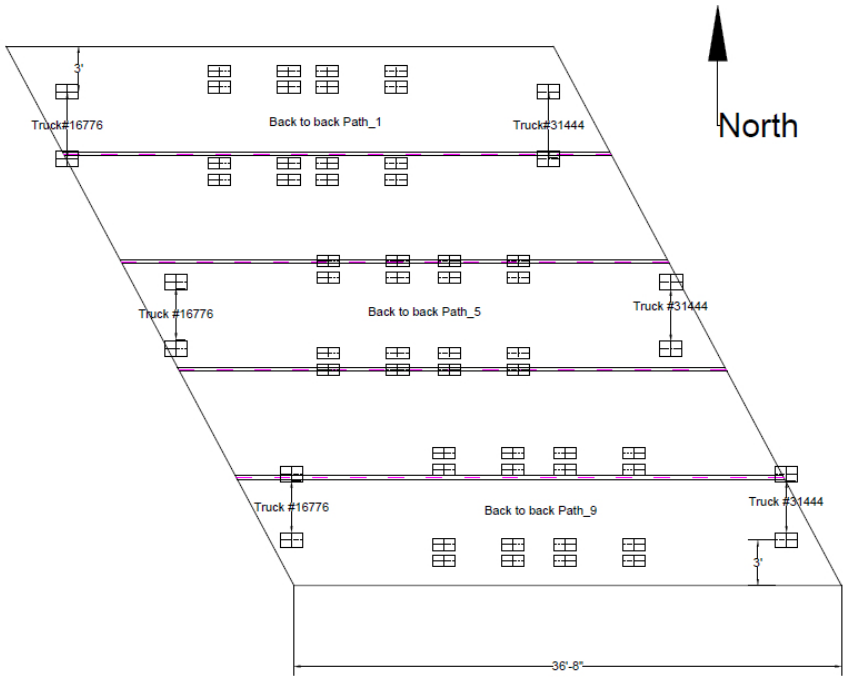

Figure 7.11. Truck positions for third phase of diagnostic testing (Bridge 8761).

Table 7.5. Maximum measured strains for first phase of diagnostic testing (Bridge 8761).

Transducer Location	Strain (με)								
	Path 1	Path 2	Path 3	Path 4	Path 5	Path 6	Path 7	Path 8	Path 9
B1S1	**62**	41	0	-3	-2	0	-2	1	-8
B1S2	58	**50**	32	6	-2	-9	-6	1	-9
B2S1	47	46	40	16	2	0	-2	1	-4
B2S2	16	18	**57**	44	22	-1	-4	1	-6
B3S1	4	6	37	**51**	42	19	4	3	-2
B3S2	-1	-1	2	22	**55**	40	21	9	-1
B4S1	-4	-3	-4	8	48	**51**	44	24	11
B4S2	-3	-3	-2	-1	4	28	**58**	51	32
B5S1	-6	-6	-5	-2	-5	17	56	**60**	51
B5S2	-5	-4	-3	-1	-2	1	2	50	**60**

Table 7.6. Maximum measured strains for second phase of diagnostic testing (Bridge 8761).

Transducer Location	Strain(με)		
	Paths 1 and 3	Paths 4 and 6	Paths 7 and 9
B1S1	99	3	0
B1S2	141	26	0
B2S1	**154**	54	3
B2S2	140	119	16
B3S1	133	**172**	46
B3S2	44	161	107
B4S1	19	136	156
B4S2	2	65	**160**
B5S1	-2	37	154
B5S2	2	5	120

Table 7.7. Maximum measured strains for third phase of diagnostic testing (Bridge 8761).

Transducer Location	Strain(με)		
	Path 1	Path 5	Path 9
B1S1	146	0	0
B1S2	**163**	3	0
B2S1	137	21	-2
B2S2	60	103	0
B3S1	25	**153**	3
B3S2	4	141	22
B4S1	-1	118	69
B4S2	0	23	144
B5S1	0	5	**177**
B5S2	1	3	153

From Table 7.5, the maximum measured strains for the first phase of testing were comparable for symmetrical truck paths and equaled 51 με for paths 4 and 6, 58 με for paths 3 and 7, and 62 με for paths 1 and 9. Only path 2 and path 8 showed a noticeable difference in maximum strains (equal to 50 με for path 2 and 60 με for path 8). Based on these comparisons, it was concluded that the shear keys for Bridge 8761 are functioning. Furthermore, the first phase results showed paths 1, 5, and 9 to be critical since the measured strains were largest for these paths. Consequently, the trucks for the double-truck tests were positioned to maximize the strains in the two exterior beams (i.e., beams 1 and 5) and the middle beam (i.e., beam 3). Table 7.6 lists the maximum strains for the second phase of testing with two trucks placed side-by-side. As shown in the table, the maximum strain for the interior beam was 172 με, which is much less than the estimated strain of 249 με, and the maximum strain for the exterior beam was 160 με, which was also much less than the estimated strain of 232 με. In summary, the maximum measured strains for the interior and exterior beams was approximately 70% of the estimated strains for the second phase of testing, which means that the AASHTO distribution factor was larger than the measured value for Bridge 8761. Recall that the AASHTO distribution factor was actually smaller for Bridge 7701 due to the broken shear keys. The diagnostic test results for Bridge 8761 provide confidence for the proof load test. From Table 7.7, it is evident that the maximum strains during the third phase of testing (i.e., back-to-back truck loading) are larger for the exterior beams compared to the second phase (i.e., side-by-side truck loading). The interior beam did not show the same behavior. In conclusion, the results from the diagnostic testing show that single lane loading controls for the exterior beams and multiple lane loading controls for the interior beam. This information was later used in planning the proof load test.

7.3 BRIDGE NO. 7722, P/C BOX GIRDER

Similar to the other two Doña Ana bridges, a diagnostic load test was performed April 15, 2014 on Bridge 7722, results of which were used to plan the proof test. The bridge was instrumented with a total of 35 strain gages (see Figure 7.12). At mid-span, 19 strain gages were mounted on the bottom flanges of the interior and exterior beams. As shown in Figure 7.13, three bottom gages were installed on beams 1, 2, 4, 6, and 7 while two gages were installed on beams 3 and 5.

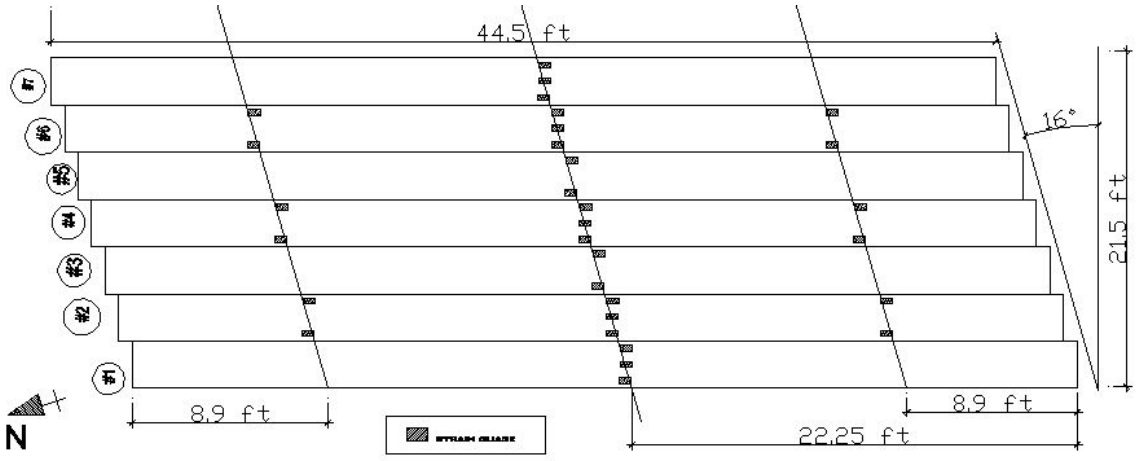

Figure 7.12. Plan view of instrumentation layout for diagnostic load testing (Bridge 7722).

An additional 12 gages were installed on the bottom flanges of interior beams 2, 4, and 6 at 20% of the span from each support and 4 gages were installed on the side faces of exterior beams 1 and 7 (not shown in Figure 7.12). As shown in Figure 7.13, gages were placed under the beam webs and also at the center of the bottom flange of selected beams at mid-span. The figure also shows the gage locations on the side faces of the exterior beams.

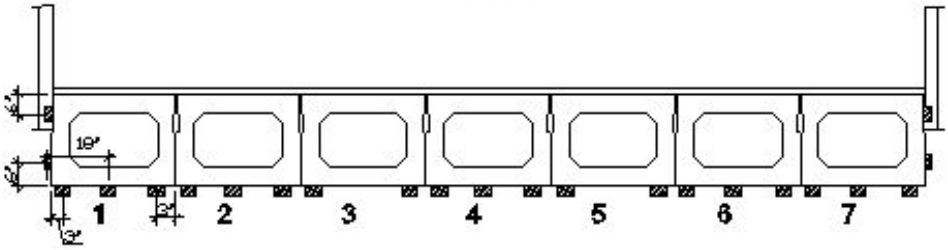

Figure 7.13. Instrumentation layout at midspan for diagnostic load testing (Bridge 7722).

Based on the number of prestressing strands determined previously, the cracking, available, target, and test truck moments for the exterior and interior beams of Bridge 7722 were computed. The cracking moment was determined using Eq. (7.1) given earlier assuming a prestress loss of 30% (which is higher than the 20% used in the Magnel diagrams for the initial prestressing strand estimate) and f_{cr} equal to 6 times the square root of f_c', thus giving a more conservative estimate of the cracking moment. The available moment was found by subtracting the dead load moment from the cracking moment and represented the additional moment the beam could resist before cracking; the dead load moment was the moment due to the beam self-weight and the asphalt wearing surface. A structural analysis was conducted to evaluate the live load moments under the Type-3 legal load and a 40-kip test truck (assuming a 31.1-kip back axle and 8.9-kip front axle). Due to the poor condition of the shear connection, the live load distribution between the exterior and interior beams was uncertain and thus, caution needed to be taken to avoid overloading the beams. Accordingly, the available strain and test truck strain were calculated using Eq. (7.2) given earlier to aid in monitoring the bridge beams during the diagnostic test. Table 7.8 summarizes the moment and strain values determined for the exterior and interior beams of Bridge 7722.

The diagnostic load test of Bridge 7722 included three patterns of loading: single dump truck; two dump trucks side-by-side; and two dump trucks back-to-back. Each dump truck weighed approximately 42.7 kips and the front and rear axle weights were approximately 12.7 kips and 30.0 kips, respectively. For the single truck loading, the truck was centered along five transverse paths (labeled path 1 through path 5) and stopped at several longitudinal locations per path. Since the bridge is skewed 16 degrees, the longitudinal axle locations are parallel to the skew. For each transverse path, the front axle wheels were centered above the loaded box beam in an effort to maximize the bending moments (Figure 7.14 shows paths 3 and 5). The box beams were numbered 1 through 7 from north to south.

Table 7.8. Preparatory calculations for diagnostic load testing of Bridge 7722.

Variable	Exterior	Interior
f_c' (psi)	4500	4500
E (ksi)	3824	3824
S_b (in^3)	3964	3964
Number of Strands	14	16
Area per Strand (in^2)	0.108	0.080
P_e (kip)	185.2	156.8
e (in.)	11.5	10.5
M_{cr} (kip-ft) *	418.3	361.4
M_{dl} (kip-ft)	195.0	170.5
$M_{available}$ (kip-ft)	223.3	190.9
M_{truck} (kip-ft) ***	74.6	74.6
M_{Type3} (kip-ft) ***	115.6	115.6
$\varepsilon_{available}$ (με) **	176.5	151.1
ε_{truck} (με) **	59.1	59.1
ε_{Type3} (με) **	91.5	91.5

Notes: * - Computed based on allowable tension of 6 times square root of f_c'.
** - Computed at bottom of beam section.
*** - Computed based on load distribution factor of 0.429 for the interior and exterior beams, and impact factor of 1.33 (for Type 3 legal load only).

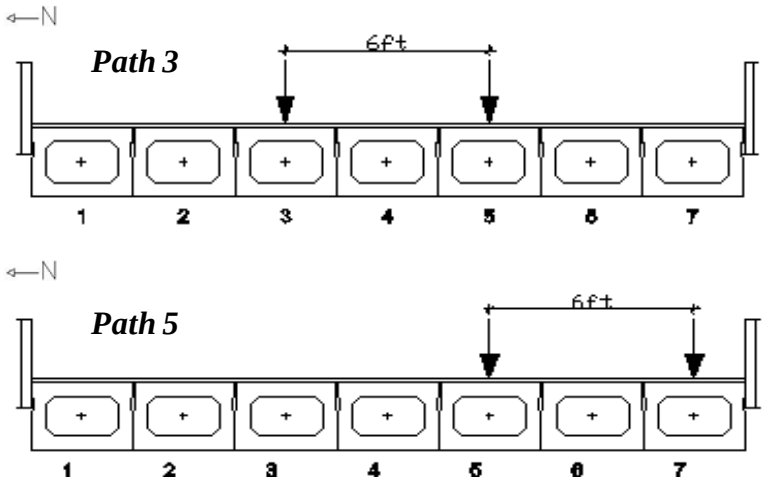

Figure 7.14. Transverse truck paths 3 and 5 for first phase of diagnostic testing (Bridge 7722).

Table 7.9 shows the measured beam strains under single truck loading for the five transverse paths with the rear axle located at midspan. The results represent the maximum strains recorded at the gages installed at the bottom of the beams at midspan. The transducers are labeled B#G# from north to south according to the beam number and gage position on the beam cross-section (e.g., B3G1 through B3G3 denotes the north, center, and south gages of beam 3).

Table 7.9. Maximum measured strains for first phase of diagnostic testing (Bridge 7722).

Transducer Location	Strain (με)				
	Path 1	Path 2	Path 3	Path 4	Path 5
B1G2	**46**	10	3	5	-3
B2G2	20	**31**	23	15	6
B3G1	20	27	31	22	10
B3G3	25	30	**31**	21	10
B4G2	20	30	27	29	15
B5G1	15	19	27	26	20
B5G3	15	20	29	22	20
B6G2	12	16	22	**38**	11
B7G2	2	0	2	4	**49**

From Table 7.9, the largest measured strains were 46 με and 49 με at the exterior beams 1 and 7, respectively, for transverse paths 1 and 5. Consequently, in the second phase of loading, two dump trucks were placed side-by-side with the first truck positioned in either path 1 or path 5 and the second truck placed adjacent to the first truck in an effort to maximize the measured strains. As shown in Figure 7.15, the dump trucks were positioned in paths 1 and 4, paths 2 and 5, and paths 2 and 4 (not shown in figure). The maximum midspan strains are reported in Table 7.10.

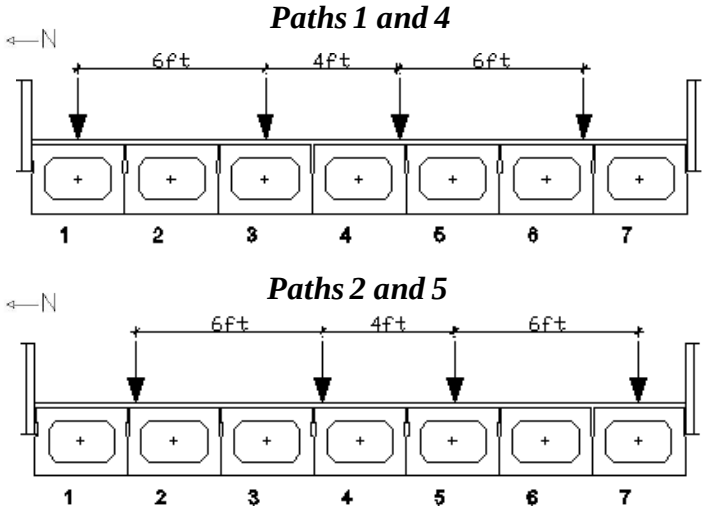

Figure 7.15. Transverse truck paths 1-4 and 2-5 for second phase of diagnostic testing (Bridge 7722).

Table 7.10. Maximum measured strains for second phase of diagnostic testing (Bridge 7722).

Transducer Location	Strain (με)		
	Paths 1 and 4	Paths 2 and 4	Paths 2 and 5
B1G2	**55**	33	19
B2G2	27	35	40
B3G1	41	38	38
B3G3	45	40	40
B4G2	42	**47**	45
B5G1	29	38	35
B5G3	26	37	34
B6G2	44	36	31
B7G2	-5	37	**51**

Comparison of the measured strains for paths 1 and 4 from Table 7.10 with paths 2 and 5 showed a strong correlation, indicating that the bridge behavior was symmetrical. The maximum strains for the different paths were 55 με (beam 1), 47 με (beam 4), and 51 με (beam 7) which are close in magnitude to the estimated strain of 59 με reported earlier in Table 7.8, particularly for the exterior beams. Based on these results, the two trucks were placed back-to-back in the third phase of testing in paths 1, 3, and 5 to maximum the strains in the two exterior beams and the middle interior beam; Table 7.11 lists the maximum measured strains during this testing phase. Strains as high as 78 με and 77 με at beam 1 and beam 7, respectively, were recorded. However, a strain of 46 με was recorded at beam 3 which is a clear indication that the shear keys between the interior beams are functioning well compared to the shear keys between the exterior and interior beams. The measured strains given in Tables 7.9, 7.10, and 7.11 were used to plan the proof load test.

Table 7.11. Maximum measured strains for third phase of diagnostic testing (Bridge 7722).

Transducer Location	Strain (με)		
	Path 1	Path 3	Path 5
B1G2	**78**	6	1
B2G2	30	39	11
B3G1	34	39	18
B3G3	31	**43**	14
B4G2	27	37	28
B5G1	18	36	27
B5G3	17	36	31
B6G2	12	36	27
B7G2	8	7	**77**

8. PROOF LOAD TESTS

Proof load tests were planned and executed on the five prestressed concrete bridges. For Bridges 7701, 8761 and 7722, diagnostic tests were used to plan the proof tests as discussed earlier. The dump trucks were loaded heavier for the proof tests and were applied along the critical transverse paths from the diagnostic tests. For box beam Bridge 8825 and I-girder Bridge 8588, no diagnostic load tests were conducted since the bridges were in good condition (i.e., there was no evidence of widening or uncertainties of the load paths that warranted diagnostic tests be conducted first).

The goal of each proof test was to maximize the midspan moment of the bridge without exceeding the cracking moment. Since the strain gauges were positioned strictly for measuring the flexural response at midspan, shear checks were also made to ensure the bridge beams would not crack near the supports due to diagonal tension. The proof tests were executed in multiple phases, with each phase using a single truck or multiple truck combination to maximize the bending moment. Ultimately, the final truck positions from each proof test were used for load rating the bridges based on serviceability as all tests were limited by concrete cracking. Final serviceability-based ratings were calculated in accordance with the AASHTO *Manual*.

8.1 BRIDGE NO. 7701, P/C DOUBLE T-BEAM

The proof load test was planned based off the critical paths determined from the diagnostic test. Under single truck loading, paths 5 and 7 (see Figure 7.1) were the most critical and under two truck loading, paths 3 and 7 loaded simultaneously side-by-side (see Figure 7.5) resulted in the highest amount of strain. From these results, a four-phase proof test was planned. For the first phase of the proof test, the tandem back axle of a single truck weighing roughly 42 kips was applied. The truck was centered in paths 5 and 7, and backed up in the same way as the diagnostic test (see Figure 7.2). Note that the more critical of the two paths (i.e., the one producing the most strain), was then used in phase three, where two trucks were placed back-to-back on the bridge to simulate single lane loading. For the second phase of the proof test, two trucks were placed side-by-side, first in paths 1 and 5 and then in paths 3 and 7. Recall that paths 3 and 7 caused the most strain in the diagnostic test; however, paths 1 and 5 were also considered to ensure the results were consistent. Similarly to phase one, the two trucks each had a back axle weight of approximately 42 kips, and were incrementally stopped along the length of the bridge. The more critical loading configuration was then used in phase four, where four trucks were placed side-by-side and back-to-back on the bridge.

The instrumentation setup for the proof test was similar to that of the diagnostic test, however, a few minor adjustments were made. For the proof test, no deflection transducers were used since the measured displacements from the diagnostic test were erroneous. In addition, it was decided that using more strain transducers for the proof test was necessary to more closely monitor the bridge response under the heavier loading along with acoustic emission sensors (see Appendix B). A total of 36 strain transducers were used with the majority placed at midspan as shown in Figure 8.1. All nine beams had at least two transducers at midspan. The diagnostic test results showed that the critical region with the highest strains was at beams 4 through 7; therefore, these four beams were instrumented with more gages at midspan. Similarly to the diagnostic test, transducers were also placed at the third points to determine if there was any support fixity.

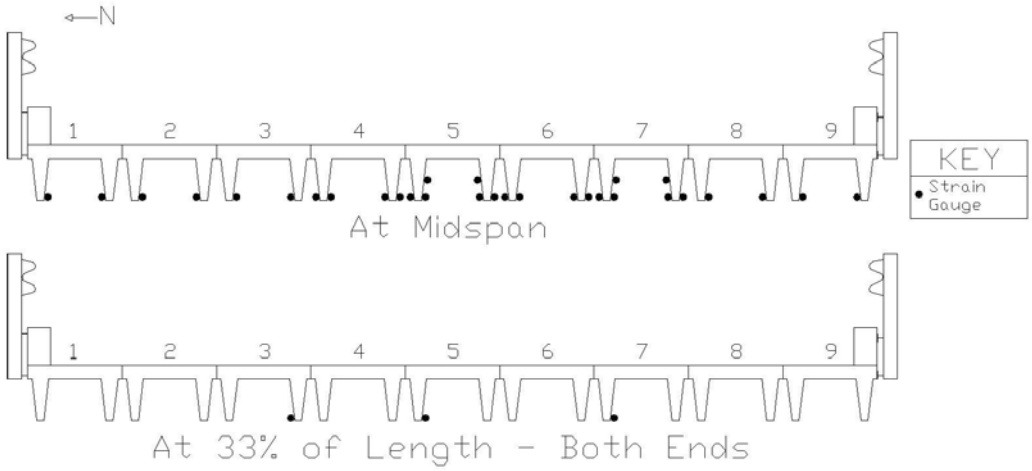

Figure 8.1. Instrumentation layout for proof load testing (Bridge 7701).

Using the modulus of rupture of $7.5(f_c')^{1/2}$ and prestress losses of 25%, the cracking and available moments amounted to 148.4 kip-ft and 112.6 kip-ft, respectively, and the available strain was 532 με. Note that this magnitude of strain is slightly larger than the value of 493 με used in preparation for the diagnostic test (see Table 7.1) which was computed assuming 30% losses. In all phases of testing, the proof test was stopped when the measured strains were approaching 532 με.

From the diagnostic test, the truck configuration that produced the maximum strain of 312 με corresponded to a single lane moment of 188 kip-ft. Using the maximum strain, the girder moment was computed to be 66.0 kip-ft by multiplying the strain, section modulus, and modulus of elasticity. The ratio of the available girder moment (112.6 kip-ft) to the girder moment from the diagnostic test was then computed as 1.71. This ratio was multiplied by the 188 kip-ft diagnostic test moment to estimate the maximum proof test moment, which amounted to 321 kip-ft. To have an idea of when this moment would be achieved during the proof test, 38-kip tandem axles were theoretically placed in two and four truck configurations. For two trucks, the applied moment was less than 321 kip-ft. However, for four trucks, the applied moment reached 321 kip-ft when the front of the tandem axles were placed approximately 6.0 feet from the supports. Based on this analysis, it was anticipated that the four truck loading would have to be stopped before the tandem axles reached the final positions on the bridge near midspan.

To check that no damage (i.e., cracking) would occur to the bridge beams due to shear, a thorough shear capacity evaluation was done. Assuming a shear distribution factor of one, the maximum shear for a single beam caused by 40-kip tandem axles placed back-to-back was computed as 20.0 kips. The web-shear cracking force, V_{cw}, was taken as the beam shear capacity and estimated using the following formula (Hawkins et al. 2005):

$$V_{cw} = f_t\sqrt{1 + \frac{f_{pc}}{f_t}}\, b_w d + V_p \qquad \text{(Eq. 8.1)}$$

where f_t is the tensile concrete strength; f_{pc} is the compressive concrete stress after all losses at beam centroid; b_w is the beam web width; d is the distance from the compression face to the centroid of the tension reinforcement (not less than 80% of overall beam depth); and V_p is the vertical component of the effective prestressing force. The tensile concrete strength varies between 2 and 4 times the square root of f_c' (equal to 5 ksi); the former value provides the better estimate for reinforced concrete members or prestressed concrete members with a low level of prestressing while the latter value is more accurate for end regions of fully prestressed members (Hawkins et al. 2005). Applying Eq. (8.1) with these two values, V_{cw} ranged between 27.2 kips and 41.9 kips, which exceeded the sum of the ultimate live load shear of 20.0 kips and dead load shear of 5.0 kips. Thus, concrete cracking due to shear was not expected.

The proof load test took place on Wednesday, March 26th, 2014 and required approximately eight hours to complete. As mentioned previously, the proof test was executed in four phases. The first phase consisted of loading the bridge with the back tandem axle of a single truck, weighing approximately 42 kips. The axle was stopped in two feet increments along the bridge length. This was done along paths 5 and 7 shown previously in Figure 7.1. In both cases, the truck was able to reach the final position (with the front of the rear axle located 14 feet from the support) without exceeding the available strain. Figure 8.2(a) shows the final longitudinal position of the two trucks. Table 8.1 lists the measured strains in phase one of the proof test. Recall that beams 4 through 7 had two transducers attached to the bottom of each stem; however, only the larger of the two recorded strains are reported for all phases of the proof test. The gages are labeled the same as the diagnostic test. It can be seen from Table 8.1 that path 5, centered along beam 6, produced the highest strain of 508 με. Consequently, path 5 was used for the third phase of the test where two trucks were placed back-to-back simulating a single loaded lane.

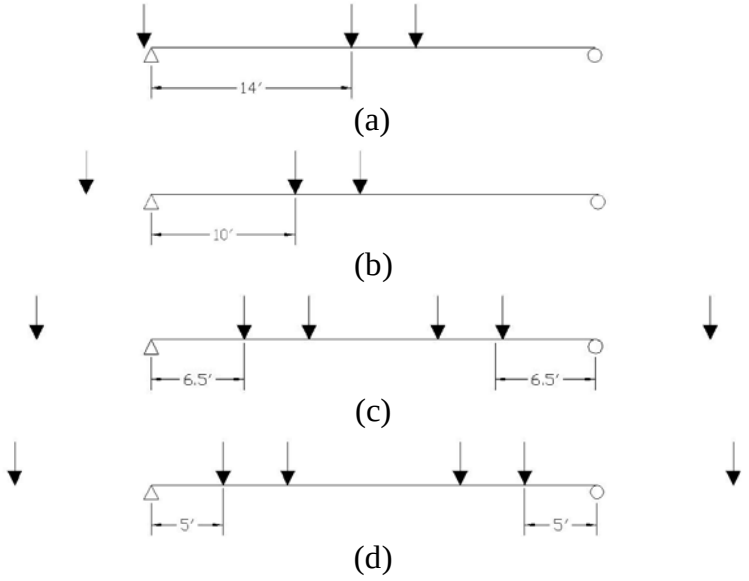

Figure 8.2. Final longitudinal truck positions for (a) first, (b) second, (c) third, and (d) fourth phase of proof testing (Bridge 7701).

Table 8.1. Maximum measured strains for first phase of proof testing (Bridge 7701).

Transducer Location	Strain (με)	
	Path 5	Path 7
B1S1	0	-2
B1S2	1	-6
B2S1	4	2
B2S2	6	-3
B3S1	3	10
B3S2	21	9
B4S1	21	21
B4S2	38	33
B5S1	**508**	94
B5S2	372	157
B6S1	339	172
B6S2	279	269
B7S1	275	**348**
B7S2	213	189
B8S1	223	186
B8S2	87	277
B9S1	79	243
B9S2	56	175

For phase two, two trucks were placed side-by-side first in paths 1 and 5, then in paths 3 and 7, which were the critical paths in the diagnostic test. In both cases, the test was stopped once the rear axles reached 10 feet (see Figure 8.2(b)) since the measured strains at one of the transducers was very close to the available strain of 532 με. Table 8.2 lists the maximum measured strains from phase two of the proof test. The table values show that paths 3 and 7 produced a higher strain than paths 1 and 5. Therefore, for phase four, the four trucks were placed side-by-side and back-to-back in paths 3 and 7 to simulate the most critical multiple lanes loaded condition.

In phase three, as mentioned previously, two trucks were placed back-to-back along the critical path 5, to simulate a single lane loaded condition. In phase four, all four trucks were placed on the bridge. On both ends of the bridge, two trucks were placed in paths 3 and 7, simulating the most critical multiple lanes loaded condition. Table 8.3 shows the measured strains for these test phases. The trucks were stopped when the rear axles were at 6.5 feet in phase three (see Figure 8.2(c)) and 5.0 feet in phase four (see Figure 8.2(d)) since the measured strain was close to the available strain.

Based on strains given in Table 8.1 through Table 8.3, a load rating factor is determined later from the proof test. For all four phases, the moments applied to the bridge from the test truck loading are used to determine the final load ratings for New Mexico legal loads in accordance with the AASHTO *Manual*. Recall that the available strain used to monitor the beams during the proof test was based on 7.5 times the square root of f_c'; to determine the final load ratings, the test truck moments that produce the available strain based on the allowable stress of concrete of 6 times the square root of f_c' will be estimated. This will lower the available moment of the bridge since the moment is based on an allowable stress limit rather than the modulus of rupture.

Table 8.2. Maximum measured strains for second phase of proof testing (Bridge 7701).

Transducer Location	Strain (με)	
	Paths 1 and 5	Paths 3 and 7
B1S1	149	62
B1S2	235	80
B2S1	228	83
B2S2	255	224
B3S1	248	191
B3S2	341	197
B4S1	363	182
B4S2	**474**	158
B5S1	448	**528**
B5S2	391	470
B6S1	367	455
B6S2	239	316
B7S1	245	443
B7S2	233	227
B8S1	247	220
B8S2	105	266
B9S1	99	250
B9S2	68	140

Table 8.3. Maximum measured strains for third and fourth phases of proof testing (Bridge 7701).

Transducer Location	Strain (με)	
	Path 5, Phase Three, Single Lane Loading	Paths 3 and 7, Phase Four, Multiple Lane Loading
B1S1	18	84
B1S2	11	115
B2S1	17	111
B2S2	28	195
B3S1	24	161
B3S2	55	203
B4S1	63	196
B4S2	82	205
B5S1	**496**	**494**
B5S2	407	456
B6S1	432	450
B6S2	348	344
B7S1	360	471
B7S2	242	289
B8S1	280	279
B8S2	146	288
B9S1	151	258
B9S2	93	228

8.2 BRIDGE NO. 8761, P/C DOUBLE T-BEAM

The proof load test of Bridge 8761 was conducted on Thursday, May 22, 2014. The goal of the test was to experimentally prove that the bridge was capable of supporting an HS-20 design truck and State legal load without cracking. To monitor the bridge response, 36 strain gauges were installed as shown in Figure 8.3. The gauges were placed at mid-span, and 20% and 80% of the bridge length on the beam stems; 32 gauges were placed 1 inch from the bottom of the beam and 4 gauges were placed 12 inches from the bottom. Both sides of the beam stems were instrumented at midspan towards the bottom since the proof test of Bridge 7701 showed significant differences in strain at these gage locations. Recall that the available strains for the exterior and interior beams of Bridge 8761 are 303 με and 562 με (see Table 7.4), respectively.

The proof load test consisted of three phases: phase one – two trucks placed side-by-side; phase two – three trucks placed side-by-side; and phase three – four trucks placed side-by-side and back-to-back. In each phase, the trucks were transversely positioned to maximize the load effects on beams 1, 3, and 5 (i.e., the two exterior beams and the center interior beam). Table 8.4 lists the axle weights of the four dump trucks used in the proof test. The axle spacings are 14.5 feet between the first and second axles, and 4.5 feet between the second and third axles. Similar to Bridge 7701, the beams of Bridge 8761 were evaluated for shear to check the possibility of web-shear cracking under proof loading. A structural analysis of the bridge resulted in an ultimate shear under dead and live load of 50.6 kips and 51.1 kips for the interior and exterior beams, respectively. Using Eq. (8.1), V_{cw} ranged from 56.8 kips to 91.9 kips for the interior beam and from 53.1 kips to 88.3 kips for the exterior beam. Thus, concrete cracking due to shear was not expected.

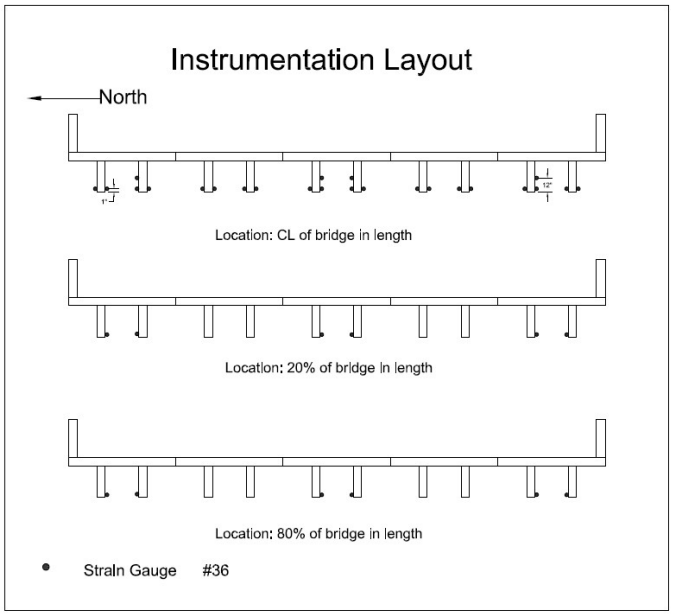

Figure 8.3. Instrumentation layout for proof load testing (Bridge 8761).

Table 8.4. Axle weights of proof test trucks (Bridge 8761).

Truck Number	Axle Weight (kips)		
	Front Single	Rear Tandem	Total
37589	16.00	40.40	56.40
31444	14.10	42.30	56.40
36977	15.84	39.88	55.72
16776	15.28	39.96	55.24

Two trucks were placed side-by-side in phase one with the front of the back axles at 0 feet, 4 feet, 8 feet, 12 feet, 16 feet, and 18 feet from the support bearing for each path. The truck positions are similar to those of the diagnostic test shown in Figure 7.10. The only difference is that truck #16776 was replaced with #37589. Table 8.5 lists the maximum strains recorded on each beam stem for phase one; the maximum strain for the interior beam was 264 με which is less than the available strain of 562 με while the maximum strain for the exterior beam was 213 με which is less than the available strain of 303 με. Note that the weights of the rear axles in the proof test were about 43% larger than the diagnostic test. The ratio of the maximum strains between the proof and diagnostic tests ranged between 1.36 and 1.51 which shows that the bridge behavior was linear. In phase two, three trucks were placed side-by-side as shown in Figure 8.4 and the maximum strains are given in Table 8.6. Compared to phase one, the strains increased in phase two (due to the larger distribution factor) but remained significantly below the available strains for the exterior and interior beams.

Table 8.5. Maximum measured strains for first phase of proof testing (Bridge 8761).

Transducer Location	Strain(με)		
	Paths 1 and 3	Paths 4 and 6	Paths 7 and 9
B1S1	203	22	9
B1S2	**213**	46	5
B2S1	**220**	93	11
B2S2	206	186	35
B3S1	201	258	115
B3S2	80	**264**	196
B4S1	25	235	**277**
B4S2	4	139	236
B5S1	-10	66	**209**
B5S2	-7	41	141

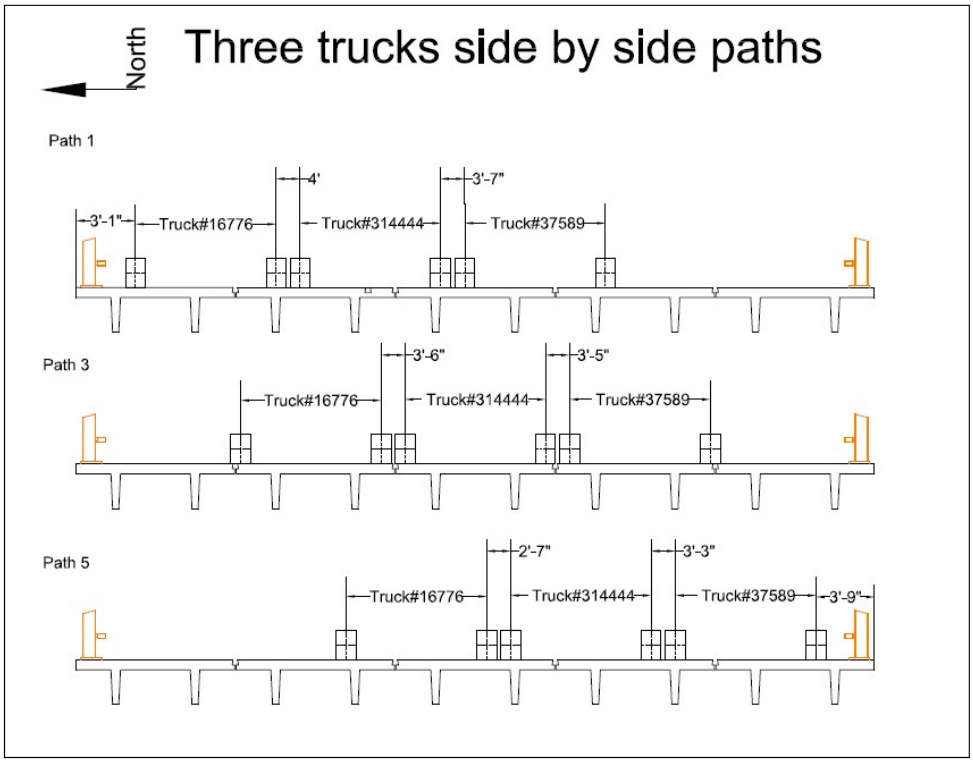

Figure 8.4. Transverse truck paths 1-3-5, 3-5-7, and 5-7-9 for second phase of proof testing (Bridge 8761).

Table 8.6. Maximum measured strains for second phase of proof testing (Bridge 8761).

Transducer Location	Strain(με)		
	Paths 1, 3, and 5	Paths 3, 5, and 7	Paths 5, 7, and 9
B1S1	212	36	32
B1S2	**218**	159	66
B2S1	230	175	136
B2S2	240	231	196
B3S1	**277**	307	**310**
B3S2	258	260	252
B4S1	227	**313**	286
B4S2	142	211	249
B5S1	66	193	**217**
B5S2	22	57	160

An important finding from phases one and two is that the test moment (per lane) produced by the dump trucks was approximately 335.0 kip-ft which is 89% of the AASHTO Type 3 moment (equal to 376.0 kip-ft) and 71% of the AASHTO HS-20 moment (equal to 471.0 kip-ft). This comparison shows that the target moment could not be achieved with side-by-side trucks only. A larger load is required since the trucks are already loaded as heavily as possible. Consequently, four trucks

were placed side-by-side and back-to-back in phase three to reach the target moments. The trucks were placed in the same paths as phase one and Table 8.7 shows the maximum measured strains.

Table 8.7. Maximum measured strains for third phase of proof testing (Bridge 8761).

Transducer Location	Strain(με)		
	Paths 1 and 3	Paths 4 and 6	Paths 7 and 9
B1S1	268	-14	7
B1S2	**323**	48	6
B2S1	280	135	17
B2S2	307	230	53
B3S1	**341**	**355**	154
B3S2	163	326	283
B4S1	67	335	**399**
B4S2	21	195	348
B5S1	-2	81	**308**
B5S2	3	6	209

As shown in Table 8.7, the maximum strain at the exterior beam was 323 με which is slightly larger than the available strain of 303 με. However, the available strain was estimated conservatively using a 28-day concrete strength of 6 ksi (which is less than the estimated strength from the Windsor probe) and also an allowable tension of 6 times the square root of f_c' (which is less than the modulus of rupture). The exterior beam was inspected carefully after the proof test and no flexural cracks were found. The maximum strain for the interior beam was 399 με which is significantly less than the available strain of 562 με. Note that the one lane moment produced by the test trucks in phase four was approximately 480 kip-ft. This moment is 102% of the HS-20 truck moment (equal to 471.0 kip-ft) and 127% of the Type 3 truck moment (equal to 376.0 kip-ft). Thus, the proof test showed the bridge supported the target load without cracking. This information will be used later to establish the final load ratings for Bridge 8761.

8.3 BRIDGE NO. 7722, P/C BOX GIRDER

The proof test of Bridge 7722 was planned based on the critical truck paths identified in the diagnostic test (discussed earlier) and was executed on September 10th, 2014. The test was completed in collaboration between the NMDOT and NMSU. Traffic was closed on the day of testing and the truck weights were measured using fixed scales by the NMDOT the day prior to the test.

The test included four patterns of loading: single dump truck; two dump trucks side-by-side; two dump trucks back-to-back; and four dump trucks (side-by-side and back-to-back). As in the diagnostic test, the loading patterns were selected to represent both one lane loaded and two or more lanes loaded conditions. The single truck loading and two trucks back-to-back loadings simulated the single lane loaded condition while two trucks side-by-side and four trucks (side-by-side and back-to-back) simulated the multiple lane loaded condition. As many as four dump trucks

were used in the proof test and each truck weighed approximately 60 kips; the front and rear axle weights averaged 15 kips and 45 kips, respectively. Table 8.8 summarizes the test vehicle axle and gross weights.

Table 8.8. Axle weights of proof test trucks (Bridge 7722).

Truck Number	Axle Weight (kips)		
	Front Single	Rear Tandem	Total
17124	14.30	44.60	58.90
17127	15.20	48.20	63.40
31765	13.80	45.60	59.40
37823	15.74	42.40	58.14

No changes were made to the instrumentation plan for the proof test of Bridge 7722. The first phase of loading consisted of a single truck centered along three transverse paths (labeled path 1, path 3 and path 5) as shown in Figure 8.5 and stopped at several longitudinal locations per path. Recall that maximum strains of 46 με and 49 με were recorded at the exterior beams 1 and 7, respectively, for paths 1 and 5 from the diagnostic test. Also, path 3 resulted in a maximum strain of 31 με for the interior beams.

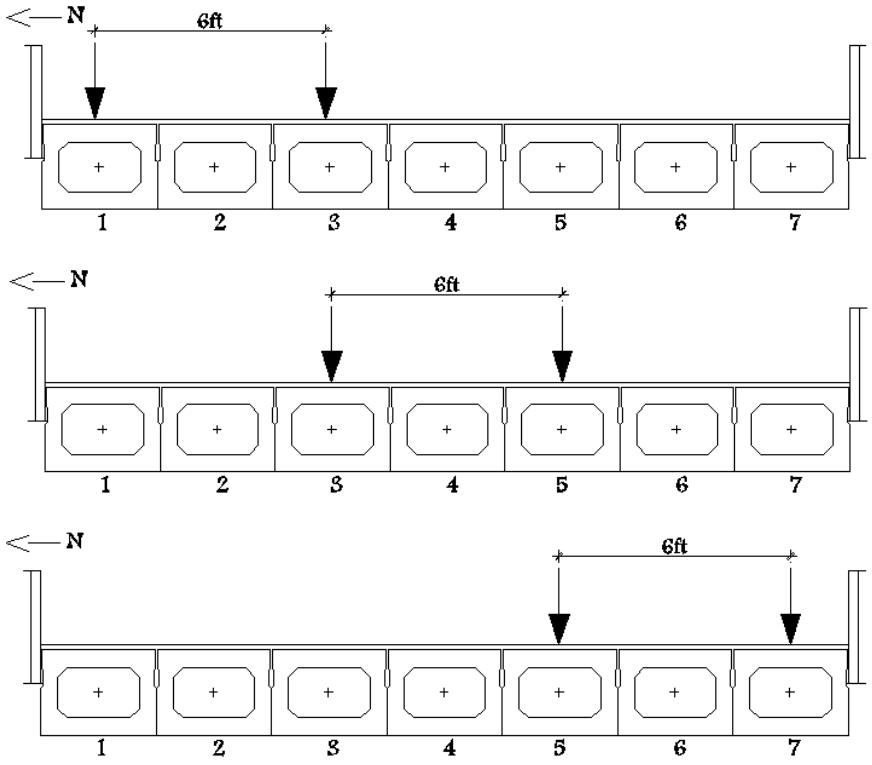

Figure 8.5. Transverse trucks paths 1, 3, and 5 for first and third phases of proof testing (Bridge 7722).

The second phase of loading was two trucks side-by-side. The trucks were backed up one at a time, leaving them staggered for only a few moments. Two trucks side-by-side loading (path 1-4 and path 2-5) are shown in Figure 8.6. The third and fourth phases of loading consisted of two trucks back-to-back and four trucks (side-by-side and back-to-back). To reduce the duration of the test, two trucks first were backed up to midspan of the bridge in the lane closest to the rail and strain measurements were taken (representing two trucks back-to-back in one lane). Subsequently, the other two trucks were backed up to midspan (adjacent to the first two trucks already at midspan) and the strains caused by four trucks (side-to-side and back-to-back) were recorded. Figures 8.5 and 8.6 show the two trucks (back-to-back) and four trucks (side-by-side and back-to-back) loading cases for phases three and four, respectively, which were similar to phases one and two.

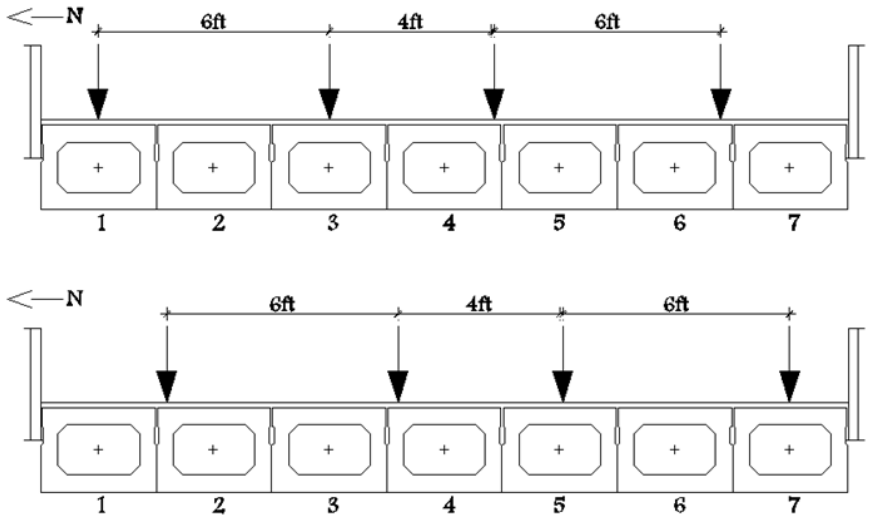

Figure 8.6. Transverse truck paths 1-4 and 2-5 for second and fourth phases of proof testing (Bridge 7722).

The preparatory calculations for the proof test of Bridge 7722 involved computation of the expected strains for the interior and exterior beams. The expected strains were computed using two methods. The first method utilized the test results from the diagnostic test. In this approach, a linear relationship between the applied load and measured strain was assumed based on the ratio between the weights of the proof test and the diagnostic test trucks (equal to approximately 1.41). The strains measured in the diagnostic test were magnified by this truck ratio to obtain an estimate of the expected strains for the proof load test. Table 8.9 reports the results of the expected strains using this method. A simple analytical model was used in the second method. Using the average truck weight of the test vehicles, the maximum moments were obtained and corresponding strains were estimated as 85 με and 125 με for single truck and two trucks back-to-back loading, respectively. Recall that the available moment was found by subtracting the dead load moment from the cracking moment and thus, represented the additional moment the beam could resist before cracking. Therefore, the available strains for the exterior and interior beams remained the same as the diagnostic test (151 με for an interior beam and 177 με for an exterior beam).

Table 8.9. Expected proof test strains based on diagnostic test results (Bridge 7722).

Loading Pattern	Beam Designation	Measured Diagnostic Test Strain (με)	Expected Proof Test Strain (με) *
Single truck	Exterior	49	69
	Interior	38	53
Two trucks side-by-side	Exterior	55	77
	Interior	47	66
Two trucks back-to-back	Exterior	78	110
	Interior	43	60

* Equal to measured diagnostic test strain times truck weight ratio of 1.41.

To check that no damage (i.e., cracking) would occur to the bridge beams due to shear, a thorough shear capacity evaluation was done. Assuming a shear distribution factor of one, the maximum shear for a single beam caused by 48.2-kip tandem axles (i.e., the largest truck axle load) placed back-to-back was computed as 24.1 kips. Using Eq. (8.1) given earlier, the web-shear cracking force, V_{cw}, was computed as the beam shear capacity and ranged between 50.4 kips and 86.0 kips, which significantly exceeded the sum of the ultimate live load shear of 24.1 kips and dead load shear of 17.0 kips. Thus, concrete cracking due to shear was not expected.

All the box beams had two or more transducers attached to the bottom flange for redundancy purposes; however, only the larger of the recorded strains were reported for all phases of the proof test. Table 8.10 shows the measured beam strains under single truck loading for the three transverse paths with the rear axle located at midspan. The values represent the maximum strains recorded at the gauges installed at the bottom of the beams at midspan.

Table 8.10. Maximum measured strains for first and second phases of proof testing (Bridge 7722).

Transducer Location	Strain (με)				
	Phase One			Phase Two	
	Path 1	Path 3	Path 5	Path 1-4	Path 2-5
B1G2	**78**	-----	-----	**81**	-----
B2G2	24	30	-----	47	-----
B3G1	38	43	15	60	54
B3G3	36	44	16	63	52
B4G2	32	**46**	31	71	80
B5G1	16	44	42	46	74
B5G3	18	44	43	49	70
B6G2	-----	32	29	-----	38
B7G2	-----	-----	**84**	-----	**90**

From Table 8.10, the largest measured strains were 78 με, 46 με, and 84 με at beams 1, 4 and 7, respectively, for paths 1, 3 and 5. Note that the reported maximum strains are substantially less

than the available strain of 151 με and 177 με for the interior and exterior beams, respectively. Furthermore, the exterior beam strains exceeded the estimated strain of 69 με (based on linear behavior) which indicates that the load distribution factor was larger for the proof test compared to the diagnostic test due to the poor shear key connection. At the interior beam the measured strain agreed with the estimated strain of 44 με since the shear keys were in better condition.

In the second phase of loading, an effort was made to maximize the measured strains at the exterior beams. Two dump trucks were placed side-by-side with the first truck positioned above beam 1 or beam 5 and the second truck was placed adjacent to the first truck. As shown previously in Figure 8.6, the dump trucks were positioned in paths 1-4 and paths 2-5; maximum midspan strains are reported in Table 8.10. The maximum strains were 81 με (beam 1) and 90 με (beam 7) which are only 6% higher than the recorded strains for single truck loading. In addition, the maximum strains for side-by-side loading remained significantly less than the available strains. Note that the target moment could not be achieved with either single truck or two trucks side-by-side loading, therefore a larger load is required. However, the trucks are already loaded as heavily as possible. To produce a larger load effect, another loading pattern is needed.

Two trucks back-to-back and four trucks (side-by-side and back-to-back) were placed in the third and fourth phases, respectively, to reach the target moments. The trucks were placed along the same paths as phases one and two (see Figures 8.5 and 8.6). Table 8.11 shows the maximum measured strains for phases three and four. Strains as high as 126 με and 136 με at beams 1 and 7, respectively, were recorded for phase three and a maximum of 132 με for phase four, also at the exterior beams. The maximum strains for the interior beams were 67 με and 116 με for phases three and four, respectively. Note that these maximum strains were 23% less than the available strains of 177 με and 151 με for the exterior and interior beams, respectively, which showed that the bridge was able to easily carry the largest test truck loading without cracking.

Table 8.11. Maximum measured strains for third and fourth phases of proof testing (Bridge 7722).

Transducer Location	Strain (με)				
	Phase Three			Phase Four	
	Path 1	Path 3 *	Path 5	Path 1-4	Path 2-5
B1G2	**126**	-----	-----	**132**	-----
B2G2	61	-----	-----	93	-----
B3G1	56	-----	30	89	85
B3G3	54	-----	23	89	75
B4G2	57	-----	47	107	116
B5G1	43	-----	62	81	104
B5G3	46	-----	67	84	102
B6G2	-----	-----	27	-----	54
B7G2	-----	-----	**136**	-----	**132**

* Path 3 was omitted in phase three since exterior beam was critical.

Based on the strains given in Tables 8.10 and 8.11, load rating factors were determined from the proof test. Later, the moments applied to the bridge from the test truck loading are used to determine the final load ratings for AASHTO and New Mexico legal loads in accordance with the AASHTO *Manual*.

8.4 BRIDGE NO. 8825, P/C BOX GIRDER

Due to the good condition of Bridge 8825, a diagnostic test was not considered necessary. A proof test was planned based on previous experience with other bridges and conducted on Tuesday, July 22, 2014. The test was successfully completed through collaboration between NMSU and several agencies including: NMDOT (dump trucks and operators); New Mexico Department of Public Safety (portable scales and axle weight measurements); and City of Albuquerque (traffic control).

The instrumentation layout was planned to evaluate the following: (1) midspan bottom flange strains of all ten beams; (2) level of fixity at the ends of three interior beams; (3) neutral axis location at midspan of the two exterior beams; and (4) lateral load distribution between beams. At mid-span, a total of 26 strain transducers were mounted on the bottom flanges of the interior and exterior beams (see Figure 8.7). As shown in Figure 8.8, three transducers were installed on the soffit of six beams (1, 3, 5, 6, 8 and 10) while two transducers were installed on four beams (2, 4, 7 and 9). The gauges were placed under the beam webs and also at the center of the bottom flange of selected beams. An additional six gauges were installed on the bottom flanges of interior beams 1, 3, and 5 at 20% and 80% of the span and four more gages were installed on the side faces of exterior beams 1 and 10 (see Figure 8.8).

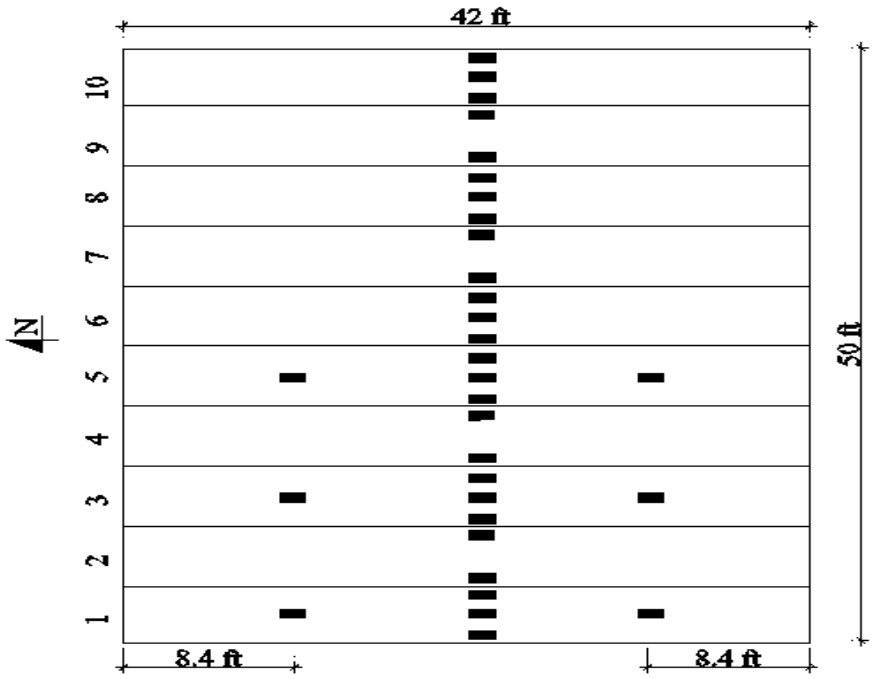

Figure 8.7. Plan view of instrumentation layout for proof load testing (Bridge 8825).

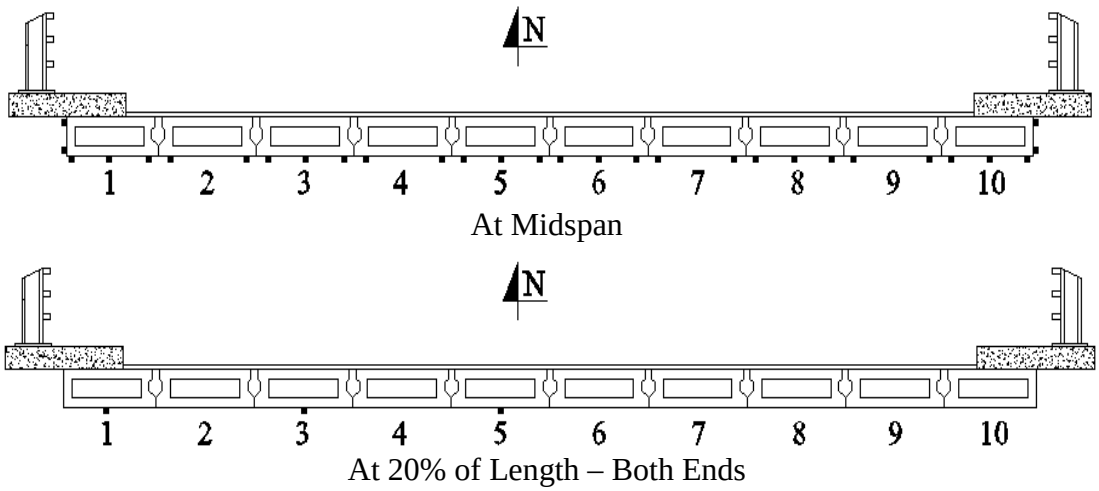

Figure 8.8. Cross section view of instrumentation layout for proof load testing (Bridge 8825).

The test included five phases of loading: phase one – single dump truck (one lane loaded); phase two – two dump trucks side-by-side (multiple lanes loaded); phase three – two dump trucks back-to-back (one lane loaded); phase four – four dump trucks side-by-side and back-to-back (multiple lanes loaded); and phase five – four trucks side-by-side (multiple lanes loaded). Figures 8.9, 8.10, and 8.11 show the truck positions for phases one, two and five, respectively. For phase four, the trucks were positioned along the same paths as phase two. To reduce the duration of the proof test, two trucks were first backed up to the midspan of the bridge (i.e., phase three) and strain measurements were taken with the trucks in paths 1 and 3 (similar to the single truck paths given in Figure 8.9). Then, the last two trucks were backed up on the bridge while keeping the first two trucks at midspan resulting in four trucks placed side-to-side and back-to-back (i.e., phase four). Each dump truck weighed roughly 58.0 kips and the front and rear axle weights were about 15.0 kips and 43.0 kips, respectively. Table 8.12 summarizes the actual weights of the test vehicles.

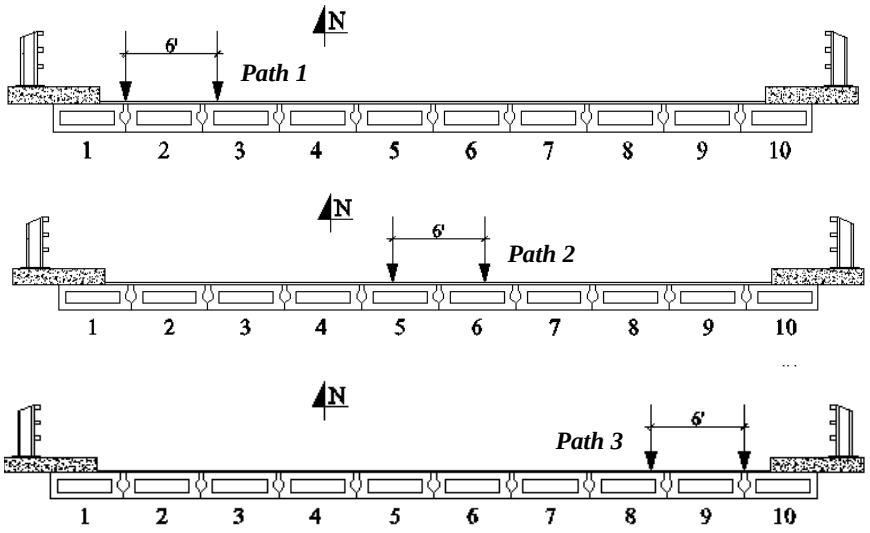

Figure 8.9. Transverse truck paths 1, 2, and 3 for first phase of proof testing (Bridge 8825).

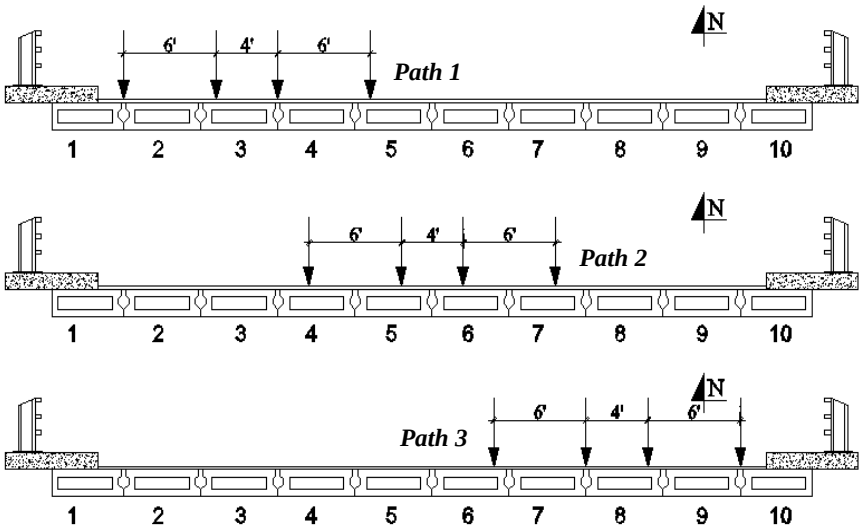

Figure 8.10. Transverse truck paths 1, 2, and 3 for second phase of proof testing (Bridge 8825).

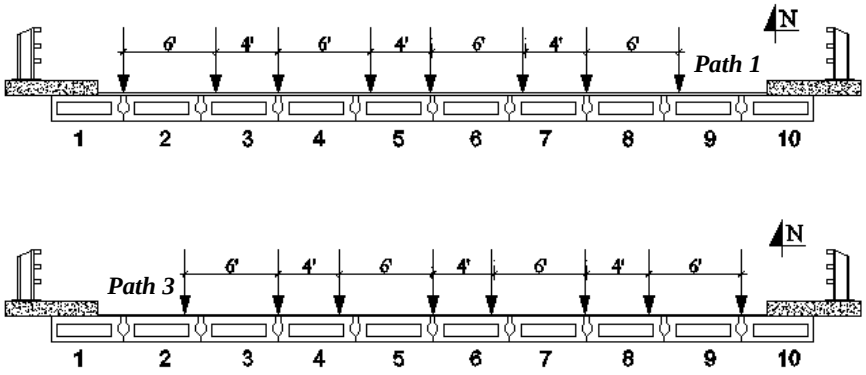

Figure 8.11. Transverse trucks paths 1 and 3 for fifth phase of proof testing (Bridge 8825).

Table 8.12. Axle weights of proof test trucks (Bridge 8825).

Truck Number	Axle Weight (kips)		
	Front Single	Rear Tandem	Total
30532	14.90	41.85	56.75
17116	14.90	41.95	56.85
50026	14.80	43.60	58.40
37525	15.55	43.30	58.85

Using the prestressing strand estimate determined earlier, the cracking, available, target, and test truck moments of the box beams were calculated similarly to Bridge 7722. In addition, the

available strain and test truck strain were computed to monitor the beams during the proof test. Table 8.13 summarizes the preparatory calculations for the proof testing of Bridge 8825.

Table 8.13. Preparatory calculations for proof load testing of Bridge 8825.

Variable	Interior and Exterior
f_c' (psi)	5000
E (ksi)	4031
S_b (in^3)	3566
Number of Strands	16
Area per Strand (in^2)	0.144
P_e (kip)	302.4
e (in.)	7.88
M_{cr} (kip-ft) *	449.9
M_{dl} (kip-ft)	238.8
$M_{available}$ (kip-ft)	211.0
M_{truck} (kip-ft) ***	155.7 (single truck in lane) 221.6 (two trucks in lane, back-to-back)
M_{Type3} (kip-ft) ***	173.7
$\varepsilon_{available}$ (με) **	177
ε_{truck} (με) **	130 (single truck in lane) 185 (two trucks in lane, back-to-back)
ε_{Type3} (με) **	145

Notes: * - Computed based on allowable tension of 6 times square root of f_c'.
** - Computed at bottom of beam section.
*** - Computed based on load distribution factor of 0.429 for the interior and exterior beams, and impact factor of 1.33 (for Type 3 legal load only).

Table 8.14 shows the measured beam strains for phase one and phase two loading with the rear axle of the dump trucks located at midspan. The results represent the maximum strains recorded at the bottom gauges of the beams at midspan. The transducers are labeled B#G# from west to east according to the beam number and gauge position (e.g., B3G1 through B3G3 denotes the west, center, and east gauges of beam 3). From Table 8.14, the largest measured strains were 49 με and 73 με at the interior and exterior beams, respectively, under single truck loading. Note that the reported maximum strains are substantially less than the available strain of 177 με reported earlier in Table 8.13. In the second phase of loading, two dump trucks were placed side-by-side and the maximum midspan strains are also reported in Table 8.14. The maximum strains for phase two were 107 με (beam 1), 87 με (beam 5), and 106 με (beam 10). The exterior beam strains were about 85% of the estimated strain of 130 με which indicates that the AASHTO live-load distribution prediction was reasonably accurate.

Table 8.14. Maximum measured strains for first and second phases of proof testing (Bridge 8825).

Transducer Location	Strain (με)					
	Phase One			Phase Two		
	Path 1	Path 2	Path 3	Path 1	Path 2	Paths 3
B1G1	**69**	-----	-----	**107**	-----	-----
B1G3	44	-----	-----	82	-----	-----
B2G1	39	-----	-----	75	-----	-----
B2G3	40	-----	-----	79	-----	-----
B3G1	38	-----	-----	76	-----	-----
B3G3	22	30	-----	79	66	-----
B4G1	50	20	-----	105	60	-----
B4G3	35	29	-----	85	66	-----
B5G1	13	**49**	-----	62	**87**	-----
B5G3	10	45	-----	41	74	-----
B6G1	-----	48	20	-----	85	56
B6G3	-----	39	24	-----	75	66
B7G1	-----	33	24	-----	71	76
B7G3	-----	16	37	-----	63	82
B8G1	-----	33	29	-----	80	69
B8G3	-----	-----	45	-----	-----	88
B9G1	-----	-----	31	-----	-----	61
B9G3	-----	-----	59	-----	-----	87
B10G1	-----	-----	64	-----	-----	98
B10G3	-----	-----	**73**	-----	-----	**106**

Note that the maximum moment per lane produced by the test vehicles in phases one and two was 155.7 kip-ft which is lower than the moment of 173.7 kip-ft for the AASHTO Type 3 legal load including impact (see Table 8.13). This shows that the target moment was not achieved and therefore, a larger load is required. Consequently, two trucks back-to-back and four trucks (side-by-side and back-to-back) were used in the third and fourth phases to reach the target moments. Table 8.15 shows the maximum measured strains for these two phases. Strains as high as 114 με were recorded for phase three (one lane loaded) and 176 με for phase four (two lanes loaded). Note that the maximum strain for the latter test phase was very close to the expected strain of 185 με and available strain of 177 με. This again confirms the AASHTO live-load distribution prediction and also that the bridge reached the critical load based on concrete tension. Since the bridge was wide enough to accommodate four trucks, the fifth and final loading consisted of four trucks side-by-side. As shown in Table 8.15, the maximum strains under four trucks (phase five) were about equal to the maximum strains under two trucks (phase three). However, both the interior and exterior beams were heavily loaded in phase five whereas only the exterior beams were heavily loaded in phase three.

Table 8.15. Maximum measured strains for third, fourth, and fifth phases of proof testing (Bridge 8825).

Transducer Location	Strain (με)						
	Phase Three		Phase Four			Phase Five	
	Path 1	Path 3	Path 1	Path 2	Path 3	Path 1	Path 3
B1G1	**114**	-----	**175**	-----	-----	**118**	-----
B1G3	70	-----	104	-----	-----	75	-----
B2G1	67	-----	98	-----	-----	74	-----
B2G3	47	-----	83	-----	-----	75	-----
B3G1	46	-----	94	-----	-----	80	-----
B3G3	30	-----	91	82	-----	96	-----
B4G1	63	-----	127	85	-----	109	-----
B4G3	55	-----	95	87	-----	96	-----
B5G1	19	-----	76	**109**	-----	114	-----
B5G3	10	-----	53	102	-----	100	-----
B6G1	-----	24	-----	**109**	56	-----	116
B6G3	-----	29	-----	96	83	-----	103
B7G1	-----	35	-----	94	99	-----	108
B7G3	-----	60	-----	78	116	-----	99
B8G1	-----	27	-----	86	81	-----	106
B8G3	-----	63	-----	-----	119	-----	109
B9G1	-----	47	-----	-----	83	-----	73
B9G3	-----	81	-----	-----	125	-----	98
B10G1	-----	92	-----	-----	150	-----	114
B10G3	-----	**110**	-----	-----	**176**	-----	**118**

Based on the maximum strains given in Tables 8.14 and 8.15, load rating factors will be determined from the proof test. For all loading phases, the moments applied to the bridge from the test trucks will be calculated and used to determine the final load ratings for AASHTO and New Mexico legal loads in accordance with the AASHTO *Manual*.

8.5 BRIDGE NO. 8588, P/C I-GIRDER

The proof load test of Bridge 8588 was executed on October 23rd, 2014. Due to the good condition of the bridge and composite girder construction, it was assumed that the live load distribution factor would be similar or smaller than the design value from the AASHO specifications and therefore, no diagnostic load test was conducted. The prestress estimate from the Magnel diagram was used together with the AASHO specifications to determine the available moments and corresponding strains for the interior and exterior girders. Bridge 8588 consists of six girders with a composite deck and diaphragms located at the beam ends and midspan. In addition, a concrete sidewalk and guardrail is located on the east side of the bridge, and only a guardrail is located on the west side. To account for composite behavior, a different equation was used to calculate the available moment (i.e., cracking moment minus dead load moments) since non-composite and

composite dead loads are applied. Accordingly, the available moment for the composite girder section was computed as:

$$M_{available} = S_c * \left[P_e * \left(\frac{1}{A} + \frac{e}{S_{nc}}\right) + f_{cr}\right] - M_{dnc} * \left(\frac{S_c}{S_{nc}}\right) - M_{dc} \quad \text{(Eq. 8.2)}$$

where S_c and S_{nc} are the composite and non-composite section moduli at the bottom of the girder, and M_{dc} and M_{dnc} are the composite and non-composite dead load moments, respectively.

Table 8.16 summarizes the preparatory calculations for Bridge 8588. The table lists the available moments and strains for four cases; average beam, interior beam, east exterior beam, and west exterior beam. For the average beam case, the composite dead loads (including the wearing surface, sidewalk, and guardrails) were equally distributed to all six girders. In the remaining three cases, the loads were generally applied based on tributary area. For the interior beam case, one-sixth of the wearing surface dead load was exclusively applied. Apart from the wearing surface, the east exterior beam was assigned the sidewalk and east guardrail weights and the west exterior beam was assigned the west guardrail weight. As a result, the east exterior beam had the lowest available strain of 182 με, while the interior and west exterior beams both had an available strain of approximately 330 με (note that the average beam case resulted in an available strain of 308 με for all the girders). Under truck loading, the expected strains were 272 με for back-to-back trucks and 160 με for one truck in a single lane for the interior and exterior beams since the live load distribution factors were about the same.

A shear evaluation was also done to check the beams for potential diagonal cracking near the supports. Assuming an average truck weight of 60 kips, the maximum undistributed shear for a single beam caused by back-to-back truck loading is 30 kips. Using the lever rule, the live load distribution factors for an interior and exterior beam are 1.38 and 1.29, respectively, and the ultimate live load shear forces are 41.6 kips and 38.7 kips. Using Eq. (8.1), the web-shear cracking force V_{cw} ranged from 121.8 kips to 176.7 kips for concrete tensile strengths of 2 to 4 times f_c'. The strands were assumed to be straight and debonded, therefore V_p was zero. Under dead and live loads, the ultimate shear forces were 87.2 kips for the west exterior girder, 88.3 kips for the interior girder, and 113.5 kips for the east exterior girder which all were less than 121.8 kips and therefore, cracking due to shear was not expected.

The instrumentation plan for Bridge 8588 was similar to the other bridges with the majority of the strain gauges placed at midspan. Each beam had four gauges at midspan, two installed on the bottom of the beam section and two on each side of the web, resulting in 24 gauges. The remaining 12 gauges were placed on beams 1, 3 and 6 at 30% and 70% of the beam length. These beams contained two gauges at these locations, one on the bottom flange and one on the web. Figures 8.12 and 8.13 show the overall instrumentation layout and gauge placement. Note that the gauges were placed in line with the skew similar to the other skewed bridges.

Table 8.16. Preparatory calculations for proof load testing of Bridge 8588.

Variable	Average	Interior	Exterior (East)	Exterior (West)
k	0.70	0.70	0.70	0.70
f_{pi} (ksi)	189	189	189	189
Number of Strands	24	24	24	24
Area per Strand (in^2)	0.153	0.153	0.153	0.153
P_e (kip)	485.8	485.8	485.8	485.8
S_c (in^3)	10014	10014	9518	10047
S_{nc} (in^3)	6186	6186	6186	6186
A (in^2)	559.5	559.5	559.5	559.5
e (in)	16.8	16.8	16.8	16.8
f_c' (girder) (psi)	5000	5000	5000	5000
f_c' (deck) (psi)	3000	3000	3000	3000
f_{cr} (ksi) *	0.424	0.424	0.424	0.424
M_{dnc} (kip-ft)	805.8	805.8	805.8	805.8
M_{dc} (kip-ft)	137.9	47.2	559.2	79.5
$M_{available}$ (kip-ft)	737.2	819.0	494.9	783.2
M_{truck} (one truck) (kip-ft) ***	-----	538.7	181.1	490.8
M_{truck} (two trucks, back-to-back) (kip-ft) ***	-----	914.1	307.4	833.0
$\varepsilon_{available}$ (με) **	219	244	155	232
ε_{truck} (one truck) (με) **	-----	160	57	146
ε_{truck} (two trucks, back-to-back) (με) **	-----	272	96	247

Notes: * - Computed based on allowable tension of 6 times square root of f_c'.
** - Computed at the bottom of beam section (gauge location).
*** - Computed based on a live load distribution factor of 1.18 (interior beam), 0.40 (east exterior beam), and 1.03 (west exterior beam), and a 60 kip dump truck.

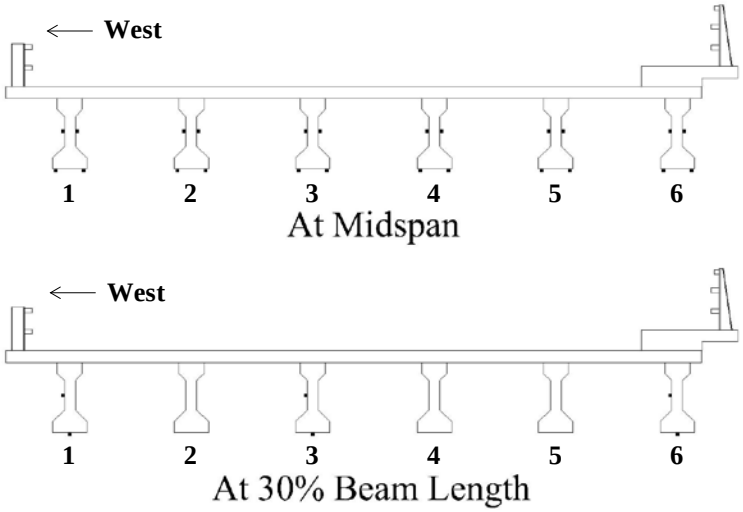

Figure 8.12. Instrumentation layout for proof load testing (Bridge 8588).

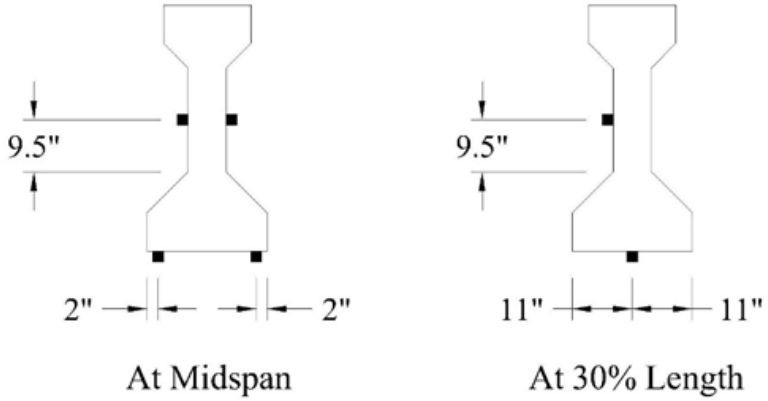

Figure 8.13. Strain transducer locations over beam height (Bridge 8588).

The proof test of Bridge 8588 was similar to that of Bridge 8825 in terms of truck loading and consisted of the following five phases: phase one – single dump truck (one lane loaded); phase two – two dump trucks side-by-side (multiple lanes loaded); phase three – three dump trucks side-by-side (multiple lanes loaded); phase four – two dump trucks back-to-back (one lane loaded); and phase five – four dump trucks side-by-side and back-to-back (multiple lanes loaded). Figures 8.14 through 8.16 show the transverse truck positions for the five phases. Note that phases one and two were used to determine the critical paths for phases four and five, respectively, while phase three was used to maximize the total midspan moment for a multiple lanes loaded condition. For phases one through three, the final longitudinal position(s) of the truck(s) were with the back axles centered at midspan of the bridge. For phases four and five, the final position(s) were with the trucks meeting back-to-back at midspan. Due to the longer bridge length (73 ft. clear span), the truck(s) were completely on the bridge in the final longitudinal position(s). Note that for shorter span bridges (i.e., Bridge 7701), only the back axles were on the bridge when the trucks were in the final position(s). Table 8.17 summarizes the measured truck weights for the proof test and Table 8.18 summarizes the maximum measured strains at the gauges located on the bottom flange

at midspan for the final longitudinal truck position(s). The gauges are labeled B#G# representing the beam number and the gauge position (1 for west, 2 for east).

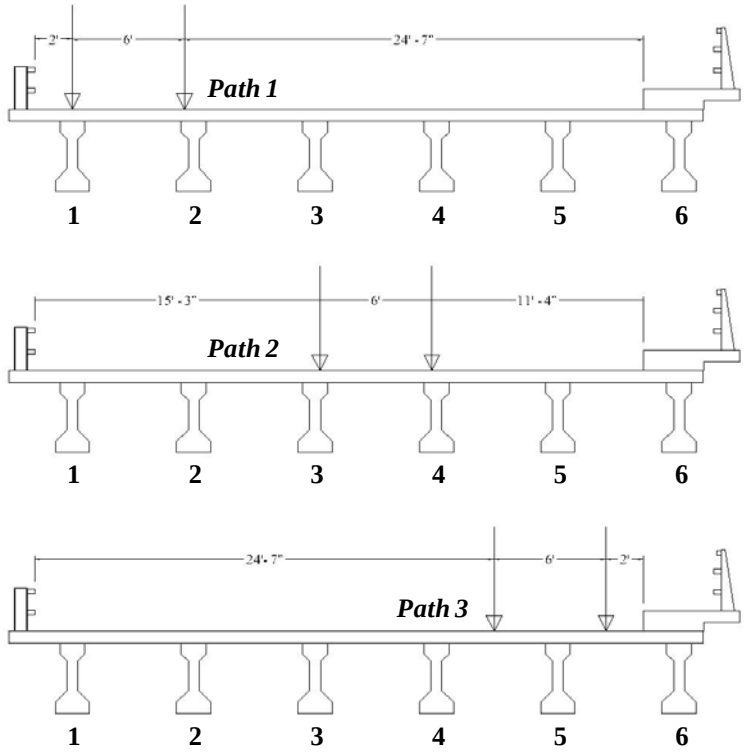

Figure 8.14. Transverse truck paths for phases one and four of proof testing (Bridge 8588).

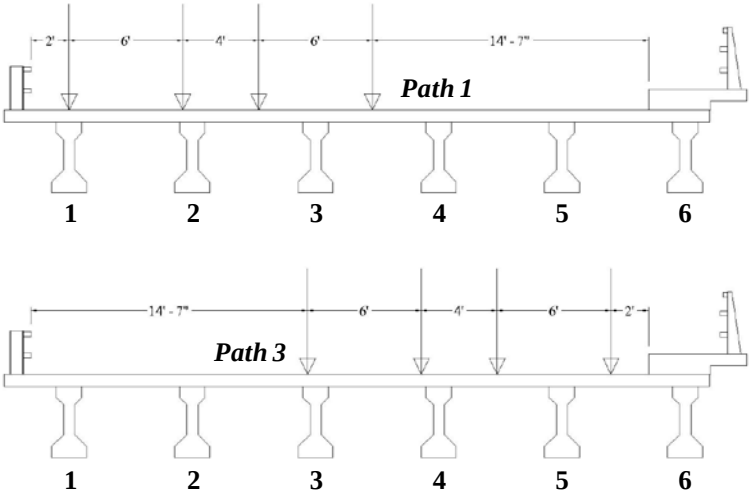

Figure 8.15. Transverse truck paths for phases two and five of proof testing (Bridge 8588).

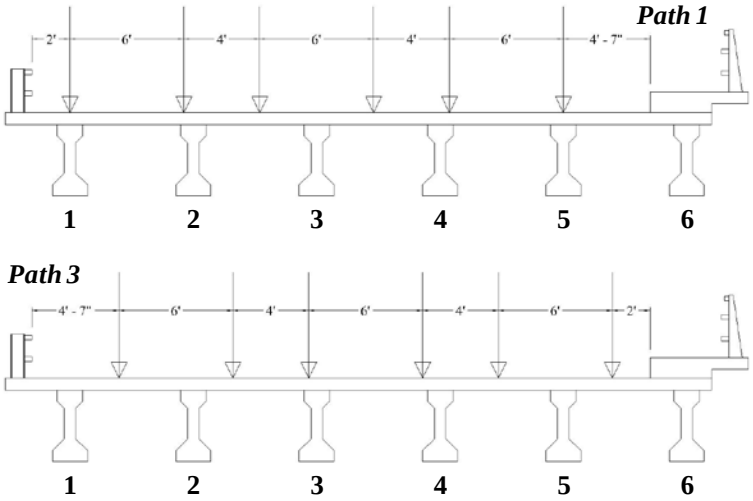

Figure 8.16. Transverse truck paths for phase three of proof testing (Bridge 8588).

Table 8.17. Axle weights of proof test trucks (Bridge 8588).

Truck Number	Axle Weight (kips)		
	Front Single	Rear Tandem	Total
30531	17.20	44.80	62.00
16580	17.30	43.70	61.00
36978	17.05	43.05	60.10
16585	17.05	41.80	58.85

Table 8.18. Maximum measured strains for all phases of proof testing (Bridge 8588).

Transducer Location	Strain (με)								
	Phase 1			Phase 2		Phase 3		Phase 4	Phase 5
	Path 1	Path 2	Path 3	Path 1	Path 3	Path 1	Path 3	Path 1	Path 1
B1G1	68	**14**	0	89	14	86	84	117	141
B1G2	**87**	-4	-4	**113**	-6	**105**	**92**	**160**	**174**
B2G1	61	31	8	115	44	122	116	107	178
B2G2	**69**	26	6	**118**	35	122	113	**117**	**181**
B3G1	30	64	22	90	79	109	109	53	152
B3G2	43	64	13	106	78	**128**	**128**	61	171
B4G1	15	60	59	49	**102**	101	112	18	98
B4G2	11	**66**	52	44	100	101	112	22	100
B5G1	3	24	57	15	71	64	77	-6	29
B5G2	5	34	**64**	31	87	82	90	6	65
B6G1	-6	-1	**44**	-6	**35**	27	43	-9	-14
B6G2	4	11	34	9	34	34	48	5	24

In the first phase of the proof test, the maximum measured strains for the interior girders were similar in paths two and three, but the largest strains were measured for the exterior girder in path one. This was expected since the truck was positioned two feet from the west rail directly above beam one. Note that path two showed a symmetrical response between the interior and exterior girders on either side of the bridge centerline (i.e., average strain for beams 1 and 6 = 5 με, beams 2 and 5 = 29 με, and beams 3 and 4 = 64 με). The exterior beams were considered critical since beam six (i.e., east exterior beam) had the lowest available strain (155 με), and beam one (i.e., west exterior beam) showed the highest measured strains in phase one (87 με). In the remaining test phases, path two (i.e., dump trucks centered on bridge) was omitted since the exterior beams were more critical and also to expedite the load testing. Phase three was conducted concurrently with phase two; with the two trucks in their final positions for phase two and after the strain data set was collected, a third truck was added in phase three and strain data was recollected during the same run in order to save time. Note that both paths in phase three resulted in about the same level of strain at the interior girders since the bridge was fully loaded in the transverse direction with three trucks. As shown in Figure 8.16, the phase three load paths are only separated by 29 in. (2 ft 7 in.). In summary, the ratios of the maximum measured strains to the available and expected strains, respectively, for phases one through three amounted to the following: interior girder (128 με / 244 με = 52%, 128 με / 160 με = 80%); west exterior girder (113 με / 232 με = 49%, 113 με / 146 με = 77%); and east exterior girder (48 με / 155 με = 31%, 48 με / 57 με = 84%). These ratios show that the measured strains were about 50% or more below the available strains, and 16% to 23% smaller than the expected strains.

Based on the measured strains from the first three phases, path one was considered the most critical for phases four and five since the west exterior girder and several adjacent interior girders were most heavily loaded simultaneously for this path. Due to the sidewalk, the east exterior beam showed low strain values in the first three phases. Since the truck load could not be positioned directly over the beam, the possibility of exceeding the available strain was very low, and therefore path three was not considered in the final two phases. In phase four, the largest measured strains for the one lane loaded condition were 160 με at the west exterior girder and 117 με at the adjacent interior girder. For the multiple lanes loaded condition (i.e., phase five), the maximum measured strains increased to 174 and 181 με for the exterior and interior girders, respectively, which are roughly 75% of the available strains and 70% of the expected strains. These percentages indicate that the AASHO distribution factors are conservative particularly for back-to-back loading since the rear tandem axles are not at midspan. The difference in expected and measured strains could also be due to an underestimation of the composite section stiffness, as well as rotational restraint at the beam ends. In all five test phases, the available strains were well above the measured strains, and thus the loading was not stopped until the trucks reached the final positions (i.e., rear tandem axle(s) centered at midspan for phases one through three, and back-to-back at midspan for phases four and five). The applied moments were subsequently calculated from the final truck positions and used to determine the legal load ratings for Bridge 8588 in the next section.

9. LEGAL LOAD RATINGS

Based on the proof test results, legal load ratings for the five prestressed concrete bridges (nos. 7701, 7722, 8588, 8761, and 8825) were determined using the AASHTO *Manual*. The AASHTO *Manual* provides guidance for load rating bridges using proof testing at the strength limit state. Since all proof tests performed in this study were monitored and controlled by concrete cracking, necessary adjustments were made to the AASHTO *Manual* procedure to accurately load rate each bridge at the service limit state. The final truck positions were used to calculate the maximum midspan moment applied to the bridges during the proof tests and corresponding legal load moments were found using the RISA and SAP2000 structural analysis programs. The experimental (i.e., proof test) and analytical (i.e., structural analysis) moments were then used in the equations given in Section 8.8.3.3 of the AASHTO *Manual* to load rate each bridge.

To comprehensively determine the safe load ratings for each bridge, the strength limit state was also checked using the AASHTOWare Bridge Rating (BrR) program. The BrR models were created using material property estimates determined from the applicable AASHTO specifications, the AASHTO *Manual*, and State provisions. In addition, the amount of reinforcement (i.e., bar size and spacing) and the concrete cover needed to create each BrR model was estimated using the Magnel diagrams and/or the results from the Ferroscan. Finally, the member dimensions needed for the bridge models were determined from field measurements taken during the site visits. Two sets of ratings (i.e., proof test ratings based on service and BrR model ratings based on strength) were computed for the prestressed concrete bridges and the final ratings were chosen using engineering judgment. Note that the final load ratings for the reinforced concrete slab bridge (no. 8676) were based solely on strength since the bridge was not load tested.

9.1 BRIDGE NO. 7701, P/C DOUBLE T-BEAM

Based on the measured strains given in Tables 8.1 through 8.3 and corresponding truck positions given in Figure 8.2, load rating factors were determined from the proof load test. For all four phases, the moments applied to the bridge from the test truck loading were used to compute the final load ratings for AASHTO and New Mexico legal loads according to the AASHTO *Manual*. Recall that the available strain of 532 με used to monitor the beams during the proof test was based on $7.5(f_c')^{1/2}$. To determine the final load ratings, however, the test truck moments associated with an available strain of 507 με, based on an allowable concrete stress of $6(f_c')^{1/2}$, were used. From Section 8.8.3.3 of the AASHTO *Manual*, the adjusted target live-load factor (X_{pA}) and the target proof load (L_T) were first determined using the following equations:

$$X_{pA} = X_p\left(1 + \frac{\Sigma\%}{100}\right) \quad \text{(Eq. 9.1)}$$

$$L_T = X_{pA}L_R(1 + IM) \quad \text{(Eq. 9.2)}$$

where X_p is the initial target load factor, Σ% is the sum of the X_p adjustment factors given in Table 8.8.3.3.1-1 of the AASHTO *Manual*, L_R is the unfactored live load due to the rating vehicle, and IM is the impact factor (equal to 1.33). The AASHTO *Manual* recommends a minimum value of 1.4 for X_p; however, since the proof test was executed based on serviceability (limiting concrete tensile stress at service load) rather than strength, a factor of 1.0 was used which is permitted for legal load rating. Also note that L_T and L_R were determined in terms of the maximum moment at midspan of the bridge rather than load since the rating vehicles and proof test trucks do not have the same axle configuration. As shown in Table 9.1, the applicable adjustment factors from the AASHTO *Manual* included one-lane loading (+15%), non-redundant load path (+10%), in-depth inspection performed (-5%), and ADTT less than 1000 (-10%).

Table 9.1. Adjustments to target load (AASHTO 2011).

Feature	Adjustment
One-Lane Load Controls	+15%
Nonredundant Structure	+10%
Fracture-Critical Details Present	+10%
Bridges in Poor Condition	+10%
In-Depth Inspection Performed	-5%
Rateable, Existing $RF \geq 1$	-5%
ADTT ≤ 1000	-10%
ADTT ≤ 100	-15%

Accordingly, X_{pA} was 1.1 for one lane loaded and 0.95 for multiple lanes loaded from Eq. (9.1). Target proof moments were then computed using Eq. (9.2) for the AASHTO legal loads (Type 3, Type 3-3, and Type 3S2) and the New Mexico legal loads (NM 2, NM 3A, and NM 5A) which are listed in Table 9.2 along with the vehicle weight, *W*.

Table 9.2. Target proof moments, rating factors, and posting loads (Bridge 7701).

Legal Load	*W* (kips)	L_R (kip-ft)	L_T (kip-ft)		RF_o	*Safe Posting Load* (tons)
			One Lane	Multiple Lanes		
HS-20	72.0	284	416	359	0.67	19.1
Type 3	50.0	235	344	297	0.81	18.2
Type 3S2	80.0	231	338	292	0.83	30.0
Type 3-3	72.0	190	278	240	1.00	N/A
NM 2	33.6	179	262	226	1.06	N/A
NM 3A	46.3	235	344	297	0.81	16.9
NM 5A	80.6	247	361	311	0.77	27.3

The target proof moments were then compared to the moments applied by the dump trucks during the actual proof test. For phases one and three (single lane loaded), the applied moments were 279

kip-ft and 368 kip-ft, respectively, while for phases two and four (multiple lanes loaded), the applied moments were 256 kip-ft and 300 kip-ft, respectively. The operating level (*OP*) capacity for the bridge was computed using the following equation from the AASHTO *Manual*:

$$OP = \frac{k_0 L_P}{X_{pA}} \quad \text{(Eq. 9.3)}$$

where k_0 is a factor that depends on how the proof test was terminated (1.0 if the target proof moment is reached and 0.88 if the test is stopped due to signs of distress) and L_P is the applied moment. Although the proof test was ended before the truck axles reached the final position, k_0 was taken as 1.0 since the concrete design strength was used rather than the actual strength to determine the available strain and prevent cracking. Consequently, the *OP* moments equaled 253 kip-ft for phase one, 270 kip-ft for phase two, 335 kip-ft for phase three, and 316 kip-ft for phase four. The final load ratings were computed based on phase one which had the smallest moment. Recall that the truck was stopped in this phase when the back axle reached 14 ft. resulting in a measured strain of 508 με which equaled the available strain. The rating factors, RF_O, for the legal load were computed using the following equation:

$$RF_O = \frac{OP}{L_R(1+IM)} \quad \text{(Eq. 9.4)}$$

The safe posting loads were then determined based on Section 6A.8.3 of the AASHTO *Manual* as follows:

$$Safe\ Posting\ Load = \frac{W}{0.7}[(RF_O) - 0.3] \quad \text{(Eq. 9.5)}$$

Table 9.2 lists the rating factors and safe posting loads for each legal load. The table shows that Bridge 7701 needs to be posted for all legal loads excluding the Type 3-3 and NM 2. For legal load rating, strength is the primary limit state for prestressed concrete bridges specified in the AASHTO *Manual*. Consequently, a legal load rating analysis of NMDOT Bridge 7701 was performed based on the bridge geometry, material properties, and steel reinforcement discussed earlier. Using the AASHTOWare BrR program, rating factors were computed according to the Load Factor Rating (LFR) and Load and Resistance Factor Rating (LRFR) methods for the strength limit state. Results from the BrR analyses are reported in Table 9.3. The LFR values were the same for the interior and exterior beams since there is no difference in the load distribution factors. For LRFR, the exterior beam had smaller rating factors since the load distribution factor is larger than the interior beam. Due to poor condition of the shear keys, the BrR analysis was also performed assuming a wheel distribution factor of 1.0 for LFR and axle distribution factor of 0.5 for LRFR. These values signify complete breakdown of the shear keys and thus, is a worst case scenario. As shown in the table, the BrR rating factors for strength (controlled by ultimate flexure) all exceeded the values for service (based on concrete cracking) determined from the proof test. This comparison confirmed that the load carrying capacity of the bridge was controlled by the optional check at the service limit state.

Table 9.3. Rating factors from proof test for service and BrR program for strength (Bridge 7701).

Legal Load	Proof Test (Service)	LFR (Strength) *		LRFR (Strength) **	
		Interior Beam	Exterior Beam	Interior Beam	Exterior Beam
HS-20	0.67	1.82 (0.90)	1.82 (0.90)	1.61 (0.80)	1.25 (0.80)
Type 3	0.81	2.29 (1.13)	2.29 (1.13)	2.03 (1.00)	1.58 (1.00)
Type 3S2	0.83	2.31 (1.14)	2.31 (1.14)	2.04 (1.01)	1.59 (1.01)
Type 3-3	1.00	2.82 (1.40)	2.82 (1.40)	2.49 (1.23)	1.94 (1.23)
NM 2	1.06	2.95 (1.46)	2.95 (1.46)	2.61 (1.29)	2.03 (1.29)
NM 3A	0.81	2.28 (1.13)	2.28 (1.13)	2.02 (1.00)	1.57 (1.00)
NM 5A	0.77	2.17 (1.07)	2.17 (1.07)	1.92 (0.95)	1.49 (0.95)

Notes: * - Values in parentheses computed using wheel distribution factor of 1.0.
** - Values in parentheses computed using axle distribution factor of 0.5.

9.2 BRIDGE NO. 8761, P/C DOUBLE T-BEAM

Based on the proof test results reported in Tables 8.5 through 8.7, load rating factors were determined for Bridge 8761 under the AASHTO and New Mexico legal loads. The adjusted target live-load factor (X_{pA}) and the target proof load (L_T) were determined using Eqs. (9.1) and (9.2) given earlier. Recall that the proof test was performed based on the limiting concrete tensile stress at service load rather than strength (i.e., X_p = 1 in Eq. (9.1)) with the purpose of determining the legal load rating. From Table 9.1, the adjustment factors that applied for Bridge 8761 included +15% for one-lane loaded, -10% for an ADTT less than 1000, and -5% for an in-depth inspection. Thus, the Σ% amounted to 0% for one-lane loading and -15% for multiple-lane loading that resulted in X_{pA} values of 1.0 and 0.85, respectively. To load rate the bridge, only multiple-lane loading was considered and an X_{pA} of 0.95 was used rather than 0.85 to limit the reductions. Single-lane loading was ignored since the measured strains from the proof test were well below the available strain for this load case.

Table 9.4 shows the unfactored live-load moments (L_R) and target proof moments (L_T) for Bridge 8761 that were computed using Eq. (9.2) for the AASHTO and New Mexico legal loads. Recall that the proof load test was conducted in three phases: phase one – two trucks placed side-by-side; phase two – three trucks placed side-by-side; and phase three – four trucks placed side-by-side and back-to-back. Based on the final positions of the test trucks, the applied moments (L_p) were approximately 330 kip-ft for phases one and two, and 480 kip-ft for phase three. It is important to note that the test trucks reached the critical positions on the bridge for each phase (which was not the case for Bridge 7701) and the measured strains neared the available strain only at the exterior beams for phase three. Using a k_0 factor of unity, the operating level (*OP*) moment capacities of the bridge were computed using Eq. (9.3) given earlier and equaled 350 kip-ft for phases one and two, and 505 kip-ft for phase three. Table 9.4 shows the rating factors (RF_o) computed for the bridge using Eq. (9.4) according to the truck configurations for phases one, two, and three.

Table 9.4. Target proof moments, rating factors, and posting loads (Bridge 8761).

Legal Load	W (kips)	L_R (kip-ft)	L_T (kip-ft) Multiple Lanes	RF_o *	*Safe Posting Load* (tons)
HS-20	72.0	348	440	0.75 (1.09)	N/A
Type 3	50.0	283	358	0.93 (1.34)	N/A
Type 3S2	80.0	270	341	0.97 (1.41)	N/A
Type 3-3	72.0	231	292	1.14 (1.64)	N/A
NM 2	33.6	212	268	1.24 (1.79)	N/A
NM 3A	46.3	279	353	0.95 (1.36)	N/A
NM 5A	80.6	290	366	0.91 (1.31)	N/A

* Value outside parentheses corresponds to phases one and two, and value in parentheses corresponds to phase three.

As shown in the table, the RF_o values were less than one for two of the AASHTO legal loads and two of the NM legal loads for phases one and two of the proof test. These values do not indicate that the bridge should be posted but rather that the target load level was not achieved using just side-by-side truck loading. The RF_o values for phase three (i.e., four trucks placed side-by-side and back-to-back) all exceeded one by more than 30% which proved that the bridge was safe under legal loading and posting was not necessary.

Similarly to NMDOT Bridge 7701, a legal load rating analysis of Bridge 8761 was performed for the strength limit state using the AASHTOWare BrR program according to the LFR and LRFR methods. As shown in Table 9.5, the LFR and LRFR ratings are comparable for the interior beam due to similarities in the load distribution factors; however, the LRFR ratings are smaller for the exterior beam since the load distribution factors are larger. Overall, the rating factors for strength (controlled by ultimate flexure) exceeded the values for service (based on concrete cracking) determined from the proof test with the exception of the LRFR ratings for the exterior beam which were slightly smaller. Since the service-based rating factors from the proof test were about equal to the LRFR strength-based rating factors for the exterior beam and smaller than the LFR ratings, the decision was made to use the service limit state to establish the legal load capacity of the bridge.

Table 9.5. Rating factors from proof test for service and BrR program for strength (Bridge 8761).

Legal Load	Proof Test (Service)	LFR (Strength)		LRFR (Strength)	
		Interior Beam	Exterior Beam	Interior Beam	Exterior Beam
HS-20	1.09	1.64	1.24	1.63	1.02
Type 3	1.34	2.14	1.57	2.13	1.28
Type 3S2	1.41	2.35	1.62	2.21	1.33
Type 3-3	1.64	2.57	1.92	2.55	1.57
NM 2	1.79	2.85	2.08	2.82	1.70
NM 3A	1.36	2.20	1.58	2.15	1.29
NM 5A	1.31	2.15	1.51	2.06	1.23

9.3 BRIDGE NO. 7722, P/C BOX GIRDER

Based on the test truck loading and measured strains presented in Figures 8.5 and 8.6, and Tables 8.10 and 8.11, the load rating factors of Bridge 7722 were determined from the proof test for AASHTO and New Mexico legal loads according to Section 8.8.3.3 of the AASHTO *Manual*. The adjusted target live-load factor (X_{pA}) and the target proof load (L_T) were first determined using Eqs. (9.1) and (9.2) given earlier. Several site conditions have an influence on the live-load factors that are accounted for through adjustments to the initial target load factor (X_p). The applicable adjustment factors for Bridge 7722 included one-lane loading (+15%), in-depth inspection performed (-5%), and ADTT less than 1000 (-10%). Accordingly, X_{pA} was 1.0 for one lane loaded and 0.85 for multiple lanes loaded from Eq. (9.1). Target proof loads were then computed using Eq. (9.2) for the AASHTO and New Mexico legal loads which are listed in Table 9.6 along with the vehicle weight, W. Note that L_T and L_R were determined in terms of the maximum midspan moment of the bridge and not load since the rating vehicles and proof test trucks do not have the same axle configuration.

Table 9.6. Unfactored moments and adjusted target moments at midspan (Bridge 7722).

Legal Load	W (kips)	L_R (kip-ft)	L_T (kip-ft)	
			One Lane	Multiple Lanes
HS-20	72.0	518	689	586
Type 3	50.0	400	532	452
Type 3S2	80.0	368	489	416
Type 3-3	72.0	332	442	375
NM 2	33.6	289	384	326
NM 3A	46.3	388	516	439
NM 5A	80.6	400	532	452

The maximum midspan moments applied in the proof test (L_p) were obtained using the axle weights and spacing of the test vehicles. For the different test phases, the associated maximum moments at midspan were 535 kip-ft (phase one), 517 kip-ft (phase two), and 753 kip-ft (phases three and four). Note that phases one and three correspond to one lane loading, and phases two and four correspond to multiple lane loading. Based on the target moments listed in Table 9.6 and the applied proof test moments just discussed, the operating level capacity (OP) was calculated using Eq. (9.3). Since the proof test was not terminated due to distress levels, k_o was taken as 1.0 for Bridge 7722. Using Eq. (9.4), the rating factors for each loading scenario of the proof test were calculated and the results are reported in Table 9.7.

As shown in Table 9.7, all the operating rating factors are greater than one. For single truck loading (phase one) and two trucks side-by-side loading (phase two), the rating factors were close to 1.0 for certain legal loads meaning that the maximum moments produced for these loading patterns during the proof test were near the legal load target moments. This is due to the limited maximum weights of the test vehicles. To produce the target moments with a single truck or two trucks side-by-side would have required heavier loading. However, the axle capacity of the trucks limits how

heavy the trucks can be loaded as well as the bed capacity (limited to 10 cubic yards). In addition, although the computed rating factors were near 1.0, the corresponding maximum strains measured under the single truck and two trucks side-by-side loads were 84 με and 90 με, respectively, which are significantly smaller than the available strains (151 με and 177 με for the interior and exterior beam, respectively). This is a clear indication that there is unused capacity. Hence, the final operating ratings were based on single lane, back-to-back truck loading (i.e., phase three in Table 9.7) due to the poor condition of the shear keys between the exterior and interior beams.

Table 9.7. Operating rating factors from proof load test (Bridge 7722).

Legal Load	Operating Rating Factors, RF_o			
	Phase One	Phase Two	Phase Three	Phase Four
HS-20	0.78	0.88	1.09	1.28
Type 3	1.01	1.14	1.41	1.67
Type 3S2	1.09	1.24	1.54	1.81
Type 3-3	1.21	1.38	1.70	2.01
NM 2	1.39	1.58	1.96	2.32
NM 3A	1.04	1.18	1.46	1.72
NM 5A	1.01	1.14	1.41	1.67

Table 9.8 provides the LFR and LRFR legal load rating results for NMDOT Bridge 7722 from the AASHTOWare BrR program for the strength limit state. In general, the rating factors were different for the interior and exterior beams due to differences in the amount of prestressing steel and mild shear reinforcement, and also load distribution. The ratings were controlled by flexural strength for LFR and shear strength for LRFR (see values given in parentheses in Table 9.8). The service-based rating factors determined from the proof test were smaller than the strength-based rating factors from the BrR program with the exception of the LRFR shear ratings for the exterior beam. Consequently, since the service-based rating factors were similar in magnitude to the LRFR ratings for the exterior beam and smaller than the LFR ratings, the bridge capacity for legal loads was set based on the service limit state.

Table 9.8. Rating factors from proof test for service and BrR program for strength (Bridge 7722).

Legal Load	Proof Test (Service)	LFR (Strength)		LRFR (Strength) *	
		Interior Beam	Exterior Beam	Interior Beam	Exterior Beam
HS-20	1.09	1.79	2.27	1.59 (1.28)	1.92 (1.01)
Type 3	1.41	2.32	2.94	2.06 (1.74)	2.49 (1.38)
Type 3S2	1.54	2.52	3.19	2.24 (1.78)	2.71 (1.40)
Type 3-3	1.70	2.80	3.54	2.49 (1.88)	3.00 (1.49)
NM 2	1.96	3.22	4.08	2.87 (2.42)	3.46 (1.92)
NM 3A	1.46	2.39	3.02	2.12 (1.83)	2.56 (1.44)
NM 5A	1.41	2.32	2.93	2.06 (1.80)	2.48 (1.42)

Notes: * - Values in parentheses computed based on shear strength.

9.4 BRIDGE NO. 8825, P/C BOX GIRDER

Similar procedures were followed to compute the load ratings for Bridge 8825. Results from the rating analyses are reported in Tables 9.9 and 9.10. Similar to Bridge 7722, the adjusted target-load factor, X_{pA}, was 1.0 for one lane loaded and 0.85 for multiple lanes loaded. The distress factor, k_o, was also taken as 1.0 for Bridge 8825 since the proof test was completed without incident. For the different test phases, the applied maximum moments at midspan, L_p, were 445 kip-ft (phases one and two), 629 kip-ft (phases three and four), and 438 kip-ft (phase five). Note that phases one and three represent one lane loading, and phases two, four, and five represent multiple lane loading. The final operating rating factors were based on phase four of the proof test which included four trucks placed side-by-side and back-to-back. This test phase controlled since the target moment and the available strain were achieved simultaneously. Recall that the maximum recorded strain was 176 με for this load case which equaled the available strain.

Table 9.9. Unfactored moments and adjusted target moments at midspan (Bridge 8825).

Legal Load	W (kips)	L_R (kip-ft)	L_T (kip-ft)	
			One Lane	Multiple Lanes
HS-20	72.0	476	633	538
Type 3	50.0	371	493	419
Type 3S2	80.0	345	458	390
Type 3-3	72.0	306	407	346
NM 2	33.6	269	358	304
NM 3A	46.3	362	482	409
NM 5A	80.6	374	498	423

Table 9.10. Operating rating factors from proof load test (Bridge 8825).

Legal Load	Operating Rating Factors, RF_o				
	Phase One	Phase Two	Phase Three	Phase Four	Phase Five
HS-20	0.70	0.83	0.99	1.17	0.81
Type 3	0.90	1.06	1.27	1.50	1.04
Type 3S2	0.97	1.14	1.37	1.61	1.12
Type 3-3	1.09	1.29	1.54	1.82	1.27
NM 2	1.24	1.47	1.76	2.07	1.44
NM 3A	0.92	1.09	1.31	1.54	1.07
NM 5A	0.89	1.05	1.26	1.46	1.04

Similarly to the other NMDOT bridges, Bridge 8825 was evaluated based on strength for legal loads using the AASHTOWare BrR program, results of which are given in Table 9.11. In both the LFR and LRFR analyses, the rating factors for the interior and exterior beams were the same since there were no differences in the steel reinforcement configurations or load distribution percentages. Note that the BrR rating factors were computed under legal load plus pedestrian loading as required

by the NMDOT for bridges with sidewalks. The rating results show that the BrR strength-based rating factors (based on ultimate flexure) exceeded the service-based rating factors (based on concrete cracking) determined from the proof test. This comparison confirmed that the optional check at the service limit state controlled the load carrying capacity of the bridge.

Table 9.11. Rating factors from proof test for service and BrR program for strength (Bridge 8825).

Legal Load	Proof Test (Service)	LFR (Strength) *		LRFR (Strength) *	
		Interior Beam	Exterior Beam	Interior Beam	Exterior Beam
HS-20	1.17	1.40	1.40	1.44	1.44
Type 3	1.50	1.78	1.78	1.82	1.82
Type 3S2	1.61	1.90	1.90	1.95	1.95
Type 3-3	1.82	2.13	2.13	2.18	2.18
NM 2	2.07	2.40	2.40	2.45	2.45
NM 3A	1.54	1.82	1.82	1.87	1.87
NM 5A	1.46	1.76	1.76	1.81	1.81

Notes: * - Values computed with legal load plus pedestrian loading.

9.5 BRIDGE NO. 8588, P/C I-GIRDER

Based on the proof test results, load rating factors were determined for Bridge 8588 under AASHTO and New Mexico legal loads. Similar to the other bridges, the AASHTO *Manual* was used to determine the final ratings. The adjusted load factor (X_{pA}) and target proof loads (L_T) were determined using Eqs. (9.1) and (9.2) given earlier. The initial load factor, X_p, was assumed equal to 1.0 since the test was based on concrete cracking (Service III) and not Strength I. Using Table 9.1, the adjustment factors which applied for Bridge 8588 were +15% for one lane loaded and -5% for an in-depth inspection. Thus, the final adjusted factors were 1.1 for one lane loaded and 0.95 for multiples lane loaded.

Recall that in all five phases of the proof test, the maximum measured strains were less than the available strains by about 25%. No tests were stopped early and all were continued until the dump trucks reached the final longitudinal positions. Thus, the multiple lanes loading condition for phase five (i.e., four trucks, side-by-side and back-to-back) was used to determine the final load ratings. Table 9.12 presents the unfactored live load moments (L_R) and the corresponding target proof moments (L_T) for the AASHTO and New Mexico legal loads based on the adjusted live load factor mentioned previously (i.e., X_{pA} = 0.95). The applied moment (L_p) corresponding to the final loading in phase five was 1532 kip-ft. Using Eqs. (9.3) and (9.4), the operating moment capacity (*OP*) and final rating factors (RF_o) were calculated. Using a k_0 factor of 1.0, *OP* amounted to 1612 kip-ft. Table 9.12 lists the final rating factors for Bridge 8588 for legal loads. For all legal loads, the rating factors are larger than 1.0 by a significant margin, indicating that Bridge 8588 is safe under legal loading and thus, no posting is necessary.

Table 9.12. Target proof moments, rating factors, and posting loads (Bridge 8588).

Legal Load	W (kips)	L_R (kip-ft)	L_T (kip-ft) Multiple Lanes	RF_o	*Safe Posting Load*
HS-20	72.0	1036	1309	1.17	N/A
Type 3	50.0	758	957	1.60	N/A
Type 3S2	80.0	843	1065	1.44	N/A
Type 3-3	72.0	801	1012	1.51	N/A
NM 2	33.6	529	668	2.29	N/A
NM 3A	46.3	720	909	1.68	N/A
NM 5A	80.6	800	1011	1.52	N/A

Table 9.13 provides the LFR and LRFR legal load rating results for NMDOT Bridge 8588 from the AASHTOWare BrR program for the strength limit state. In general, the rating factors were different for the interior and exterior beams primarily due to differences in load distribution. The ratings were controlled by shear strength for LFR and shear or flexural strength for LRFR (see note given in Table 9.13). The service-based rating factors determined from the proof test were all significantly lower than the strength-based rating factors from the BrR program. Consequently, the bridge capacity for legal loads was set based on the service limit state.

Table 9.13. Rating factors from proof test for service and BrR program for strength (Bridge 8588).

Legal Load	Proof Test (Service)	LFR (Strength)		LRFR (Strength)	
		Interior Beam	Exterior Beam	Interior Beam	Exterior Beam
HS-20	1.17	1.64	1.77	1.80 *	1.68 **
Type 3	1.60	2.27	2.44	2.46 **	2.26 **
Type 3S2	1.44	1.93	2.07	2.21 *	2.06 **
Type 3-3	1.51	1.93	2.07	2.29 *	2.15 **
NM 2	2.29	3.20	3.43	3.46 **	3.19 **
NM 3A	1.68	2.38	2.58	2.58 **	2.38 **
NM 5A	1.62	1.91	2.05	2.27 *	2.17 **

Notes: LFR rating factors controlled by shear strength and LRFR rating factors controlled by shear strength (*) or flexural strength (**); all rating factors computed with legal load plus pedestrian loading.

9.6 BRIDGE NO. 8676, R/C SLAB

Design and legal load rating analyses were performed for Bridge 8676. The LFR method was used to compute the design load rating under HS-20 loading and both the LFR and LRFR methods were used to compute the legal load rating under state and federal legal loading. No load tests were performed on this bridge, only the BrR analysis was done. As discussed before, the reinforcement layout of Bridge 8676 was determined with the Hilti Ferroscan system and the reinforcement was

input based on the as-built drawings shown in Figures 5.23 and 5.24. The bottom mat longitudinal reinforcement consisted of #6 and #8 bars alternately spaced every 12 in. Since the bridge is simple-supported, the top reinforcement was not needed. Grade 60 reinforcement and 4 ksi concrete were used based on the construction year. There are no utilities on this bridge.

For quality assurance purposes, a one-ft strip model and whole system model of Bridge 8676 were developed in the BrR program. There are two basic differences between the two models. First, only one-ft reinforcement needs to be input for the one-ft strip model while the whole system model requires the input of all reinforcement. Second, the distribution factor for the one-ft model must be calculated by hand according to the AASHTO *Manual* while the factor is automatically calculated for the whole system model. The two rating models gave the same HS-20 design rating factors based on the LFR method. The inventory rating factor was 0.524 at 60% of the bridge length and concrete flexure was the controlling limit state. The operating rating factor of the bridge was 0.875 at the same location. According to NMDOT policy (operating rating greater than 0.85), a legal load rating analysis was not necessary; however, the analysis was performed to determine the need for load posting.

Table 9.14 shows the legal load rating results for the whole system model and the one-ft strip model for Bridge 8676 based on the LFR and LRFR methods. Again, the two analysis models produced the same results which verified the accuracy of the BrR input properties. For all legal loads, the controlling location is at midspan of the bridge and the limit state is concrete flexure. The LRFR results show that the bridge is only adequate for Type 3-3 and NM 2 loading since the legal load rating factors are 1.05 and 1.13, respectively. For Type 3, Type 3S2, NM 3A, and NM 5A, the rating factors are 0.85, 0.87, 0.85, and 0.81, respectively, which signifies the bridge needs to be load posted for these four legal loads. The safe posting loads were determined using Eq. (9.5) given earlier and are reported in Table 9.14. Note that the LFR results all exceed one signifying that load posting is not necessary.

Table 9.14. BrR legal load rating factors and posting loads (Bridge 8676).

Legal Load	*W* (kips)	*LFR Rating Factor*	*LRFR Rating Factor*	*Safe Posting Load* (tons) *
HS-20	72.0	0.88	0.69	20.1
Type 3	50.0	1.07	0.85	19.6
Type 3S2	80.0	1.10	0.87	32.6
Type 3-3	72.0	1.33	1.05	N/A
NM 2	33.6	1.43	1.13	N/A
NM 3A	46.3	1.07	0.85	19.6
NM 5A	80.6	1.03	0.81	29.4

Notes: * - Computed based on the LRFR rating factors.

10. SUMMARY AND CONCLUSIONS

10.1 SUMMARY

Project NM13STR-01 consisted of four major tasks including the collection of data pertaining to the concrete bridges without plans selected for load testing in New Mexico (**Task 1**); survey of the load rating procedures used in other state DOTs to evaluate planless bridges (**Task 2**); review of the literature related to domestic and international research and best practices for load testing and rating of bridges without plans (**Task 3**); and the development of experimental and analytical load rating procedures for simple-supported prestressed concrete and reinforced concrete slab bridges with no plans (**Task 4**). Attention was given to the load testing and rating of prestressed concrete bridges since the evaluation procedures for reinforced concrete and steel bridges are much better established. Furthermore, five of the six concrete bridges evaluated in this project are prestressed.

This final report covers the in-depth inspection results, Magnel diagram estimates, Ferroscan and Windsor probe evaluations, diagnostic and proof tests, and load rating of the prestressed concrete bridges. Furthermore, this report contains the inspection observations, Ferroscan and Windsor probe results, and load ratings of the reinforced concrete bridge. Testing was omitted for this bridge since the Ferroscan provided accurate results of the reinforcement layout and the load rating is controlled by the strength limit state. Also included in this report is a detailed guide for using the Hilti Ferroscan and Windsor probe instruments (see Appendix A). The guide provides background information on both instruments and specific recommendations on the operation based on bridge type. In Appendix B, a paper containing the test procedures and results from acoustic emission monitoring of NMDOT Bridge 7701 are presented. In Appendix C, the final load ratings for all bridges are documented in the NMDOT standard load rating forms.

Apart from the final report, an implementation plan and multimedia presentation were created for Project NM13STR-01. The implementation plan provides a step-by-step guide for load rating the remaining simple-span prestressed concrete and reinforced concrete slab bridges without plans in New Mexico. The implementation plan was developed directly from the findings from Project NM13STR01 and evaluates each bridge based on the structure's unique characteristics and corresponding design specifications. The multimedia presentation documents the evaluation of each bridge involved in this project. The presentation covers the analysis of each bridge, and includes images and results from the diagnostic and proof tests, as well as the final load ratings.

10.2 CONCLUSIONS

Based directly on the bridges evaluated in Project NM13STR-01, a multiple-step load rating procedure was developed for simple-span prestressed concrete and reinforced concrete slab bridges without plans in New Mexico. The implementation of both procedures yielded the following conclusions:

- The literature review provided little guidance on proof testing of prestressed concrete bridges without plans. Although testing has been conducted for load rating purposes, the majority of recent tests were diagnostic rather than proof. In addition, proof tests have been performed mainly on reinforced concrete bridges rather than prestressed concrete.
- Conducting load tests of prestressed concrete bridges based on serviceability, or the Service III limit state (concrete cracking), was necessary to ensure the bridges remained uncracked. It was important to take precaution in the testing, particularly for bridges with missing or damaged shear keys between beams, since the actual live load distribution is uncertain.
- Diagnostic load tests were helpful in planning the proof tests of prestressed concrete bridges in cases where the live load path was uncertain (e.g., missing or damaged shear keys). These tests provided useful information on the actual bridge behavior under truck loading below the estimated cracking load.
- The monitoring of strain was effective in controlling the proof tests to avoid overloading the prestressed concrete bridges. Preparatory calculations were required to determine the available strains that the bridges could endure without cracking, and the proof tests were monitored by ensuring that the measured beam strains did not exceed the available strains.
- Based on the dump truck positions that induced the available strains, the applied moments were computed and compared to the target moments for the AASHTO and New Mexico legal loads. These comparisons were then used in accordance with the AASHTO *Manual* to develop rating factors and safe posting loads for prestressed concrete bridges. Load testing exposed the true bridge behavior and showed that load ratings determined assuming complete shear transfer between beams may overestimate the capacity of damaged bridges.
- An AASHTOWare BrR load rating analysis should be performed for prestressed concrete bridges to check the strength limit state (i.e., flexural and shear capacity) and compare the ratings with those determined based on the proof test results for serviceability. In addition, the BrR analysis should be done using the LFR and LRFR methods for both prestressed concrete and reinforced concrete slab bridges in order to select the most appropriate load ratings using engineering judgement. Discrepancies between LFR and LRFR ratings were found from bridge to bridge, thus making it imperative to check both.
- The Hilti Ferroscan proved to be extremely effective in determining the size, spacing, and concrete cover of the steel reinforcement in the reinforced concrete slab bridge and marginally effective for the prestressed concrete bridges. Due to the high accuracy of the Ferroscan results, load testing was omitted and the reinforcement measurements were used along with the structural dimensions and estimated material properties to perform the load rating using the AASHTOWare BrR program.
- The Windsor probe was effective in verifying the estimated strength of cast-in-place concrete. Both the slab bridge and the deck of the prestressed concrete I-girder bridge were successfully tested and the test measurements showed the concrete strength to be higher than the assumed strength. However, the Windsor probe proved to be less effective for precast prestressed concrete, as the probe did not fully embed in most cases.

This study provided valuable information for future evaluations of prestressed concrete bridges without plans. For instance, if an in-depth inspection is performed and no excessive signs of damage or distress are found, a diagnostic test may be excluded if there is confidence that the bridge behavior can be predicted. Furthermore, if high quality images of the prestressing strands can be obtained from a rebar scanner and the bridge is in good condition, load testing may be

avoided altogether since the bridge may be modeled and rated analytically based on the bridge properties determined from the design specifications and Magnel diagrams. The implementation plan that accompanies this report provides a detailed guide for evaluating the remaining prestressed concrete bridges.

It is important to note that even though the AASHTO *Manual* was generally used in this study, there are no specific guidelines in the manual that address the load rating of prestressed concrete bridges through proof load testing. The manual provides guidance for proof testing based on strength but not serviceability. Although common testing procedures were employed herein, the procedures were adapted to the service limit state for concrete tension, which required a unique approach not given in the AASHTO *Manual*. In addition, the literature review done prior to this evaluation uncovered just a few publications (mainly reports from state DOTs or consultants) that gave minimal direction for the load rating of bridges via proof testing, in particular prestressed concrete bridges without design plans.

Apart from prestressed concrete bridges, this study provided valuable info for future evaluations of simple-supported reinforced concrete slab bridges without plans. As mentioned earlier, the Hilti Ferroscan proved to be very effective in detecting mild steel reinforcement, thus eliminating the need for load testing. The results from the scan, along with estimated material properties and field measurements, can be used to perform an AASHTOWare BrR analysis. With an accurate reinforcement layout, the BrR load ratings provide reasonable estimates of the bridge capacity.

APPENDIX A: BASIC FERROSCAN AND WINDSOR PROBE GUIDE

This appendix provides information related to the general and bridge-specific operation of the non-destructive-testing equipment including the Hilti PS 250 Ferroscan System and Windsor Probe WP-534 System. The test procedures and interpretation of results from the Ferroscan and Windsor Probe systems largely depend on the bridge type and thus, guidance is provided for the different bridges tested in Project NM13STR-01 including reinforced concrete slab, prestressed concrete double T-beam, prestressed concrete box girder, and prestressed concrete I-girder bridges.

A.1 GENERAL OPERATION

A.1.1 FERROSCAN

A Hilti PS 250 Ferroscan system may be used to scan the location, size, and cover of the steel reinforcement (i.e., longitudinal strands and transverse rebars) in prestressed concrete beams and reinforced concrete slabs. The Ferroscan has certain limitations that must be considered. First, the scanner is generally capable of providing accurate results only for the first layer of reinforcement and a minimum ratio of 2:1 is required for the center-to-center rebar spacing (s) to clear concrete cover of the steel bar (c) as shown in Figure A.1. Second, the accuracy of the rebar size estimate is ±1 standard bar diameter and the bar location must be greater than 0.4 in. and less than 2.4 in. from the concrete surface to obtain an accurate depth measurement. Third, the Ferroscan is most accurate for detecting steel reinforcing bars that meet the ASTM A615 / A615M-01b Standard Specification for Deformed and Plain Carbon-Steel Bars for Concrete Reinforcement. In general, for prestressed concrete bridges, the scans of the steel strand are not as accurate due to the seven-wire arrangement. The Ferroscan provides better results of the transverse shear reinforcement in prestressed concrete beams which are typically deformed or plain bars and similarly the longitudinal reinforcement in concrete slab bridges. The Hilti PS 250 Ferroscan system is operated by moving the scanner directly over the concrete surface. The data collected is automatically stored in the scanner and subsequently, can be wirelessly transferred to the monitor for viewing of the scans in the field. Figure A.2 shows the scanner and monitor components of the Ferroscan.

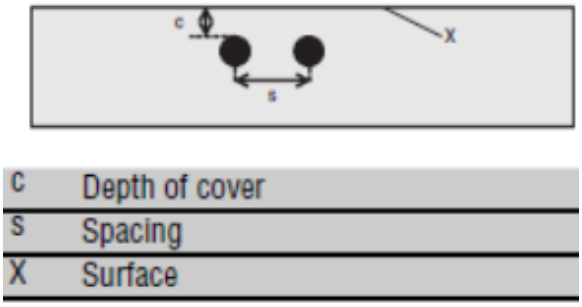

Figure A.1 Bar spacing and depth of cover used by Ferroscan (Hilti 2013).

Figure A.2 Scanner and monitor components of Ferroscan (Hilti 2013).

Three different types of scans can be generated with the Ferroscan: quickscans, imagescans, and blockscans. Quickscans require that the scanner be moved over the concrete surface at right angles to the steel reinforcement. The scanner will most accurately detect reinforcing bars oriented at right angles to the scanner direction; incorrect depths will result if the bars lie diagonal to the scanner. The accuracy of the quickscans is improved if the bar diameter and/or spacing is/are known and entered into the scanner. Quickscan data can be easily recorded and transferred to the monitor, and finally to a computer for detailed evaluation of the cover depth and spacing. During a quickscan, the approximate bar cover is shown on the scanner display (see Figure A.3) and a signal tone is emitted when the scanner is positioned over the center of a rebar. The scanner should not be positioned directly over a rebar at the beginning or ending of a quickscan recording. Furthermore, the scanner must remain in contact with the concrete surface at all times during recording. Up to 98 feet can be recorded with the scanner before the data must be transferred.

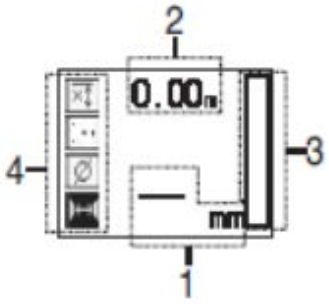

1	Bar depth
2	Distance traveled
3	Signal strength
4	Settings: minimum depth, scan direction, bar diameter, bar spacing

Figure A.3 Ferroscan quickscan screen during recording (Hilti 2013).

Imagescans are generated by moving the scanner along eight different paths (four horizontal and four vertical) over a 2 ft by 2 ft reference grid positioned in the area of interest. To start, the imagescan mode is selected in the scanner. The rows and columns of the grid are displayed and an arrow is displayed at a default starting point; the starting point may be reassigned to different corners to facilitate scanning. The scanner must be placed on the reference grid at the same starting point as the one chosen on the scanner screen and the alignment marks on the scanner must line up correctly with the reference grid. Incorrect alignment can lead to imagescan results with incorrect reinforcement information. Furthermore, imagescan data will only be generated for areas of the grid that have been scanned both vertically and horizontally. Figure A.4 shows the starting point and horizontal / vertical paths needed for the imagescan. Imagescan data can be evaluated once transferred to the Ferroscan monitor or computer. Estimates of the size, location, and concrete depth of the reinforcement will be shown. Up to nine imagescans can be recorded with the scanner before the data must be transferred.

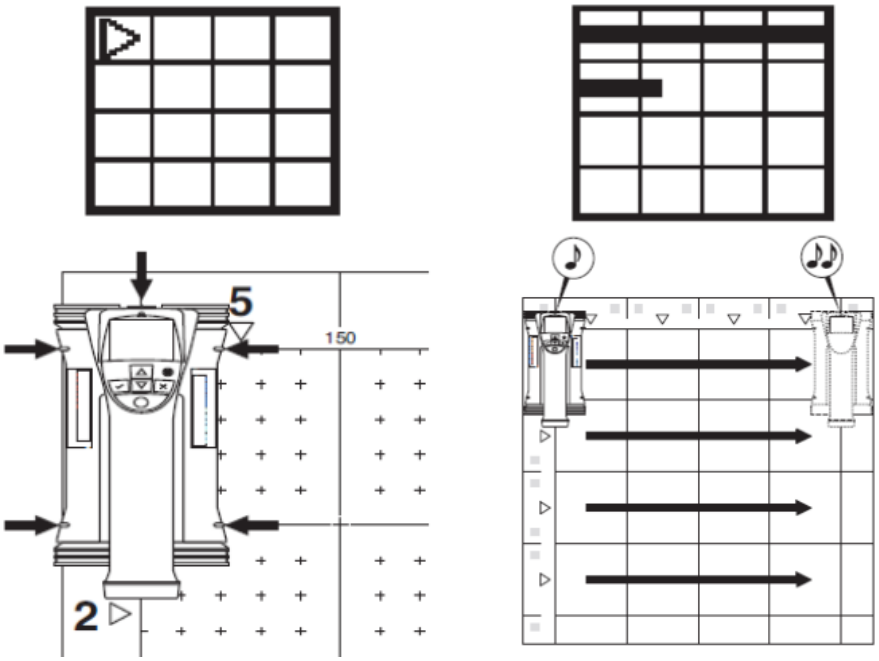

(a) (b)

Figure A.4 (a) Starting point and (b) horizontal / vertical paths for imagescan (Hilti 2013).

Blockscans are generated by overlapping several imagescans collected over a selected area. For example, a blockscan of a 6 ft by 6 ft area can be produced with nine imagescans on a 3 by 3 grid. As the blockscan proceeds from imagescan to imagescan, the guide holes in the 2 ft by 2 ft reference grids must be lined up as shown in Figure A.5. The scanner automatically stitches the imagescans into a blockscan, thus giving the reinforcement configuration over a larger area than an individual imagescan. Estimates of the rebar position, concrete cover, and size are provided similar to an imagescan.

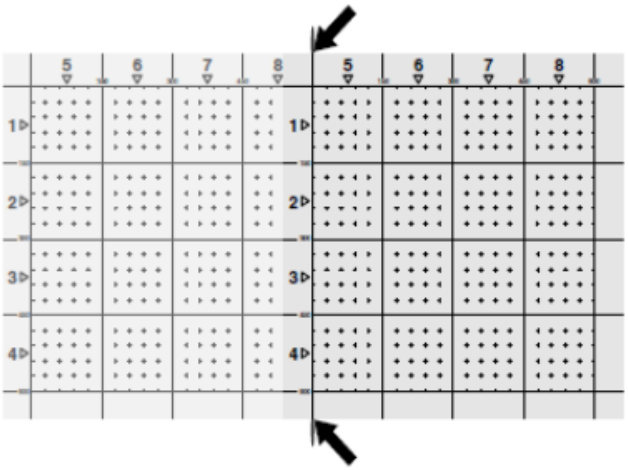

Figure A.5 Alignment of imagescan reference grids for blockscan (Hilti 2013).

The scanner display shows the imagescan slots available for creating a blockscan (see Figure A.6). Note that a blockscan does not require that all nine imagescan locations be used, only those needed to capture the area of interest (e.g., a 2 ft by 6 ft blockscan of a concrete beam can be generated with just the first row of three imagescans). As previously mentioned, up to nine imagescans can be recorded as shown in Figure A.6 before data transfer is required. Hence, a 6 ft x 6 ft blockscan may be generated from nine imagescans or smaller size blockscans may be produced from a fewer number of imagescans. For ease of scanning, the 2 ft by 2 ft reference grid should be adhered to a rigid (e.g., plastic, cardboard) backing. The backing is particularly handy for scanning beams with shallow depths since the backing provides a smooth surface for the scanner to travel past the bottom of the beam. In addition, the reference grid can be more easily handled and consistently placed in the field.

(a) (b)

Figure A.6 (a) Starting slot and (b) available imagescan slots for blockscan (Hilti 2013).

A.1.2 WINDSOR PROBE

The Windsor Probe penetration test is a non-destructive testing method for estimating the compression strength of in-situ concrete. Manufacturers have claimed that the test can be used to

estimate the compressive strength of concrete up to 17,000 psi and calibration charts are devised for different aggregate hardness values. The Windsor Probe System WP-534 consists of a driver and probes as shown in Figure A.7. In a typical test, a probe is shot into the concrete with the driver and the depth of probe penetration is measured. Probes are 3.125 in. long and there are two types, PRS-01 silver and PRS-03 gold. Silver probes have a 0.25 in. step diameter as shown in Figure A.8 and are used to test standard weight concrete (greater than 125 pcf) with standard coarse aggregate. Gold probes are 0.3125 in. in diameter throughout the probe length and are used to test lightweight concrete with densities less than 125 pcf (Malhotra 2004).

Figure A.6 Driver and probes of Windsor Probe System WP-534 (Windsor 2010).

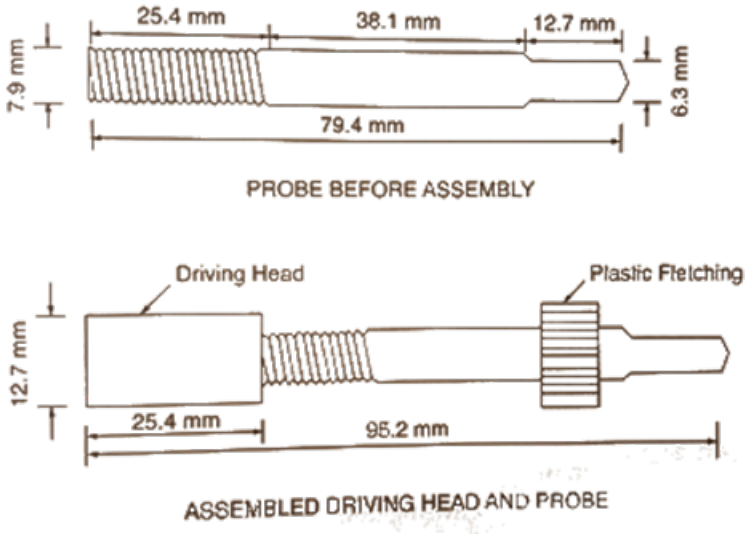

Figure A.7 PRS-01 silver probe configuration for normal-weight concrete (Malhotra 2004).

The correlation between the probe penetration depth and the concrete compressive strength varies with the hardness of the coarse aggregate. In general, the harder the coarse aggregate, the longer the exposed length of the driven probe. Equipment manufacturers provide both low and standard power tables to relate the exposed probe length with the coarse aggregate hardness. The hardness is found using a Mohs' test kit with nine minerals listed here in increasing hardness from #1 to #9: talc, gypsum, calcite, fluorite, apatite, feldspar, quartz, beryl, and corundum. The Mohs' test starts by scratching the coarse aggregate with the hardest mineral (i.e., #9) and the test continues with the softer minerals in descending order of hardness until the mineral is found that does not scratch the coarse aggregate. The Mohs' hardness number of the softest mineral that does not leave a scratch represents the coarse aggregate hardness used in the power tables. If there is no coarse aggregate in the concrete, a Mohs' hardness of #3 may be assumed. As mentioned before, coarse aggregate hardness is directly related to the compressive strength estimate for the concrete. Studies have found that the consistency of aggregate hardness will affect the accuracy of the concrete strength estimate. Thus, several samples of coarse aggregate should be taken from the concrete specimen and tested for consistency. Coarse aggregate directly exposed to the environment should not be used since the hardness may have been affected by the exposure to the elements.

The WP-534 power tables show the correlation between the height of the exposed probe and the concrete compressive strength (based on Mohs' hardness of the coarse aggregate). The power tables are calibrated to the probe velocity in the standard power mode. Standard power is recommended for estimating the compressive strength of concrete that has been cured for longer than 28 days or with strengths greater than 3,000 psi. The low power mode of the WP-534 instrument is set by positioning the probe lower in the driver barrel which drives the probe at a lower velocity and power. The low power table is calibrated for this difference in velocity. The low and standard power tables give similar exposed lengths for strengths approximately 3,600 psi. However, the low power table will provide more accurate results for concrete strengths around 3,000 psi. Tables A.1 and A.2 show a typical standard power and low power table, respectively, for the WP-534 system. As shown in both tables, the concrete compressive strength is estimated based on the exposed probe length and Mohs' hardness of the coarse aggregate.

In 1972, ASTM Committee C-9 began the development of a standard for penetration resistance testing that included probe penetration that was introduced in 1975 (Malhotra 2004). The ASTM C 803 Standard Test Method for Penetration Resistance of Hardened Concrete gives the procedures for proper execution of Windsor probe testing. The latest version gives the following guidance (ASTM C 803):

> 1) This test method is applicable to assess the uniformity of concrete and to delineate zones of poor quality or deteriorated concrete in structures.

Table A.1 Typical standard power table for Windsor Probe System WP-534 (Windsor 2010).

Exposed Probe inches (mm)	Mohs' No. 3 psi (MPa)	Mohs' No. 4 psi (MPa)	Mohs' No. 5 psi (MPa)	Mohs' No. 6 psi (MPa)	Mohs' No. 7 psi (MPa)
1.275 (3.239)					
1.300 (3.302)					
1.325 (3.366)					
1.350 (3.429)					
1.375 (3.493)					
1.400 (3.556)	3000 (20.6)				
1.425 (3.620)	3175 (21.9)				
1.450 (3.683)	3325 (22.9)				
1.475 (3.747)	3500 (24.1)				
1.500 (3.810)	3675 (25.3)	3000 (20.6)			
1.525 (3.874)	3825 (26.3)	3175 (21.9)			
1.550 (3.937)	4000 (27.5)	3350 (23.1)			
1.575 (4.001)	4175 (28.8)	3525 (24.3)			
1.600 (4.064)	4325 (29.8)	3700 (25.5)	3050 (21.0)		
1.625 (4.128)	4500 (31.0)	3875 (26.7)	3225 (22.2)		
1.650 (4.191)	4675 (32.2)	4050 (27.9)	3400 (23.4)		
1.675 (4.255)	4825 (33.2)	4225 (29.1)	3600 (24.8)		
1.700 (4.318)	5000 (34.4)	4400 (30.3)	3775 (26.0)	3000 (20.6)	
1.725 (4.382)	5175 (35.7)	4575 (31.5)	3950 (27.2)	3200 (22.0)	
1.750 (4.445)	5325 (36.7)	4750 (32.7)	4150 (28.6)	3400 (23.4)	
1.775 (4.509)	5500 (37.9)	4925 (33.9)	4325 (29.8)	3600 (24.8)	
1.800 (4.572)	5675 (39.1)	5100 (35.1)	4500 (31.0)	3800 (26.2)	3000 (20.8)
1.825 (4.636)	5825 (40.1)	5275 (36.3)	4700 (32.4)	4000 (27.5)	3225 (22.2)
1.850 (4.699)	6000 (41.3)	5450 (37.5)	4875 (33.6)	4200 (23.9)	3425 (23.6)
1.875 (4.763)	6175 (42.6)	5625 (38.8)	5050 (34.8)	4400 (30.3)	3650 (25.1)
1.900 (4.826)	6325 (43.6)	5800 (40.0)	5250 (36.2)	4600 (31.7)	3875 (26.7)
1.925 (4.890)	6500 (44.8)	5975 (41.2)	5425 (37.4)	4800 (33.1)	4100 (28.2)

Table A.2 Typical low power table for Windsor Probe System WP-534 (Windsor 2010).

Exposed Probe inches (mm)		Mohs' No. 3 psi (MPa)		Mohs' No. 4 psi (MPa)		Mohs' No. 5 psi (MPa)		Mohs' No. 6 psi (MPa)		Mohs' No. 7 psi (MPa)	
1.125	(28.575)	525	(3.62)								
1.150	(29.210)	625	(4.31)								
1.175	(29.845)	725	(5.00)	450	(3.10)						
1.200	(30.480)	800	(5.51)	525	(3.62)						
1.225	(31.115)	900	(6.20)	600	(4.13)						
1.250	(31.75)	1000	(6.89)	675	(4.65)						
1.275	(3.239)	1075	(7.41)	750	(5.17)						
1.300	(3.302)	1175	(8.10)	825	(5.69)	450	(3.10)				
1.325	(3.366)	1250	(8.62)	900	(6.20)	525	(3.62)				
1.350	(3.429)	1325	(9.14)	975	(6.72)	600	(4.13)				
1.375	(3.493)	1400	(9.65)	1075	(7.41)	700	(4.82)				
1.400	(3.556)	1500	(10.3)	1150	(7.93)	775	(5.34)				
1.425	(3.620)	1575	(10.8)	1225	(8.45)	875	(6.03)	400	(2.75)		
1.450	(3.683)	1650	(11.3)	1300	(8.96)	975	(6.72)	500	(3.44)		
1.475	(3.747)	1725	(11.9)	1400	(9.65)	1050	(7.24)	600	(4.13)		
1.500	(3.810)	1850	(12.7)	1500	(10.3)	1150	(7.93)	700	(4.82)		
1.525	(3.874)	1925	(13.2)	1575	(10.8)	1250	(8.62)	800	(5.51)		
1.550	(3.937)	2000	(13.7)	1675	(11.5)	1325	(9.14)	900	(6.20)	450	(3.10)
1.575	(4.001)	2075	(14.3)	1750	(12.0)	1425	(9.83)	1000	(6.89)	550	(3.79)
1.600	(4.064)	2150	(14.8)	1850	(12.7)	1525	(10.5)	1100	(7.58)	650	(4.48)
1.625	(4.128)	2250	(15.5)	1950	(13.4)	1600	(11.0)	1200	(8.27)	750	(5.17)
1.650	(4.191)	2325	(16.0)	2025	(13.9)	1700	(11.7)	1300	(8.96)	875	(6.03)
1.675	(4.255)	2400	(16.5)	2100	(14.4)	1800	(12.4)	1400	(9.65)	975	(6.72)
1.700	(4.318)	2500	(17.2)	2200	(15.1)	1875	(12.9)	1500	(10.3)	1075	(7.41)
1.725	(4.382)	2575	(17.7)	2275	(15.6)	1975	(13.6)	1600	(11.0)	1175	(8.10)
1.750	(4.445)	2650	(18.2)	2375	(16.0)	2075	(14.3)	1700	(11.7)	1275	(8.79)
1.775	(4.509)	2750	(18.9)	2450	(16.9)	2150	(14.8)	1800	(12.4)	1400	(9.65)
1.800	(4.572)	2825	(19.4)	2550	(17.5)	2250	(15.5)	1900	(13.1)	1500	(10.3)
1.825	(4.636)	2900	(20.0)	2650	(18.2)	2350	(16.2)	2000	(13.7)	1600	(11.0)

2) This test method is applicable to estimate in-place strength, provided that a relationship has been experimentally established between penetration resistance and concrete strength. Such a relationship must be established for a given test apparatus, using similar concrete materials and mixture proportions as in the structure. Use the procedures and statistical method in ACI 228.1R for developing and using the strength relationship.
3) Steel probes are driven with a high-energy, powder-actuated driver, and probes may penetrate some aggregate particles. Probe penetration resistance is affected by concrete strength as well as the nature of the coarse aggregate. Steel pins are smaller in size than probes and are driven by a low energy, spring-actuated driver. Pins are intended to penetrate the mortar fraction only; therefore, a test in which a pin strikes a coarse aggregate particle is disregarded.
4) This test method results in surface damage to the concrete, which may require repair in exposed architectural finishes.

As illustrated in Figure A.8, a Windsor probe test is conducted by holding the driving head of the WP-534 instrument perpendicular to the surface of the concrete, placing it on the firing template, and firing the probe into the concrete. A measuring cap and plate are then installed on the embedded probe and a calibrated micrometer is used to measure the exposed probe length to the nearest 0.025 inch. The mineral scratch test is finally done on the coarse aggregate to obtain the Mohs' hardness value and together with the exposed probe length are used to determine the concrete compressive strength from the table. In NMDOT Project NM13STR-01, the standard power mode was used since the compressive strengths of the selected concrete bridges for load testing were all expected to be larger than 3,000 psi. In addition, PRS-01 silver probes were used rather than PRS-03 gold probes since the former are designed to penetrate concrete with compressive strengths up to 17,000 psi.

Figure A.8 Windsor probe penetration test

A minimum of three embedded probe measurements are necessary to obtain statistically significant results. The ASTM C 803 standard provides a table that gives the range difference allowed between the three measurements (see Table A.3). If the three exposed probes fall outside this range, a

fourth measurement is required. To properly test the concrete, ASTM C 803 states that the probes cannot penetrate more than half the thickness of the concrete member and must be four inches from any edge of the concrete surface and seven inches from any other probe. Furthermore, the probes must be fully embedded in the concrete and any loose probes must be discarded. A small hammer can be used to tap the probes to ensure proper embedment.

Table A.3 Precision for resistance testing with probes (ASTM C 803).

Maximum Size of Aggregate	Limit	Maximum Range of Three Individual Measurements	Limit Maximum Difference Between Two Tests (Each test calculated as the average of three measurements)
inches (mm)	inches (mm)	inches (mm)	inches (mm)
No. 4 (Mortar)	0.08 (2.0)	0.26 (6.6)	0.13 (3.3)
1 (25)	0.1 (2.5)	0.33 (8.4)	0.16 (4.1)
2 (50)	0.14 (3.6)	0.46 (11.7)	0.22 (5.6)

A.2 BRIDGE-SPECIFIC INSTRUCTIONS

A.2.1 R/C SLAB BRIDGES

Simple-supported slab bridges require use of the Hilti PS 250 Ferroscan to identify the bottom steel mat reinforcement configuration which is the principal variable affecting the load capacity. Due to symmetry, only a quarter of the bridge needs to be scanned to determine the bottom steel reinforcement. Recall that only the steel layer closest to the concrete surface generally is measurable. Large blockscans (e.g., 6 ft x 6 ft) can be used to facilitate the scanning process. From the blockscans, the rebar locations and lengths can be determined as illustrated in Figure A.9. Other locations along the slab can be scanned to ensure consistency in the measurements. The Ferroscan software can estimate the bar size and location. The frequency of the reinforcement bar sizes are estimated and the most consistent size is used for the load rating. If the reinforcement is the same size throughout the slab, the Ferroscan results are generally more accurate.

Once the reinforcement bar size and spacing has been estimated from the imagescans or blockscans, the concrete cover and rebar spacing can be further evaluated using quickscans. Quickscans cannot estimate the bar size and thus, a reinforcement bar size must be entered to obtain the most accurate results. If the slab has alternating rebar sizes, the variations may be visible in the quickscan. Figure A.10 shows the typical quickscan results for a slab bridge. The x-axis represents the rebar locations and the y-axis is the corresponding concrete cover. As shown in the figure, the concrete cover varies in a regular pattern which suggest the rebar sizes are alternating.

The depth cover is measured from the concrete surface to the edge of the reinforcement; hence, as the rebars alternate, so do the concrete cover depths.

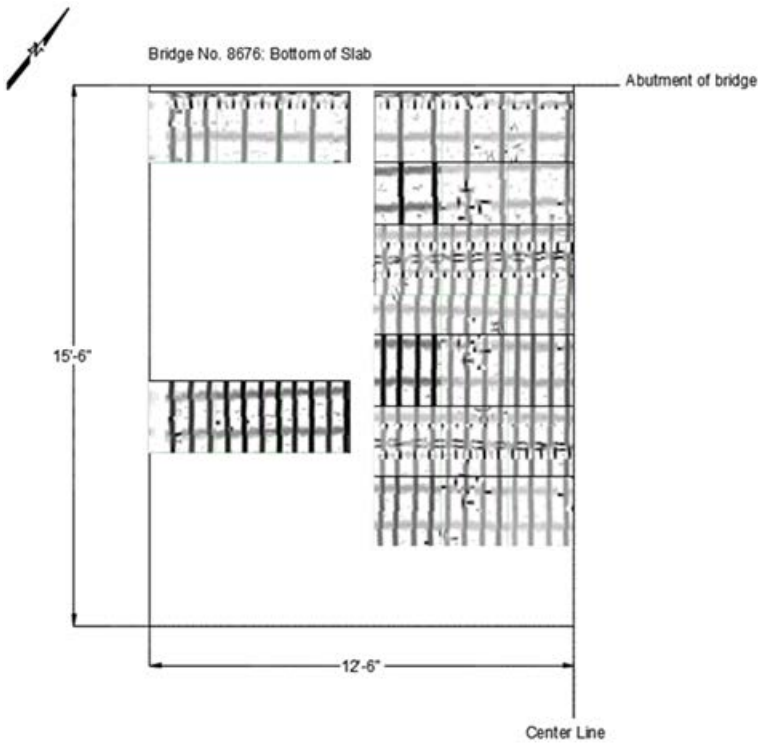

Figure A.9 Typical blockscan results for reinforced concrete slab bridge.

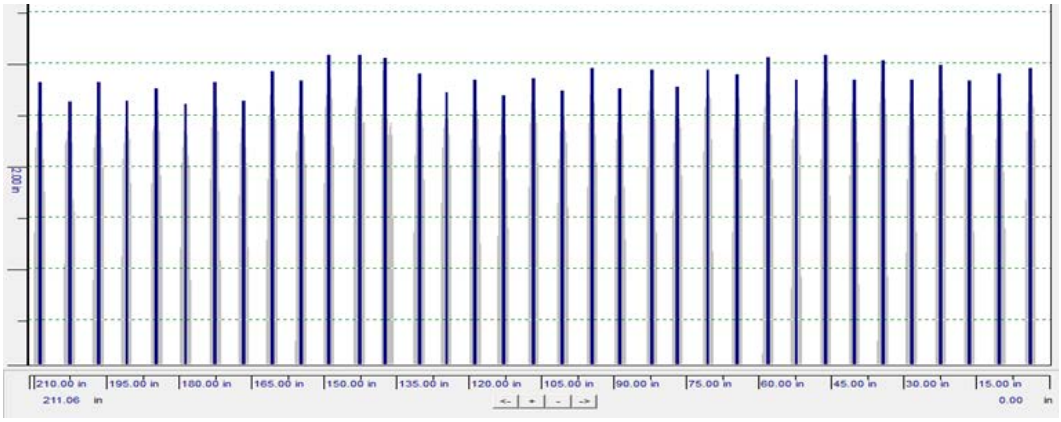

Figure A.10 Typical quickscan results for reinforced concrete slab bridge.

The Windsor probe penetration test is a practical method for cast-in-place reinforced concrete slab bridges, since the concrete is lower strength and the topside of the slab may be exposed. Slab bridges that have a wearing surface may alternatively be tested on the bottom side. Test locations over the slab area should be chosen four inches from any edge and preferably away from traffic

on the topside (i.e., shoulder areas). Before the penetration test, the quickscan feature of the Ferroscan should be used to locate the reinforcement. This ensures that the Windsor probe will be driven through the concrete without hitting the steel which can compromise the compressive strength estimates. Once the Windsor probe has been shot, a small divot or spall may occur where the probe penetrated. Coarse aggregates may be gathered from these areas for the Mohs' hardness test before the concrete is repaired with non-shrink grout.

A.2.2 P/C DOUBLE T-BEAM BRIDGES

With the HILTI PS 250 Ferroscan system, an attempt can be made to determine the prestressing strand configuration of double T-beam bridges by scanning along the height and length of the beam stems. Figure A.11 shows a typical beam cross-section and the scanning setup. The hatched region represents the paths where the Ferroscan is moved. The figure also illustrates the placement of a plastic backing between the Ferroscan and the concrete surface to ensure the entire beam depth is scanned.

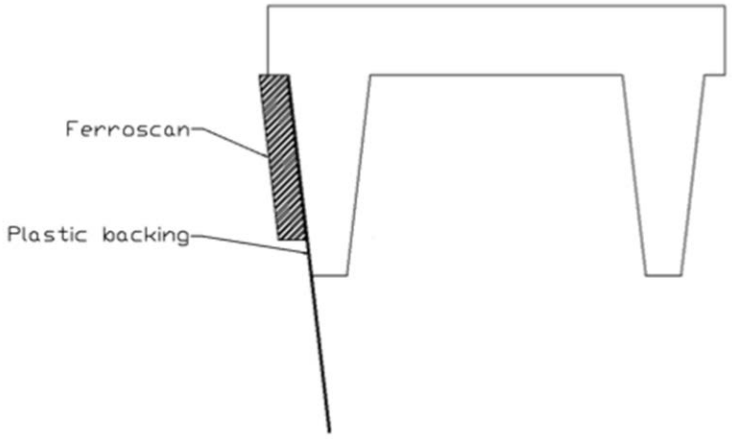

Figure A.11 Typical Ferroscan measurement setup for double T-beam bridges.

Blockscans should be taken near midspan and as close to the abutments as possible for both an interior and exterior beam. Both beams should be scanned to verify that the beams are the same since the bridge may have been widened resulting in different longitudinal prestressing strand and/or transverse shear reinforcement details. The abutment and midspan blockscans may be compared to determine any changes in the stirrup spacing and also to check if the prestressing strands are harped. Figure A.12 shows a typical blockscan along a double T-beam web near the harp point. Due to the close strand spacing, it may not be possible to distinguish individual strands near midspan; however, strand deviation (if present) will result in larger spacing between the strand groups near the beam ends. In general, strands are harped at 0.4L and the prestressing strands are tightly spaced (i.e., less than or equal to 2 in.) in the middle 20% of the beam length which

complicates the size estimate. Furthermore, due to the seven-wire strand arrangement (rather than standard bars), the imagescans may result in a wide range of bar size estimates.

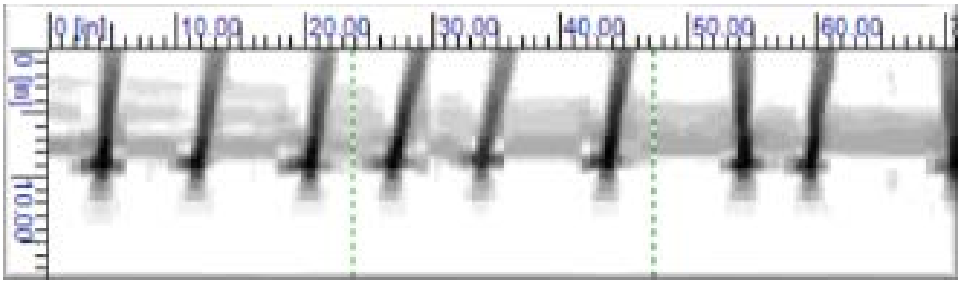

Figure A.12 Typical blockscan of double T-beam web near harp point.

The HILTI PS 250 Ferroscan can provide accurate bar estimates of the vertical shear reinforcement in double T-beam bridges using the imagescan or blockscan feature. However, care must be taken to ensure that the bar size estimates correspond to the stirrups. Locations where the stirrups overlap with the prestressing strand will produce larger than actual bar sizes that should be discarded. The stirrup spacing and concrete cover can be determined most easily from the quickscan results as discussed earlier for reinforced concrete slab bridges. To determine the number of stirrup legs in each beam stem, imagescans should be taken on the inside and outside faces of the stem as shown in Figure A.13. The depth range viewer of the HILTI PS 250 Ferroscan software provides a useful tool to compare the two imagescans. The viewer shows the internal reinforcement at different concrete depths as shown in Figure A.14. Thus, if the beam has double-leg stirrups, the stirrup will be the last visible on both sides of the stem as the depth range is decreased which signifies that the stirrup is closest to the concrete surface (see Figure A.15). However, if the beam has single-leg stirrups, the stirrup will appear closest to the concrete surface one side of the stem and the opposite side will show the prestressing strands to be closest (see Figure A.16).

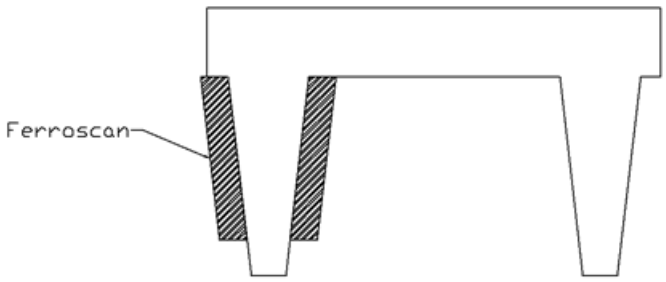

Figure A.13 Ferroscan measurements on interior and exterior faces of double T-beam stem.

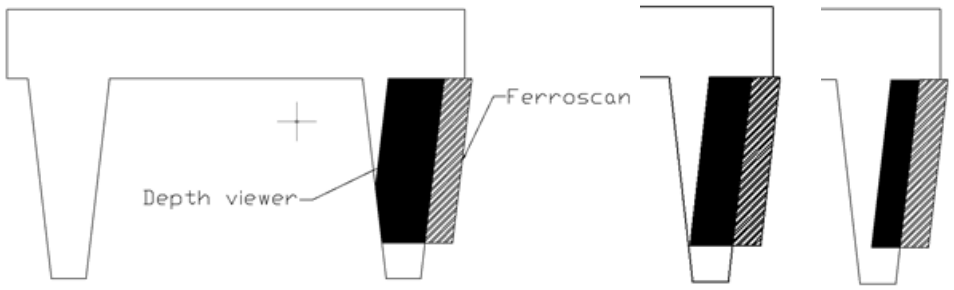

Figure A.14 Depth range viewer of Ferroscan.

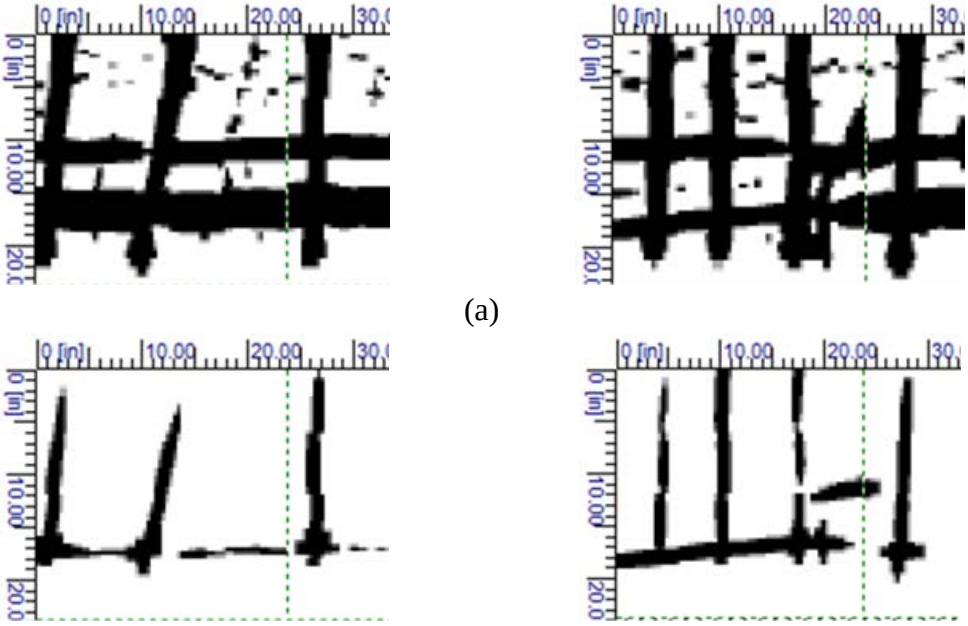

(a)

(b)

Figure A.14 Typical imagescan results for double-leg stirrup viewed at (a) large depth range and (b) small depth range.

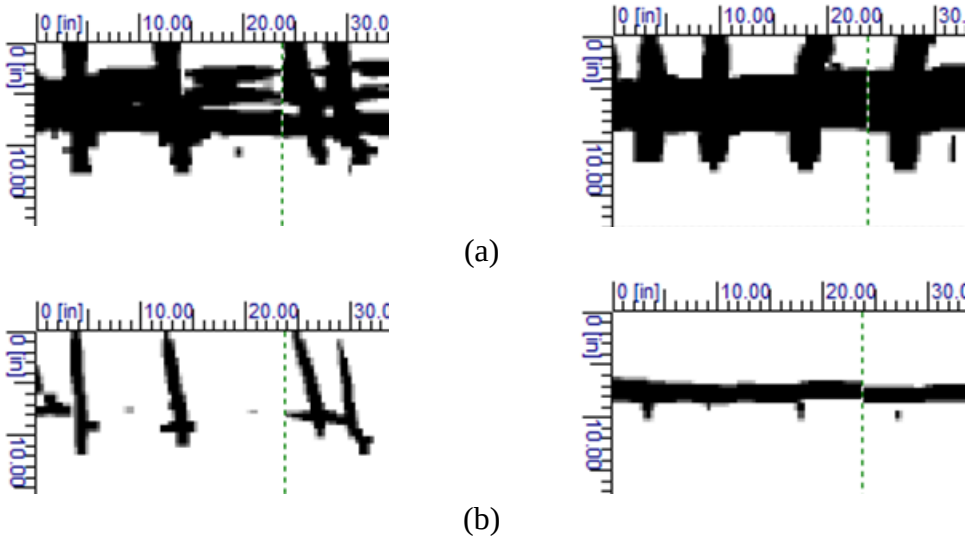

Figure A.14 Typical imagescan results for single-leg stirrup viewed at (a) large depth range and (b) small depth range.

The Windsor probe penetration test remains a practical method for precast, prestressed concrete double T-beam bridges since the topside of the beam flanges may be exposed. However, the coarse aggregate may be harder and/or the concrete strength may be higher than cast-in-place construction which creates difficulties in embedding the probes. Double T-beam bridges that have a wearing surface may alternatively be tested on the bottom side of the flanges or the stem. Care should be taken in testing the stems since the probe cannot penetrate more than half the thickness as mentioned previously which can be an issue for thin stems. Test locations over the flange or stem area should be chosen four inches from any edge and preferably away from traffic on the flange topside (i.e., shoulder areas). Before the penetration test, the steel reinforcement should first be located to ensure that the Windsor probe will be driven through concrete without hitting the steel which can compromise the compressive strength estimates. Once the Windsor probe has been shot, a small divot or spall may occur where the probe penetrated. Coarse aggregates may be gathered from these areas for the Mohs' hardness test before the concrete is repaired with non-shrink grout.

A.2.3 P/C BOX GIRDER BRIDGES

The HILTI PS 250 Ferroscan system is generally more effective in detecting the mild transverse shear reinforcement than the longitudinal prestressing strands of box beam bridges. Imagescans or blockscans, depending on the size of the box beam and the area of coverage, should be taken along the bottom flanges and webs near the abutments and at midspan. Interior and exterior beams should be scanned to determine if the box beams have similar characteristics or differences due to widening. The prestressing strands in box beams typically have 0.375 in. or 0.5 in. diameters and are spaced approximately 2 in. on center. Because of the close spacing and seven-wire strand

arrangement, characterizing the prestressing strand configuration is difficult with the Ferroscan. Another major factor affecting the quality of the imagescan is the concrete cover depth; a small cover results in a clear image of the prestressing strands while a large cover results in a noisy image as shown in Figure A.15.

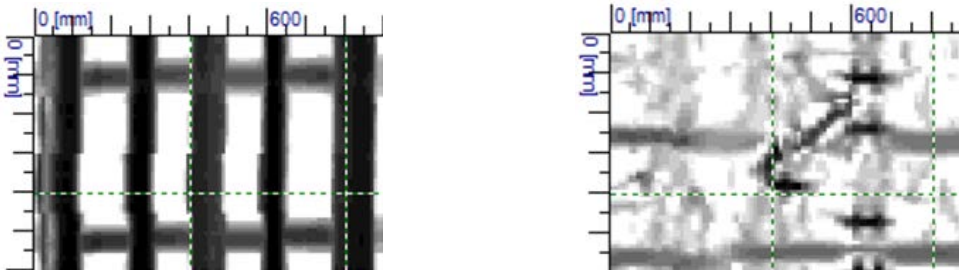

(a) (b)

Figure A.15 Typical imagescan results for box beam flange with (a) small concrete cover and (b) large concrete cover.

The HILTI PS 250 Ferroscan is most accurate for the first layer of reinforcement and additional layers may be difficult to understand. As shown in Figure A.16, box beams with large strand spacing and small concrete cover will provide the best quality results. The imagescans show various shades of gray with varying strip widths due to different cover depths and spacings of the steel reinforcement. In general, the darker strips may be caused by multiple reinforcement layers, close strand spacing, and/or small cover depth. The depth range tool of the Ferroscan software may be able to discern the steel configuration by analyzing the larger bar strips at different depths to check if the visible strand strips separate or disappear. The tool allows the user to pan in and out of the imagescan through the depth of the beam flange. Subsequently, thin lines in the imagescans begin to blur and disappear from view at shallower depths which indicates that the strands are only in one layer. On the other hand, thick lines may begin to separate into two or more lines which are possible indications of multiple strands and/or layers. Note that the depth range analysis only provides an estimate of the steel configuration in the box beam and further confirmation with standard box beam drawings (if available) is recommended.

Unlike the longitudinal prestressing strand, the transverse shear stirrups in box beam bridges are easier to detect with the Ferroscan. Figure A.17 shows an imagescan of a box beam web viewed at different depths. The stirrup locations are clear and the Ferroscan also provides a more accurate bar size estimate compared to prestressing strand.

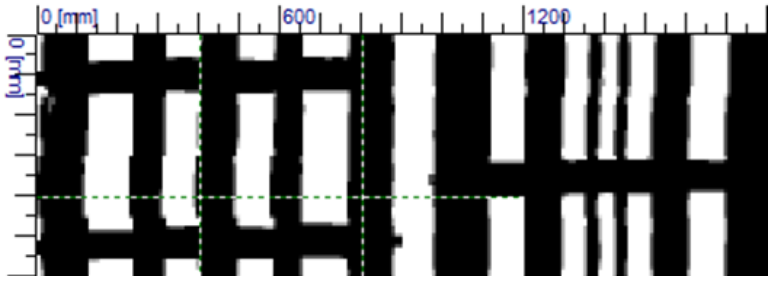

(a)

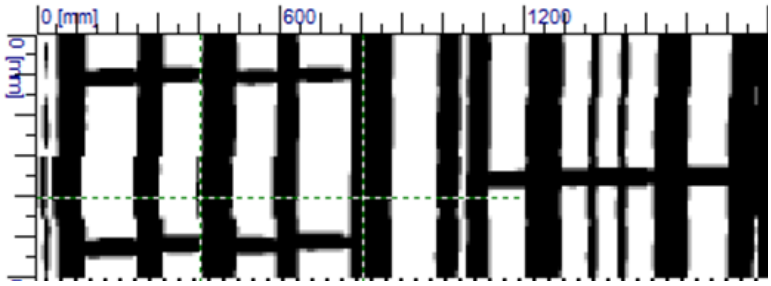

(b)

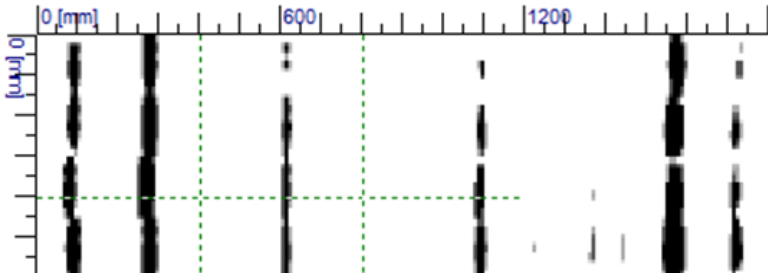

(c)

Figure A.16 Typical blockscan results for box beam flange viewed at (a) large depth range, (b) medium depth range, and (c) small depth range.

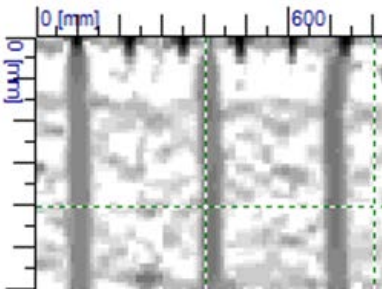

(a)

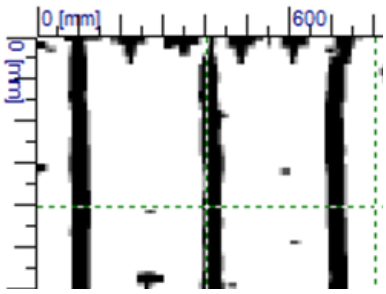

(b)

Figure A.17 Typical imagescan results for box beam web viewed at (a) large depth range and (b) small depth range.

The Windsor probe penetration test remains a practical method for precast, prestressed concrete box girder bridges since the top flange may be exposed. However, driving the probes may be difficult since the coarse aggregate may be harder and/or the concrete strength may be higher than cast-in-place construction. Box beam bridges with a wearing surface may alternatively be tested on the girder bottom flanges or webs of the exterior girders. Care in testing the flanges or webs should be taken since the probe cannot penetrate more than half the thickness as previously mentioned. Test locations over the flange or web area should be chosen four inches from any edge and preferably away from traffic on the top flange (i.e., shoulder areas). Before the test, the steel reinforcement should first be located to ensure that the Windsor probe will be driven through concrete without hitting the steel. Once the Windsor probe has been shot, a small divot or spall may occur where the probe penetrated. Coarse aggregates may be gathered from these areas for the Mohs' hardness test before the concrete is repaired with non-shrink grout.

A.2.4 P/C I-GIRDER BRIDGES

The HILTI PS 250 Ferroscan provides a good estimate of the bar size, spacing, and concrete cover of the transverse shear stirrups in prestressed I-girders but has limited usefulness for detecting the prestressing strand configuration. The standard strand spacing for an I-girder is 2 in. and the strand diameters range between 0.375 in. and 0.6 in. In addition, the strands may be bundled in certain areas which violates the 1.4 in. spacing requirement for the Ferroscan. There are usually several layers of strands in the bottom flange and a few layers in the web. The Ferroscan is generally not capable of detecting steel reinforcement past the first layer which along with the close spacing and multiple layers complicates the measurements of the girder bottom flange.

Imagescans or blockscans may be taken along the bottom flange and webs of an I-girder. An interior and exterior girder should be scanned to verify that the girders are the same and the scans should be taken near the abutments and at midspan for reasons discussed earlier. Similar to box beams, the Ferroscan depth range feature can be used to attempt to distinguish different strands and/or layers. However, the Ferroscan results for an I-girder generally provide limited information of the prestressing strands. The reader is referred to the previous discussion for the double T-beam and box girder bridges on the application of the depth range feature. Figure A.18 shows typical imagescans taken on the side of the web, underside of the bottom flange, and side of the bottom flange. As shown in part (a) of the figure, the Ferroscan provides clear images of the transverse shear reinforcement. Quickscans are also useful for finding the spacing of the shear stirrups.

For an I-girder bridge, the Windsor probe penetration test should be completed on the cast-in-place deck and attempted on the precast girder. The test procedure for the deck is similar to a reinforced concrete slab bridge and similar to the other prestressed concrete bridge components (i.e., double T-beam, box girder) discussed earlier for the I-girder.

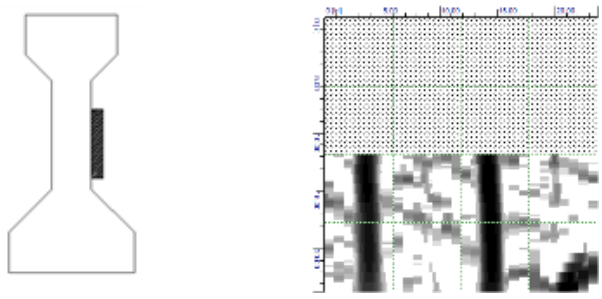

(a)

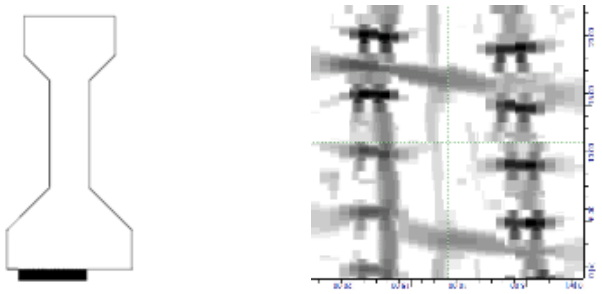

(b)

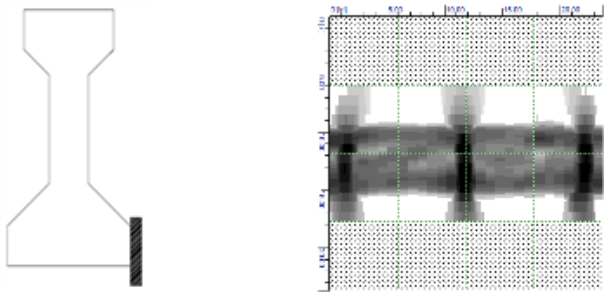

(c)

Figure A.18 Typical imagescans of I-girder on (a) side of web, (b) underside of bottom flange, and (c) side of bottom flange.

APPENDIX B: ACOUSTIC EMISSION MONITORING OF BRIDGE 7701

This appendix contains a paper highlighting the results from acoustic emission monitoring of Bridge 7701, the prestressed concrete double T-beam bridge located in District 1, Doña Ana County. The monitoring was performed during the proof test of the bridge and was a joint effort between New Mexico State University (NMSU) and the University of South Carolina.

On-Site Acoustic-Emission Monitoring for Assessment of a Prestressed Concrete Double-Tee-Beam Bridge without Plans

Rafal Anay[1], Tamara M. Cortez[2], David V. Jáuregui[3], Mohamed K. ElBatanouny[4], Paul Ziehl[5]

Abstract

Acoustic emission was used in this study to assess the condition of a simple-span, prestressed concrete bridge located in southern New Mexico during a proof test. The 40-year old bridge is county owned and no design plans were available. AE data was collected under several loading conditions from two groups of sensors placed near the support and midspan of an interior double-tee beam. Strain measurements were also taken at midspan and used to direct the test and determine the maximum loading. AE data analysis methods were applied to evaluate the response of the structure under increasing loads and to develop crack maps. Analysis of the AE data showed signs of internal beam micro-crack development near the supports (shear region) as well as in the midspan (moment region). The AE data indicated that damage in the form of crack growth was more prevalent in the region near the supports.

Key words: Load testing; Load rating; Load posting; Nondestructive evaluation; Acoustic emission; Prestressed concrete bridges; No plans.

[1]Rafal Anay, Graduate Research Assistant
University of South Carolina, 300 Main Street, Columbia, SC, USA, 29208
[2]Tamara Cortez, Graduate Research Assistant
New Mexico State University, Hernandez Hall, Box 30001, MSC 3CE 31 Las Cruces, NM 88003.
[3]David V. Jáuregui, Professor
New Mexico State University, Hernandez Hall, Box 30001, MSC 3CE 31 Las Cruces, NM 88003.
[4]Mohamed ElBatanouny, Postdoctoral Fellow
University of South Carolina, 300 Main Street, Columbia, SC, USA, 29208
[5]Paul Ziehl, Professor
University of South Carolina, 300 Main Street, Columbia, SC, USA, 29208

Introduction

Bridge load rating is the process of determining the safe load-carrying capacity of a bridge using analytical methods, experimental methods, or a combination of the two. In the United States, bridge load rating procedures are specified by the American Association of State Highway and Transportation Officials (AASHTO) in the AASHTO Manual for Bridge Evaluation (AASHTO 2011). Load ratings are used by the New Mexico Department of Transportation (NMDOT) to manage the State's bridge infrastructure to assure public safety, assist in the efficient allocation of bridge repair and replacement resources, and facilitate the movement of goods and services on the State's public roadways (Jáuregui et al. 2013).

The majority of New Mexico bridges have documentation such that the load ratings can be readily determined by analytical methods. However, there are approximately 170 concrete bridges (50% reinforced concrete and 50% prestressed concrete) in the State that have no plans; and therefore are difficult to evaluate solely by analytical means. In the absence of plans, conservative assumptions are usually made to define the reinforcement layout and concrete properties for use in the analysis. In some cases, the load ratings are established based on engineering judgment and an assessment of the current bridge condition without an actual structural analysis. Ratings determined under these conditions may result in high levels of uncertainty and have a low confidence level.

The AASHTO Manual (AASHTO 2011) states that "Many older reinforced concrete and prestressed concrete beam and slab bridges whose construction plans, design plans, or both are not available need proof testing to determine a realistic live load capacity". For prestressed concrete bridges, however, proof testing is a challenge due to the high likelihood of exceeding the cracking moment in trying to achieve the target proof load specified in the AASHTO Manual (2011). The

use of non-destructive evaluation (NDE) methods is very important in proof testing of concrete bridges without plans due to the unknown material strengths and hidden reinforcement. Acoustic emission (AE) is a modern NDE method that provides the capability to effectively monitor the structure's internal condition under increasing load and assist in establishing a safe load limit (Olaszek et al. 2010). Conventional testing methods for concrete structures do not provide the full information about the severity of defects (Golaski et al. 2002) or potential degradation. The use of acoustic emission monitoring during load testing can supplement the data gathered during load testing, and in particular may be useful in assessing damage in the shear region and also in the flexural region (midspan).

This study presents the assessment of a double-tee beam prestressed concrete bridge in New Mexico during proof testing. The proof test was planned and conducted based on the serviceability limit state (i.e., concrete tension) for prestressed concrete bridges rather than strength to determine the legal load rating without inducing damage to the bridge. Strain measurements were taken at strategic locations to monitor the bridge response and to determine the maximum loading (Aguilar et al., 2015). In addition, internal signs of concrete cracking were monitored using AE, results of which are the focus of this paper.

Bridge Description

The subject bridge is a single-span, prestressed concrete bridge with a 9.45 m (31 ft.) span located in southern New Mexico and owned by Doña Ana County. The bridge was constructed in 1974 and consists of nine double-tee beams, each of which is 0.83 m (33 in.) wide, 0.45 m (19.5 in.) deep, and 9.75 m (32 ft.) long. The bridge beams are placed directly next to one another, allowing for the beam flanges to act as the deck, and the beam ends rest on 0.3 m (12 in.) long bearing seats. Each beam has seven shear keys on the top flange at 1.29 m (4 ft. 3 in.) center-to-

center spacing. The shear keys consist of two steel angles connected by a short piece of rebar. There is no wearing surface and the overall bridge width is 7.13 m (24 ft. 9 in.), while the roadway width is 7.13 m (23 ft. 5 in.) from curb to curb. The exterior beams have concrete curbs that are 0.20 m (8 in.) wide and 0.33 m (13 in.) deep. In addition, the exterior beams have side mounted guardrails, with W6 I-beam posts spaced at 1.29 m (51 in.) and extending 0.66 m (26 in.) above the concrete curb. The guardrail is 0.31 m (12.5 in.) deep and runs along the entire bridge length. ***Figure 1*** shows photographs of the top and bottom of the bridge.

Figure 1: Prestressed Concrete Double-Tee Beam Bridge
in Southern New Mexico

Visual Inspection

Based on the most recent inspection report (dated November 9th, 2011), at the time of the proof test the National Bridge Inventory (NBI) condition ratings were a ‘6’ for the deck and superstructure, and a ‘7’ for the substructure (out of ‘9’). The beams were numbered from north to south and the abutments were numbered from west to east. The topside of the beam flanges showed transverse, longitudinal, and map cracking up to 0.79 mm (1/32 in.) in width with heavy abrasion and small spalls. The exterior beams had less abrasion and damage, most likely due to less exposure to traffic. The shear keys nearest to the curbs were all covered with grout and appeared to be functioning. Between interior beams 4 and 5, all the keys except one (i.e., six out of seven)

were broken. In addition, the keys between interior beams 6 and 7 were damaged and not functioning properly as shown by the poor distribution of load between beams from the strain measurements (Aguilar et al. 2015). The underside of the flanges had map and longitudinal cracks up to 0.79 mm (1/32 in.) in width with minor spalls, some of which were between the stems and flanges of the beams. The beam stems had horizontal cracks up to 3.2 mm (1/8 in.) in width at the supports. Beam 6 showed some vertical cracking up to 0.79 mm (1/32 in.) in width originating from the flange-stem transition; however, these cracks were not full depth. Beam 9 had a few spalls up to six inches by six inches with four inches of exposed shear reinforcement on the south side of the stem, near abutment one. No flexural cracks were observed in any of the beams.

Acoustic Emission

The application of nondestructive evaluation (NDE) methods can assist in proper assessment of the condition of existing structures having limited documentation. Acoustic emission (AE) is defined by ASTM as transient elastic waves generated by a rapid release of energy from localized sources within a material (ASTM E1316, 2014). AE has significant potential for monitoring concrete bridges without plans; especially to determine the serviceability, in terms of cracking, of such structures (Olaszek et al., 2010). In addition, AE has the ability to detect and locate different types of defects based on measured parameters (ElBatanouny et al., 2014b, Hamdi et al., 2013). Different approaches were developed to quantify damage in reinforced and prestressed concrete structures as discussed in details in the following sections. The Intensity Analysis method has been used to characterize damage in structural elements (Fowler et al. 1989, Golaski et al. 2002, ElBatanouny et al. 2014a), and the cumulative signal strength (CSS) parameter and source location techniques have been used to detect cracks and their locations, respectively (ElBatanouny et al. 2012). Other approaches have also been applied in AE monitoring of concrete

structures, and several studies have shown a relationship between AE data and fracture of a reinforced concrete specimen (Pollock 1981, Shiotani et al. 2001, Colombo et al. 2003, Farhidzadeh et al. 2012, ElBatanouny et al. 2014b). Furthermore, AE data may be displayed in real time depending on the capabilities of the data acquisition system. ***Figure 2*** shows the AE wave features that may be extracted from each AE hit on an AE data acquisition system (ElBatanouny et al., 2014a). The features of the waveform associated with each hit can be used to calculate parameters such as amplitude, rise time, duration, signal strength, and counts. Definitions of these and other terms related to acoustic emission are provided at the end of this paper.

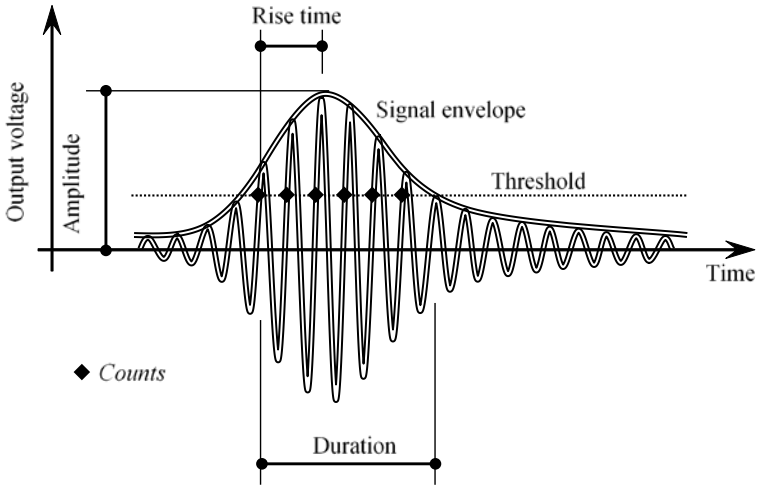

Figure 2: Schematic showing acoustic emission waveform (ElBatanouny et al. 2014a)

Intensity Analysis

Intensity Analysis is a method developed to characterize damage in structural elements and was originally developed to detect the degree of damage in FRP vessels (Fowler et al., 1989). To calculate the intensity of an emission source, the historic index and severity are calculated for data collected during the test. The intensity of AE activity is determined by plotting the maximum historic index (HI) and severity values on a chart (Golaski et al., 2002). The H(t) function given by equation (1.a) is used to estimate changes in the slope of the cumulative signal strength with

respect to time and estimate the level of damage using a historical methodology (ratio of the cumulative signal strength of recent hits to the cumulative signal strength from all hits). The severity, S_r, represents the average for the 50 events having the highest signal strength as defined by equation (1.b) (Fowler et al. 1989, ElBatanouny et al. 2014a):

$$H(t) = \frac{N}{N-K} \frac{\sum_{i=K+1}^{N} S_{oi}}{\sum_{i=1}^{N} S_{oi}} \quad (1.a)$$

$$S_r = \frac{1}{50} \sum_{i=1}^{i=50} S_{oi} \quad (1.b)$$

where N is the number of hits up to a specific time (t), S_{oi} is the signal strength of the i-th event, and K is an empirically derived factor that varies with the number of hits. One value of K that has been suggested is as follows (Nair and Cai 2010, ElBatanouny et al. 2014a): a) N/A if $N \leq 50$, b) N-30 if $51 \leq N \leq 200$, c) 0.85N if $201 \leq N \leq 500$, and d) N-75 if $N \geq 501$.

Experimental Program and Instrumentation

Instrumentation

Eight AE sensors were installed on the stem of the middle beam (beam number 5), four of which were positioned near the west support (shear region) and the other four were placed at midspan (moment region) as shown in ***Figure 3***. Note that only beam 5 was instrumented with AE sensors since this beam showed the largest strains during a previous diagnostic test (Aguilar et al. 2015) and also due to the channel limitations of the AE system. Strain transducers were also installed at midspan on the bottom of each beam stem and used to guide the proof test and determine the maximum loading.

Load test procedure

Four 9.14 cu. meter (ten cu. yard) dump trucks [71.2 kN (16-kip) front single axle, 18.7 kN (42-kip)] rear tandem axle] were used for loading the bridge in four phases.

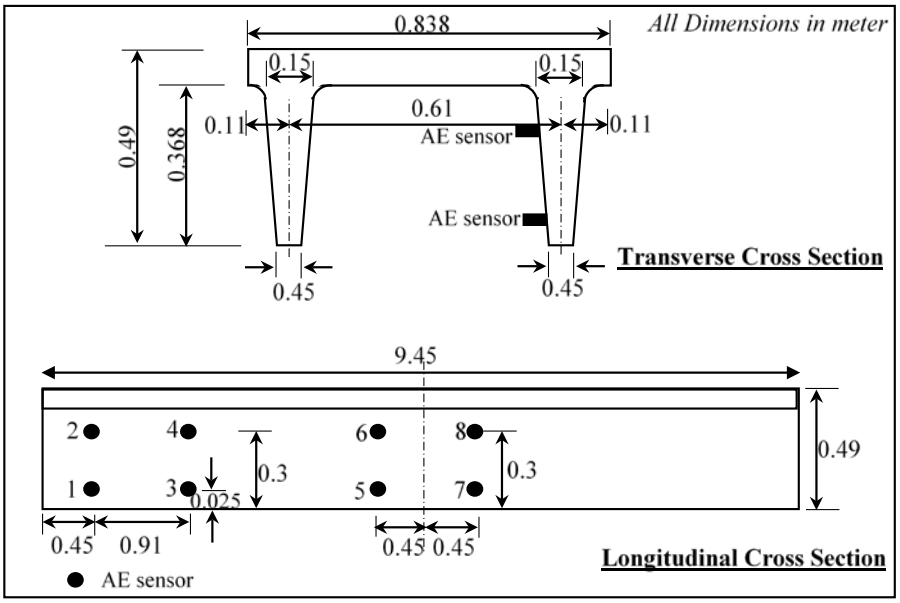

Figure 3: AE sensor positions on middle beam of bridge (not to scale)

In the first phase, one lane loading was simulated with a single truck placed transversely at a distance of 1.49 m (59 in.) (path 5) and 0.61 m (0.24 in.) (path 7) from the south curb. ***Figure 4*** shows pictures of the truck backing into position during phase one. In the second phase, two trucks were placed side-by-side to simulate multiple lane loading. ***Figure 5*** shows the two load cases applied in phase two that includes two new transverse paths (numbered 1 and 3).

Figure 4: Truck positioning during test phase one

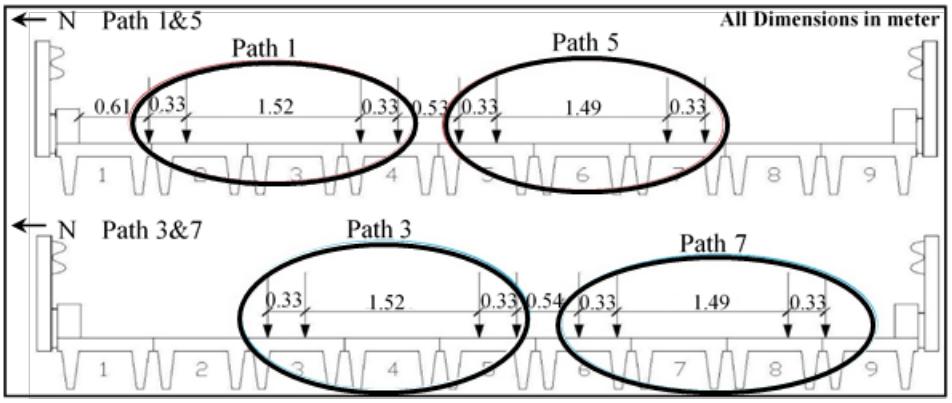

Figure 5: Transverse truck positions for all load paths

The third phase was a repeat of phase one path 5 using two trucks placed back-to-back and the fourth phase was a repeat of phase two paths 3 and 7 using four trucks placed side-by-side and back-to-back. In each phase, the trucks were backed up and halted at incremental longitudinal positions. ***Figure 6*** shows the longitudinal truck positions for phase two and ***Table 1*** summarizes the middle axle position from the abutment for all test phases. Strain measurements were monitored at all nine beams and the truck loading was stopped when the strain readings approached the available strain or the final truck positions were reached. Since the bridge has no design plans, the number of prestressing strands was estimated using Magnel diagrams based on the serviceability limit state (concrete tension) which amounted to a total of 6 strands (3 per stem).

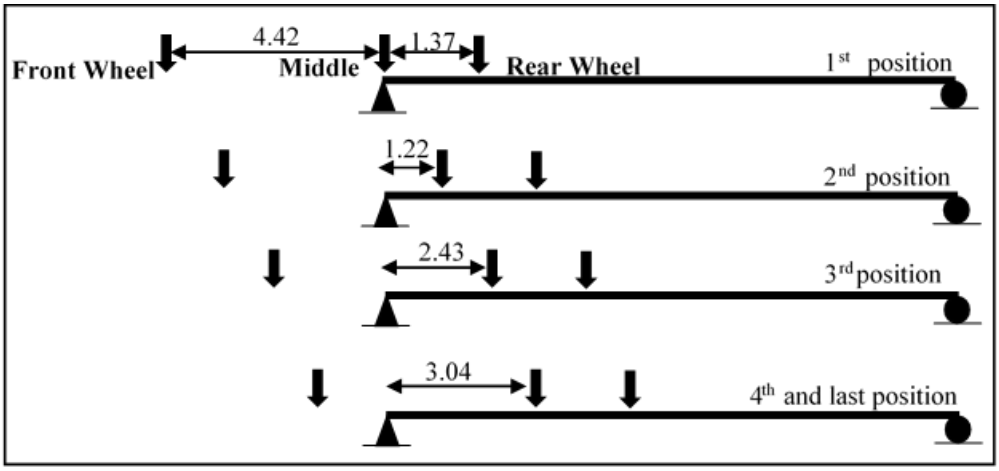

Figure 6: Longitudinal truck position steps for phase two

Table 1: Middle axle location of test truck

Truck Position	Middle Axle Location, m (ft)			
	Phase One	Phase Two	Phase Three	Phase Four
1	0	0	0	0
2	1.22 (4)	1.22 (4)	0.61 (2)	0.61 (2)
3	2.43 (8)	2.43 (8)	1.22 (4)	1.22 (4)
4	3.04 (10)	3.04 (10)	1.52 (5)	1.52 (5)
5	3.65 (12)	-----	1.98 (6.5)	-----
6	4.26 (14)	-----	-----	-----

Based on the strand estimate, the cracking moment was computed as:

$$M_{cracking} = S_b * \left[P_e * \left(\frac{1}{A} + \frac{e}{S_b}\right) + f_{cr}\right] \quad (2)$$

where S_b is the section modulus at the bottom of the beam; A is the cross-sectional area of the beam; P_e is the effective prestressing force; e is the eccentricity of the prestressing steel; and f_{cr} is the modulus of rupture (equal to 7.5 times the square root of f'_c). Subtracting the dead load moment from the cracking moment gave the available moment, $M_{available}$, for the beam before cracking. The available strain, $\varepsilon_{available}$, was then determined using the following equation:

$$\varepsilon_{available} = \frac{M_{available}}{S * E_{design}} \quad (3)$$

where S is the section modulus at the transducer location (1.0 in. or 25.4 mm from the bottom of the beam stem) and E_{design} is the modulus of elasticity of the beam. Strains measured during the load test were closely monitored to not exceed the available strain of 532 με and prohibit cracking the beam. Further details can be found in Aguilar et al. (2015).

Figure 7 shows footprints of the final truck locations for the different test phases and ***Table 3*** gives the maximum strains recorded at the bottom of the beam stems. The beams are numbered 1 to 9 from north to south (***Figure 5***). As shown in ***Table 2***, beam 5 experienced the largest strains and was also the beam monitored with the AE system as discussed earlier. The table also shows large differences in strain and poor load distribution between beams due to the damaged shear keys

(e.g., 38 με at beam 4 and 508 με at beam 5 for path 5 of phase one). Note that the flexural response of the beam at midspan was monitored by strain and AE measurements while the shear response at the support was monitored only by AE measurements. In addition, the available strain presented above is merely an estimate that depends on the initial prestressing force and prestress losses resulting from elastic shortening, creep, shrinkage, and relaxation. Computing the available moment before cracking is a challenge even for bridges with design plans and thus, including both types of measurements (strain and AE) provides a more robust monitoring system for proof testing.

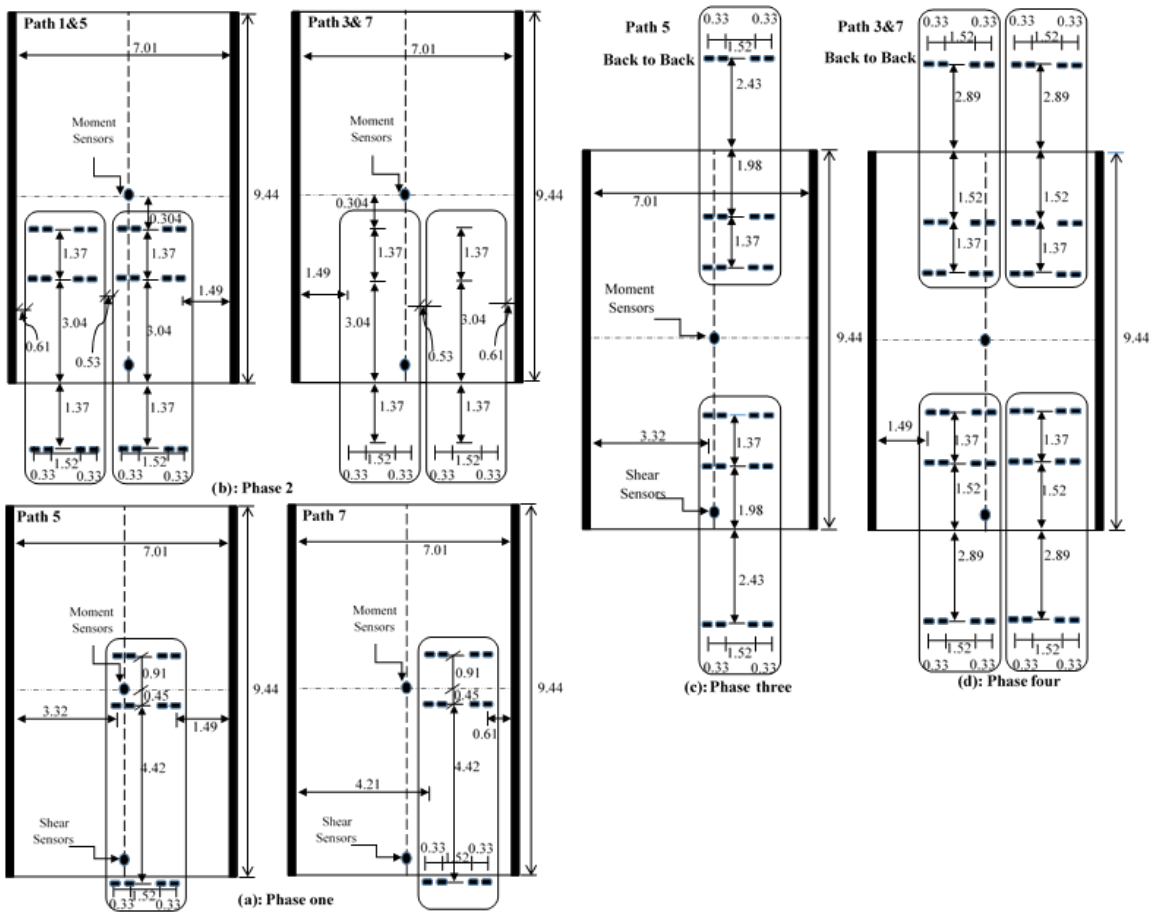

Figure 7: Load paths: (a) phase one, (b) phase two, (c) phase three, (d) phase four

Table 2. Maximum measured strains for proof load test

Beam Number	Strain (με)					
	Phase One		Phase Two		Phase Three	Phase Four
	Path 5	Path 7	Paths 1 and 5	Paths 3 and 7	Path 5	Paths 3 and 7
1	1	0	235	80	18	115
2	6	2	255	224	28	195
3	21	10	341	197	55	203
4	38	33	**474***	182	82	205
5	**508***	157	448	**528***	**496***	**494***
6	339	269	367	455	432	450
7	275	**348***	245	443	360	471
8	223	277	247	266	280	288
9	79	243	99	250	151	258

* The numbers in bold mean maximum measured strain for each load path

Reduction and Treatment of Acoustic Emission Data

The acoustic emission data was collected during the load test with an amplitude threshold of 45 dB. There is no standard threshold setting for bridge load testing, therefore this threshold was selected based on past experience with laboratory specimens. It is understood that not all acoustic emission data corresponds to the physical response of the tested structure. Wave reflections and mechanical noise, such as rubbing, are two examples of sources that generate 'non-genuine' or 'spurious' data. Therefore, more than one filter should be applied to eliminate undesirable data. The test was conducted on-site; therefore, it was impossible to control the noise generated by many sources (i.e., friction between tires and the deck and wind-born debris). Field testing has inherent challenges in comparison to laboratory testing where external noise sources are often more readily minimized.

In the recording of an AE waveform, system timing parameters including peak definition time (PDT, enables determination of the true peak time of the AE waveform), hit definition time (HDT, enables determination of the end of the hit and close out of the measurement processes),

and hit lockout time (HLT, inhibits the measurement of signals after the hit is stored to minimize the recording of reflections) are selected. In this study, the PDT, HDT, and HLT values were set at 200 micro-s, 400 micro-s, and 800 micro-s, respectively (ElBatanouny et al., 2014b). During the load test, the graphical interface of AEwin software was set to show the AE activity versus time for data detected from each channel; which gives a simple indication regarding the amount of damage developing near each sensor.

Three post-processing filters were developed to reduce the recorded data after each phase of testing. The first was an amplitude filter which rejected hits with amplitudes below a specific threshold, which was set to 60 dB based on the very large amount of data below this level and the characteristics of the AE signals observed during the load test. This filter was used only to establish the AE evaluation criteria for the Intensity Analysis and cumulative signal strength analysis with the objective of simplifying and adapting the process for field use. The second filter used combinations of duration and amplitude to reject AE data related to wave reflections. This filter is referred to as D–A filter (for duration-amplitude), and is similar to a Swansong II filter (Tinkey et al. 2002). A similar filtration procedure has been previously applied by the authors to filter AE data collected during testing of a glass fiber reinforced polymer reinforced concrete beams (ElBatanouny et al. 2014b); and prestressed concrete beams (ElBatanouny et al. 2014a). The third filter was developed based on the relationship between rise time and amplitude (R–A) (ElBatanouny et al. 2014a). The second and third filters (D-A and R-A) were used exclusively for source triangulation purposes. ***Table 3*** shows the data rejection limits used in the second and third filters.

Table 3: Data Rejection Limits for AE Filters

D-A filter		R-A filter	
Amplitude (dB)	Duration (μs)	Amplitude (dB)	Rise time (μs)
60-67	>2000	60-67	>300
68-75	>4000	68-75	>450
76-83	>6000	76-83	>600
84-91	>8000	84-91	>750
92-100	>10000	92-100	>900

Results and Discussion

Detection and Assessment of Active Crack Growth

The detection of cracking, either visible or non-visible, is generally associated with AE signals having high signal strength and also sharp changes in slope of the cumulative signal strength (CSS) curve (ElBatanouny et al. 2012). ***Figure 8*** shows the magnitude of CSS for all load cases. For each case, the loading was repeated once for two tests (labeled 1st Run and 2nd Run). It can be seen from ***Figure 8*** that the value of CSS for sensors 1 through 4 in the shear region for all load paths was higher than the value of CSS for sensors 5 through 8 in the moment region. In addition, phase one path 7 had small values of CSS in the shear and moment regions since beam 5 was not loaded directly as in path 5 (***Figure 5***) due to the truck position and the poor load distribution between beams (attributed to damage in the shear keys). Also, this signifies that the first indication of cracking happened within the timeframe of the first load path (path 5) compared with the second load path (path 7). Similar to the AE measurements, ***Table 2*** shows low strain values for beam 5, path 7. Furthermore, it can be seen from ***Figure 8*** that there was a gradual increase in CSS for sensors 1 through 4 as the test was continued through phases two and three which means that the level of cracking was more severe in the shear region under back-to-back loading than side-by-side. This behavior was expected as the maximum shear doubles in magnitude when the trucks are placed back-to-back as compared to side-to-side.

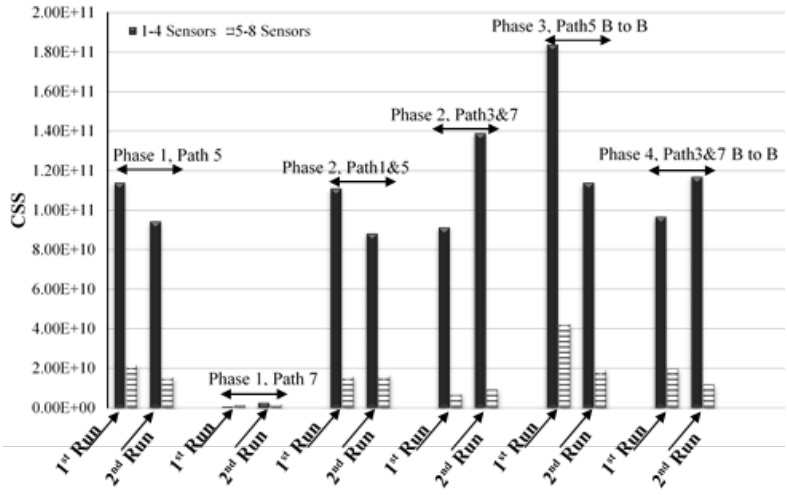

Figure 8: Cumulative Signal Strength for all test phases

This was confirmed by AE data as comparison of phase two path 1 and 5 with phase three showed roughly a two-fold increase in CSS. In addition, there was virtually no CSS change (2.63%), between phase one path 5 and phase two paths 1 and 5, which indicates that the truck in path 1 had no measurable effect on beam 5 (again attributed to damage in the shear keys).

The CSS for sensors 5 through 8 was less than the CSS for sensors 1 through 4 in ***Figure 8***, which indicates higher acoustic emission activity (additional micro- and macro-cracking) in the shear region as compared to the moment region. ***Figure 9*** shows more profound changes in the slope of the CSS within the timeframe of the second load phase (path 1 and 5) for sensors 1 through 4 compared with sensors 5 through 8, which further indicates that there was more cracking in the shear region than in the moment region. In addition, sensors 5 through 8 experienced sharper changes in slope in the latter part of the loading which coincides with the truck approaching midspan, which causes larger bending moments.

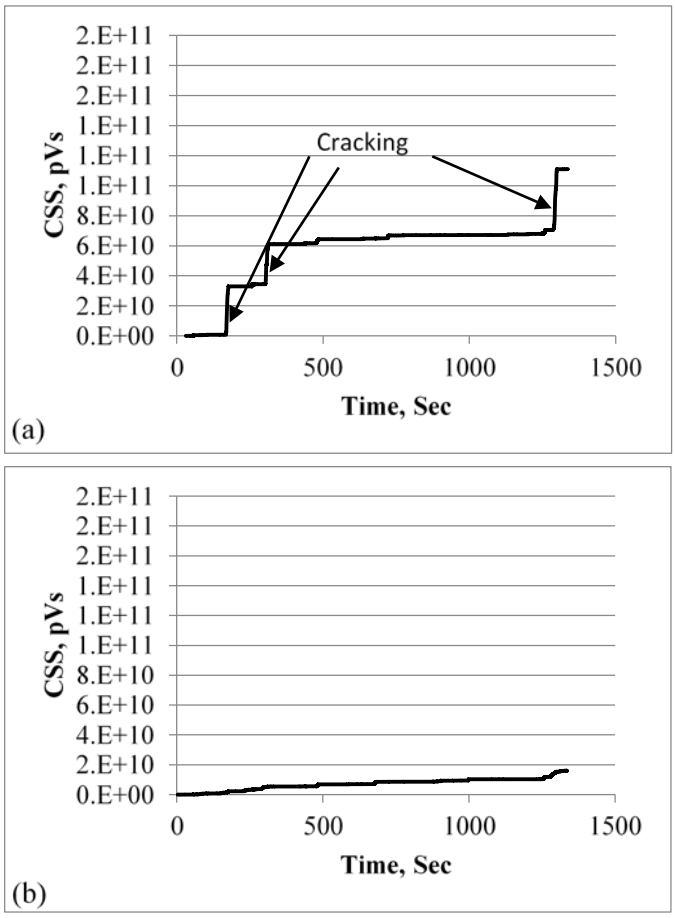

Figure 9: CSS versus time for phase 2 path 1&5 1st run: (a): AE sensors (1-4), (b) AE sensors (5-8)

Source Location of Acoustic Emission Events

Source triangulation algorithms based on time of flight were utilized to produce crack maps resulting from the proof load test. One important issue in source location for concrete is that waves are often reflected due to cracking and structural boundaries. As a result, AE data filters should be used as discussed earlier to produce more reasonable source location results. ***Figure 10a*** shows the substantial amount of unfiltered data that was gathered during phases three and four from the two groups of sensors (at shear and moment regions), much of which can be attributed to wave reflections. After filtering of the collected data, the crack maps provide visibility of possible crack locations in the shear region and no indications in the moment region as shown in ***Figure 10b***.

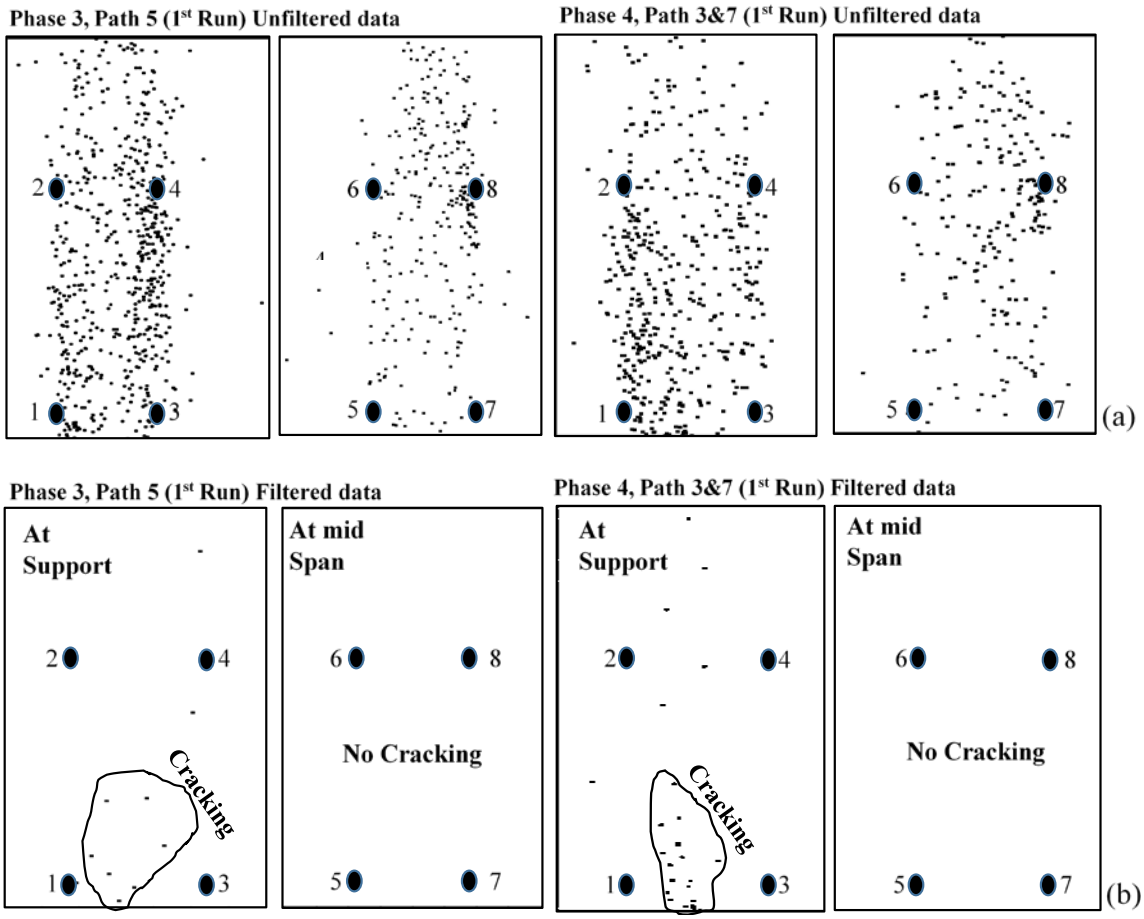

Figure 10: AE source location: (a) unfiltered data, and (b) filtered data

This is not to say that no cracking occurred in the moment region. Rather, the magnitude of that cracking was not sufficient to allow for source location based on time of flight and the settings utilized in this study. Note that this general behavior is consistent with the CSS data shown in ***Figure 8*** and ***Figure 9***, and also with the maximum strains reported in ***Table 2*** since the measured strains did not exceed the available strain of 532 με associated with cracking. Furthermore, the number of potential crack locations increased from phase three to four which is reasonable since the magnitude of loading increased. The filtered data generally demonstrates that the AE method has the ability to detect and assess crack locations and may potentially be utilized to provide an alert prior to formation of visible cracking.

Intensity Analysis of Acoustic Emission Data

An Intensity Analysis was conducted for all test phases based on the AE data collected from sensors 1 through 4 and 5 through 8 using Equations (1.a) and (1.b) to evaluate the level of potential damage occurring in the shear and moment regions. ***Figure 11*** shows the Intensity Analysis chart which indicates that the most severe damage occurred in the shear region as five of six load cases had high historic index and high severity values situated at the upper right corner of this chart. Less damage occurred in the moment region because all of the six points had lower historic index and severity values than the shear region. The least damage was detected in phase one path 7 which corresponded to the smallest truck weight and indirect loading of beam 5. The figure shows that phase three path 5 was the most damaging for both shear and moment, and phase one path 7 was the least damaging. These results related to the shear and moment regions agreement with the results obtained using the CSS parameter and source location. By comparing these results, it can be seen that the shear region experienced significant damage, in the form of crack formation and growth.

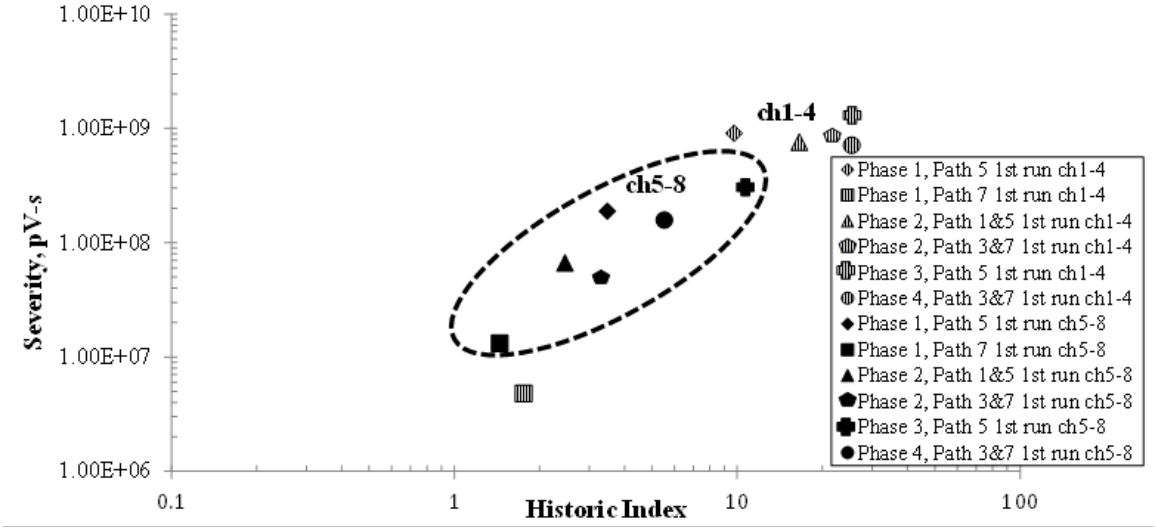

Figure 11: Intensity Analysis condition assessment charts

Conclusions

This study summarizes an effort to supplement proof load testing with NDE techniques, particularly AE, to evaluate the condition of an existing prestressed concrete double-tee beam bridge with no plans. The results illustrate the ability of AE to detect and locate cracks and provide additional insight regarding critical loading paths/conditions and its effect on the performance of the structure. Conclusions are as follows:

1. Cumulative signal strength (CSS) can be utilized to detect crack formation. The parameter provided an indication of the susceptibility of the bridge to crack in the shear region, as well as in the moment region. This was achieved by comparing the sharp changes in slope of CSS collected from both regions. Given its relative simplicity, this method has the potential to assess the integrity of the tested structure in real-time.
2. Intensity analysis gives an indication of the level of damage under certain loading conditions. This can aid in the determination of reliable load posting for in-service structures. The AE data filters associated with the method are straightforward and can be set as front end filters to make this method more applicable for real-time condition assessment. Additional field applications would be beneficial to further the development of real-time assessment capability.
3. The importance of applying appropriate filters for AE source triangulation was confirmed by comparing unfiltered data, which gave unclear indications of cracking, with filtered data that gave clear indications of cracking in the shear region. Furthermore, the results of source location analysis are in agreement with the results of cumulative signal strength and Intensity Analysis.

4. Damage was detected by AE whereas no indication of local damage was detected by the more conventional instrumentation. AE has the potential to be used as the primary instrumentation utilized during proof testing, particularly when crack growth during testing is of primary interest.
5. Measured strains for flexure at midspan did not exceed the available strain associated with cracking which generally agreed with the lower indications of cracking from AE data in the moment region. No strain measurements were taken at the support to check if the available strain in the shear region was exceeded to validate the higher indications of cracking from the AE data. Hence, strain and AE monitoring in the moment and shear regions is advised to more thoroughly determine the load limits from proof testing.

Based on the midspan strains and corresponding truck positions given in ***Table 2*** and ***Figure 7***, respectively, load rating factors were determined from the proof test for federal and state legal loads. Aguilar et al. (2015) showed that load posting was necessary for all legal loads except the Type 3-3 and NM 2. The safe posting loads for the remaining vehicles were 18.2 tons (Type 3), 30.0 tons (Type 3S2), 16.9 tons (NM 3A), and 27.3 tons (NM 5A). Before the proof test, the bridge was not load posted since the operating rating factor for design loading was larger than 1.0. The initial ratings were determined by the NMDOT based on historical data for off-system bridges in Doña Ana Country, New Mexico. Based on the proof test, shear transfer between beams was shown to be an issue due to the poor condition of the shear keys which led to reductions in the load ratings and ultimately, the bridge needed to be load posted for legal loads as discussed above. Note that the final posting decisions were made based on the lower indications of cracking from the strain and AE data in the moment region of the bridge and not just the AE data in the shear region that although showed stronger indications of cracking, no visible cracks were detected during the

proof test. Future research will address the implementation of strain and AE monitoring of the shear response for proof testing.

The current state-of-practice presented in this study indicates the potential of AE for real-time crack detection. For crack location, post-processing filters are needed to increase the reliability of the detected crack events. Given the potential of AE for early real-time crack detection, future research should address the implementation of the method as the primary 'stop' criterion in proof load tests where cracking and serviceability are of interest.

Acknowledgements

This project was funded by the New Mexico DOT, grant number NM13STR01. The support is gratefully acknowledged.

Terminology related to Acoustic Emission

Hit: The process of detection and measurement of an AE signal on an individual sensor cannel (ASTM E1316): ***Amplitude:*** The largest voltage peak in the AE signal waveform; customarily expressed in decibels relative to 1 μV at the preamplifier input (dB) assuming a 40 dB preamp (ASTM E1316): ***dB:*** A unit of measurement for AE signal amplitude A, defined by $A\ (dB) = 20\ log\ V_p$; where V_p is the peak signal voltage in μV referred to the preamplifier input (ASTM E1316); ***Duration****:* The time from the first threshold crossing to the end of the last threshold crossing of the AE signal from the AE threshold (ASTM E1316); ***Rise time:*** The time from an AE signal's first threshold crossing to its peak (ASTM E1316); ***Counts:*** The number of times the AE signal crosses the detection threshold (ASTM E1316); ***Signal Strength****:* The measured area of the rectified AE signal with units proportional to volt seconds (specified by the AE instrument manufacturer) (ASTM E1316).

References

Aguilar, C., Jáuregui, D., Newtson, C., Weldon, B., and Cortez, T. (2015). "Load Rating a Prestressed Concrete T-Beam Bridge Without Plans by Proof Testing." *Proceedings of the TRB 2015 Annual Meeting*. Washington D.C. *(in press).*

American Association of State Highway and Transportation Officials (AASHTO). (2011). Manual for Bridge Evaluation, 2nd Edition, Washington, D.C.

ASTM E1316. Standard Terminology for Nondestructive Examinations. American Standard for Testing and Materials; 2013. 1–33.

Colombo, S., Main, I. and Forde, M. (2003). "Assessing Damage of Reinforced Concrete Beam Using *b*-value Analysis of Acoustic Emission Signals." *ASCE Journal of Materials in Civil Engineering*. 15(3), 280–286.

ElBatanouny, M., Larosche, A., Ziehl, P. and Yu, L., (2012) "Wireless Acoustic Emission Monitoring on in-situ Decommissioning for Nuclear Structures." *NPIC&HMIT*. San Diego, CA.

ElBatanouny, M., Ziehl, P., Larosche, A., Mangual, J., Matta, F. and Nanni A., (2014a). "Acoustic Emission Monitoring for Assessment of Prestressed Concrete Beams." *Construction and Building Materials*, 58, 46–53.

ElBatanouny, M., Larosche, A., Mazzoleni, P., Ziehl, P., Matta, F. and Zappa E., (2014b). "Identification of Cracking Mechanisms in Scaled FRP Reinforced Concrete Beams Using Acoustic Emission." *Experimental Mechanics*, 54, 69-82.

Farhidzadeh, A., Salamone, S., Dehgghan-Niri, E., Luna, B. and Whittaker A., (2012). "Damage Assessment of Reinforced Concrete Shear Walls by Acoustic Emission." *ASNT conference proceeding*. *NDE/NDT for highways and bridges*: Structural Materials Technology NY.

Fowler, T., Blessing, J. and Conlisk, P., (1989). "New Directions in Testing." *In: Proc. 3rd international symposium on AE from composite materials*, Paris, France.

Golaski, L, Gebski, P. and Ono K., (2002). "Diagnostics of Reinforced Concrete by Acoustic Emission. *Journal of Acoustic Emission*." 20, 83–98.

Hamdi, S., Le Duff, A., Simon, L., Plantier, G., Sourice, A. and Feuilloy, M., (2013). "Acoustic Emission Pattern Recognition Approach Based on Hilbert–Huang Transform for Structural Health Monitoring in Polymer-Composite Materials." *Applied Acoustics*, 74 (5), 746-757.

Jáuregui, D., Newtson, C. and Weldon, B., (2013). *Load Rating Bridges with No as-Built Plans or Non-Engineered Bridges*. FY 2014 Quarterly Report, New Mexico Department of Transportation, Research Bureau, Santa Fe, NM (in press).

Nair, A. and Cai, C., (2010). "Acoustic Emission Monitoring of Bridges: Review and Case Studies." *Engineering Structures*. 32 (6), 1704–1714.

Olaszek, P., Swit, G., and Casas, J., (2010). "Proof Load Testing Supported by Acoustic Emission: An Example of Application." *A: International IABMAS Conference on Bridge Maintenance, Safety and Management. V International IABMAS Conference on Bridge Maintenance, Safety and Management*. Philadelphia: CRC Press, 472-479.

Pollock, A., (1981). "Acoustic Emission Amplitude Distributions." *International Advances in Nondestructive Testing* 7, 215–39.

Shiotani, T., Ohtsu, M. and Ikeda, K., (2001). "Detection and Evaluation of AE Waves Due to Rock Deformation." *Construction and Building Materials*. 15(5–6), 235–46.

Tinkey, B., Fowler, T. and Klingner, R., (2002). *Nondestructive testing of prestressed bridge girders with distributed damage*. Research Report 1857-2, 106.

APPENDIX C: NMDOT LOAD RATING FORMS

This appendix contains the final NMDOT load rating forms for the six concrete bridges evaluated in Project NM13STR-01. The prestressed concrete bridges include two double T-beam bridges in District 1 (nos. 7701 and 8761), two box beam bridges in District 1 (no. 7722) and District 3 (no. 6), and one I-girder bridge in District 2 (no. 8588). The reinforced concrete slab bridge is located in District 1 (no. 8676).

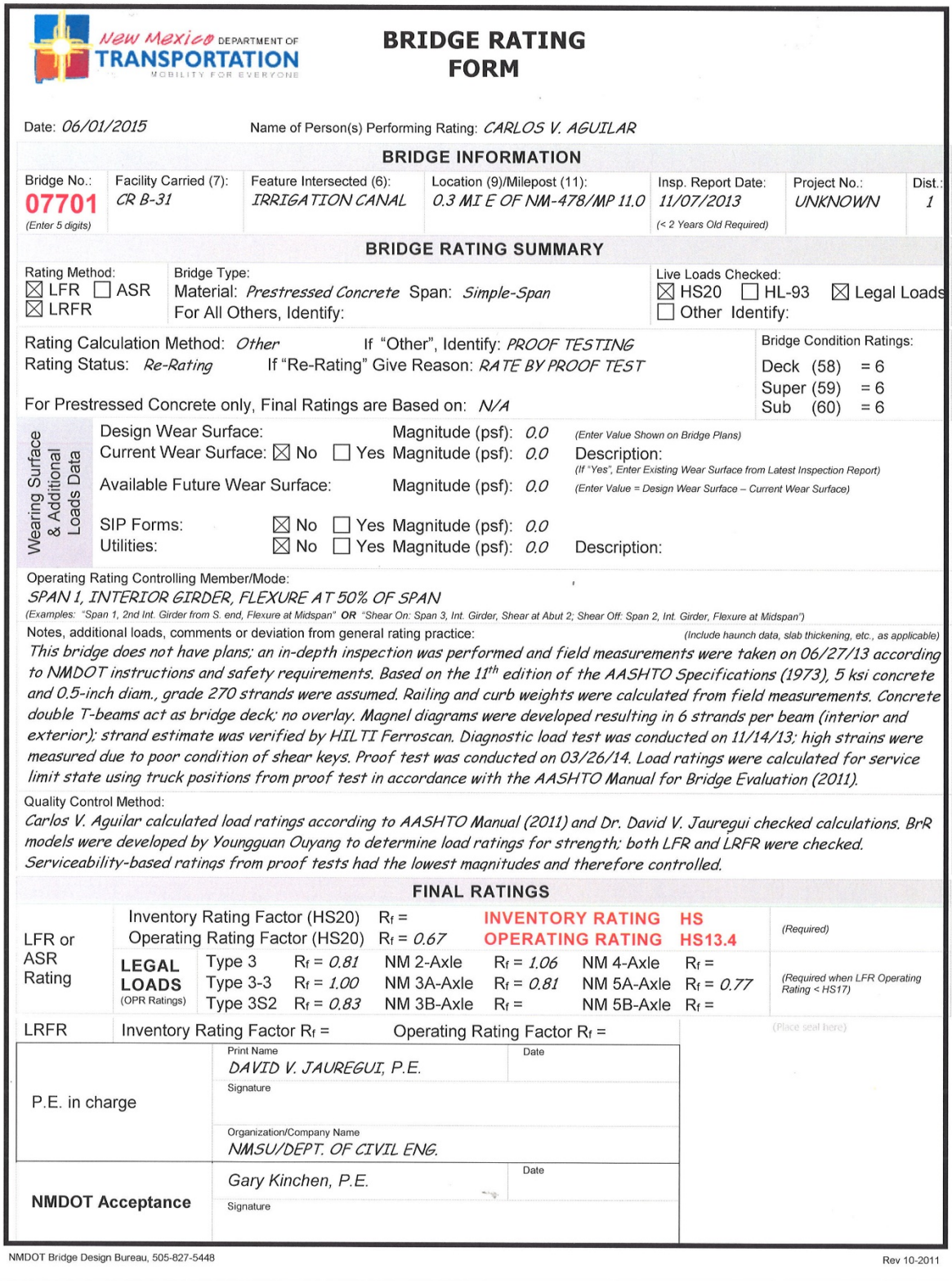

New Mexico DEPARTMENT OF TRANSPORTATION
MOBILITY FOR EVERYONE

BRIDGE RATING FORM

Date: 06/01/2015 Name of Person(s) Performing Rating: CARLOS V. AGUILAR

BRIDGE INFORMATION

Bridge No.:	Facility Carried (7):	Feature Intersected (6):	Location (9)/Milepost (11):	Insp. Report Date:	Project No.:	Dist.:
07701 (Enter 5 digits)	CR B-31	IRRIGATION CANAL	0.3 MI E OF NM-478/MP 11.0	11/07/2013 (< 2 Years Old Required)	UNKNOWN	1

BRIDGE RATING SUMMARY

Rating Method: ☒ LFR ☐ ASR ☒ LRFR

Bridge Type: Material: Prestressed Concrete Span: Simple-Span For All Others, Identify:

Live Loads Checked: ☒ HS20 ☐ HL-93 ☒ Legal Loads ☐ Other Identify:

Rating Calculation Method: Other If "Other", Identify: PROOF TESTING

Rating Status: Re-Rating If "Re-Rating" Give Reason: RATE BY PROOF TEST

For Prestressed Concrete only, Final Ratings are Based on: N/A

Bridge Condition Ratings: Deck (58) = 6; Super (59) = 6; Sub (60) = 6

Wearing Surface & Additional Loads Data

Design Wear Surface: Magnitude (psf): 0.0 (Enter Value Shown on Bridge Plans)

Current Wear Surface: ☒ No ☐ Yes Magnitude (psf): 0.0 Description: (If "Yes", Enter Existing Wear Surface from Latest Inspection Report)

Available Future Wear Surface: Magnitude (psf): 0.0 (Enter Value = Design Wear Surface – Current Wear Surface)

SIP Forms: ☒ No ☐ Yes Magnitude (psf): 0.0

Utilities: ☒ No ☐ Yes Magnitude (psf): 0.0 Description:

Operating Rating Controlling Member/Mode:

SPAN 1, INTERIOR GIRDER, FLEXURE AT 50% OF SPAN

(Examples: "Span 1, 2nd Int. Girder from S. end, Flexure at Midspan" **OR** "Shear On: Span 3, Int. Girder, Shear at Abut 2; Shear Off: Span 2, Int. Girder, Flexure at Midspan")

Notes, additional loads, comments or deviation from general rating practice: (Include haunch data, slab thickening, etc., as applicable)

This bridge does not have plans; an in-depth inspection was performed and field measurements were taken on 06/27/13 according to NMDOT instructions and safety requirements. Based on the 11th edition of the AASHTO Specifications (1973), 5 ksi concrete and 0.5-inch diam., grade 270 strands were assumed. Railing and curb weights were calculated from field measurements. Concrete double T-beams act as bridge deck; no overlay. Magnel diagrams were developed resulting in 6 strands per beam (interior and exterior); strand estimate was verified by HILTI Ferroscan. Diagnostic load test was conducted on 11/14/13; high strains were measured due to poor condition of shear keys. Proof test was conducted on 03/26/14. Load ratings were calculated for service limit state using truck positions from proof test in accordance with the AASHTO Manual for Bridge Evaluation (2011).

Quality Control Method:

Carlos V. Aguilar calculated load ratings according to AASHTO Manual (2011) and Dr. David V. Jauregui checked calculations. BrR models were developed by Youngguan Ouyang to determine load ratings for strength; both LFR and LRFR were checked. Serviceability-based ratings from proof tests had the lowest magnitudes and therefore controlled.

FINAL RATINGS

LFR or ASR Rating

Inventory Rating Factor (HS20) R_f = INVENTORY RATING HS

Operating Rating Factor (HS20) R_f = 0.67 OPERATING RATING HS13.4 (Required)

LEGAL LOADS (OPR Ratings)

Type 3	R_f = 0.81	NM 2-Axle	R_f = 1.06	NM 4-Axle	R_f =
Type 3-3	R_f = 1.00	NM 3A-Axle	R_f = 0.81	NM 5A-Axle	R_f = 0.77
Type 3S2	R_f = 0.83	NM 3B-Axle	R_f =	NM 5B-Axle	R_f =

(Required when LFR Operating Rating < HS17)

LRFR Inventory Rating Factor R_f = Operating Rating Factor R_f =

(Place seal here)

P.E. in charge	Print Name: DAVID V. JAUREGUI, P.E.	Date
	Signature	
	Organization/Company Name: NMSU/DEPT. OF CIVIL ENG.	
NMDOT Acceptance	Gary Kinchen, P.E.	Date
	Signature	

NMDOT Bridge Design Bureau, 505-827-5448 Rev 10-2011

Figure C.1. NMDOT load rating form for Bridge No. 7701 (P/C T-beam, District 1).

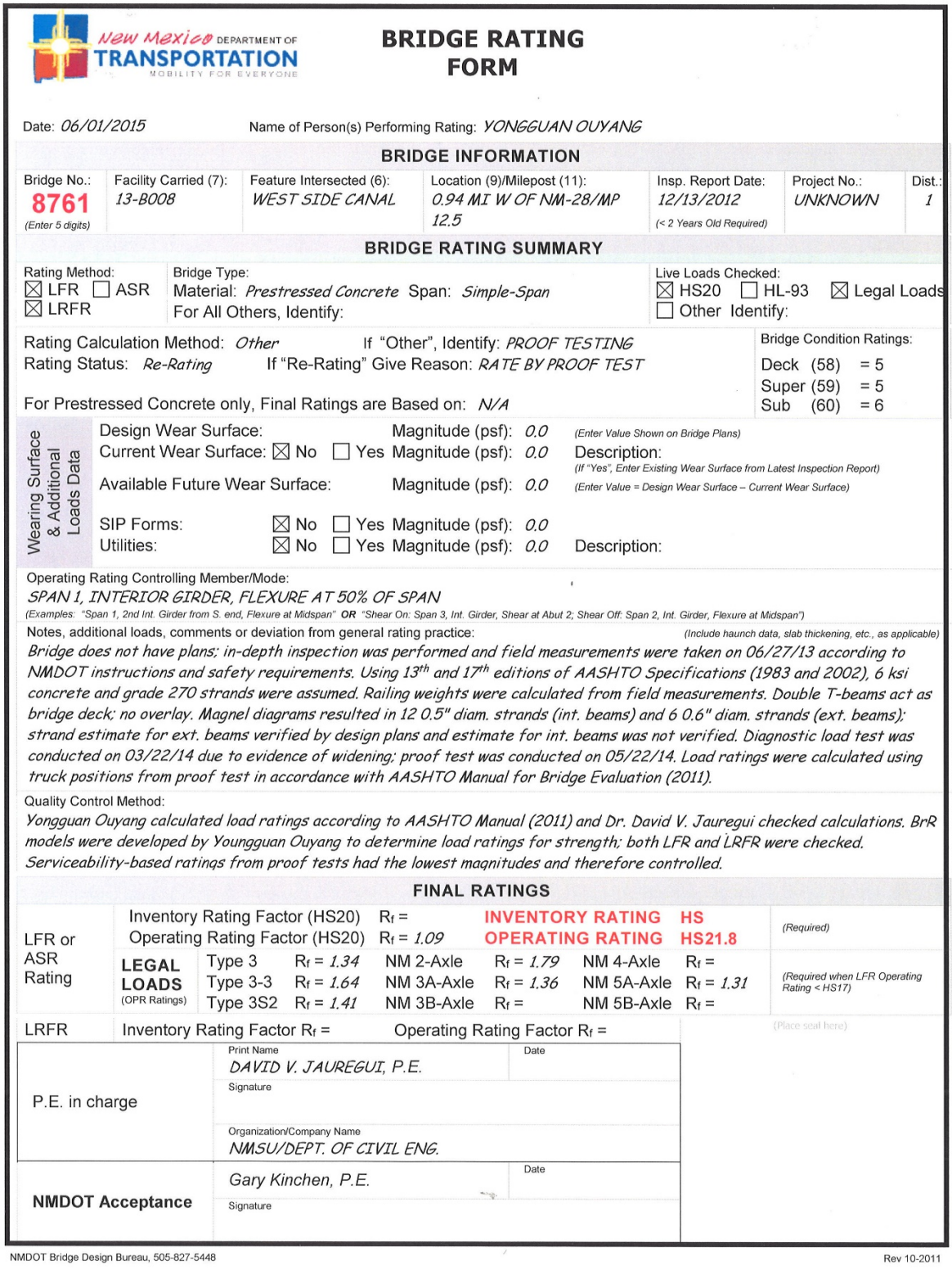

New Mexico DEPARTMENT OF TRANSPORTATION
MOBILITY FOR EVERYONE

BRIDGE RATING FORM

Date: 06/01/2015 Name of Person(s) Performing Rating: YONGGUAN OUYANG

BRIDGE INFORMATION

Bridge No.:	Facility Carried (7):	Feature Intersected (6):	Location (9)/Milepost (11):	Insp. Report Date:	Project No.:	Dist.:
8761 (Enter 5 digits)	13-B008	WEST SIDE CANAL	0.94 MI W OF NM-28/MP 12.5	12/13/2012 (< 2 Years Old Required)	UNKNOWN	1

BRIDGE RATING SUMMARY

Rating Method: ☒ LFR ☐ ASR ☒ LRFR

Bridge Type: Material: Prestressed Concrete Span: Simple-Span For All Others, Identify:

Live Loads Checked: ☒ HS20 ☐ HL-93 ☒ Legal Loads ☐ Other Identify:

Rating Calculation Method: Other If "Other", Identify: PROOF TESTING

Rating Status: Re-Rating If "Re-Rating" Give Reason: RATE BY PROOF TEST

For Prestressed Concrete only, Final Ratings are Based on: N/A

Bridge Condition Ratings: Deck (58) = 5; Super (59) = 5; Sub (60) = 6

Wearing Surface & Additional Loads Data

Design Wear Surface: Magnitude (psf): 0.0 (Enter Value Shown on Bridge Plans)

Current Wear Surface: ☒ No ☐ Yes Magnitude (psf): 0.0 Description: (If "Yes", Enter Existing Wear Surface from Latest Inspection Report)

Available Future Wear Surface: Magnitude (psf): 0.0 (Enter Value = Design Wear Surface – Current Wear Surface)

SIP Forms: ☒ No ☐ Yes Magnitude (psf): 0.0

Utilities: ☒ No ☐ Yes Magnitude (psf): 0.0 Description:

Operating Rating Controlling Member/Mode:

SPAN 1, INTERIOR GIRDER, FLEXURE AT 50% OF SPAN

(Examples: "Span 1, 2nd Int. Girder from S. end, Flexure at Midspan" **OR** "Shear On: Span 3, Int. Girder, Shear at Abut 2; Shear Off: Span 2, Int. Girder, Flexure at Midspan")

Notes, additional loads, comments or deviation from general rating practice: (Include haunch data, slab thickening, etc., as applicable)

Bridge does not have plans; in-depth inspection was performed and field measurements were taken on 06/27/13 according to NMDOT instructions and safety requirements. Using 13th and 17th editions of AASHTO Specifications (1983 and 2002), 6 ksi concrete and grade 270 strands were assumed. Railing weights were calculated from field measurements. Double T-beams act as bridge deck; no overlay. Magnel diagrams resulted in 12 0.5" diam. strands (int. beams) and 6 0.6" diam. strands (ext. beams); strand estimate for ext. beams verified by design plans and estimate for int. beams was not verified. Diagnostic load test was conducted on 03/22/14 due to evidence of widening; proof test was conducted on 05/22/14. Load ratings were calculated using truck positions from proof test in accordance with AASHTO Manual for Bridge Evaluation (2011).

Quality Control Method:

Yongguan Ouyang calculated load ratings according to AASHTO Manual (2011) and Dr. David V. Jauregui checked calculations. BrR models were developed by Youngguan Ouyang to determine load ratings for strength; both LFR and LRFR were checked. Serviceability-based ratings from proof tests had the lowest magnitudes and therefore controlled.

FINAL RATINGS

LFR or ASR Rating

Inventory Rating Factor (HS20) R_f = INVENTORY RATING HS

Operating Rating Factor (HS20) R_f = 1.09 OPERATING RATING HS21.8 (Required)

LEGAL LOADS (OPR Ratings)

Type 3	R_f = 1.34	NM 2-Axle	R_f = 1.79	NM 4-Axle	R_f =		
Type 3-3	R_f = 1.64	NM 3A-Axle	R_f = 1.36	NM 5A-Axle	R_f = 1.31	(Required when LFR Operating Rating < HS17)	
Type 3S2	R_f = 1.41	NM 3B-Axle	R_f =	NM 5B-Axle	R_f =		

LRFR Inventory Rating Factor R_f = Operating Rating Factor R_f =

(Place seal here)

P.E. in charge	Print Name: DAVID V. JAUREGUI, P.E.	Date
	Signature	
	Organization/Company Name: NMSU/DEPT. OF CIVIL ENG.	
NMDOT Acceptance	Gary Kinchen, P.E.	Date
	Signature	

NMDOT Bridge Design Bureau, 505-827-5448 Rev 10-2011

Figure C.2. NMDOT load rating form for Bridge No. 8761 (P/C T-beam, District 1).

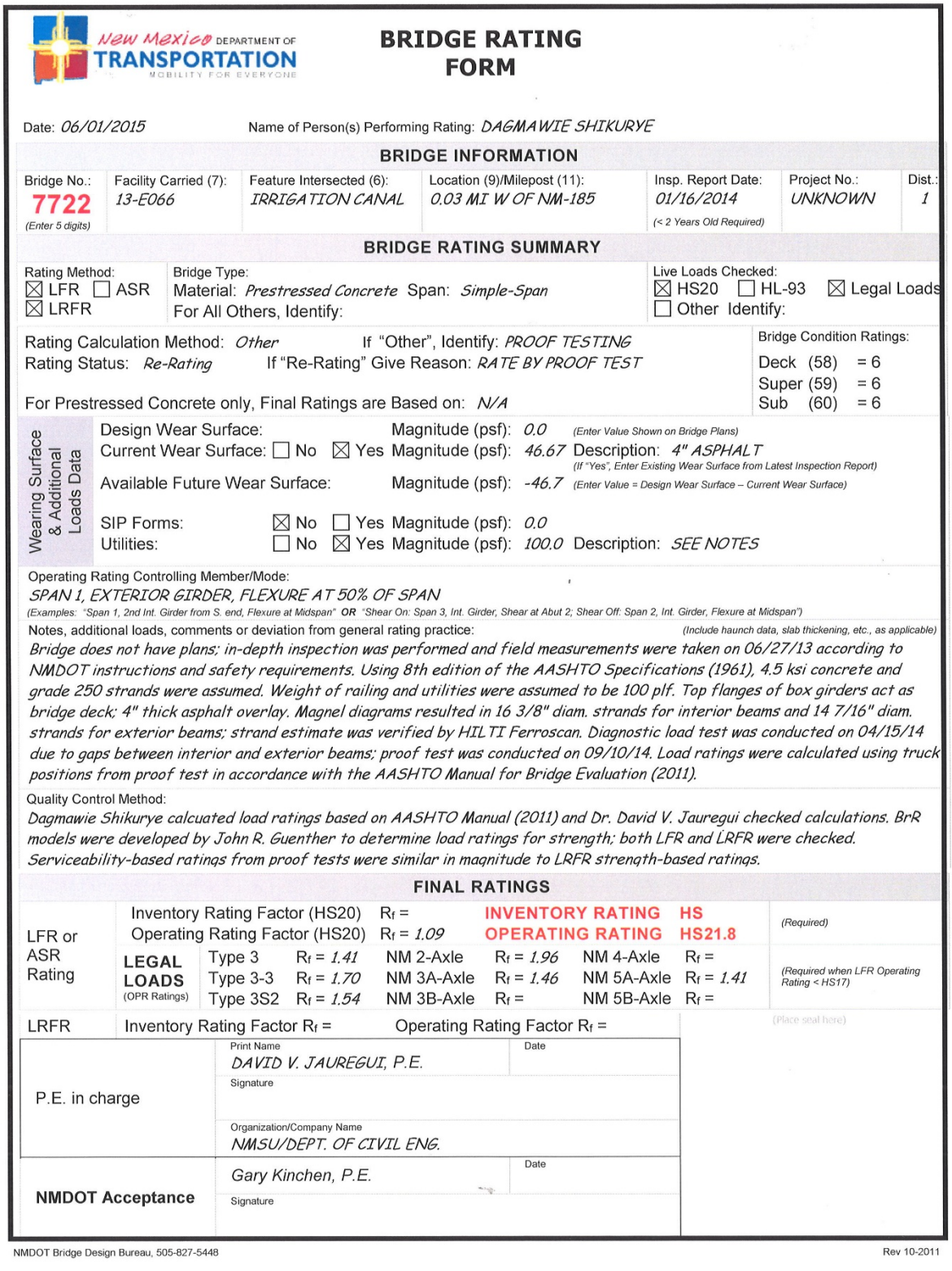

New Mexico DEPARTMENT OF TRANSPORTATION
MOBILITY FOR EVERYONE

BRIDGE RATING FORM

Date: 06/01/2015 Name of Person(s) Performing Rating: DAGMAWIE SHIKURYE

BRIDGE INFORMATION

Bridge No.:	Facility Carried (7):	Feature Intersected (6):	Location (9)/Milepost (11):	Insp. Report Date:	Project No.:	Dist.:
7722 (Enter 5 digits)	13-E066	IRRIGATION CANAL	0.03 MI W OF NM-185	01/16/2014 (< 2 Years Old Required)	UNKNOWN	1

BRIDGE RATING SUMMARY

Rating Method: ☒ LFR ☐ ASR ☒ LRFR

Bridge Type: Material: Prestressed Concrete Span: Simple-Span For All Others, Identify:

Live Loads Checked: ☒ HS20 ☐ HL-93 ☒ Legal Loads ☐ Other Identify:

Rating Calculation Method: Other If "Other", Identify: PROOF TESTING

Rating Status: Re-Rating If "Re-Rating" Give Reason: RATE BY PROOF TEST

For Prestressed Concrete only, Final Ratings are Based on: N/A

Bridge Condition Ratings:
Deck (58) = 6
Super (59) = 6
Sub (60) = 6

Wearing Surface & Additional Loads Data

Design Wear Surface: Magnitude (psf): 0.0 (Enter Value Shown on Bridge Plans)

Current Wear Surface: ☐ No ☒ Yes Magnitude (psf): 46.67 Description: 4" ASPHALT (If "Yes", Enter Existing Wear Surface from Latest Inspection Report)

Available Future Wear Surface: Magnitude (psf): -46.7 (Enter Value = Design Wear Surface – Current Wear Surface)

SIP Forms: ☒ No ☐ Yes Magnitude (psf): 0.0

Utilities: ☐ No ☒ Yes Magnitude (psf): 100.0 Description: SEE NOTES

Operating Rating Controlling Member/Mode:
SPAN 1, EXTERIOR GIRDER, FLEXURE AT 50% OF SPAN
(Examples: "Span 1, 2nd Int. Girder from S. end, Flexure at Midspan" **OR** "Shear On: Span 3, Int. Girder, Shear at Abut 2; Shear Off: Span 2, Int. Girder, Flexure at Midspan")

Notes, additional loads, comments or deviation from general rating practice: (Include haunch data, slab thickening, etc., as applicable)

Bridge does not have plans; in-depth inspection was performed and field measurements were taken on 06/27/13 according to NMDOT instructions and safety requirements. Using 8th edition of the AASHTO Specifications (1961), 4.5 ksi concrete and grade 250 strands were assumed. Weight of railing and utilities were assumed to be 100 plf. Top flanges of box girders act as bridge deck; 4" thick asphalt overlay. Magnel diagrams resulted in 16 3/8" diam. strands for interior beams and 14 7/16" diam. strands for exterior beams; strand estimate was verified by HILTI Ferroscan. Diagnostic load test was conducted on 04/15/14 due to gaps between interior and exterior beams; proof test was conducted on 09/10/14. Load ratings were calculated using truck positions from proof test in accordance with the AASHTO Manual for Bridge Evaluation (2011).

Quality Control Method:

Dagmawie Shikurye calcuated load ratings based on AASHTO Manual (2011) and Dr. David V. Jauregui checked calculations. BrR models were developed by John R. Guenther to determine load ratings for strength; both LFR and LRFR were checked. Serviceability-based ratings from proof tests were similar in magnitude to LRFR strength-based ratings.

FINAL RATINGS

LFR or ASR Rating

Inventory Rating Factor (HS20) R_f = INVENTORY RATING HS (Required)

Operating Rating Factor (HS20) R_f = 1.09 OPERATING RATING HS21.8

LEGAL LOADS (OPR Ratings)

Type 3	R_f = 1.41	NM 2-Axle	R_f = 1.96	NM 4-Axle	R_f =		
Type 3-3	R_f = 1.70	NM 3A-Axle	R_f = 1.46	NM 5A-Axle	R_f = 1.41	(Required when LFR Operating Rating < HS17)	
Type 3S2	R_f = 1.54	NM 3B-Axle	R_f =	NM 5B-Axle	R_f =		

LRFR Inventory Rating Factor R_f = Operating Rating Factor R_f =

(Place seal here)

P.E. in charge	Print Name: DAVID V. JAUREGUI, P.E.	Date
	Signature	
	Organization/Company Name: NMSU/DEPT. OF CIVIL ENG.	
NMDOT Acceptance	Gary Kinchen, P.E.	Date
	Signature	

NMDOT Bridge Design Bureau, 505-827-5448 Rev 10-2011

Figure C.3. NMDOT load rating form for Bridge No. 7722 (P/C box girder, District 1).

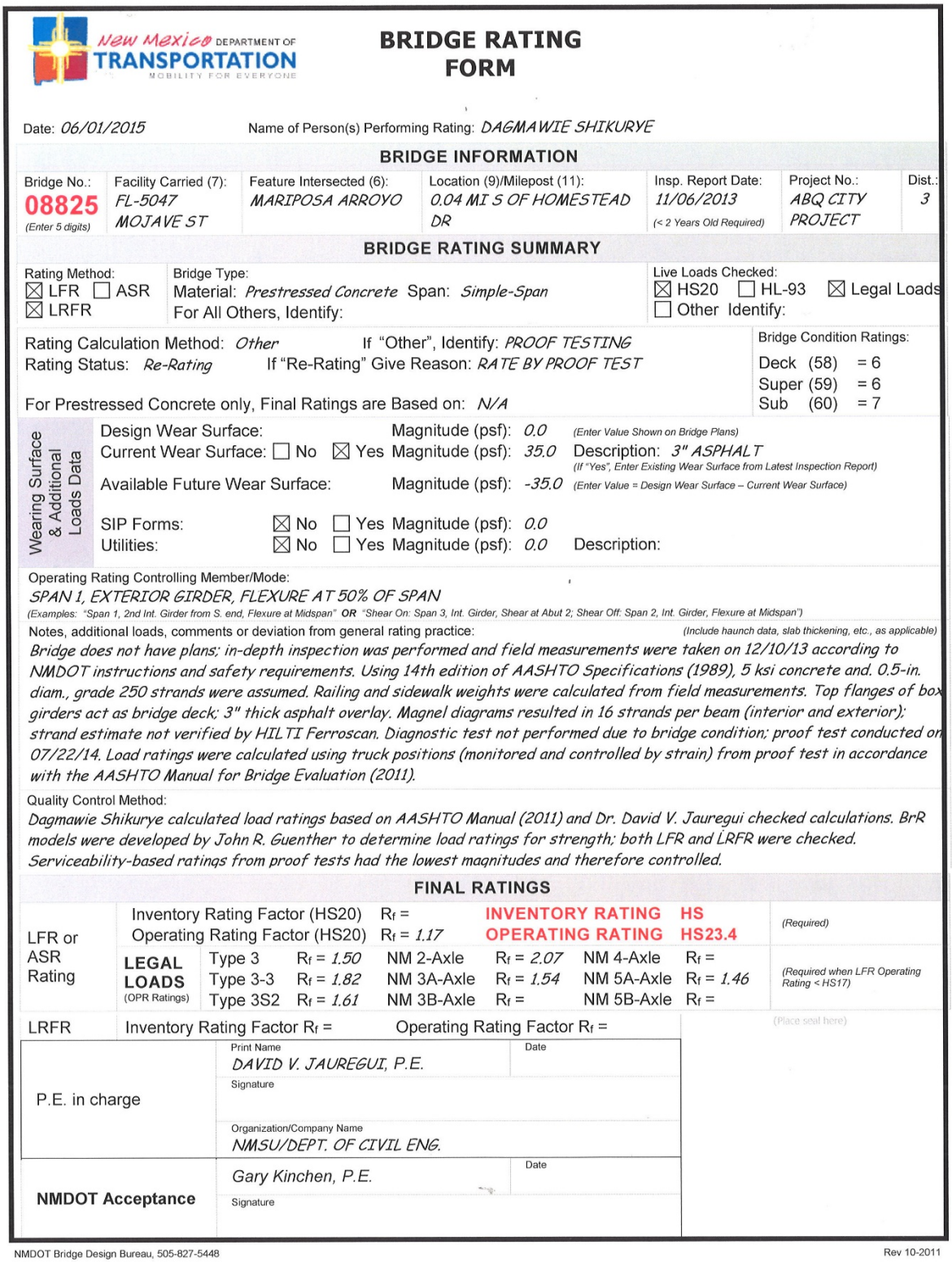

New Mexico DEPARTMENT OF TRANSPORTATION
MOBILITY FOR EVERYONE

BRIDGE RATING FORM

Date: 06/01/2015 Name of Person(s) Performing Rating: DAGMAWIE SHIKURYE

BRIDGE INFORMATION

Bridge No.:	Facility Carried (7):	Feature Intersected (6):	Location (9)/Milepost (11):	Insp. Report Date:	Project No.:	Dist.:
08825 (Enter 5 digits)	FL-5047 MOJAVE ST	MARIPOSA ARROYO	0.04 MI S OF HOMESTEAD DR	11/06/2013 (< 2 Years Old Required)	ABQ CITY PROJECT	3

BRIDGE RATING SUMMARY

Rating Method: ☒ LFR ☐ ASR ☒ LRFR

Bridge Type: Material: Prestressed Concrete Span: Simple-Span For All Others, Identify:

Live Loads Checked: ☒ HS20 ☐ HL-93 ☒ Legal Loads ☐ Other Identify:

Rating Calculation Method: Other If "Other", Identify: PROOF TESTING

Rating Status: Re-Rating If "Re-Rating" Give Reason: RATE BY PROOF TEST

For Prestressed Concrete only, Final Ratings are Based on: N/A

Bridge Condition Ratings:
Deck (58) = 6
Super (59) = 6
Sub (60) = 7

Wearing Surface & Additional Loads Data

Design Wear Surface: Magnitude (psf): 0.0 (Enter Value Shown on Bridge Plans)

Current Wear Surface: ☐ No ☒ Yes Magnitude (psf): 35.0 Description: 3" ASPHALT (If "Yes", Enter Existing Wear Surface from Latest Inspection Report)

Available Future Wear Surface: Magnitude (psf): -35.0 (Enter Value = Design Wear Surface – Current Wear Surface)

SIP Forms: ☒ No ☐ Yes Magnitude (psf): 0.0

Utilities: ☒ No ☐ Yes Magnitude (psf): 0.0 Description:

Operating Rating Controlling Member/Mode:
SPAN 1, EXTERIOR GIRDER, FLEXURE AT 50% OF SPAN
(Examples: "Span 1, 2nd Int. Girder from S. end, Flexure at Midspan" **OR** "Shear On: Span 3, Int. Girder, Shear at Abut 2; Shear Off: Span 2, Int. Girder, Flexure at Midspan")

Notes, additional loads, comments or deviation from general rating practice: (Include haunch data, slab thickening, etc., as applicable)

Bridge does not have plans; in-depth inspection was performed and field measurements were taken on 12/10/13 according to NMDOT instructions and safety requirements. Using 14th edition of AASHTO Specifications (1989), 5 ksi concrete and. 0.5-in. diam., grade 250 strands were assumed. Railing and sidewalk weights were calculated from field measurements. Top flanges of box girders act as bridge deck; 3" thick asphalt overlay. Magnel diagrams resulted in 16 strands per beam (interior and exterior); strand estimate not verified by HILTI Ferroscan. Diagnostic test not performed due to bridge condition; proof test conducted on 07/22/14. Load ratings were calculated using truck positions (monitored and controlled by strain) from proof test in accordance with the AASHTO Manual for Bridge Evaluation (2011).

Quality Control Method:
Dagmawie Shikurye calculated load ratings based on AASHTO Manual (2011) and Dr. David V. Jauregui checked calculations. BrR models were developed by John R. Guenther to determine load ratings for strength; both LFR and LRFR were checked. Serviceability-based ratings from proof tests had the lowest magnitudes and therefore controlled.

FINAL RATINGS

LFR or ASR Rating

Inventory Rating Factor (HS20) R_f = INVENTORY RATING HS (Required)

Operating Rating Factor (HS20) R_f = 1.17 OPERATING RATING HS23.4

LEGAL LOADS (OPR Ratings) (Required when LFR Operating Rating < HS17)

Type 3	R_f = 1.50	NM 2-Axle	R_f = 2.07	NM 4-Axle	R_f =
Type 3-3	R_f = 1.82	NM 3A-Axle	R_f = 1.54	NM 5A-Axle	R_f = 1.46
Type 3S2	R_f = 1.61	NM 3B-Axle	R_f =	NM 5B-Axle	R_f =

LRFR Inventory Rating Factor R_f = Operating Rating Factor R_f = (Place seal here)

P.E. in charge	Print Name: DAVID V. JAUREGUI, P.E.	Date
	Signature	
	Organization/Company Name: NMSU/DEPT. OF CIVIL ENG.	
NMDOT Acceptance	Gary Kinchen, P.E.	Date
	Signature	

NMDOT Bridge Design Bureau, 505-827-5448 Rev 10-2011

Figure C.4. NMDOT load rating form for Bridge No. 8825 (P/C box girder, District 3).

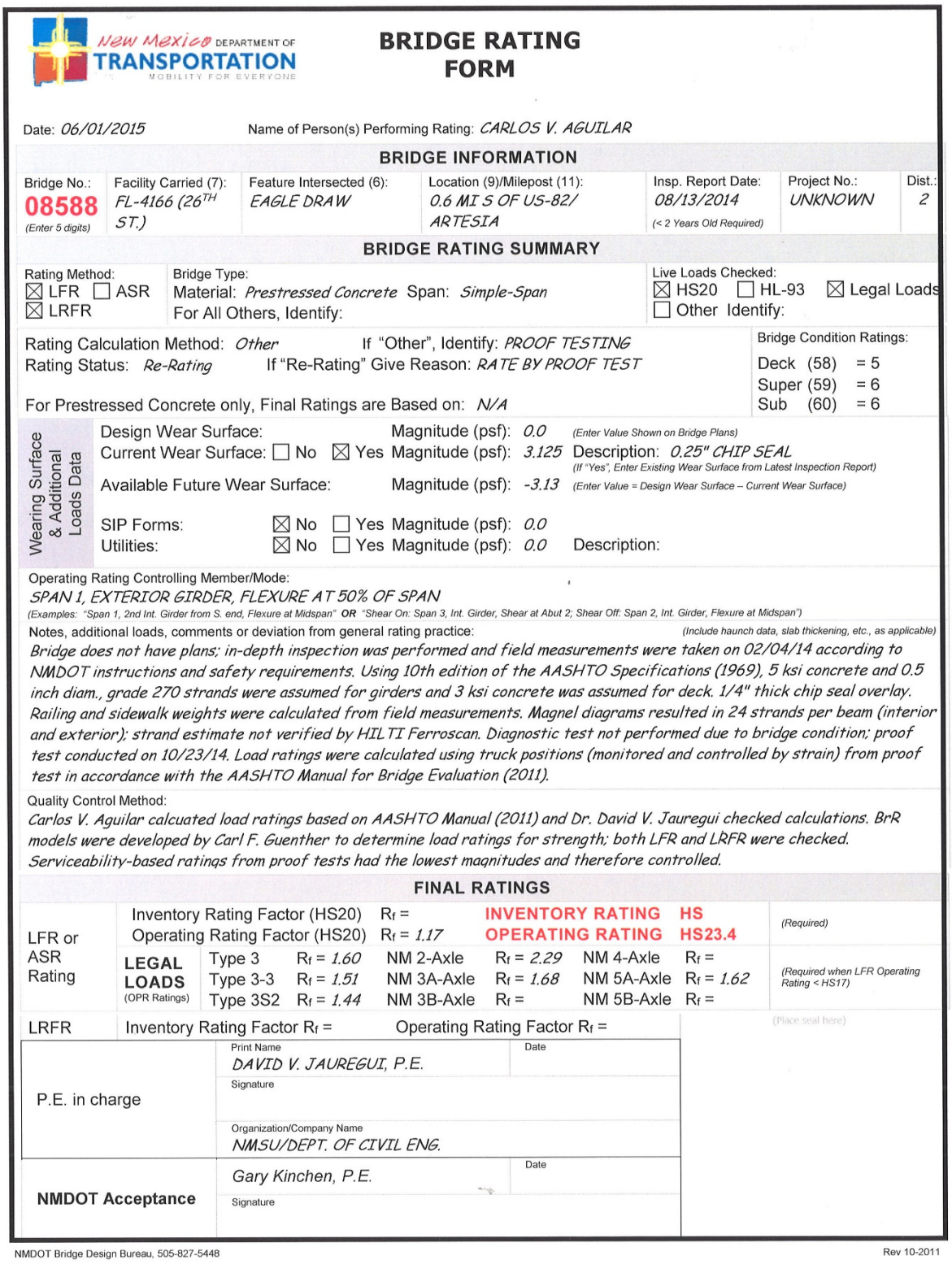

New Mexico DEPARTMENT OF TRANSPORTATION
MOBILITY FOR EVERYONE

BRIDGE RATING FORM

Date: 06/01/2015 Name of Person(s) Performing Rating: CARLOS V. AGUILAR

BRIDGE INFORMATION

Bridge No.:	Facility Carried (7):	Feature Intersected (6):	Location (9)/Milepost (11):	Insp. Report Date:	Project No.:	Dist.:
08588 (Enter 5 digits)	FL-4166 (26TH ST.)	EAGLE DRAW	0.6 MI S OF US-82/ ARTESIA	08/13/2014 (< 2 Years Old Required)	UNKNOWN	2

BRIDGE RATING SUMMARY

Rating Method: ☒ LFR ☐ ASR ☒ LRFR

Bridge Type: Material: Prestressed Concrete Span: Simple-Span For All Others, Identify:

Live Loads Checked: ☒ HS20 ☐ HL-93 ☒ Legal Loads ☐ Other Identify:

Rating Calculation Method: Other If "Other", Identify: PROOF TESTING

Rating Status: Re-Rating If "Re-Rating" Give Reason: RATE BY PROOF TEST

For Prestressed Concrete only, Final Ratings are Based on: N/A

Bridge Condition Ratings:
Deck (58) = 5
Super (59) = 6
Sub (60) = 6

Wearing Surface & Additional Loads Data

Design Wear Surface: Magnitude (psf): 0.0 (Enter Value Shown on Bridge Plans)

Current Wear Surface: ☐ No ☒ Yes Magnitude (psf): 3.125 Description: 0.25" CHIP SEAL (If "Yes", Enter Existing Wear Surface from Latest Inspection Report)

Available Future Wear Surface: Magnitude (psf): -3.13 (Enter Value = Design Wear Surface – Current Wear Surface)

SIP Forms: ☒ No ☐ Yes Magnitude (psf): 0.0

Utilities: ☒ No ☐ Yes Magnitude (psf): 0.0 Description:

Operating Rating Controlling Member/Mode:
SPAN 1, EXTERIOR GIRDER, FLEXURE AT 50% OF SPAN
(Examples: "Span 1, 2nd Int. Girder from S. end, Flexure at Midspan" **OR** "Shear On: Span 3, Int. Girder, Shear at Abut 2; Shear Off: Span 2, Int. Girder, Flexure at Midspan")

Notes, additional loads, comments or deviation from general rating practice: (Include haunch data, slab thickening, etc., as applicable)

Bridge does not have plans; in-depth inspection was performed and field measurements were taken on 02/04/14 according to NMDOT instructions and safety requirements. Using 10th edition of the AASHTO Specifications (1969), 5 ksi concrete and 0.5 inch diam., grade 270 strands were assumed for girders and 3 ksi concrete was assumed for deck. 1/4" thick chip seal overlay. Railing and sidewalk weights were calculated from field measurements. Magnel diagrams resulted in 24 strands per beam (interior and exterior); strand estimate not verified by HILTI Ferroscan. Diagnostic test not performed due to bridge condition; proof test conducted on 10/23/14. Load ratings were calculated using truck positions (monitored and controlled by strain) from proof test in accordance with the AASHTO Manual for Bridge Evaluation (2011).

Quality Control Method:
Carlos V. Aguilar calcuated load ratings based on AASHTO Manual (2011) and Dr. David V. Jauregui checked calculations. BrR models were developed by Carl F. Guenther to determine load ratings for strength; both LFR and LRFR were checked. Serviceability-based ratings from proof tests had the lowest magnitudes and therefore controlled.

FINAL RATINGS

LFR or ASR Rating

Inventory Rating Factor (HS20) R_f = INVENTORY RATING HS (Required)

Operating Rating Factor (HS20) R_f = 1.17 OPERATING RATING HS23.4

LEGAL LOADS (OPR Ratings)

						(Required when LFR Operating Rating < HS17)
Type 3	R_f = 1.60	NM 2-Axle	R_f = 2.29	NM 4-Axle	R_f =	
Type 3-3	R_f = 1.51	NM 3A-Axle	R_f = 1.68	NM 5A-Axle	R_f = 1.62	
Type 3S2	R_f = 1.44	NM 3B-Axle	R_f =	NM 5B-Axle	R_f =	

LRFR Inventory Rating Factor R_f = Operating Rating Factor R_f =

(Place seal here)

P.E. in charge	Print Name: DAVID V. JAUREGUI, P.E.	Date
	Signature	
	Organization/Company Name: NMSU/DEPT. OF CIVIL ENG.	
NMDOT Acceptance	Gary Kinchen, P.E.	Date
	Signature	

NMDOT Bridge Design Bureau, 505-827-5448 Rev 10-2011

Figure C.5. NMDOT load rating form for Bridge No. 8588 (P/C I-girder, District 2).

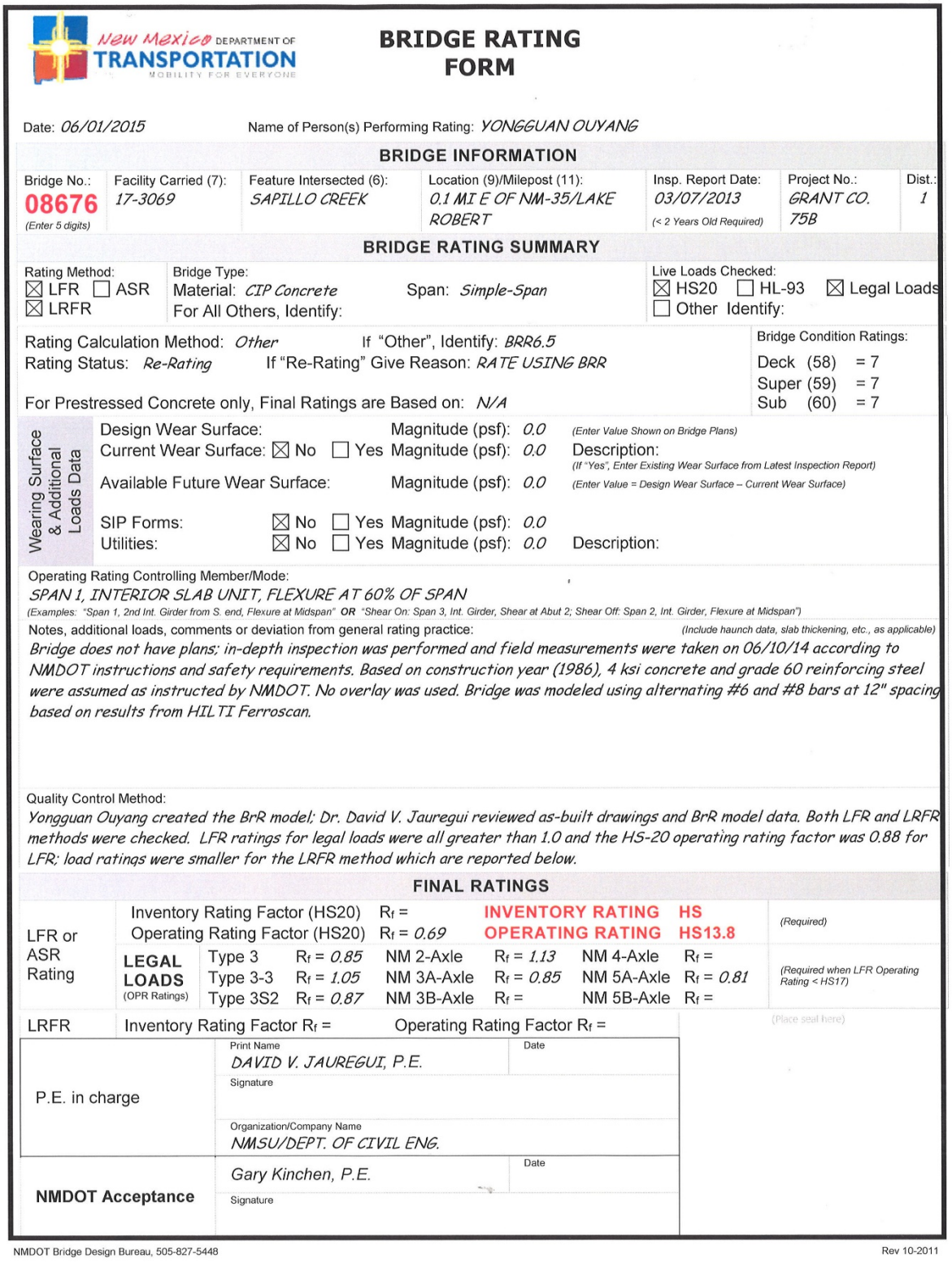

New Mexico DEPARTMENT OF TRANSPORTATION
MOBILITY FOR EVERYONE

BRIDGE RATING FORM

Date: 06/01/2015 Name of Person(s) Performing Rating: YONGGUAN OUYANG

BRIDGE INFORMATION

Bridge No.:	Facility Carried (7):	Feature Intersected (6):	Location (9)/Milepost (11):	Insp. Report Date:	Project No.:	Dist.:
08676 (Enter 5 digits)	17-3069	SAPILLO CREEK	0.1 MI E OF NM-35/LAKE ROBERT	03/07/2013 (< 2 Years Old Required)	GRANT CO. 75B	1

BRIDGE RATING SUMMARY

Rating Method: ☒ LFR ☐ ASR ☒ LRFR

Bridge Type: Material: CIP Concrete Span: Simple-Span For All Others, Identify:

Live Loads Checked: ☒ HS20 ☐ HL-93 ☒ Legal Loads ☐ Other Identify:

Rating Calculation Method: Other If "Other", Identify: BRR6.5

Rating Status: Re-Rating If "Re-Rating" Give Reason: RATE USING BRR

For Prestressed Concrete only, Final Ratings are Based on: N/A

Bridge Condition Ratings: Deck (58) = 7 Super (59) = 7 Sub (60) = 7

Wearing Surface & Additional Loads Data

Design Wear Surface: Magnitude (psf): 0.0 (Enter Value Shown on Bridge Plans)

Current Wear Surface: ☒ No ☐ Yes Magnitude (psf): 0.0 Description: (If "Yes", Enter Existing Wear Surface from Latest Inspection Report)

Available Future Wear Surface: Magnitude (psf): 0.0 (Enter Value = Design Wear Surface – Current Wear Surface)

SIP Forms: ☒ No ☐ Yes Magnitude (psf): 0.0

Utilities: ☒ No ☐ Yes Magnitude (psf): 0.0 Description:

Operating Rating Controlling Member/Mode:

SPAN 1, INTERIOR SLAB UNIT, FLEXURE AT 60% OF SPAN

(Examples: "Span 1, 2nd Int. Girder from S. end, Flexure at Midspan" **OR** "Shear On: Span 3, Int. Girder, Shear at Abut 2; Shear Off: Span 2, Int. Girder, Flexure at Midspan")

Notes, additional loads, comments or deviation from general rating practice: (Include haunch data, slab thickening, etc., as applicable)

Bridge does not have plans; in-depth inspection was performed and field measurements were taken on 06/10/14 according to NMDOT instructions and safety requirements. Based on construction year (1986), 4 ksi concrete and grade 60 reinforcing steel were assumed as instructed by NMDOT. No overlay was used. Bridge was modeled using alternating #6 and #8 bars at 12" spacing based on results from HILTI Ferroscan.

Quality Control Method:

Yongguan Ouyang created the BrR model; Dr. David V. Jauregui reviewed as-built drawings and BrR model data. Both LFR and LRFR methods were checked. LFR ratings for legal loads were all greater than 1.0 and the HS-20 operating rating factor was 0.88 for LFR; load ratings were smaller for the LRFR method which are reported below.

FINAL RATINGS

LFR or ASR Rating

Inventory Rating Factor (HS20) R_f = INVENTORY RATING HS (Required)

Operating Rating Factor (HS20) R_f = 0.69 OPERATING RATING HS13.8

LEGAL LOADS (OPR Ratings)

Type 3	R_f = 0.85	NM 2-Axle	R_f = 1.13	NM 4-Axle	R_f =	(Required when LFR Operating Rating < HS17)
Type 3-3	R_f = 1.05	NM 3A-Axle	R_f = 0.85	NM 5A-Axle	R_f = 0.81	
Type 3S2	R_f = 0.87	NM 3B-Axle	R_f =	NM 5B-Axle	R_f =	

LRFR Inventory Rating Factor R_f = Operating Rating Factor R_f =

(Place seal here)

P.E. in charge	Print Name: DAVID V. JAUREGUI, P.E.	Date
	Signature	
	Organization/Company Name: NMSU/DEPT. OF CIVIL ENG.	
NMDOT Acceptance	Gary Kinchen, P.E.	Date
	Signature	

NMDOT Bridge Design Bureau, 505-827-5448 Rev 10-2011

Figure C.6. NMDOT load rating form for Bridge No. 8676 (R/C slab, District 1).

REFERENCES

American Association of State Highway Officials (AASHO). (1961). *Standard Specifications for Highway Bridges*, 8th Edition, Washington, D.C.

American Association of State Highway Officials (AASHO). (1969). *Standard Specifications for Highway Bridges*, 10th Edition, Washington, D.C.

American Association of State Highway Officials (AASHO). (1973). *Standard Specifications for Highway Bridges*, 11th Edition, Washington, D.C.

American Association of State Highway and Transportation Officials (AASHTO). (1983). *Standard Specifications for Highway Bridges*, 13th Edition, Washington, D.C.

American Association of State Highway and Transportation Officials (AASHTO). (1989). *Standard Specifications for Highway Bridges*, 14th Edition, Washington, D.C.

American Association of State Highway and Transportation Officials (AASHTO). (2002). *Standard Specifications for Highway Bridges*, 17th Edition, Washington, D.C.

American Association of State Highway and Transportation Officials (AASHTO). (2011). *Manual for Bridge Evaluation*, 2nd Edition, Washington, D.C.

Bakht, B. and Jaeger, L. G. (1990). "Bridge Testing – A Surprise Every Time." *Journal of Structural Engineering*, Vol. 116, No. 5, pp. 1370-1383.

Bernhardt, R. P. and DeKolb, S. P. (2003). "Inspection and Load Testing of Three Bridges." *Final Report*, Project No. DE-01739-2P, US Army Signal Center, Fort Gordon, GA.

Bernhardt, R. P., DeKolb, S. P., and Kwiatkowski, T. L. (2004). "Proof Testing of Reinforced Concrete Bridges: A Useful Way to Provide Load Rating." *TECHBrief 2004 No. 3*, Burns & McDonnell, pp. 3-5.

Casas, J. R. and Gómez, J. D. (2013). "Load Rating of Highway Bridges by Proof Loading." *KSCE Journal of Civil Engineering*, Vol. 17, No. 3, pp. 556-567.

Casas, J. R., Olaszek, P., Sajna, A., Znidarie, A., and Lavric, I. (2009). "Sustainable Development, Global Change and Ecosystems (Sustainable Surface Transport): Deliverable D16: Recommendations on the Use of Soft, Diagnostic, and Proof Load Testing." *Document No. ARCHES-02-DE16*, Assessment and Rehabilitation of Central European Highway Structures (ARCHES) Management Group.

Chajes, M.J., and Shenton, H.W. (2006), "Using Diagnostic Load Tests for Accurate Load Rating of Typical Bridges," *Journal of Bridge Structures*, Vol. 2, No. 1, pp. 13-23.

Conner, G. H., Stallings, J. M., McDuffie, T. L., Campbell, J. R., Fulton, R. Y., Shelton, B. A., and Mullins, R. B. (1997). "Bridge Load Testing in Alabama." Transportation Research Board.

Commander, B., Valera-Ortiz, W., Stanton, T. R., and Diaz-Alvarez, H. (2009). "Field Testing and Load Rating Report, Bridge FSBR-514, Fort Shafter, Hawaii." *Final Report No. ERDC/GSL TR-09-9*, US Army Corp of Engineers, Arlington, VA.

Ellingwood, B. R., Zureick, A.-H., Wang, N., and O'Malley, C. (2009). "Condition Assessment of Existing Bridge Structures: Report of Task 4 – Development of Guidelines for Condition Assessment, Evaluation and Rating of Bridges in Georgia." *Report of GTRC Project No. E-20-K90 and GDOT Project No. RP05-01*, Georgia Department of Transportation and Georgia Institute of Technology, Atlanta, GA.

Federal Highway Administration (FHWA). "ACTION: Revisions to the Recording and Coding Guide for the Structure, Inventory and Appraisal of the Nation's Bridges." *Memorandum* from M. Myint Lwin, Director, Office of Bridge Technology, February 2, 2011.

Jeffrey, A., Breña, S. F., and Civjan, S. A. (2009). "Evaluation of Bridge Performance and Rating through Non-destructive Load Testing." *Final Report*, Research Report 2009-1, Vermont Agency of Transportation.

Gómez, J. D. and Casas, J. R. (2008). "Assessment of Bridge Capacity through Proof Load Testing." *Proceedings of IALCCE – International Symposium on Life-Cycle Civil Engineering*, pp. 559-564.

Gómez, J. D. and Casas, J. R. (2010). "Target Proof Load Factors for Highway Bridge Assessment in Central and Eastern European Countries." *Bridge Maintenance, Safety, Management, and Life-Cycle Optimization*, D. Frangopol, R. Sause, and C. Kusko, eds., Taylor and Francis Group, London, England, pp. 3220-3227.

Hag-Elsafi, O. and Kunin, J. (2006). "Load Testing for Bridge Rating: Dean's Mill over Hannacrois Creek." *Report FHWA/NY/SR-06/147*, Transportation Research and Development Bureau, New York State Department of Transportation.

Hawkins, N. M., Kuchma, D. A., Mast, R. F., Marsh, M. L., and Reineck, K.-H. (2005). "Simplified Shear Design of Structural Concrete Members." *Final Report*, NCHRP Report 549, National Cooperative Highway Research Program, Washington, D.C.

Kissane, R. J., Beal, D. B., and Sanford, J. A. (1980). "Load Rating Of Short-Span Highway Bridges." *Interim Report on Research Project 156-1*, Research Report 79 (US DOT/FHWA), Engineering Research and Development Bureau, New York State Department of Transportation.

Krishnamurthy, N. (1983). "Magnel Diagrams for Prestressed Concrete Beams." *ASCE Journal of Structural Engineering*, Vol. 109, No. 12, pp. 2761-2769.

Ladner, M. (1985). "In Situ Load Testing of Concrete Bridges in Switzerland." symposia paper presented at *ACI Convention Strength Evaluation of Existing Concrete Bridges*, ACI Committee 437 (Strength Evaluation of Existing Concrete Structures), pp. 59-79.

Lichtenstein, A. G. (1993). "Bridge Rating Through Nondestructive Load Testing." *Final Draft Report for NCHRP Project 12-28(13)A*, Transportation Research Board, National Research Council, Washington, D. C.

Malhotra, V. (2004). *Handbook on Nondestructive Testing of Concrete*, 2nd Edition, Boca Raton, Florida.

Markey, I. (1991). "Load Testing of Swiss Bridges." *Steel Construction Today*, Vol. 5, No. 1, pp. 15-20.

Michigan Department of Transportation (MDOT). "Guidance for the use of Field Evaluation and Documented Engineering Judgment." *Bridge Advisory 2012-02* from Bradley Wagner, Load Rating Program Manager, October 16, 2012.

Moses, F., Lebet, J. P., and Bez, R. (1994). "Applications of Field Testing to Bridge Evaluation." *Journal of Structural Engineering*, Vol. 120, No. 6, pp. 1745-1762.

New Mexico State Highway Department (NMSHD). (1970). *Standard Specifications for Road and Bridge Construction*, Santa Fe, NM.

O'Malley, C., Wang, N., Ellingwood, B. R., and Zureick, A.-H. (2009). "Condition Assessment of Existing Bridge Structures: Report of Tasks 2 and 3 – Bridge Testing Program." *Report of GTRC Project No. E-20-K90 and GDOT Project No. RP05-01*, Georgia Department of Transportation and Georgia Institute of Technology, Atlanta, GA.

Oregon Department of Transportation (ODOT). (2013a). *Section 8: Load Rating Concrete Bridge Without Existing Plans*. ODOT Load and Resistance Factor Rating (LRFR) Manual.

Oregon Department of Transportation (ODOT). (2013b). *ODOT Approximate Load Rating Procedure for Concrete Bridges with No Existing Plans*.

Pennsylvania Department of Transportation (PennDOT). (2010a). *Chapter 3: Bridge Analyses and Load Ratings*. PennDOT Bridge Safety Inspection Manual, Publication 238 (3-10).

Pennsylvania Department of Transportation (PennDOT). (2010b). *Appendix IP 03-B: Guidelines for Live Load Rating of Selected Concrete Bridges Without Plans Using Engineering Judgment*. PennDOT Bridge Safety Inspection Manual, Publication 238 (3-10).

Pinjarkar, S. G., Guedelhoefer, O. C., Smith, B. J., and Kritzler, R. W. (1990). "Nondestructive Load Testing for Bridge Evaluation and Rating." *Final Report for NCHRP Project 12-28(13)*, Transportation Research Board, National Research Council, Washington, D. C.

Saraf, V., Sokolik, A. F., and Nowak, A. S. (1996). "Proof Load Testing of Highway Bridges." *Transportation Research Record*, No. 1541, pp. 51-57.

Shahawy, M. E. and Garcia, A. M. (1990). "Structural Research and Testing in Florida." *Transportation Research Record*, No. 1275, pp. 76-80.

Shahawy, M. A. (1995). "Nondestructive Strength Evaluation of Florida Bridges." Proceedings of SPIE – The International Society of Optical Engineering (Nondestructive Evaluation of Aging Bridges and Highways), Society of Photo-Optical Instrumentation Engineers, Vol. 2456, pp. 101-123.

Shenton III, H. W., Chajes, M. J., and Huang, J. (2007). "Load Rating of Bridges Without Plans." *Final Report*, Research Report DCT 195, Delaware Center for Transportation.

Taylor, Z., Amini, O., and van de Lindt, J. W. (2011). "Approach for Establishing Approximate Load Carrying Capacity for Bridges with Unknown Design Properties." *Report No. MPC-11-236*, North Dakota State University - Upper Great Plains Transportation Institute, Fargo: Mountain-Plains Consortium.

Texas Department of Transportation (TxDOT). (2013). *Chapter 5, Section 3: Rating Concrete Bridges with No Plans*. TxDOT Bridge Inspection Manual.

Wang, N., Ellingwood, B. R., Zureick, A.-H., and O'Malley, C. (2009). "Condition Assessment of Existing Bridge Structures: Report of Task 1 – Appraisal of State-of-the-Art of Bridge Condition Assessment." *Report of GDOT Project No. RP05-01*, Georgia Department of Transportation, Atlanta, GA.

Wang, N., O'Malley, C., Ellingwood, B. R., and Zureick, A.-H. (2011a). "Bridge Rating Using System Reliability Assessment. I: Assessment and Verification by Load Testing." *ASCE Journal of Bridge Engineering*, Vol. 16, No. 6, pp. 854-862.

Wang, N., Ellingwood, B. R., and Zureick, A.-H. (2011b). "Bridge Rating Using System Reliability Assessment. II: Improvements to Bridge Rating Practices." *ASCE Journal of Bridge Engineering*, Vol. 16, No. 6, pp. 863-871.

Wipf, T. J., Phares, B. M., Klaiber, F. W., Wood, D. L., Mellingen, E., and Samuelson, A. (2003). "Development of Bridge Load Testing Process for Load Evaluation." *Final Report on Iowa DOT Project TR-445 / CTRE Project 00-65*, Research Report TR-445, Iowa Highway Research Board, Iowa Department of Transportation.

Wisniewski, D. F., Casas, J. R., and Ghosn, M. (2012). "Codes for Safety Assessment of Existing Bridges – Current State and Further Development." *Structural Engineering International*, Vol. 22, No. 4, pp. 552-561.